MOULD BEHAVIOUR AND PRODUCT QUALITY IN CONTINUOUS CASTING OF SLABS

By

Rama Ballav Mahapatra

B.Tech.(Hons.), Indian Institute of Technology, Kharagpur, 1981
M.A.Sc., The University of British Columbia, 1985

A THESIS SUBMITTED IN PARTIAL FULFILLMENT OF
THE REQUIREMENTS FOR THE DEGREE OF
DOCTOR OF PHILOSOPHY

in

THE FACULTY OF GRADUATE STUDIES
(Department of Metals and Materials Engineering)

We accept this thesis as conforming
to the required standard

THE UNIVERSITY OF BRITISH COLUMBIA

October 1989

In presenting this thesis in partial fulfilment of the requirements for an advanced degree at the University of British Columbia, I agree that the Library shall make it freely available for reference and study. I further agree that permission for extensive copying of this thesis for scholarly purposes may be granted by the head of my department or by his or her representatives. It is understood that copying or publication of this thesis for financial gain shall not be allowed without my written permission.

Department of Metals and Materials Engineering

The University of British Columbia
Vancouver, Canada

Date October 11, 1989

Abstract

An extensive study has been conducted to elucidate mould behaviour and to examine its influence on product quality during continuous casting of slabs. The study essentially comprised of industrial measurements, mathematical modelling and metallographic examination. The industrial measurements consisted of mould temperature measurements; an operating slab mould was instrumented with 114 thermocouples and the temperature of the mould at different locations was successfully measured for a wide range of casting conditions. A three-dimensional heat flow model of the mould was developed to quantitatively characterize the heat fluxes in the mould from a knowledge of the mould temperature data. Futhermore, a one-dimensional solidification model was developed to simulate solidification of steel and also, a heat flow model was developed to examine the mould flux behaviour by characterizing the slag rim thickness at the meniscus. Slab samples collected during the industrial trial campaign were metallographically examined to study the different aspects of solidification in the mould, sub-surface structure, solidification bands, cracks and oscillation marks.

The thermocouple measurements revealed the occurrence of metal level fluctuation in the mould, the magnitude of which was appreciable. Thus, implementation of a metal level control system has been recommended. The time-averaged mould temperature data was converted into heat fluxes and it has been well demonstrated that a three-dimensional model of the mould wall was essential for accurate computation of heat fluxes in the mould. The measurements have clearly established the strong dependence of heat transfer in the mould on the mould flux employed during casting. A reduction in the viscosity and melting temperature of the mould flux will lead to enhancement of heat transfer in the mould. It was also found that the heat transfer in the mould can be influenced by changes in casting speed, submergence depth, steel carbon content; the effect of these variables on heat transfer has been explained mostly on the basis of their influence on the mould flux

behaviour at the meniscus. Furthermore, heat extraction characteristics on the two broad faces were different which was a consequence of differences in mould flux behaviour resulting from differences in mould wall thickness between the two broad faces.

The heat-flux profiles were employed as a boundary condition in the solidification model to compute the shell thickness in the mould for a wide range of casting conditions. The casting speed has a significant influence on the shell profile in the mould; an increase in the casting speed led to a reduction in the shell thickness. The non-uniformity of the shrinkage of the solid shell in the mould was evident from the slab surface-temperature profile which clearly revealed the advantages of a non-linear taper of the narrow face compared to the conventional single taper. From a knowledge of heat-flux profile and metallographic analysis, a mechanism towards formation of longitudinal cracks/depression was formulated. Mathematical analysis performed on the mould flux at the meniscus revealed the presence of a slag rim adjacent to the mould wall; the dimensions of the slag rim thickness were computed at different casting speed and mould wall thickness. It was shown that oscillation marks are formed by the interaction of the slag rim with the partially solidified meniscus; the depth of the oscillation marks is strongly governed by the thickness of the slag rim at the meniscus.

This study has unambiguously shown that the dimension of the slag rim at the meniscus is quite critical from the standpoint of heat transfer and product quality of slabs. Based on the findings of the present study, for the first time, links have been established between the mould wall thickness and heat transfer in the mould. The slag rim thickness at the meniscus can be reduced by increasing the mould wall thickness. It is anticipated that an increase in the casting speed and thus, a corresponding increase in production rate can be accomplished by changing the design of the mould.

Table of Contents

List of Tables

List of Figures

List of Symbols

c_{pw}	Specific heat of water, J/kg K
c_{ps}	Specific heat of steel, J/kg K
c_{psol}	Specific heat of steel at solidus temperatute, J/kg K
c_{pliq}	Specific heat of steel liquidus temperature, J/kg K
c_{pm}	Specific heat of steel in the mushy region, J/kg K
c_{pflux}	Specific heat of mould flux, J/kg K
D_H	Hydraulic diameter, mm
f	Mould oscillation frequency, cpm
h_w	Heat transfer coefficient, $W/m^2\ ^0C$
k_m	Thermal conductivity of mould wall, W/m K
k_w	Thermal conductivity of water, W/m K
k_s	Thermal conductivity of steel, W/m K
k_{flux}	Thermal conductivity of mould flux, W/m K
L	Length of cooling channel, mm
L_s	Latent heat of steel, J/kg
Pr	Prandtl number
q_m	Heat flux from shell to mould wall, kW/m^2
q_{flux}	Heat flux from flux to mould wall, kW/m^2
R_{flux}	Resistance of flux/mould wall interface, $K\ m^2W^{-1}$
Re	Reyonlds number
s	Mould stroke length, mm
t	Time, s
t_n	Negative strip time, s
t_{ch}	Depth of the cooling channel, mm
T_m	Mould wall temperature, ^0C

T_w	Cooling water temperature, ^{0}C
T_{iwat}	Water inlet temperature, ^{0}C
T_s	Temperature of steel, ^{0}C
T_p	Initial temperature of steel, ^{0}C
T_{liq}	Liquidus temperature, ^{0}C
T_{sol}	Solidus temperature, ^{0}C
T_{old}	Temperature before a time step, ^{0}C
T_{new}	Temperature end of time step, ^{0}C
T_{cor}	Corrected temperature, ^{0}C
T_{flux}	Temperature of the mould flux, ^{0}C
T_{iflux}	Initial temperature of mould flux, ^{0}C
T_{sur}	Surface temperature of the mould flux, ^{0}C
u_w	Velocity of water, m/s
u_s	Strand velocity, m/s
v	Casting speed, m/min
w_{ch}	Half width of cooling channel, mm
ρ_w	Density of water, kg/m^3
ρ_s	Density of steel, kg/m^3
ρ_{flux}	Density of mould flux, kg/m^3
μ_w	Viscosity of water, N s/m^2

Acknowledgement

I would like to express my sincere thanks to Professors I.V. Samarasekera and J.K. Brimacombe for their invaluable guidance and advice throughout the course of this research. The assistance of Mr. Neil Walker during the industrial trial and other parts of the work was invaluable and sincerely appreciated. The assistance of Mr. Nick Hemingway in the metallographic examination is deeply appreciated.

I would like to thank Stelco Inc. for their financial assistance. The cooperation and assistance of Mr. Jack Young, Mr. Gene Patterson and Mr. Blair Otterman of Stelco during the plant trials and other parts of the work is very much appreciated.

I would like thank Mr. N. Tuffrey, Mr. Y. Nagasaka, Mr. J. Rechberger, Mr. R. Kamat, Dr. E. Osinski, Mr. A. Shook, Mr. B. Hernandez and Mr. K. Mukunthan for all their encouragement and discussions.

Finally I would like to thank my wife Veena for her constant support, encouragement, patience and for all the discussions throughout the course of this work.

Chapter 1 - INTRODUCTION

The continuous casting process essentially consists of pouring of molten steel at a controlled rate into a water cooled, reciprocating copper mould as shown in Fig. 1.1. It may be noted that during continuous casting of slabs the pouring of liquid steel into the mould is accomplished through a refractory tube extending from the bottom of the tundish into the mould commonly referred to as submerged entry nozzle. This results in partial solidification of the steel in the mould. Subsequently, the partially solidified strand is continuously withdrawn and solidification of steel is completed below the mould, where secondary cooling is accomplished by spraying water onto the surface of the strand. Mould flux is frequently used during continuous casting of slabs primarily to improve lubrication between the shell and the mould wall and also to control the heat extraction rates in the mould. The rapid increase in the adoption of this process over the past 20 years can be seen in Fig.1.2. More than 50% of the current steel production in the world is continuously cast whilst in Japan this figure exceeds 90% [1]. The continuous casting process has been established worldwide due to its higher yield, enhanced productivity and more uniform quality compared to the conventional ingot casting process. Moreover, significant savings in energy can be realized, if the continuously cast steel is directly hot-charged into the reheat furnace prior to rolling [2]. Figure 1.3 shows a comparison of the total energy consumption associated in the reheating of the slabs with cold and hot charging, and direct rolling after casting. Undoubtedly, hot charging and direct rolling can considerably reduce the energy consumption compared to the conventional cold charging practice. However, hot charging can be implemented successfully, only if the cast steel is free from surface defects and therefore, the ensuing requirement for inspection and surface grinding is eliminated.

It is interesting to note that the magnitude of the surface area of the cast product generated during continuous casting is much larger than that in ingot casting. Needless to say, the most predominant quality problems associated with continuously cast slabs are surface defects. These defects originate primarily in the mould which is rationalized on the basis that steel has low ductility and mechanical strength close to the solidus temperature [3,4] and this region of poor ductility occurs near the surface just below the meniscus. Heat transfer and solidification in the mould are the most crucial aspects of the continuous casting process owing to their strong links to the quality of the cast product [5,6]. Heat transfer from the strand to the mould is an exceedingly complex phenomenon due to the presence of a gap separating the strand from the inner surface of the mould. In the continuous casting of slabs, mould flux is known to have a dominant influence on the heat extraction capability of the mould primarily by its ability to alter the thermal resistance of the gap which offers the maximum resistance to heat flow. A number of researchers have revealed the profound influence of mould flux on the quality as well as production problems. For instance, oscillation marks present on the surface of the slabs are formed as a result of direct interaction between the partially solidified steel meniscus and the mould flux. The depth of the oscillation mark is strongly related to the viscosity of the mould flux, which is also known to have a significant effect on the surface cracks. Furthermore, inadequate lubrication at the meniscus will enhance sticking between the steel shell and the mould and thus can lead to a break-out; this phenomenon is generally attributed to the mould flux, since it has a strong influence on the lubrication.

Owing to overwhelming evidences linking mould flux to the quality and operating problems, there has been extensive research on the development of mould flux in the past two decades. Attempts have been made to elucidate the role played by mould flux during continuous casting in a qualitative manner by simply considering the behaviour of the flux film present between the strand and the mould wall. It is normally accepted that certain features of the flux film, primarily its thickness and the proportion of the solid and liquid flux will have a significant bearing on the heat transfer and lubrication in the

mould. Therefore, viscosity and crystallization temperature are considered to be critical variables of the mould flux. Such a rationalization need not necessarily be true, because the gap is not entirely filled with mould flux. For instance, despite using a mould flux with optimum physical properties, the lubrication and the heat transfer in the mould can be considerably influenced, if the depth of the molten mould flux at the meniscus is not adequate. It has been reported that the presence of a thick slag rim adjacent to the mould wall at the meniscus can impede the flow of mould flux and thus, is very detrimental from the standpoint of lubrication. Therefore, it is more realistic to state that, in addition to the physical properties, the performance of the mould flux is strongly dependent on its behaviour at the meniscus. Nonetheless, the research conducted on mould flux has been primarily aimed at improving its physical properties like viscosity, crystallization temperature, melting rate. Two different approaches have been taken to attain this; majority of the researchers have attempted to improve the properties of the mould flux by adjusting its chemical composition. The second approach has been to control the mineralogical phases present in the mould flux during melting and solidification to obtain its desired properties. However, to evaluate the performance and suitability of a mould flux during casting, trial and error methods and empirical relationships have been utilized. Researchers in the past have ignored the most important aspect of the mould flux, namely, its behaviour at the meniscus under the prevailing conditions in an operating slab mould. Therefore, links between the mould flux and the quality and operating problems have not been fully ascertained. A lack of appropriate analysis on the mould flux has been mainly due to a paucity of information on the heat flux distribution in the mould. Consequently, heat transfer and the ensuing solidification in the mould is not well understood.

In contrast, the results of studies at UBC on billet casting [5,6] has enhanced our knowledge on heat transfer and solidification in a billet mould. The effect of steel composition and water velocity on heat transfer in the mould has been elucidated and has led to the formulation of a mechanism for oscillation mark formation. Moreover, it has

led to a better understanding of quality problems like rhomboidity and off-corner interal cracks, such that recommendation could be made to prevent these defects. Unfortunately, a study of similar nature has not been conducted on slab moulds and is therefore the objective of the proposed research.

The present work was undertaken to examine the mould-related quality problems. Measurements were made on an operating slab caster to determine the heat extraction rates in the mould for different casting speeds, submerged entry nozzle configuration, mould flux types and steel grades. Subsequently, this information has been utilized to perform mathematical analyses on the mould flux and steel. Knowledge of the temperature distribution in the mould flux was immensely useful in assessing its behaviour at the meniscus. In addition, the behaviour of the mould flux has been ascertained for different casting paramaters and design of the mould. Mathematical analysis was also performed on the steel to understand solidification in the mould. Also, samples of slabs were subjected to metallographic examination to evaluate its quality. Subsequently, results from plant measurements, mathematical models and metallographic examination were simultaneously analysed to understand the mould related quality problems. This study has lead to a better insight on the links between mould flux, quality and operating problems and provided guidelines for the improvement of slab surface quality and operating practice.

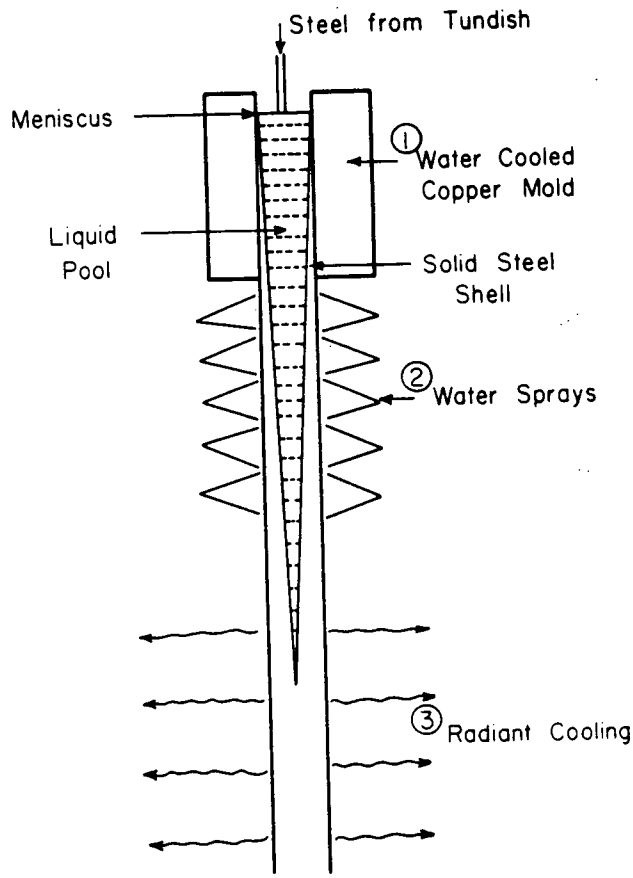

Figure 1.1. Schematic drawing of the continuous casting machine showing the different zones of heat extraction.

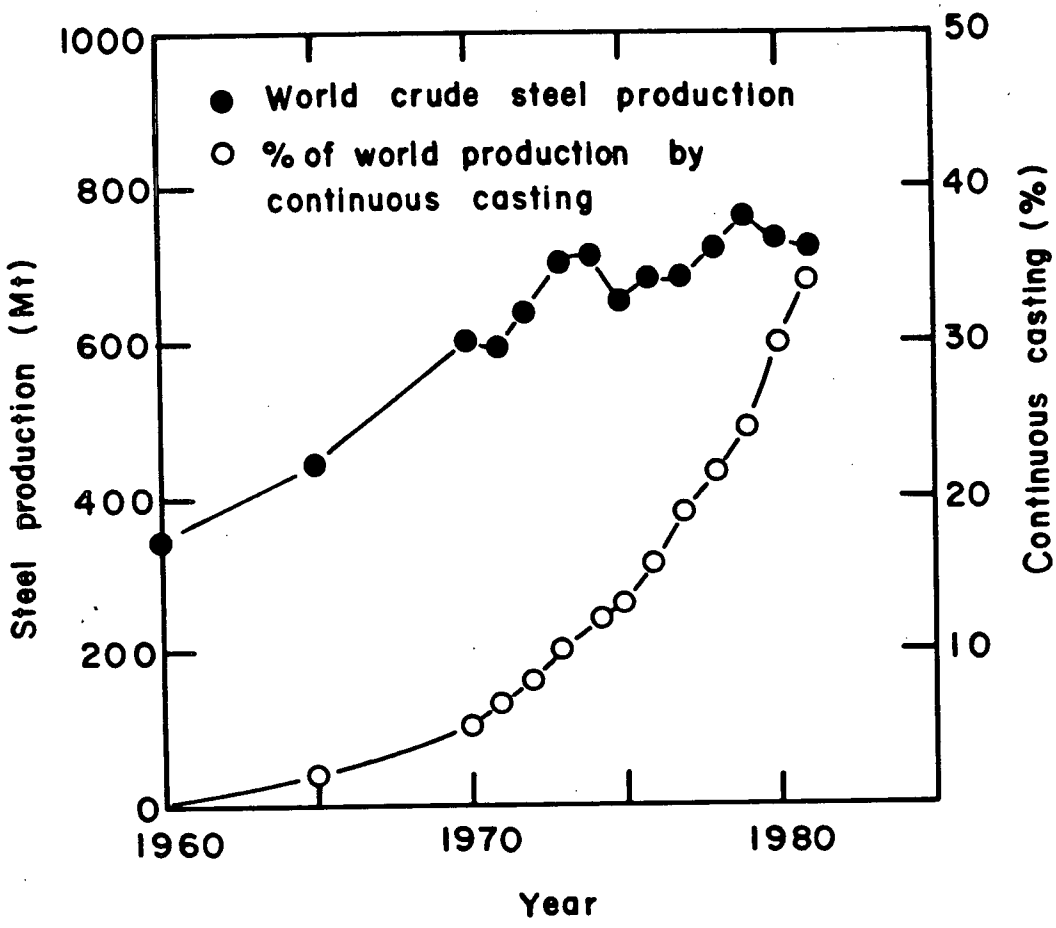

Figure 1.2. Total steel production in the world and the proportion of continuous casting [1].

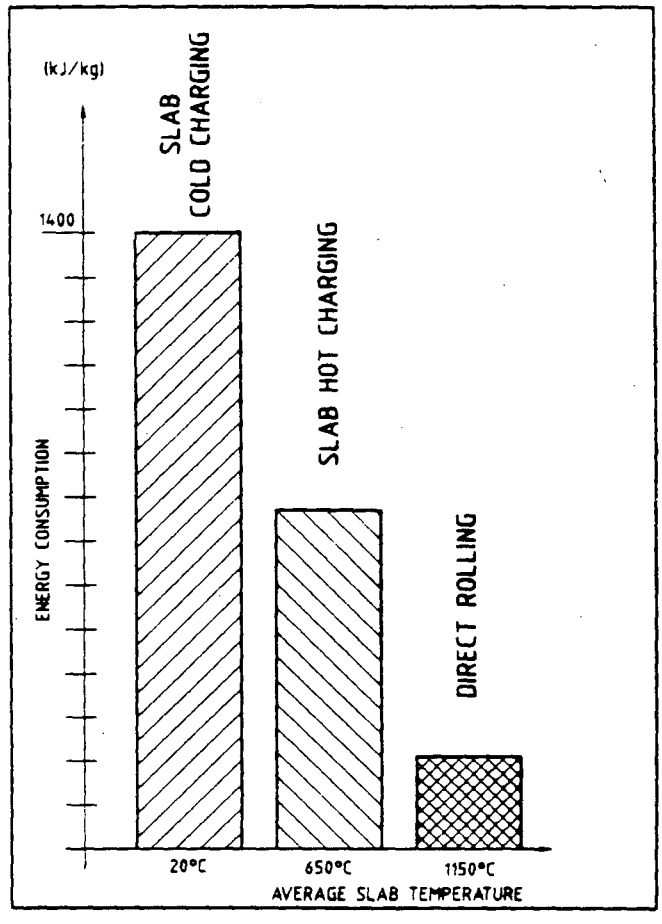

Figure 1.3. Comparison of the total energy consumption in slab reheating with cold and hot charging and direct rolling [20].

Chapter 2 - LITERATURE REVIEW

The following sections will review the various quality and operating problems encountered during continuous casting of slabs. Based on the information available in the literature the underlying causes and the origin of these problems will be established and discussed in the subsequent sections.

2.1 Quality Aspect of Continuously Cast Slabs

2.1.1 Longitudinal Cracks

Longitudinal surface cracks frequently appear on the mid-face and near the corners of continuously cast slabs [7]. These cracks vary in length from a few millimeters to several hundred millimeters or more, and may necessitate extensive surface treatments such as scarfing or grinding.

2.1.1.1 Longitudinal Mid-Face Cracks

Longitudinal mid-face cracks have been studied extensively in the past. A typical example of a longitudinal mid-face crack on a slab is shown in Fig. 2.1. Brimacombe et al. [8] have found that longitudinal mid-face cracks are interdendritic in nature and form by hot tearing close to the solidification front. From the location of these cracks and with the aid of a heat flow model to calculate the shell thickness, they have shown that the cracks originate in the mould. Also, analysis of the cracks with a scanning electron microscope revealed the presence of mould flux. Clearly, these findings confirm that the longitudinal mid-face cracks form in the mould.

Nakano et al. [9] of Nippon Steel have measured the temperature of the mould in an attempt to study the relationship between mould heat extraction and the occurrence of longitudinal cracks. They essentially made the measurements over two periods, one in which the cracks were formed and other in which they were absent. Figure 2.2 shows that large fluctuations in temperature of the mould occur during the formation of the cracks. Byrne et al. [10] of British Steel Corporation have reported the presence of deep

longitudinal cracks on rounds cast with mould flux in the beginning of a heat. They have succeded in reducing this type of cracks simply by using a different type of mould flux exclusively at the start of the cast which minimized the fluctuation of mould heat transfer in the initial stages of casting.

The links between the uniformity of the heat transfer in the mould and the occurrence of longitudinal cracks is not difficult to understand. Non-uniform cooling in the mould leads to the development of localized hot spots in which tensile stresses will concentrate in the solidifying shell and can lead to the formation of a crack. The strong relationship between the mould flux and the incidence of longitudinal cracking has also been reported by Chihara et al. [11] of Nippon Steel Corporation. There is strong evidence in the literature suggesting that an uneven flow of the mould flux at the meniscus will generate non-uniform cooling in the mould and lead to the formation of longitudinal cracks [12,13,14,15].

Owing to the dependence of longitudinal cracks on the type of mould flux, a number of attempts have been made to relate the properties and the consumption rate of the flux during casting to these cracks. The effect of viscosity of the mould flux on longitudinal mid-face cracks has been studied by a number of investigators. Delhalle et al. [16] and Funanokawa et al. [17] have reported that low viscosity mould flux will prevent the formation of longitudinal cracks. Contrary findings on the effect of viscosity of the mould flux also have been reported [18,19]. Figure 2.3 shows the results of Sorimachi et al. [19] which clearly reveal the advantages of using higher viscosity mould flux. However, it is important to realize that various investigators have characterized the viscosity of the mould flux exclusively at a temperature of 1300^0C in their studies to assess its effect on the incidence on longitudinal cracking. This does not represent the viscosity of the mould flux at the meniscus in an operating slab mould under the prevailing casting conditions. Nevertheless, it is clear from the literature that the mould flux viscosity has to be controlled to reduce the incidence of longitudinal cracks.

The effect of recrystallization temperature of the mould flux on longitudinal cracks also has been investigated [21,22]. Wada et al. [21] of Nippon Kokan have reported that as the recrystallization temperature of the mould flux is lowered, the occurrence of longitudinal cracking is enhanced. On the contrary, Vereecke et al. [22] have implied that longitudinal cracks can be diminished by reducing the recrystallization temperature of the mould flux.

Mairy et al. [23], while attempting to measure the friction in the mould with a sensor, called M.L.TEKTOR, observed that the longitudinal cracks are formed over periods during which the frictional forces between the solidifying shell and the mould are high as shown in Fig. 2.4. The increase in the friction has been attributed to a reduction in the consumption rate of mould flux and has led to a number of investigations, in which attempts have been made to relate the consumption rates of the mould flux to the occurrence of longitudinal cracks. Nakano et al. [9] have reported that the incidence of longitudinal cracks is increased when the depth of the molten mould flux at the meniscus is low which has been explained on the basis of reduced consumption of the mould flux owing to a reduction in its depth. The strong relationship between the molten flux depth and the occurrence of longitudinal cracks also has been reported by Ogibayashi et al. [24]. In order to elucidate the precise influence of the molten flux depth, Nakano et al. [25] of Nippon Steel have proposed that the mould flux at the meniscus adjacent to the mould wall solidifies and results in the formation of a slag rim which moves with the mould during its oscillation. Therefore, the presence of the slag rim can inhibit the flow of mould flux at the meniscus and the influence of the slag rim is prominent particularly when the depth of the molten flux at the meniscus is not adequate. Delhalle et al. [16] have found that a rise in the metal level in the mould enhances the formation of longitudinal cracks as shown in Fig. 2.5. It is likely that in the presence of a slag rim at the meniscus, the metal level increase in the mould will result in the obstruction of mould

flux inflow at the meniscus. Furthermore, Yanagida et al. [26] have found that the incidence of longitudinal cracks can be enhanced with a decrease in the ratio of the melting rate and infiltration rate of the mould flux.

It has been found that longitudinal cracks are also strongly dependent on the carbon content of the steel. Steel having carbon in the range of 0.08%-0.15% [16,18,27,28] is particularly prone to this type of cracks, the findings of Irving et al. [27] are shown in Fig. 2.6.

2.1.1.2 Longitudinal Corner Cracks

The design of the mould, in particular the taper of the narrow face copper plates, plays an important role in the formation of longitudinal corner cracks [14,15,16,17]. In the early stages of solidification, the heat extraction at the corner of the slab is enhanced due to two-dimensional heat transfer resulting in a thicker steel shell. The solidified shell near the corner of the slab is strong enough to withstand the ferrostatic pressure of the molten steel which leads to the formation of an air gap, at and off the corner. The presence of large gap near the corner leads to a reduction in the heat extraction causing reheating of the solidified shell which leads to the development of hot spot near the corners. In the presence of transverse tensile strains, longitudinal corner cracks can form.

Funanokawa et al. [17] have found that with an increase in the taper of the narrow plates the incidence of longitudinal corner cracks is reduced as shown in Fig. 2.7. However, excessive taper is not desirable because it can increase the strand/mould wall friction [23]. Moreover, Nakata et al. [30] have suggested that in addition to the narrow plates, the wide plates should also be tapered to reduce the occurrence of longitudinal cracks. Fujiyama et al. [31] of Kawasaki Steel have experimented with a mould where the taper at the corner of the narrow plate is greater than that at the centre and have reported a reduction in the frequency of longitudinal corner cracks. They have explained this in terms of the new mould design which can reduce the air gap and inhibit development of

hot spots near the corner. It is evident that the design of the mould has a strong effect on the incidence of longitudinal cracks mainly by its ability to affect the heat transfer in the mould.

2.1.2 Longitudinal Depressions

Longitudinal depressions are usually found on the wide faces of the slab near the corner. Extensive studies have not been conducted on this type of quality problem. Yamamoto et al. [33] have attempted to find the origin of these depressions and have adjusted the secondary cooling conditions to prevent their occurrence; but, the longitudinal depressions remained the same. Based on these results, they have reported that these depressions originate in the mould. Thomas et al. [34] also have confirmed that these depressions originate in the mould and have recommended that the taper of the end plates must be adjusted to prevent this kind of problem.

2.1.3 Oscillation Marks

The surface of a continuously cast slab is characterized by the presence of oscillation marks resulting from the reciprocating action of the mould. A typical example of a slab surface exhibiting oscillation marks is shown in Fig. 2.8. Oscillation marks can have a deleterious effect on slab quality because the bottom of the oscillation mark may act as a notch, which localizes the stress and increases the propensity for transverse crack formation, especially during straightening of the strand [12,18,35]. Segregation of phosphorous and manganese which may enhance cracking is found at the bottom of the oscillation marks and in the vicinity of the sub-surface hooks [36,37,38]. The presence of oscillation marks also locally increases the width of the gap between the strand and the mould wall. Consequently, there is a significant drop in heat transfer [39] and a local reduction in the thickness of the solid shell. This can eventually lead to a break-out below the mould if the shell cannot withstand the ferrostatic pressure of the molten steel. In summary, the presence of an oscillation mark, particularly if deep, is undesirable since it has an adverse effect on both slab quality and casting operation.

2.1.3.1 Pitch and Depth of Oscillation Marks

Each oscillation mark is formed during one cycle of oscillation of the mould. The pitch of the oscillation marks is governed by the casting speed and the frequency of the mould oscillation as given below [13],

$$Pitch = \frac{v}{f} \tag{2.1}$$

The depth of oscillation marks (obtained mostly from measurements on the narrow face) is known to be related to the steel carbon content, negative strip time (a function of frequency, stroke of mould oscillation and the casting speed) and the type of mould flux. The carbon content of steel has a pronounced effect on the depth of the oscillation marks [40,41]. Cramb et al. [40] have reported that oscillation marks are relatively deep in steel grades having a carbon content in the range of 0.10 to 0.16 percent as shown in Fig. 2.9.

Many investigators have reported the influence of the negative strip time of the mould oscillation on the depth of oscillation marks [20,28,40,42-47]. The negative strip time is defined as the time during one oscillation cycle, when the mould travels downward at a speed greater than the strand withdrawal. For sinusoidal oscillation of the mould, the negative strip time is expressed as,

$$t_n = \frac{60}{\pi f}\cos^{-1}\left(\frac{v}{\pi fs}\right) \tag{2.2}$$

It is evident from the literature that the depth of oscillation marks is enhanced with increasing negative strip time as shown in Fig. 2.10. The stroke length of the mould oscillation is known to influence the oscillation mark depth [13,47]; a decrease in the stroke length reduces the oscillation mark depth [47]. The frequency of the mould oscillation is also known to influence oscillation mark depth [40,45], an increase leads to a reduction in the depth of the oscillation marks. Furthermore, oscillation mark depth is decreased with increasing casting speed [40] as shown in Fig. 2.11.

In addition to the the mould oscillation characteristics, the mould flux also is known to have an effect on the depth of oscillation marks. The viscosity of the mould flux, in particular, is known to influence the depth of the oscillation marks [48,49]. Takeuchi [48] found that the depth of the oscillation mark is deeper in Al-killed steel compared to Si-killed steel which was rationalized on the basis of the higher viscosity of the mould flux during casting of Al-killed steel owing to an increase in the quantity of entrained alumina. On the contrary, Ando et al. [49] have reported that an increase in the viscosity of the mould flux reduces the depth of oscillation marks.

2.1.3.2 Mechanisms of Oscillation Mark Formation

A number of mechanisms have been suggested in the literature for the formation of oscillation marks [12,13,41,51-55]. Saucedo [55] has proposed that the formation of oscillation marks is solely governed by the extent of solidification of steel at the meniscus and the ensuing overflow of molten steel over the partially solidified meniscus. Based on this rationale, it is hard to explain the strong dependence of the oscillation mark depth on the nature of the mould lubricant. It is reported that the heat transfer at the meniscus is enhanced when oil is used as a lubricant in comparison to mould flux [57], but the depth of the oscillation mark is reduced [56] despite larger extent of solidification at the meniscus. Owing to these shortcomings, Takeuchi and Brimacombe [41] have proposed a mechanism for oscillation mark formation on slabs which is based on the response of the partially solidified shell at the meniscus to the fluid pressure development in the mould flux channel between the strand and the mould wall. With the aid of a fluid flow model of the mould flux channel, they have reported that a positive pressure develops in the mould flux during negative strip and a negative pressure during the upstroke of the mould oscillation. A schematic representation of the events in one oscillation cycle leading to the formation of an oscillation mark is shown in Fig. 2.12. They have reported that the depth of oscillation marks is dependent on the extent of solidification at the meniscus and also on the mould oscillation characteristics, casting speed, viscosity of the mould flux

and also on the metal level fluctuations during casting. It emerges clearly from the literature that in addition to the strong effect of the mould oscillation, the initial solidification at the meniscus, both in the steel as well in the mould flux, plays an important role in the formation of oscillation marks.

2.1.3.3 Countermeasures to Prevent Oscillation Marks

Numerous studies have been conducted to establish countermeasures to minimize the depth of oscillation marks, mostly by simulating continuous casting in the laboratory. The results indicate that the depth of the oscillation marks can be reduced by controlling the mould oscillation characteristics [12,56,58] and the initial solidification at the meniscus [50,59]. Yasanuka et al. [58] of Kobe Steel have reported that the depth of oscillation marks can be reduced to zero by increasing the oscillation frequency of the mould to 30 Hz as shown in Fig. 2.13. Similar findings also have been reported by Howe et al. [56] of British Steel. However, it may be noted that in an actual operation, the frequency of the mould oscillation is always in the range of 1-3 Hz. The reluctance to adopt higher oscillation frequency of the mould has been mainly due to the fact that mould flux consumption is drastically reduced [58] which results in poor lubrication in the mould.

Delhalle et al. [59] have attempted to reduce the depth of the oscillation marks by controlling solidification of steel at the meniscus. The mould used in their experiments consisted of insulating sleeves (stainless steel, chromium carbide) at the meniscus which was referred to as hot top mould. They have reported that the depth of oscillation marks can be reduced with these hot top moulds and a comparison between the conventional and the hot top mould is given in Table 2.1. However, the hot top moulds are not in operation in plants, mainly due to difficulties related to peeling of the insulating sleeves, reduced life of the mould.

2.1.3.4 Initial Solidification at the Meniscus

Owing to the strong dependence of the depth of oscillation marks on the initial solidification at the meniscus, it is clear that the understanding of this phenomena requires that the extent of solidification at the meniscus be known in a quantitative manner. There has been a number of attempts to study this aspect mathematically [41,60-65]. Saucedo et al. [62] and Laki et al. [63] have modelled solidification at the meniscus by assuming values of heat transfer coefficients for different grades of steel to characterize the heat flux from the steel to the mould. The results indicate that the heat transfer conditions at the meniscus and the superheat of the steel will have an effect on the extent of solidification at the meniscus. But, they have not performed any calculations to determine the temperature distribution in the mould flux. Takeuchi and Brimacombe [41] also have studied the extent of solidification at the meniscus, both in the steel and the mould flux, using a two-dimensional heat transfer model. They have utilized the mould temperature measurements made by Nakato et al. [66] to calculate the heat flux at the meniscus which has been employed in their model to calculate temperature distribution in the steel and the mould flux. However, it is important to note that the temperature measurements in the mould have not been made at sufficient number of locations, especially in the vicinity of the meniscus and thus, the heat flux at the meniscus may not be accurate. Besides, the heat flux data is valid only for a particular steel composition, casting speed, mould flux and pouring conditions that prevailed during the mould temperature measurements.

The positive pressure developed in the mould flux channel during negative strip of the mould oscillation [41] is related to the depth of the oscillation marks and therefore, Tada et al. [64] have attempted to characterize the influence of the size of the slag rim at the meniscus adjacent to the mould wall on the pressure developed in the mould flux channel, a schematic representation is shown in Fig. 2.14. They have reported that a decrease in the thickness of the slag rim will result in a reduction in the pressure. These

results clearly indicate the importance of the size of the slag rim and therefore an accurate knowledge of the temperature distribution in the mould flux is essential. Recently, Takawa et al. [65] have attempted to analyse the initial solidification at the meniscus and the calculations have been primarily aimed at quantifying the dimensions of the slag rim adjacent to the mould wall. However, they have assumed values of heat transfer coefficients in the model to characterize the heat transfer from the steel to the mould.

The preceding review clearly shows that inspite of the profound influence of the initial solidification on the depth of oscillation marks, this phenomena has not been studied quantitatively using the heat transfer conditions existing in an operating mould which has been mainly due to a lack of heat flux data in the vicinity of the meniscus.

2.1.4 Transverse Cracks

Transverse cracks are one of the most common surface defects found on continuously cast slabs and therefore have attracted numerous studies. These cracks are located along the bottom of the oscillation marks perpendicular to the casting direction [12,14,16]. A typical example of transverse cracks on a longitudinal section of the slab is shown in Fig. 2.15.

Fujiyama et al. [31] have reported that transverse cracks are formed in the sub-mould region because steel has a low strength and ductility in the temperature range prevailing in this region [67]. The longitudinal tensile strains generated in the straightener or in the spray chamber can cause transverse cracks in the above mentioned temperature range. Steel containing Al, Nb, V, Cb, N [28] and carbon in the range of 0.08-0.14 percent [16] are particularly more susceptible to transverse cracks.

Soejima et al. [68] of Kobe Steel have found that the occurrence of transverse cracks is increased at higher depth of oscillation marks. Irving et al. [28] have reported that the incidence of transverse cracks is reduced with decreasing negative strip time which is known to reduce the depth of oscillation marks. Takeuchi and Brimacombe [36] also have found that transverse cracks are associated with deep oscillation marks and

these cracks are interdendritic in nature and some of the cracks contained mould flux. They have formulated a mechanism on the formation of transverse cracks based on metallographic studies and a heat flow model. Oscillation marks result in non-uniformity in the thickness of the shell between the top and the bottom of an oscillation mark as shown in Fig 2.16. Therefore, deep oscillation marks will result in a thin shell at the bottom of the mark. Furthermore, the thickness of the segregated layer at the bottom of the mark increases with increase in the depth of oscillation marks. Subsequently, the thin and weak shell at the bottom of an oscillation mark can crack when subjected to longitudinal tensile strains. Tanaka et al. [69] have said that the friction between the shell and the mould, which is related to the mould flux, can generate longitudinal strains. It is evident from the literature that transverse cracks initiate in the mould.

2.2 Operating Problems During Continuous Casting of Slabs

2.2.1 Strand Break-out

Break-out of the continuously cast strand below the mould is about the most serious problem a caster can encounter, since this can significantly lower the production rate. Break-outs can occur due to a number of reasons. Tsuneoka et al. [70] of Nippon Steel and Tsai et al. [71] of Inland steel have examined the causes that led to break-outs in their respective plants and their findings are shown in Fig. 2.17. Clearly, majority of the break-outs can be attributed to sticking between the shell and the mould wall.

Sticking invariably initiates at the meniscus [72,73]; Fig. 2.18a schematically shows the sequence of events that take place in the mould from the initiation of sticking to the eventual break-out. It can also be seen from Fig. 2.18b that the entire process results in rapid changes in the mould temperature at any given location. Therefore, mould temperatures are often monitored to detect sticking in the mould. Poor lubrication in the mould can result in sticking between the shell and mould and thus, the occurrence of break-out due to sticking is increased as the frictional forces in the mould is enhanced [74]. It has been established that the lubrication in the mould is dependent on the mould

flux, hence sticker type break-out is strongly related to the mould flux. Increase in the mould flux viscosity will increase the friction in the mould and consequently the propensity for break-outs [74].

Sorimachi et al.[75] of Kawasaki Steel have reported that sticker type break-out is dependent on the tendency of the mould flux to recrystallize into a phase referred to as cuspidine($3CaO.2SiO_2.CaF_2$) during solidification; the presence of cuspidine in the mould flux film will deteriorate the lubrication between the shell and the mould. They have suggested that the silica content of the mould flux should be increased to prevent the formation of cuspidine in order to minimize the break-out frequency. However, it should be noted that an increase in silica will lead to an increase in the mould flux viscosity and thus can be detrimental from the standpoint of sticking. Imai et al.[76] also have emphasized on the need to control the recrystallization tendency of the mould flux into cuspidine. They have reported that introduction of gases like Ar, H_2, Air into the mould flux can increase the quantity of cuspidine and also the mould flux viscosity and thus can result in sticking due to poor lubrication.

Lubrication in the mould is also dependent on the consumption rate of the mould flux and mould oscillation characteristics. Koyano et al. [77] have observed that the frequency of sticker type break-out is increased particularly, when the casting speed is greater than 1.5 m/min and this is attributed to the reduction in the consumption of the mould flux. Based on the plant experience, they have recommended a minimum mould flux consumption rate of 0.3 kg/m^2 to prevent sticking in the mould. Maeda et al. [78] have found a strong relationship between mould flux consumption and the carbon content of steel; an increase in the carbon content will reduce the consumption rates which can result in sticking. This observation has led to the development of mould fluxes for exclusive application in high carbon steel. Furthermore, it has been shown that the carbon present in the mould flux can influence the occurrence of sticker type break-out. This has been explained on the basis that the carbon from mould flux can dissolve in molten steel and thus, resulting in its recarburization [86]. Subsequently, the liquidus temperature of

the steel is lowered and thus, the presence of molten steel at the meniscus will enhance sticking. Therefore to prevent recarburization of steel, attempts are being made develop new mould fluxes in which carbon is substituted by Boron Nitride [87].

Some researchers have reported that lubrication can be improved, if the mould is vibrated ultrasonically perpendicular to the casting direction [79,80]. This observation has not been explained, however, it is possible that vibration of the mould may result in breaking of the slag rim adjacent to the mould and thereby improving the mould flux inflow at the meniscus. The oscillation characteristics of the mould is also known to influence the frequency of break-outs due to sticking. Nakato et al. [81] of Kawasaki Steel have reported that an increase in the frequency of mould oscillation will lead to a reduction in the flux film thickness between the shell and the mould and therefore, break-out due to sticking can occur at higher frequencies. Attempts have been made to prevent sticker type break-out by optimizing the mould oscillation cycle [82-85]. In Nippon Kokan, experiments simulating continuous casting have been conducted with the aim of evaluating lubrication in the mould under two different oscillation modes. A comparison of the mould velocity and displacement against the time characteristics for the sinusoidal and the non-sinusoidal mode of oscillation of the mould is schematically shown in Fig. 2.19. Mizukami et al. [84] have measured the frictional forces in the mould, when it was subjected to the two different type of oscillation. Measurements indicate that the total friction in the mould was lower during non-sinusoidal oscillation of the mould; they have attributed this to an increase in the mould flux consumption and also to a reduction in the relative velocity between the mould and the strand during the upward motion of the mould (Fig. 2.19).

Break-out of the strand is also attributed in a few cases to the presence of deep cracks on the slab [70]. The occurrence of deep oscillation marks on the slab, which is again related to the mould flux can lead to a break-out by reducing the heat extraction in the mould. Ogibayashi et al. [24] of Nippon Steel have reported that the total heat removed in the mould must be optimized to prevent a break-out, as can be seen from Fig.

2.20. Reduction of heat extraction rates in the mould will result in a thin shell which can rupture below the mould, if the shell cannot withstand the ferrostatic pressure of the molten steel. On the otherhand excessive heat removal in the mould will lead to a reduction in the temperature of the strand surface and thus, due to the presence of solid flux film adjacent to the shell, the friction forces in the mould will be increased and thus a break-out can occur.

2.3 Conclusions From Literature Review on the Quality Aspect and Operating Problems During Continuous Casting of Slabs.

Continuously cast slabs are plagued by a number of quality problems. Also, operating problems are encountered during casting, namely, break-outs. The preceding review clearly indicates that many of these quality problems, like, oscillation marks, surface cracks originate in the mould and it is conclusive that the critical factors which have a significant effect on the quality problems are the mould flux, mould design and the heat transfer in the mould. Needless to say, the break-out of the strand below the mould is also related to the events occurring in the mould. Mould flux, in particular is seen to have a profound influence on the incidence of break-outs. It emerges clearly from the literature that the behaviour of the mould flux at the meniscus is important. For example, the slag rim formed at the meniscus adjacent to the mould wall can be detrimental as it can inhibit the flow of mould flux and thereby, influence the heat transfer and lubrication. A review of the important parameters during casting, like mould flux, mould design and the heat transfer in the mould will be presented in the following sections.

2.4 Mould Flux

Mould fluxes were originally developed for application in the casting of bottom pouring ingots. Currently, mould fluxes are routinely used in continuous casting process essentially to accomplish several key functions. McCauely et al. [88] have reported on the differences in the properties of mould flux for application in bottom pouring and continuous casting. They also reported that the requirements in the properties of the

mould fluxes differ substantially from casting of slabs to blooms. Continuous casting mould fluxes are essentially synthetic slags in powder form and their composition is usually based on the $CaO.SiO_2Al_2O_3$ system with some additions of alkali oxides and fluorides. Majority of the mould fluxes also contain 3 to 6 percent of graphite to control its melting characteristics and thermal insulation capability. Depending on the manufacturing method, mould fluxes are normally classified under three categories, namely, fly ash based, synthetic powders and prefused or granulated powder. The fly ash based and synthetic powders are blends of powdered raw materials, whereas, granulated powders are blends which have been melted and sized after mechanical mixing of raw materials. In general, the use of granulated mould fluxes is increasing [89].

2.4.1 Functions of the Mould Flux

The mould flux above the meniscus in an operating mould exists in three different states, namely, molten, sintered and powdered, as schematically shown in Fig. 2.21. The desired functions of the mould flux during casting are given below,

(i) To prevent reoxidation of the molten steel at the meniscus.

(ii) To prevent freezing of the steel at the meniscus by providing thermal insulation.

(iii) To absorb and dissolve the inclusions which rise upto the meniscus and thereby prevent their entrapment in the solid shell.

(iv) To provide lubrication between the solid shell and the mould and hence facilitate in the withdrawal of the strand from the mould.

(v) To control the heat transfer from the strand surface to the mould wall.

McCauely et al. [90-94] have reported on the requirements of the mould flux with respect to its physical properties for accomplishing the above functions. It clearly emerges that the properties of the mould flux which need to be controlled are its viscosity, recrystallization temperature, melting rate. Branion [95] and Layni et al.[96] have emphasized that, in addition to the physical properties of the mould flux, the

temperatures of the hot face of the mould wall and steel shell are also crucial, since these parameters would influence the behaviour of the mould flux film in the gap between the shell and the mould.

2.4.2 Research Towards Development of the Mould Flux

A number of researchers have attempted to alter the chemical composition of the mould flux to improve its physical properties [95-99]. The melting rate can be controlled by the type and quantity of carbon in the mould flux. Softening and melting temperature of the mould flux is frequently estimated by heating a sample and observing the changes in its shape during this period [95]. Scheel et al. [99] have reported that the melting and softening temperature of the mould flux can be changed by varying the quantity of Na_2O ,CaO, Al_2O_3 and its basicity. Viscosity of the mould flux is very sensitive to its temperature and it can be seen from Fig. 2.22 that there is a dramatic increase in the viscosity below the recrystallization temperature of the mould flux. This has led to a number of studies towards controlling the viscosity of the mould flux. Increase in the alumina content of the mould flux will increase its viscosity, whereas an increase in the quantity of fluorides will reduce the viscosity of the mould flux. Attempts also have been made to characterize the combined effect of all the oxides in the mould flux on its properties by establishing a new chemical parameter called the glass ratio [100]. Grievson et al. [101] have reported that the mineralogical phases present in the mould flux during its melting and solidification have a greater influence compared to the chemical composition in controlling the viscosity and the melting characteristics of the mould flux.

Layni et al. [96] based on the results obtained from an operating caster have reported that two mould fluxes of similar chemical composition and viscosity showed significant differences in their consumption rates. The mould flux that tended to gum up at the meniscus (thick slag rim) resulted in a low consumption rate and this observation has not been explained. However, it is possible that the slag rim will restrain the inflow of

the mould flux at the meniscus and thereby, reduce the consumption rate. Gray et al. [27] of British Steel also have reported that the slag rim at the meniscus must be minimized to improve the lubrication and the heat transfer in the mould. Therefore, the performance of the mould flux during casting is also dependent on its behaviour at the meniscus in conjunction to its physical properties. But, the development work on the mould fluxes have mostly emphasized on improving their physical properties. Therfore, it is essential that the behaviour of the mould flux at the meniscus in an operating slab mould be characterized.

2.5 Continuous Casting Slab Mould

Slab moulds are usually straight or curved as shown in Fig. 2.23. Plate type moulds are used in slab casting compared to the tubular mould in billet casting. The plate type moulds have relatively greater wall thickness compared to the tubular moulds [102]. The slab mould comprises of four copper plates, which are bolted to steel backup plates to provide rigidity to the copper plates [102,103,104]. These plates are assembled to form a mould cavity of desired dimensions. The narrow plates are frequently tapered between 0.9-1.3 %/m to compensate for the shrinkage of steel during solidification, whereas, the broad plates are parallel primarily due to difficulties in aligning these plates with the sub-mould region of the casting machine [105]. The length of the mould usually varies between 700 to 900 mm. These moulds are cooled by water flowing through longitudinal channels machined from the outer face of the copper plates. The average water velocity in the cooling channels is around 6 m/s [105].

During casting the mould is reciprocated and the most extensive mode of oscillation of the mould is sinusoidal. The most significant parameters of oscillation are the frequency, stroke length and the negative strip time. It should be noted that the oscillation characteristics of the mould vary from plant to plant.

The life of a mould is normally in the range of 100 to 500 heats [105]. The wide scatter is due to the different sizes of the heat and sections cast in various plants. Mould

life is also quantified in terms of total length of the strand cast through it. The copper plates are usually coated [106,108] with chrome and/or nickel to increase its life. An example of a typical coating on the copper plate with dimensions are shown in Fig. 2.24 [106]. The narrow faces of the moulds tend to have a shorter life than the wide plates. These plates are normally remachined after 5000 to 7000 m cast length compared to 10000 to 15000 m for the wide plates [105]. It is a standard practice to remachine the copper plates for its further use. During each remachining, 1.5-2.5 mm of copper is removed from the plates and the same plate is used as many as nine times after remachining [105]. It may be noted that, this is equivalent to a reduction in the copper thickness by 10-20 mm from its original value.

Brimacombe et al. [108] have formulated several criteria towards the design of billet mould. However, despite the strong links between the mould to the heat transfer and the final product quality, there are no explicit guidelines towards the design of a slab mould.

2.6 Heat Transfer in the Mould

The literature review on the quality as well as operating problems during continuous casting has revealed the significance of heat transfer in the mould. The following sections will review the mechanism of heat transfer, heat flux measurements and finally the effect of a number of operating variables, steel grade and mould flux on the heat transfer in the mould will also be presented.

2.6.1 Mechanism of Heat Transfer in the Mould

Heat transfer from the surface of the strand to the mould is quite complex due to the presence of a gap separating the strand from the mould wall as shown in Fig. 2.25. The gap assumes importance because its resistance to heat flow is approximately 84 percent of the total [39]. Irving with the aid of mathematical calculations has shown that in the presence of air, the primary mode of heat transfer through the gap is by conduction[109]. Therefore, the gap dimensions have a strong impact on the heat transfer in the mould.

However, in the continuous casting of slabs, the gap will usually comprise of mould flux existing in three different of states, namely, liquid, crystalline and glassy, as shown in Fig. 2.26. It should be noted that the different states of the mould flux in the gap and their proportions will depend on the temperatures of the hot face of the mould, the surface of the strand and the solidification characteristics of the mould flux [95].

In the presence of flux film in the gap, the heat transfer through the gap can take place by conduction and radiation and hence it is necessary to clarify the dominant mode of heat transfer through the gap in the slab mould. Mitchell [110] has reported that in addition to conduction, heat transfer through slag can also occur by radiation. The mechanism of heat transfer by radiation through slag consists of successive absorption and emission of radiant energy by different layers of the slag which is also referred to as radiation-conduction. Turkdogan has recommended that in addition to thermal conductivity, the calculations of heat transfer through slag must incorporate a new parameter called the radiative conductivity, to take care of the component of heat transfer due to radiation [111]. It should be noted that the magnitude of the radiative conductivity of a slag is proportional to the cube of its temperature and the thickness of the slag layer. Mills et al. [112] have conducted experiments in the laboratory by simulating the gap and have reported that the heat transfer by radiation through a layer of the mould flux is relatively small. This is rationalized on the basis that the thickness of the mould flux film in the gap is small, the recrystallized layer has a high absorption coefficient and finally the temperature of the glassy layer adjacent to the mould wall is quite low. Similarily, to ascertain the mode of heat transfer through the gap, Scheel et al. [99] have conducted laboratory experiments by simulating the gap and have found that the thickness of the gap containing mould flux has a significant effect on the heat transfer, as shown in Fig. 2.27. These measurements have been rationalized on the basis that the magnitude of the component due to radiation-conduction is directly proportional to the thickness of the

mould flux film [113] and therefore, the inverse relationship between heat transfer and the gap thickness (Fig. 2.27) can be explained only on the basis that the mode of heat transfer through the gap is primarily by conduction.

Since it was established that conduction is the dominant mode of heat transfer across the gap, it was therefore assumed that in addition to the gap dimensions, the thermal conductivity of the mould flux will be vital from the standpoint of assessing the heat transfer in the mould. Thus, Taylor et al. [113] have measured the thermal diffusitives of a large number of mould fluxes and have utilized this data to obtain the thermal conductivity. Their results indicate that the thermal conductivity of the mould flux is quite similar over a wide range of composition. Therefore, the observed variation in the heat transfer with different mould fluxes can not be justified on the basis of their thermal conductivity. In other words, the resistance of the gap can not be calculated from the thermal conductivity of the mould flux, even for known dimension of the gap. Kyoden et al. [116] have reported the presence of numerous pores in the recrystallized mould flux which will further add to the difficulties in characterizing the resistance of the gap.

From the preceding review, it clearly emerges that the heat fluxes in the mould can not be calculated, owing to a large number of unknown parameters involved in the calculation of the thermal resistance of the gap. Furthermore, the gap width in an operating slab mould is known to vary in both transverse and longitudinal directions. Therefore, calculation of mould heat fluxes from the first principles is not possible, as the phenomena affecting the gap dimensions and its thermal resistance are exceedingly complex.

2.6.2 Mould Heat Flux Measurements

A number of attempts have been made [99,112,115,117] to measure the heat extraction in the mould by simulating the gap between the shell and the mould. In these experiments, the strand surface and the hot face of the mould are simulated using a heated

steel plate and a copper plate respectively and the gap is simulated by maintaining a distance between the steel and the copper plate. Prior to the measurements, the gap is filled with a certain type of mould flux and then the heat transfer is determined from the inlet and outlet temperature of the cooling water. However, it is important to note that in an operating mould, the inflow of the mould flux at the meniscus into the gap is dependent on the conditions prevailing at the meniscus, particularly, the molten flux pool depth, dimensions of slag rim and also the mould oscillation characteristics; the above mentioned experiments do not simulate the conditions existing at the meniscus in an operating slab mould. Owing to these apparent limitations, the measurements do not exactly denote the heat transfer in an slab mould.

The temperature of the inlet and outlet cooling water in the mould are often monitored in most of the plants. This information is also utilized to estimate the heat extraction in the mould. Needless to say, the heat flux distribution in the mould cannot be obtained from these measurements.

Mould temperature measurements have been employed to measure the heat extraction rates in the mould. Samarasekera et al. [6] and Singh et al. [118] have quantified the heat flux distribution in a billet mould utilizing mould temperature measurements. A two-dimensional model of heat-flow in the mould wall was employed to convert the mould temperatures into axial heat flux profiles [6]. To determine the heat flux distribution in the slab mould, temperature measurements of the copper plate also have been made [24,29,31,119,120,121]. However, appropriate techniques have not been employed to obtain the heat flux profiles from the mould temperatures. Nakai et al. [29] in their heat-flow model, have considered only a tranverse section of the mould wall as shown in Fig. 2.28 and have ignored the heat conduction along the length of the mould wall. Samarasekera et al. [122] have shown that the axial component of heat conduction in the mould wall, particularly in the meniscus region, is large due to the presence of steep axial temperature gradients. Therefore, the neglect of axial heat flow will result in an underestimate of heat flux values in the vicinity of the meniscus. Pozhivanov et al.

[120] also have developed a mathematical model of the mould wall to convert the mould temperatures into heat fluxes. They have considered the heat flow in the axial direction, but, have ignored the heat conduction along the width of the copper plate. The mathematical model of a slab mould necessitates the incorporation of heat flow along the thickness, length and the width of the mould wall. It is also important to note that, in addition to the inadequacies of these mathematical models, sufficient number of mould temperature measurements have not been made in the vicinity of the meniscus. In general, there is a lack of reliable data on the heat flux distribution in the slab mould.

2.6.3 Effect of Operating Variables, Steel Grade and Mould Flux on the Heat Transfer in the Mould

As mentioned earlier, the rate controlling factor in the heat transfer from the strand to the mould is the resistance of the gap. The effect of a number of variables on the mould heat transfer has been explained in terms of their effect on the thermal resistance of the gap. This information is based on work done in laboratory and plant measurements on billet and slab moulds.

2.6.3.1 Casting Speed

Many investigators have attempted to study the effect of casting speed on the heat transfer in the mould [16,30,57,114,115,120,123-128]. The casting speed is known to have a strong impact on the heat transfer in the mould; an increase in the casting speed will lead to an enhancement in the heat transfer rates as shown Fig. 2.29. This is known to be gap related because with higher casting speeds, the thickness of the steel shell is reduced at a given level in the mould so that the ferrostatic pressure is effective in pushing the shell against the mould wall and therby reducing the width of the gap. In addition to the changes in the width of the gap at different casting speeds, it should also be noted that, the inflow of mould flux at the meniscus into the gap is influenced by casting speed and, thereby, this can affect the resistance of the gap. Yasanuka et al. [129] have employed autoradiographic technique and have reported that the shell thickness at

the bottom of an oscillation mark is always thinner than other locations and therefore, heat transfer in the mould is dependent on the depth of oscillation mark which in turn is related to the casting speed. Overall, it can be seen that casting speed has a strong effect on the heat transfer in the mould.

2.6.3.2 Superheat of the Molten Steel in the Mould

It has been reported that with increase in superheat of the steel, the heat fluxes in the mould are enhanced [57,124] as shown in Fig. 2.30. This is apparently due to a reduced thickness of the steel shell at higher superheat so that the contact of the shell with the mould due to ferrostatic pressure is improved and the width of the gap is reduced. It is also likely that the viscosity of the mould flux at the meniscus will depend on the steel temperature, and therefore, superheat also can affect the inflow of mould flux at the meniscus.

2.6.3.3 Pouring Conditions

Open stream pouring is always practiced in billet casting, whereas submerged entry nozzles are used in slab casting. It has been reported that open stream pouring increases the heat flux in the mould, particularly near the meniscus region as compared to submerged entry nozzles [57,130] and this is explained on the basis that the depth of penetration of the stream in the open stream pouring is less compared to close stream pouring through submerged entry nozzles [SEN]. Consequently, with open stream pouring, the convection in the vicinity of the meniscus is enhanced resulting in reduced thickness of the solid shell. Thus, the ferrostatic pressure is effective in reducing the width of the gap. The design of the SEN also can influence the heat transfer in the mould. This is because the flow patterns in the molten steel is dependent on features like the number of ports [35], submergence depth [16] and the jet angle [124]. It is probable that the flow patterns in the molten steel near the meniscus may be critical from the standpoint of the heat transfer from the steel to mould flux and thereby, can influence the behaviour of the mould flux at the meniscus.

2.6.3.4 Water Velocity

Mills et al. [35] have suggested that water velocity will not have significant effect on heat transfer in the slab mould, because, the water side resistance is not a major part of the overall thermal resistance to heat flow. Wolf [57] claims that the average heat flux in the mould is decreased when the water velocity is increased from 7.6 m/s to 10 m/s, as shown in Table 2.2 and the observation has not been explained. In a recent investigation at Kobe Steel [114], the influence of the design of the cooling channel and water velocity on the heat flux at different casting speeds has been examined. Figure. 2.31 reveals that at casting speed near 1.5 m/min, with slit type design of the cooling channel, the heat flux is higher at a water velocity of 5.5 m/min (denoted by open circles) compared to 7.6 m/min. But, this observation has not been explained.

2.6.3.5 Mould Design

Mould design is known to influence the heat transfer in the mould, particularly, the taper of the narrow plates [121,123]. Deshimaru et al. [121] have attempted to enhance the heat extraction near the corner of the narrow face by incorporating a new design in which the copper plate has a higher taper at the corner compared to the centre of the plate. This resulted in an increase in heat extraction rates near the corner compared to the conventional design. The findings of Wolf [123] as shown in Table 2.3, also reveals that the heat flux in the mould is enhanced with increase in the taper of the narrow face and this is a result of reduction of the gap width. However, excessive taper is undesirable, as it can result in sticking between the shell and the mould wall.

2.6.3.6 Mould Oscillation Characteristics

Russian investigators have reported that the frequency of the mould oscillation has an impact on the heat transfer [120], it can be seen from Fig. 2.32 that an increase in frequency from 50 to 100 cycles per minute resulted in an increase in the heat transfer particularly near the meniscus and this observation has not been explained. On the contrary, Suzuki et al. [127] of NKK have found that an increase in the frequency from

55 to 90 cpm had no effect on the heat transfer. The frequency is known to affect the mould flux inflow at the meniscus, however, its influence on the heat transfer need not be the same from plant to plant, since the inflow of mould flux would also be dependent on the mould flux behaviour at the meniscus. Suzuki et al. [46] also have found that the heat transfer in the mould, especially near the meniscus, is decreased when the nature of the mould oscillation was non-sinusoidal, compared to the conventional sinusoidal mode. This observation has not been explained, it is possible that differences in the mould oscillation mode will affect the consumption rate of the mould flux and thus, the heat transfer in the mould. It should also be noted that the heat transfer can be influenced by the mould oscillation conditions, since the depth of the oscillation mark is also related to the negative strip time.

2.6.3.7 Steel Composition

The composition of steel, carbon in particular, has a significant effect on the mould heat transfer [6,57,130,131,132]. Singh and Blazek [131] have measured the heat flux in a non-reciprocating mould for a variety of steel grades. They have found that for the same casting speed the average mould heat flux is minimum for 0.10 carbon steel and remains essentially constant for steel grades containing more than 0.25 percent carbon as shown in Fig. 2.33. Grill and Brimacombe [132] also have determined the average mould heat fluxes in commercial billet casting machines and have reported that the heat flux is a minimum for 0.1 percent carbon steel, reaching a maximum at 0.3-0.4 percent-carbon steel. Samarasekera et al. [6] have obtained mould heat-flux profiles for a number of steel grades from the temperature measurements of billet moulds. They found that in the upper region of the mould, the magnitude of the heat flux rises with increasing carbon level in the range of 0.14-0.36 percent. Evidently, there is a good agreement on the findings of different investigators on the effect of carbon content on heat flux in billet casting. The explanation for the observed effects of carbon on mould heat flux is related to the peritectic reaction ($\delta + L = \gamma$] and the solid state δ - γ transformation [132]. The reason,

for a reduction in the heat flux for low carbon steel is attributed to greater shrinkage due to phase transformation when compared to high carbon steel which results in the generation of large gap. [132].

However, there has not been similar studies on the heat transfer in the slab mould for an extended range of steel grades. This is primarily due to the fact that several types of mould fluxes are used in the casting of different grades of steel and thus, a comparison of heat transfer will not be meaningful . However, Wolf [57] has reported that in the presence of mould flux, the effect of carbon on the heat transfer in the mould is diminished. But, no measurements have been made to substantiate this.

In addition to carbon, phosphorous and sulphur can also influence the mould heat transfer [6,57,118]. Samarasekera et al. [6] found that in the range of 0.016-0.028 percent-phosphorous, for medium carbon steels, higher phosphorous levels lead to a reduction in heat transfer particularly at the meniscus and this is a result of increase in the depth of oscillation marks. Similarly, increase in sulphur level in 0.037-0.046 percent range leads to a reduction in heat transfer.

2.6.3.8 Mould Flux

Mould flux is used in a slab mould to accomplish a number of functions. The influence of mould flux on the heat transfer in the mould has been studied by a number of investigators [24,99,115,116,117]. Riboud et al. [115] have reported that lubrication with oil as practiced in billet casting, leads to a higher heat transfer when compared to mould flux lubrication. On the contrary, it also has been reported that when mould flux is substituted for oil, the total heat extraction in the mould is affected only to a minor degree [7]. Singh and Blazek [131] have reported that the effect of mould flux on the heat transfer in the mould is dependent on the type of steel grade that is being cast. They have made measurements of heat transfer in the mould with a 0.1% carbon steel using oil and mould flux as lubricants. It can be seen from Fig. 2.34, that in the presence of mould flux,

the heat transfer is increased in the upper part of the mould and decreased in the lower part. The chemical composition, viscosity and the recrystallization characteristics of the mould flux are known to have an impact on the mould heat transfer.

Scheel et al. [99] from laboratory experiments have found that SiO_2 and Na_2O would have an effect on the heat transfer as shown in Fig. 2.35. FeO in the mould flux will affect the heat transfer in the mould [117]; an increase in the quantity of FeO can reduce the heat transfer as it makes the mould flux less transparent and thus the component of heat transfer due to radiation is reduced. However, it has been established that heat transfer through the gap mainly occurs by conduction.

The viscosity of the mould flux is known to have an impact on the heat transfer in the mould, namely, with increasing viscosity, the heat transfer in the mould is diminished [16,99,124]. Whereas, Emi et al. [13] have reported that both viscous and fluid mould fluxes will result in higher heat transfer in the mould as shown in Fig. 2.36. Viscosity will influence the inflow of the mould flux at the meniscus and thereby affect the resistance of the gap.

The recrystallization characteristics of the mould flux will influence the heat transfer in the mould [116,117]. Increase in the recrystallization temperature of the mould flux will reduce the heat transfer [116,117] and this observation has not been explained. Kyoden et al. [116] have examined the microstructure of the recrystallized mould flux and have found the presence of numerous pores in it. They have measured the area covered by the pores and have reported that as this quantity is increased the heat transfer in the mould is reduced.

Table 2.1 - Comparison of oscillation mark depth obtained during casting in the conventional and hot top mould [59].

STEEL GRADE	OSCILLATION PARAMETERS	DEPTH OF MARKS µm	
		Conventional	Hot top mold
Low carbon (C < 0.08 %)	Frequency : 110 min^{-1}	240	160
Middle carbon (C = .1 %)	Stroke : 6 mm	280	200

Table 2.2 - Effect of water velocity on the average heat flux in the mould [123].

Water velocity (m/s)	7.6	10.0
Mould heat flux ($kcal/m^2min$)	26 475	18 978

Table 2.3 - Effect of taper of the narrow face on the average heat flux in the mould [123].

Taper (%/m)	0	1.5	2.2	2.6
Mould heat flux ($kcal/m^2min$)	15 008	16 704	19 575	*

*Strand is sticking in the mould.

Figure 2.1. An example of a slab showing the presence of longitudinal mid-face crack.

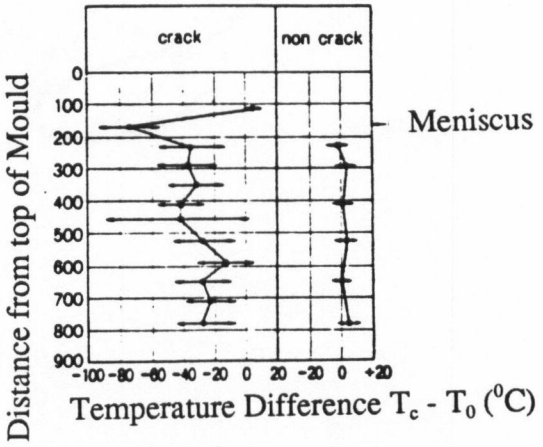

Figure 2.2. Measure mould temperatures in the presence and absence of longitudinal cracks [9]. (T_C ant T_O denote the mould temperatures in the presence and absence of cracks respectively)

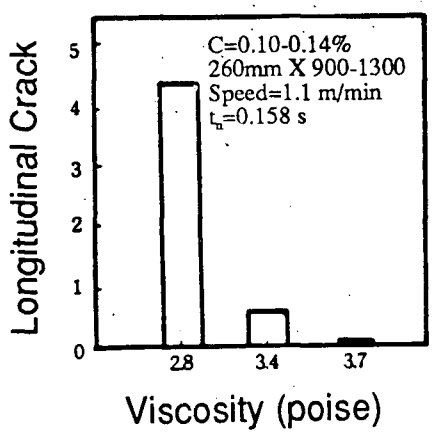

Figure 2.3. Influence of mould flux viscosity on the occurrence of longitudinal cracks [19]

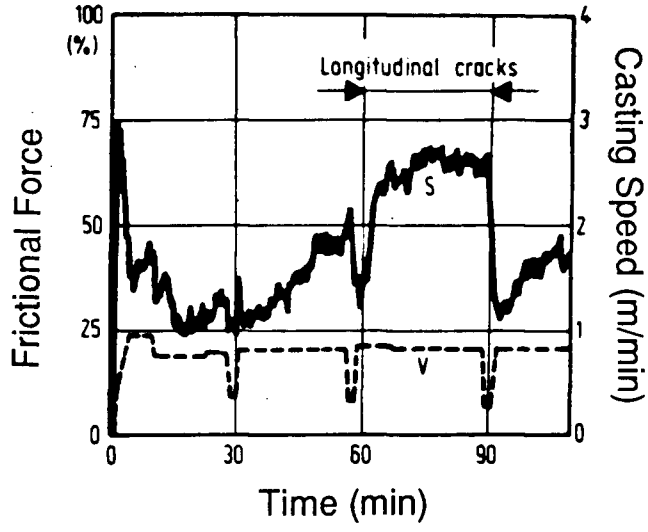

Figure 2.4. Effect of friction in the mould on the incidence of longitudinal cracks [23].

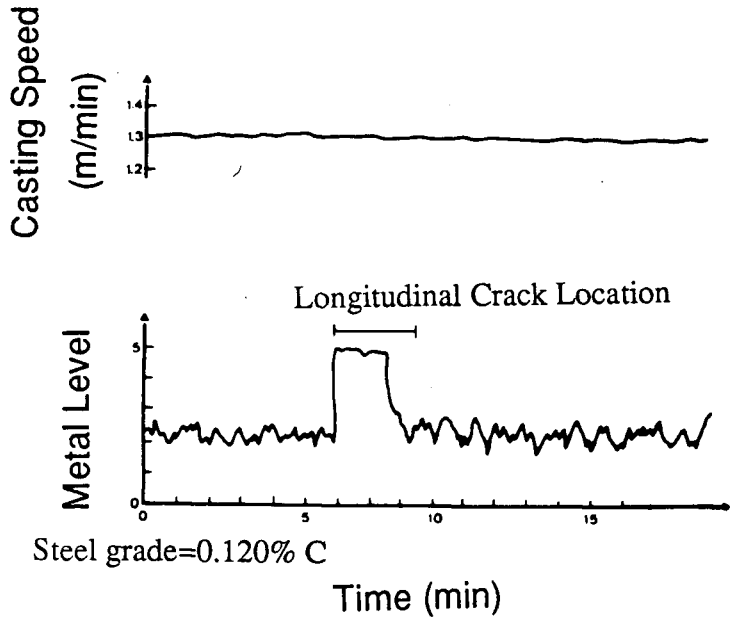

Figure 2.5. Influence of the metal level increase in the mould on the incidence of longitudinal cracks [16].

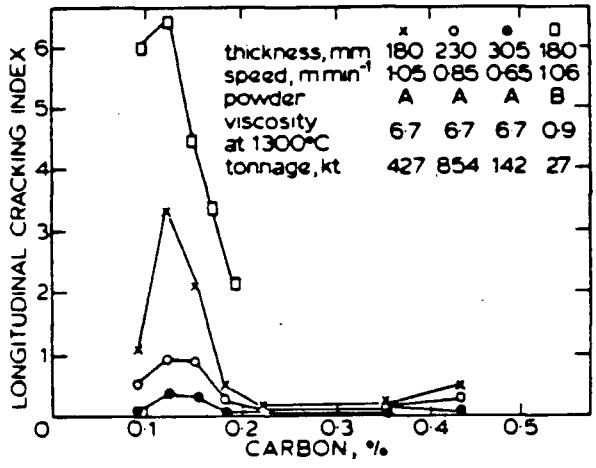

Figure 2.6. Effect of carbon content of steel on longitudinal cracks [27].

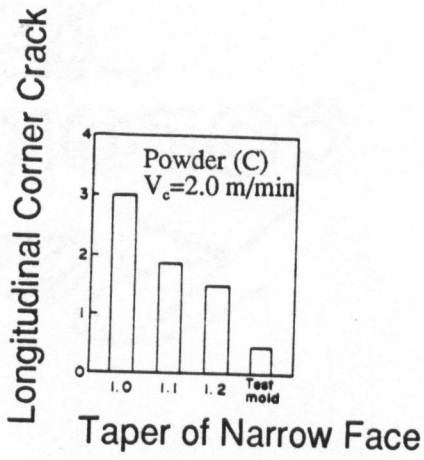

Figure 2.7. Effect of the taper of the narrow face on the occurrence of longitudinal corner cracks [17].

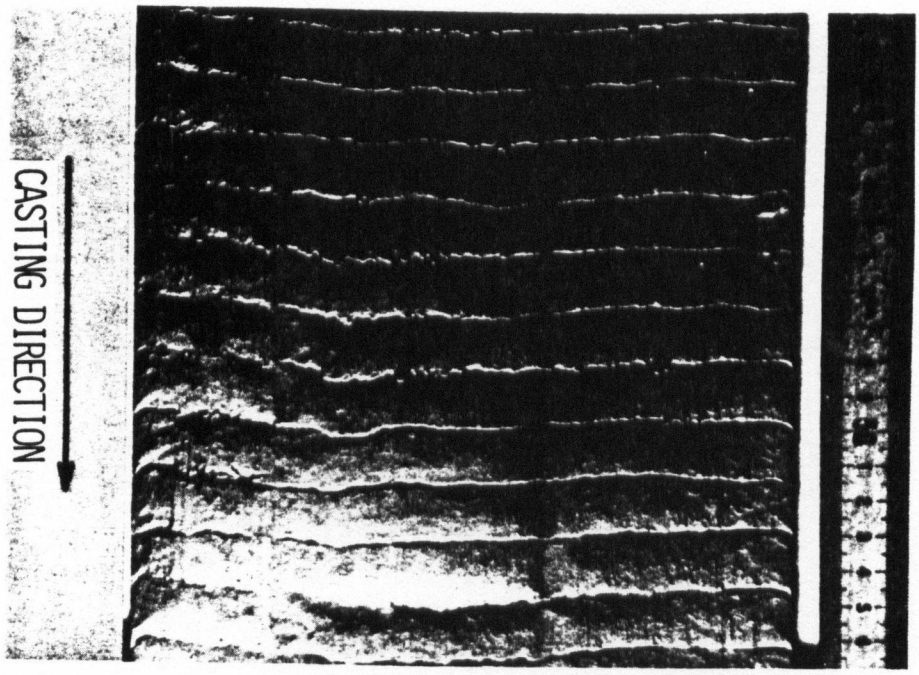

Figure 2.8. Surface of the slab showing the presence of oscillation marks [41].

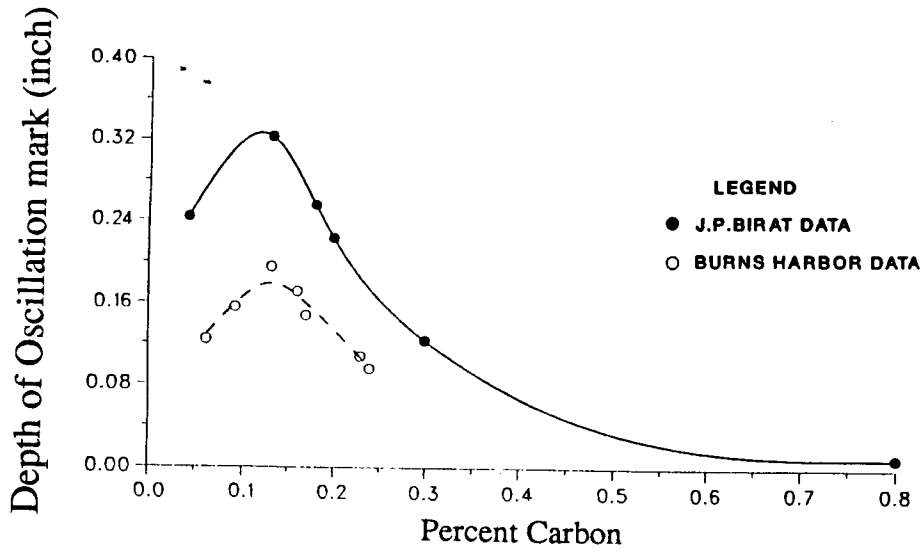

Figure 2.9. Effect of carbon content of steel on depth of oscillation marks [40].

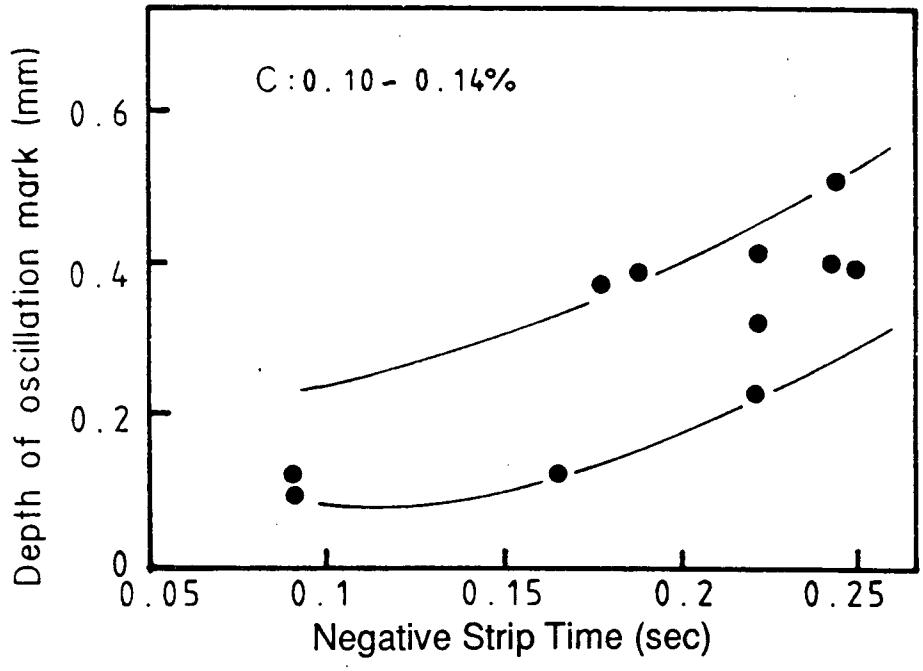

Figure 2.10. Influence of negative strip time on the depth of the oscillation marks [20].

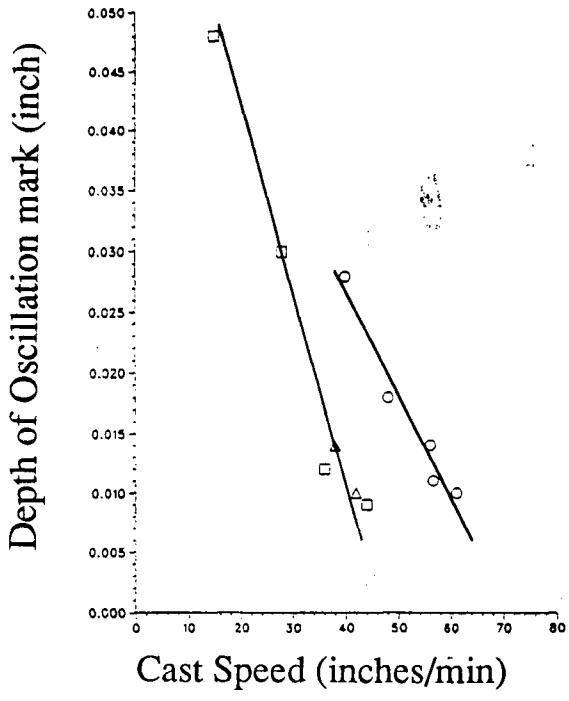

Figure 2.11. Effect of casting speed on the depth of oscillation marks [40].

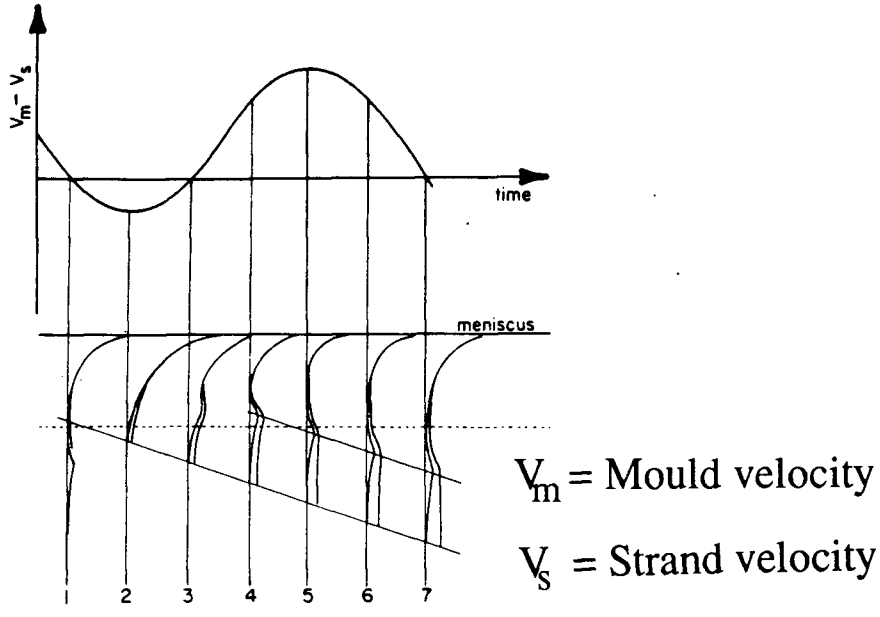

Figure 2.12. Schematic representation of events in the mould during an oscillation cycle leading to the formation of an oscillation mark [41].

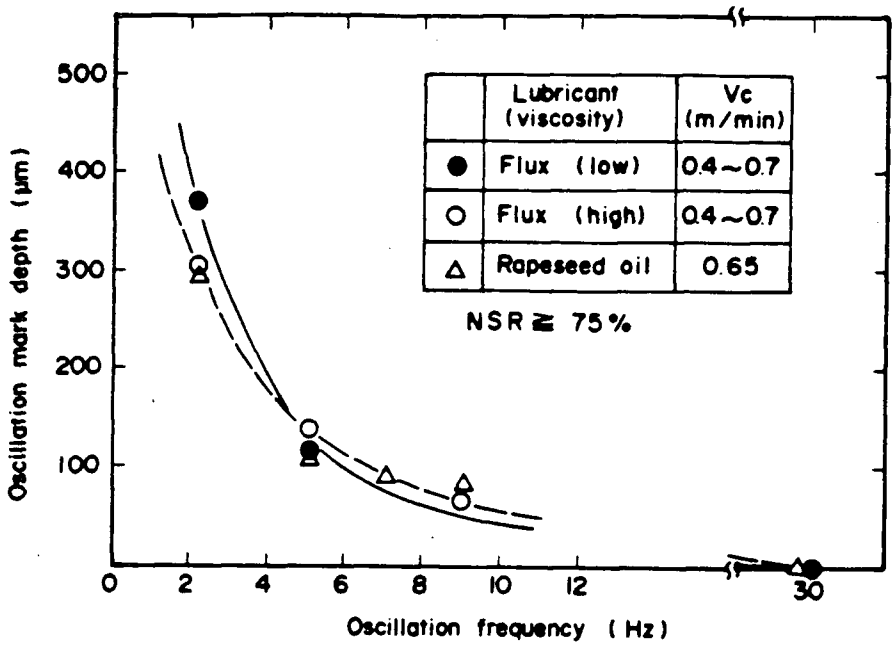

Figure 2.13. Effect of the mould oscillation frequency on the oscillation mark depth [58].

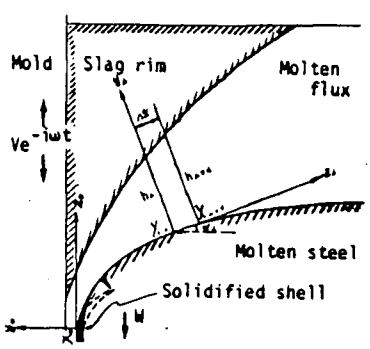

Figure 2.14. Schematic representation of the slag rim at the meniscus considered in the mathematical model. [64].

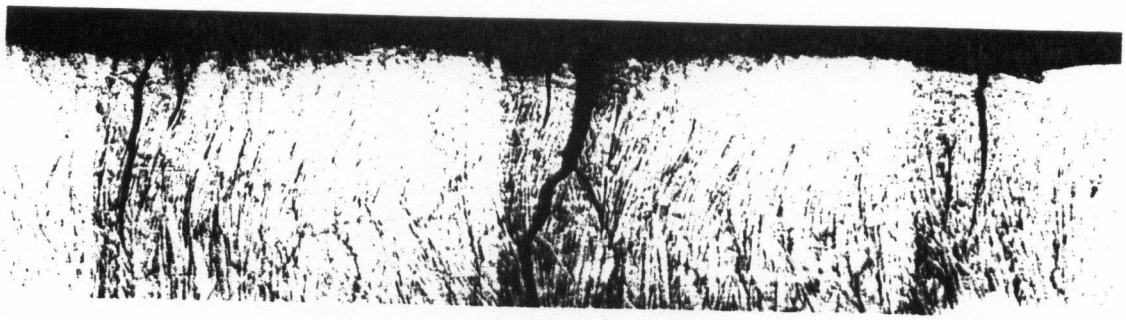

Figure 2.15. Longitudinal section of a slab showing the presence of transverse cracks at the bottom of oscillation marks [36]

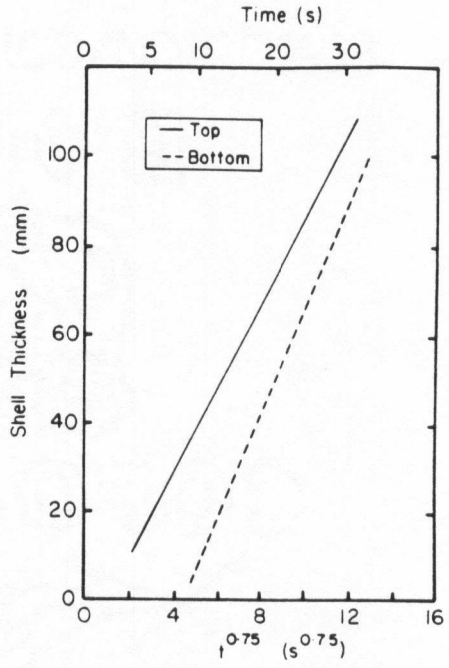

Figure 2.16. Comparison of shell thickness between the top and bottom of an oscillation mark [36].

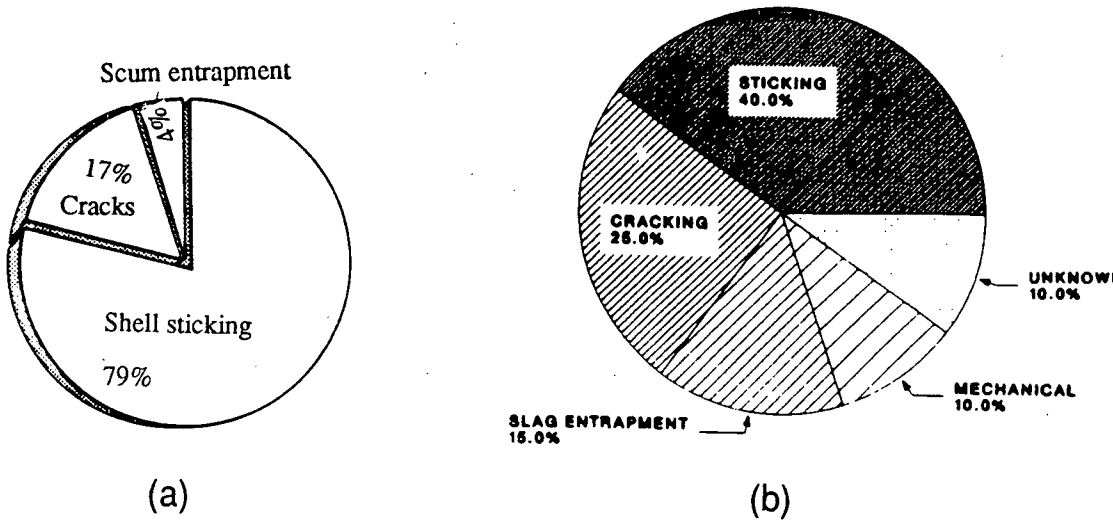

Figure 2.17. Causes of Break-outs (a) Nippon Steel [70] (b) Inland Steel [71]

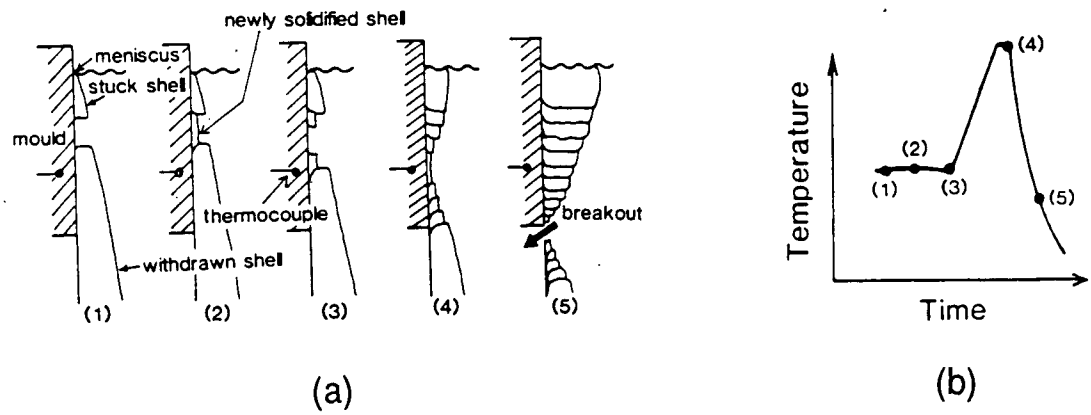

Figure 2.18. (a) Mechanism of sticker type break-out [72] (b) Response of the mould interms of its temperature from the initiation of sticking to the eventual break-out [72].

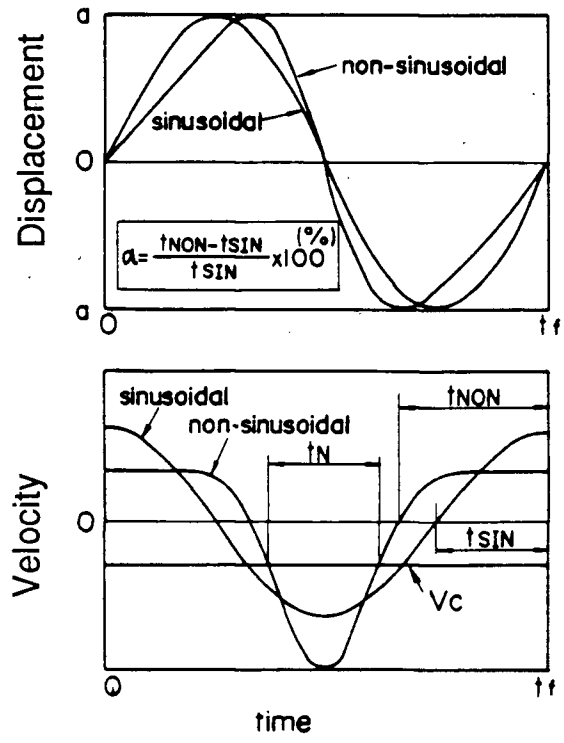

Figure 2.19. Comparison of the mould velocity and displacement between sinusoidal and non-sinusoidal oscillation of the mould [83].

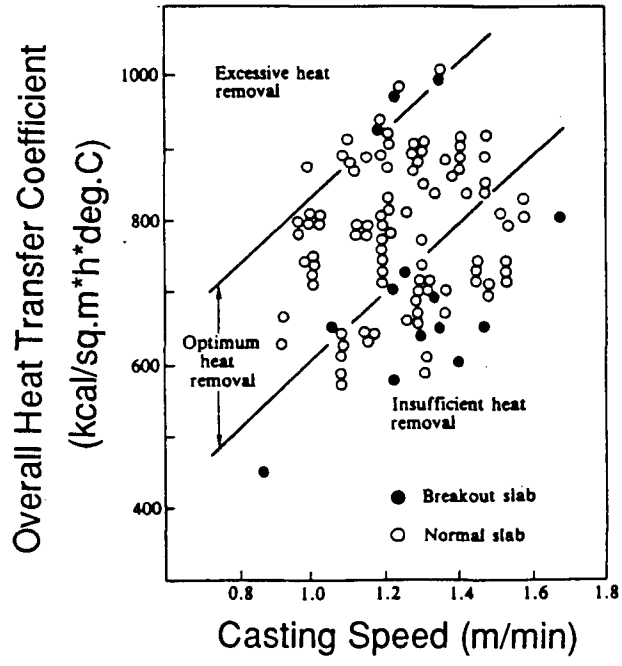

Figure 2.20. Relationship between the heat extraction in the mould on the incidence of break-outs [24].

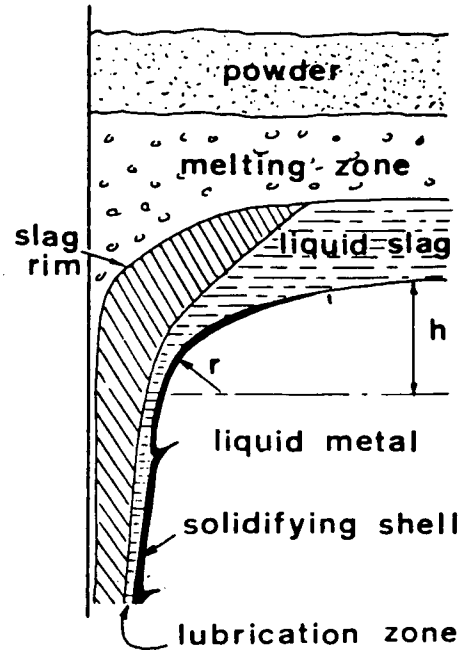

Figure 2.21. Schematic diagram to illustrate the different physical states of the mould flux present above the meniscus [97].

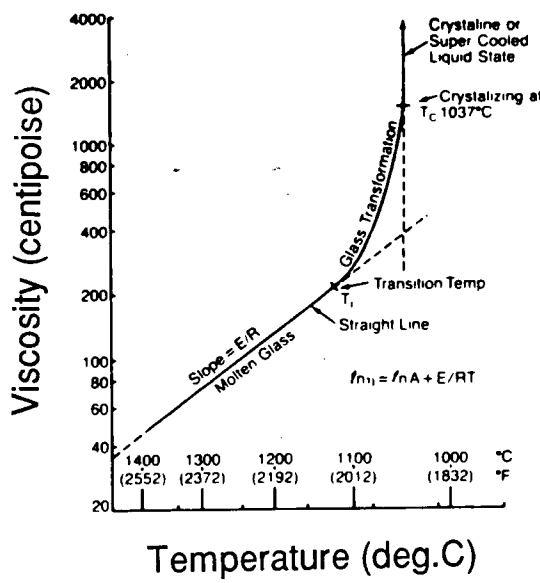

Figure 2.22. Typical relationship between mould flux viscosity and temperature [95].

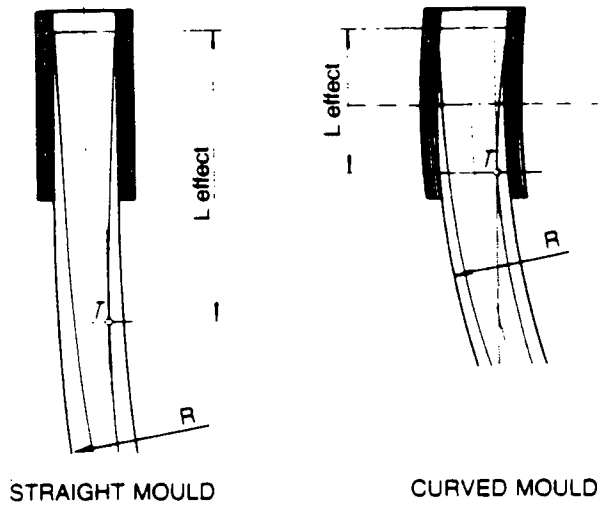

Figure 2.23. Different types of slab mould.

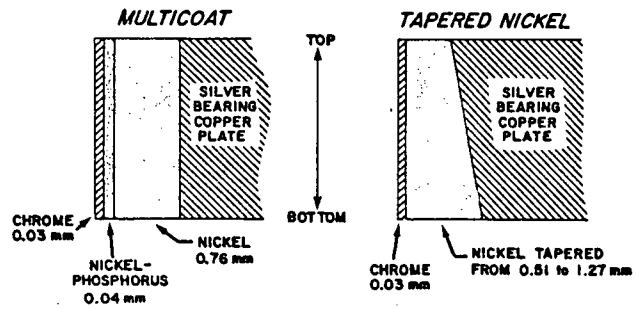

Figure 2.24. Different types of coating employed at the hot face of the copper plate [106].

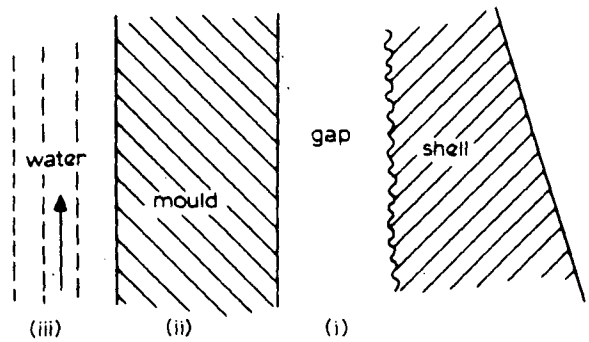

Figure 2.25. Schematic diagram to illustrate the various thermal resistances to heat flow in the mould.

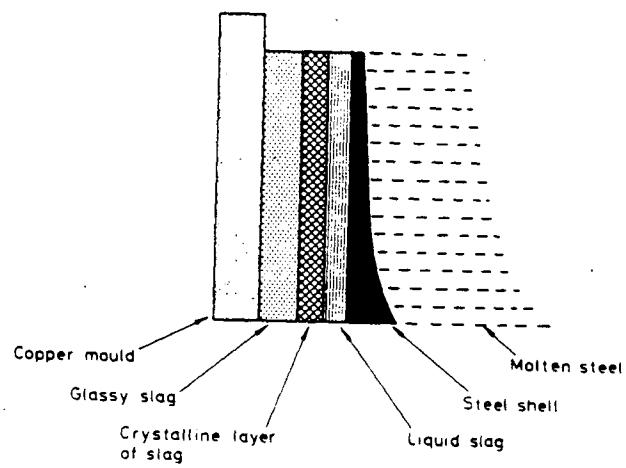

Figure 2.26. Schematic drawing of the mould flux film present in the gap [112].

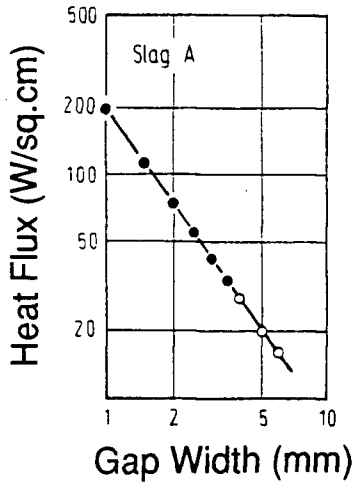

Figure 2.27. Influence of the thickness of the gap containing mould flux on the heat flux [99].

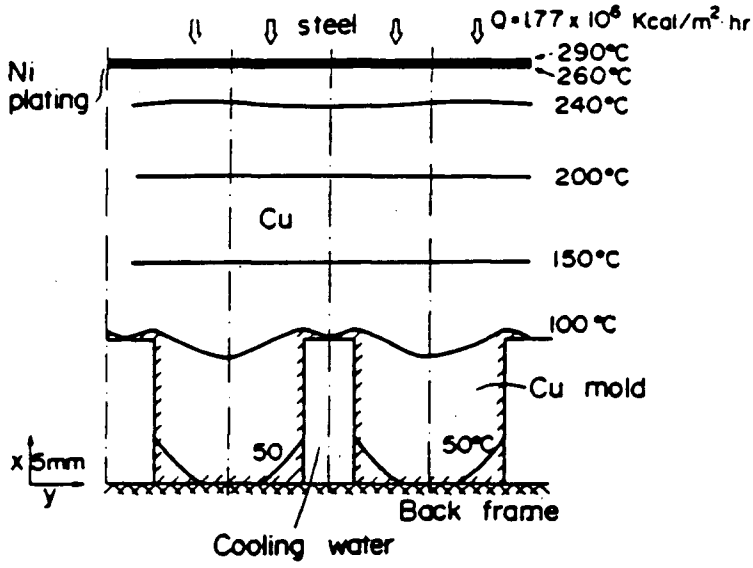

Figure 2.28. Transverse slice of the mould wall employed in the heat flow model to calculate heat fluxes [29].

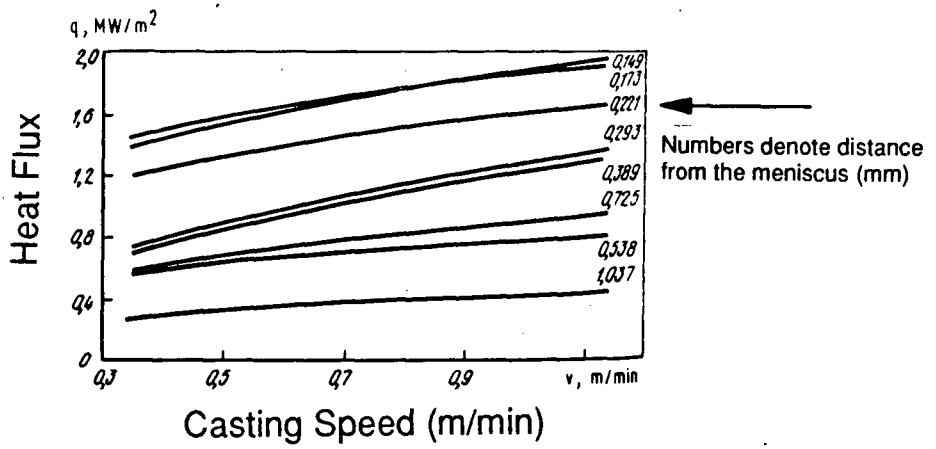

Figure 2.29. Effect of casting speed on the heat transfer in the mould [120].

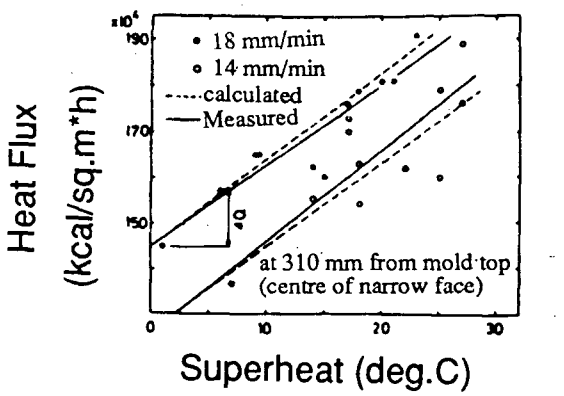

Figure 2.30. Influence of superheat on heat flux in the mould at a distance of 310 mm from the mould top [124].

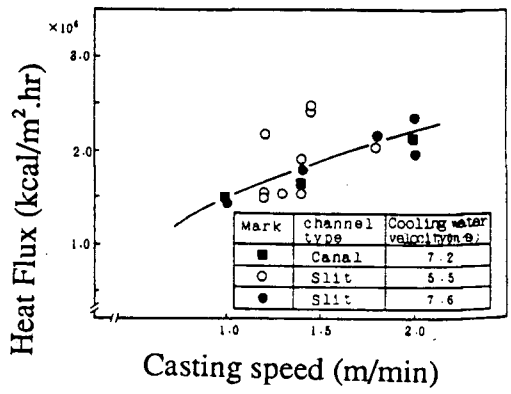

Figure 2.31. Effect of water velocity on the heat flux at the meniscus. [114]

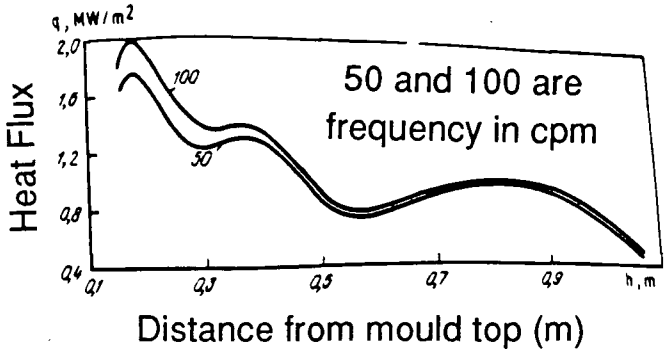

Figure 2.32. Effect of mould oscillation frequency on the heat fluxes in the mould [120].

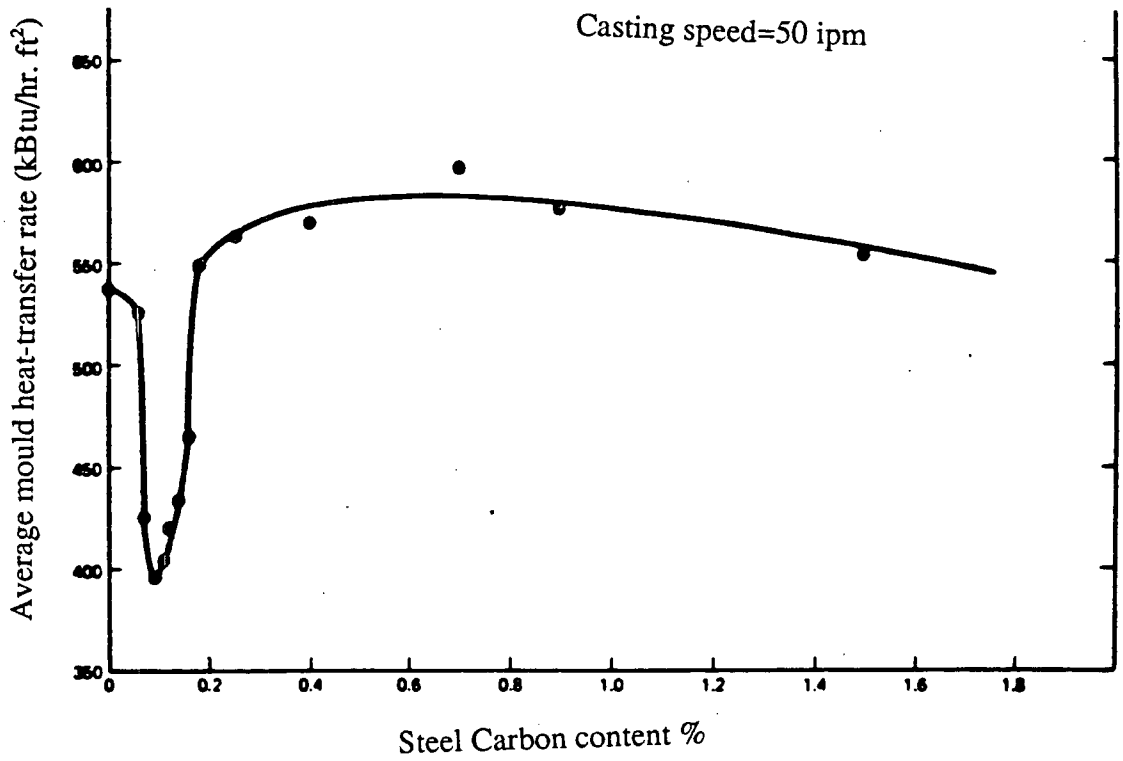

Figure 2.33. Effect of steel carbon content on the average heat flux in billet mould [131].

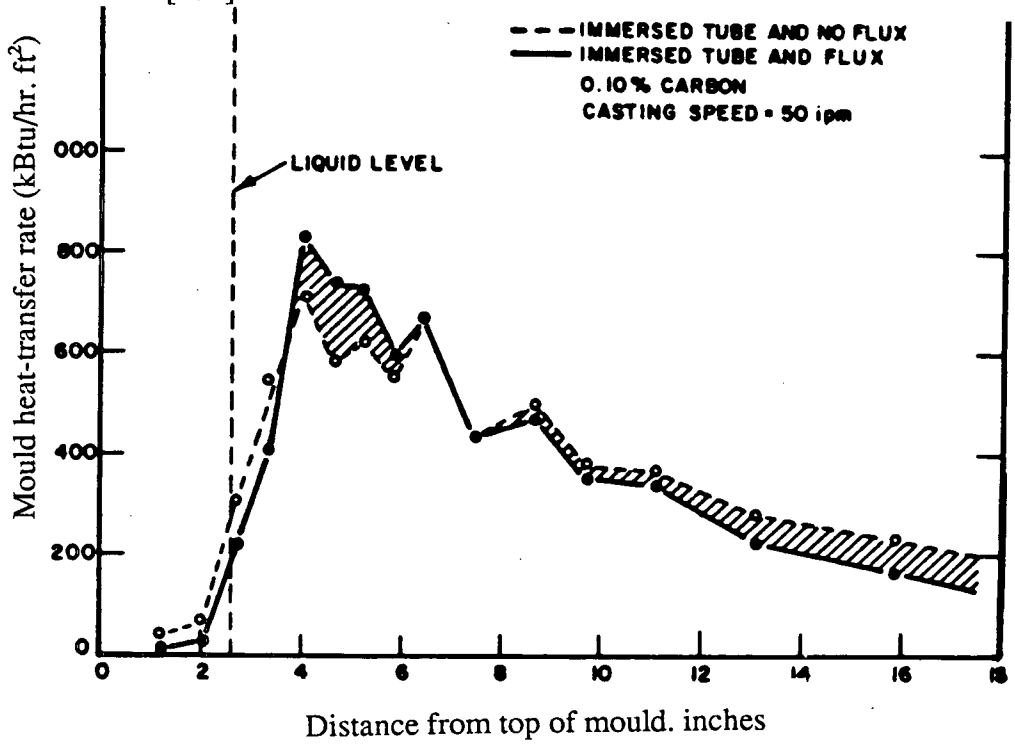

Figure 2.34. Heat-flux profiles in the mould with mould flux and oil used as lubricants [131].

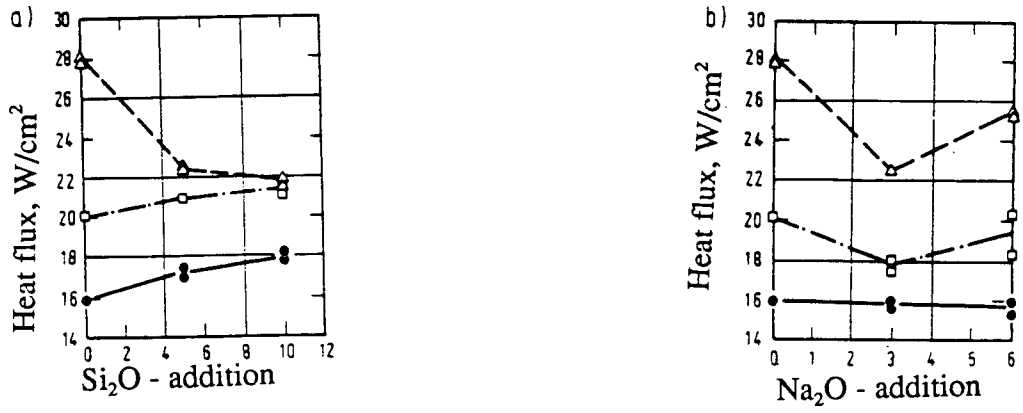

Figure 2.35. Effect of (a) SiO_2 (b) Na_2O in the mould flux on heat flux obtained from laboratory measurements [99].

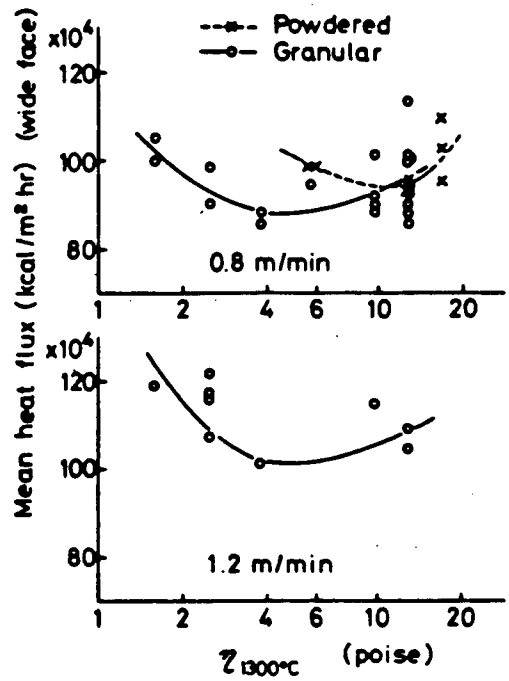

Figure 2.36. Effect of viscosity of the mould flux on the average heat flux in the mould [13].

Chapter 3 - SCOPE AND OBJECTIVES OF THE PRESENT WORK

It is evident from the literature that continuously cast slabs are plagued by a number of quality problems, many of which can be traced to the mould. It emerges from the literature that heat transfer and lubrication in the mould are the most crucial aspects of the casting process owing to their strong links to the final product quality and the smoothness of the casting operation. Needless to say, the heat transfer in the mould is a complicated phenomenon and is dependent on a large number of variables. Nonetheless, from a fundamental understanding of the mechanism of heat transfer in the mould, it appears that the extent to which a variable will affect the heat transfer is likely to be governed by its influence on the behaviour of the mould flux at the meniscus and in the gap between the shell and the mould wall. Moreover, lubrication in the mould is also primarily dependent on the type of mould flux used during casting. It may be interesting to note that despite numerous efforts directed at quality and the operating problems encountered during continuous casting of slabs, there is a dearth of studies elucidating the behaviour of the mould flux at the meniscus. An understanding of the behaviour of the mould flux during casting clearly necessitates a quantitative characterization of the thermal field in the mould flux. It is anticipated that a knowledge of heat transfer in the mould particularly at the meniscus will provide further insight into the role played by mould flux during casting and subsequently will assist in the understanding of the quality and operating problems encountered during continuous casting of slabs.

3.1 Objectives of the Research Programme

The main purpose of the research was to characterize the heat extraction rates in a slab mould in a quantitative manner which required appropriate measurements in the plant owing to the inadequacies of theoretical methods as discussed in the earlier chapter.

A knowledge of heat transfer in the mould has been utilized to examine in-depth the mould related quality and operating problems. The various objectives of this research in striving towards the ultimate goal were as given below.

(i) To determine the influence of mould flux type, steel grade, casting speed and the design of submerged entry nozzle on the mould wall temperature based on measurements on an operating slab mould.

(ii) To develop mathematical model of the mould wall capable of calculating the heat extraction rates in the mould from the measured mould wall temperatures as a function of the above mentioned variables.

(iii) To develop mathematical models to simulate solidification phenomenon occurring in steel and to elucidate the mould flux behaviour at the meniscus.

(iv) To examine the quality aspects of the slabs (cracks, oscillation marks) by conducting metallurgical investigation of the slab samples collected during the industrial trial.

(v) To establish links between mould design, heat transfer and the mould flux behaviour at the meniscus to the mould related quality problems.

(vi) To formulate recommendations towards improvement in mould design and operating practice to improve slab quality.

Chapter 4 - METHODOLOGY

This chapter is devoted to the experimental procedures employed in the industrial trial and the laboratory work which essentially consisted of metallographic examination. The section on industrial trials will largely focus on design, installation of thermocouples and the mould temperature measurements.

4.1 Industrial Trials

4.1.1 Salient Features of the Continuous Casting Machine

The industrial trial was undertaken at Stelco's Lake Erie Works. This plant has a twin-strand Demag slab casting machine with a radius of curvature of 10.5 m. The oscillation mode of the mould is sinusoidal and the frequency and stroke length of mould oscillation are fixed. The pouring of the steel from the tundish into the mould is achieved through a submerged entry nozzle which is attached to the bottom of the tundish. The metal level in the mould is controlled manually by adjusting the stopper rod on the tundish and is usually aimed between 75 to 100 mm from the top of the mould and furthermore, the feeding of mould flux into the mould is performed manually. The width of the mould is changed during casting so as to enable casting of slabs of different widths which varied between 1100 mm to 2030 mm and this is accomplished by moving only one narrow face copper plate. The mould is equipped with devices to measure the temperature of the inlet water, outlet water and the water flow rates. These measurements are made on a regular basis on each of the four faces of the mould. A summary of the salient features of the slab caster is given in Table 4.1.

4.1.1.1 Mould Design

The mould on which measurements were conducted in the present study was of curved type with a radius of curvature of 10.5 m. The copper plates on the broad face of

the mould were coated with two separate layers of chromium and nickel of coating thickness 0.020" (0.508 mm) and 0.003" (0.076 mm) respectively, whilst the narrow face copper plates had no coating. Prior to the instrumentation of the mould with thermocouples, the dimensions of the copper plate, cooling channel on each of the four faces of the mould were measured and these measurements were eventually incorporated into the mathematical model of the mould which will be discussed later. Figure 4.1 shows a plot of the copper thickness at different distances from the top of the mould on the inside radius, outside radius and the narrow face. Evidently, the thickness of the inside and outside radius copper plates is not uniform along the length. The non-uniformity in the copper thickness is a consequence of curved type mould since this design necessitates curvature of the copper plates at the hot face, whilst the cold face is vertical to facilitate their attachment to the stainless steel backing plates. The copper thickness measured on the two opposite broad faces are given in Table 4.2 and it may be interesting to note that at any particular distance from the top of the mould, there is a significant difference in the copper thickness between the two broad faces which is more prominent near the meniscus.

The mould is cooled by water flowing through a series of vertical channels machined on the copper plate and these cooling channels can be seen clearly in the photograph of a copper plate (narrow face) shown in Fig. 4.2. The copper plate is fastened to a steel backup plate which is also referred to as a water jacket and a photograph of the water jacket on the narrow face is shown in Fig. 4.3. The cooling channels are of rectangular cross-section and a schematic drawing of the cooling channels on the broad and narrow faces with relevant dimensions are shown in Fig. 4.4a and Fig. 4.4b respectively. There are a total of 66 cooling channels on the broad face and 9 on the narrow face. The depth and width of the cooling channels are 20 mm and 6 mm

respectively. The spacing between two consecutive cooling channels on the broad and the narrow faces are not identical (Figs. 4.4a and 4.4b) and besides, it should also be noted that this spacing is increased in the presence of bolts as can be seen in Fig. 4.2.

4.1.2 Mould Temperature Measurements

The technique implemented to measure the slab mould temperatures was similar to that applied successfully in billet mould studies conducted by Brimacombe et al. [133] at Western Canada Steel. They utilized an intrinsic copper/constantan type of thermocouple to measure the temperature of the mould wall. It should be noted that copper/constantan type of thermocouple can accurately measure up to a maximum temperature of 350^0C [134]. In order to assess the suitability of a copper/constantan type thermocouple for the present measurements, the measured values of the mould temperatures obtained from a few preliminary experiments conducted by Stelco personnel were examined. In these experiments the thermocouples were located at 15 mm from the hot face and a total of 5 thermocouples were employed. Figure 4.5 shows a plot of the measured axial mould temperature profile at three different casting speeds. Evidently, the highest temperature of the mould is well within the measurable range of copper/constantan type of thermocouple. However, in the present study, it was intended to make the temperature measurements 6 mm from the hot face. Subsequently, the temperature of the mould wall 6 mm from the hot face was estimated from a knowledge of the preliminary mould temperature measurements (15 mm from hot face) and it was established that a copper/constantan type of thermocouple can be utilized to measure the mould temperature in the present study.

4.1.2.1 Design and Installation of the Thermocouples

Each thermocouple consisted of a single wire of constantan with a diameter of 0.76 mm. Prior to its installation, one end of the constantan wire was beaded using a heli-arc torch and the bead served as the hot junction of the thermocouple. Subsequently, this bead was flattened with a file and then the constantan wire was insulated electrically and

inserted through a tiny hole at the centre of a threaded copper plug. Flat bottom holes were drilled at each location on the copper plate where a temperature measurement was to be made. Finally, the copper plug containing the constantan wire was screwed into the copper plate through the flat bottom hole and thus, the hot junction of the thermocouple was forced mechanically against the copper. Furthermore, it should be noted that on each of the copper plates, two copper wires (one redundant) were also installed and these wires were electrically ground and thus, served as the copper part of the intrinsic copper/constantan thermocouple.

The installation of a thermocouple on the mould wall is schematically shown in Fig. 4.6. It should be noted that a poor contact between the thermocouple bead and the copper will result in inaccurate measurements and therefore, the design of the threaded copper plug in particular, assumes a critical role in ensuring an excellent contact between the thermocouple bead and the mould. Consequently, prior to the instrumentation of the mould, numerous tests were performed to ascertain an optimum design of the copper plug. These tests were conducted on scrap copper plate on which plugs of different design were installed and thereafter, the copper plate was cut across the centreline of the copper plugs and the cut section was visually examined to assess the contact between the bottom of the plug and the copper. The design of the copper plugs on the narrow and broad face which eventually proved to be the most effective are shown in Fig. 4.7a and Fig. 4.7b respectively and was adopted for the trials. It should be noted that the sizes of the plugs used on the broad and narrow faces were 10 mm and 5 mm in diameter respectively. On the narrow face, the spacing between the cooling channels was 10 mm (Fig. 4.4 b) which restricted the diameter of the copper plug to 5 mm. On the contrary, the larger spacing between the cooling channels on the broad face (Fig. 4.4a) permitted a 10 mm diameter copper plug and it should be noted that a large sized copper plug is desirable as it is easy to install it on the mould wall. Owing to a larger diameter of the copper plug on the broad face and requirements towards closer spacing between the

thermocouples near the meniscus (10 mm), it was not possible to install all the thermocouples along the same axis. This necessitated in the installation of the thermocouples near the meniscus on the broad face along two vertical rows (Fig. 4.15). A special type of tool was fabricated for screwing in the copper plugs without damaging the constantan wire, a photograph of which is shown in Fig. 4.8. During installation of these thermocouples, special checks were made to ensure that excellent electrical contact was preserved between the thermocouple bead and the mould.

Photographs of the installed thermocouples on the narrow face and broad face are shown in Fig. 4.9 and Fig. 4.10 respectively. It should be noted that the perimeter of the copper plugs were peened to prevent them from loosening during the trial and this can be seen clearly from the photograph shown in Fig. 4.11. After installation, the thermocouples on each plate of the mould were bundled together, wrapped with heat shrink tubing into cables which were extracted through the water jackets as shown in Fig. 4.12 and Fig. 4.13. Finally, all the four plates along with the respective water jackets were assembled to form the mould cavity and a photograph of the instrumented mould is shown in Fig. 4.14. All the thermocouple leads were connected to bananna plugs on the two junction boxes located on the mould frame; the temperature of the box was also monitored and referred to as the cold junction temperature. The thermocouple leads from the junction boxes were eventually connected to the data acquisition system using a shielded copper cable.

4.1.2.2 Arrangement of the Thermocouples

A total of 114 thermocouples were employed to measure the temperature of the mould. These thermocouples were mainly installed along vertical rows at the centreline and near the corner of a given face as shown in Fig. 4.15. The layout of the thermocouples on the narrow and the broad face is schematically shown in Fig. 4.16. It should be noted that the spacing between the thermocouples in the vicinity of the meniscus has been reduced due to the significance of initial solidification at the meniscus.

Also, thermocouples are located above the metal level (90 to 100 mm) primarily to assist in the understanding of the behaviour of the mould flux at the meniscus. From the measurements of the depth of the flat bottom hole and the copper plate thickness, the distance between the thermocouple bead and the hot face of the mould was determined. The location of the thermocouples and their respective distances from the hot face on each of the four faces of the mould is given in Tables 4.3a-d.

4.1.2.3 Data Acquisition

The voltage signals from the thermocouples were fed into a data acquisition system, namely, Fluke, 2280B Datalogger. This particular system has been successfully used earlier in steel plant environment. Prior to the measurements, the datalogger was programmed primarily to specify the scanning order and rate. The normal scanning interval used was 8 seconds. Two strip chart recorders were employed in conjunction with the datalogger to monitor a few specified thermocouples as a backup in the event of malfunctioning of the datalogger. Besides mould temperature, the casting speed was also recorded with the datalogger. The data was stored on cassette tapes and eventually transferred to the Amdhal computer for further analysis. Also, data on the temperature and flow rates of mould cooling water and the temperature of the steel in the tundish were obtained from the appropriate recorders on the casting machine.

4.1.2.4 Details of the Trials

Mould temperature measurements were carried out for a large number of heats and the details of steel composition and casting conditions of the different heats are given in Tables 4.4 and 4.5 respectively. It may be noted that plain carbon steel grades have been examined in which the carbon content varied between 0.04 to 0.36 percent. The influence of variables like, steel carbon, mould flux, casting speed, submerged entry nozzle on the mould temperatures were also examined.

4.2 Laboratory Work

Slab samples were collected from selected heats during the plant trial. Figure 4.17 schematically shows a cross-section of the slab illustrating the locations from where samples were cut. Metallographic examination was conducted at the University of British Columbia on different samples to determine the surface and sub-surface structure and locate the position of cracks if any.

Surface analysis included the investigation of the oscillation marks. The oscillation marks on the broad faces are deformed by the containment rolls present in the sub-mould region and therefore the measurement of oscillation mark depth was carried out on the samples from the narrow face. Prior to the measurements, the surface of the sample was shot blasted to remove the oxide layers. The depth of the oscillation marks were measured using a profilometer designed at UBC; the details of this profilometer are described by Bakshi et al. [135].

Slices were cut from the samples for sub-surface analysis. Transverse slices were macroetched in a 50 % Hydrochloric Acid solution at 70^0 C. The macrostructures were examined for solidification bands and sub-surface cracks. Also, longitudinal slices were surface ground and later polished to a 0.3 micron level and etched with picric acid to examine the sub-surface structure in the vicinity of the oscillation marks.

Table 4.1 - Salient features of the slab casting machine at Lake Erie Works, Stelco.

Mould Type	Curved, 10.5m radius
Mould Dimensions	Length 900mm Width 1130-2030 mm Thickness 240 mm
Width Adjustment	Only one end plate is moved
Water flow rate	Broad face 66 l/sec Narrow face 6.5 l/sec
Oscillation conditions	Stroke 11 mm Frequency 90 cpm Negative strip time 0.24 to 0.29 s
Metal level control	Manually, aimed at 75-100 mm from top of the mould
Mould flux feeding	Manually

Table 4.2 - Comparison of the thickness of the inside and outside radius copper plates.

Distance from the top of mould (mm)	Copper thickness (mm)	
	Inside radius	Outside radius
0	36	48
100	39	44
200	42	41
300	44	40
400	45	39
500	45	39
600	44	40
700	42	42
800	39	45
900	36	48

Table 4.3a - Location and distance between thermocouple tip and the hot face on the inside radius face.

Distance from the top of mould (mm)	Distance between the thermocouple and the hot face of the mould (mm)		
	East	Center	West
70	6.35	6.10	6.07
80	6.35	5.74	5.95
90	6.18	5.67	6.02
100	5.92	5.80	5.74
110	6.45	5.74	5.92
120	5.81	5.61	5.69
130	5.92	5.95	5.13
140	6.02	5.61	5.49
150	5.77	5.82	5.90
160	6.07	5.59	5.72
200	5.89	6.83	
240	6.02	5.92	
340	5.97	5.97	
440	5.66	5.49	
540	6.41	5.97	
640	6.38	6.25	
740	10.87	10.79	
850	10.46	10.54	

Table 4.3b - Location and distance between thermocouple tip and the hot face on the outside radius face.

Distance from top of the mould (mm)	Distance between thermocouple and the hot face of the mould (mm)	
	East	Centre
70	6.24	6.10
80	6.12	5.98
90	5.53	5.81
100	6.13	5.98
110	5.86	6.01
120	6.1	5.92
130	6.17	5.87
140	6.07	5.88
150	6.31	5.91
160	6.11	5.69
200		6.20
240		6.12

Table 4.3c - Location and distance between thermocouple tip and the hot face on the narrow face (movable).

Distance from top of the mould (mm)	Distance between thermocouple and the hot face of the mould (mm)	
	Centre	Off-corner
70	5.99	5.97
80	6.02	6.15
90	5.97	6.05
100	6.07	6.12
110	6.17	5.97
120	5.89	5.97
130	6.20	5.84
140	5.82	5.94
150	5.97	6.17
160	6.02	6.07
200	6.12	5.97
240	6.22	5.97
340	6.12	5.82
440	10.05	9.72
540	10.08	9.19
640	12.17	11.94
740	15.14	15.03
850	15.03	15.11

Table 4.3d - Location and distance between thermocouple tip and the hot face on the narrow face (fixed).

Distance from top of the mould (mm)	Distance between thermocouple and the hot face of the mould (mm)
	Centre
70	5.72
80	5.84
90	5.74
100	5.66
110	5.77
120	5.74
130	5.87
140	5.84
150	5.77
160	5.79

Table 4.4 - Steel composition of heats cast during the trial.

Heat No	C (%)	Mn (%)	P (%)	S (%)	Si (%)	Cu (%)	Ni (%)	Cr (%)
816951	0.04	0.26	0.004	0.013	0.008	0.028	0.013	0.059
816952	0.04	0.29	0.005	0.015	0.010	0.021	0.009	0.059
816953	0.09	0.30	0.007	0.021	0.017	0.028	0.008	0.058
772591	0.04	0.26	0.007	0.018	0.011	0.024	0.009	0.057
772592	0.10	0.40	0.009	0.019	0.013	0.014	0.028	0.043
772593	0.18	0.78	0.011	0.014	0.13	0.009	0.010	0.029
772594	0.19	1.23	0.011	0.017	0.14	0.009	0.010	0.024
772595	0.18	0.44	0.008	0.010	0.007	0.015	0.013	0.049
816954	0.17	0.45	0.009	0.009	0.012	0.010	0.010	0.035
816955	0.19	0.75	0.010	0.007	0.14	0.010	0.010	0.036
816956	0.07	0.39	0.007	0.007	0.011	0.013	0.011	0.030
816957	0.20	0.93	0.009	0.008	0.15	0.015	0.012	0.037
816958	0.17	0.44	0.008	0.008	0.010	0.012	0.008	0.030
816959	0.17	0.48	0.009	0.010	0.010	0.009	0.006	0.041
772599	0.05	0.49	0.006	0.008	0.019	0.010	0.008	0.017
772600	0.05	0.48	0.007	0.008	0.012	0.012	0.009	0.022
772601	0.05	0.47	0.007	0.008	0.015	0.012	0.008	0.018
772602	0.06	0.49	0.007	0.007	0.013	0.016	0.015	0.028
772611	0.07	1.34	0.008	0.005	0.30	0.036	0.019	0.18
772612	0.08	1.36	0.009	0.006	0.29	0.020	0.014	0.19
772613	0.09	0.40	0.006	0.008	0.001	0.039	0.014	0.026
816967	0.10	0.40	0.005	0.007	0.006	0.026	0.015	0.026
816968	0.05	0.28	0.005	0.009	0.007	0.028	0.017	0.062
816970	0.07	0.40	0.007	0.011	0.008	0.020	0.009	0.022
816979	0.06	0.49	0.006	0.007	0.014	0.018	0.014	0.018
816983	0.29	1.23	0.014	0.005	0.18	0.023	0.009	0.030
816984	0.29	1.25	0.016	0.005	0.19	0.016	0.012	0.040
772629	0.05	0.28	0.004	0.009	0.016	0.043	0.017	0.016
772636	0.19	0.74	0.008	0.006	0.14	0.024	0.009	0.026
816991	0.35	0.83	0.015	0.013	0.014	0.009	0.006	0.026
816992	0.36	0.81	0.018	0.007	0.019	0.012	0.007	0.027
816993	0.36	0.80	0.013	0.006	0.013	0.012	0.007	0.025
816994	0.09	0.40	0.006	0.009	0.011	0.024	0.012	0.017
816995	0.09	0.39	0.007	0.007	0.007	0.017	0.009	0.023
816996	0.09	0.41	0.006	0.007	0.009	0.015	0.009	0.016
816997	0.09	0.40	0.005	0.007	0.009	0.017	0.013	0.020
816999	0.21	1.40	0.013	0.005	0.14	0.013	0.009	0.028
817007	0.05	0.26	0.005	0.013	0.011	0.037	0.015	0.060
817008	0.05	0.27	0.005	0.007	0.009	0.041	0.016	0.067
817009	0.09	0.41	0.006	0.007	0.009	0.031	0.014	0.026
817014	0.05	0.27	0.006	0.009	0.007	0.022	0.012	0.060
772758	0.05	0.28	0.008	0.009	0.010	0.022	0.023	0.066
772759	0.05	0.28	0.005	0.009	0.007	0.021	0.021	0.064
817187	0.09	0.37	0.010	0.009	0.025	0.016	0.010	0.043
817190	0.28	1.24	0.012	0.006	0.17	0.016	0.013	0.044

Table 4.5 - Casting conditions of heats cast during the trial.

Heat No	Casting Speed (m/min)	Slab Width (mm)	Mould Flux	Port Angle (°)	Tundish Temp. (°C)	Water Flow Rate (l/sec)	
						Narrow Face	Broad Face
816951	0.75	1580	Pemco	7.5 up	1550	6.5	66.0
816952	0.5, 0.75	1580	Pemco	7.5 up	1550	6.5	66.0
816953	0.6,0.7	1580	Pemco	7.5 up	1540	6.5	66.0
772591	1.0, 1.10	1580	Pemco	7.5 up	1550	6.5	66.0
772592	1.0, 1.2	1580	Pemco	7.5 up	1550	6.5	66.0
772593	0.75	1730	Stg	7.5 up	1535	6.5	66.0
772594	0.6, 0.7	1730	Stg	7.5 up	1540	6.5	66.0
772595	0.7	1680	Stg	7.5 up	1540	6.5	66.0
816954	0.7	1680	Stg	7.5 up	1550	6.5	66.0
816955	0.6, 0.8	1680	Stg	7.5 up	1540	6.5	66.0
816956	0.8, 1.0	1330	Pemco	7.5 up	1548	6.5	66.0
816957	0.7, 0.9	1280	Stg	7.5 up	1535	6.5	66.0
816958	0.8	1280	Stg	7.5 up	1540	6.5	66.0
816959	0.9	1280	Stg	7.5 up	1540	6.5	66.0
772599	1.0	1280	Pemco	7.5 up	1545	6.5	66.0
772600	1.0	1280	Pemco	7.5 up	1555	6.5	66.0
772601	0.9, 1.0	1280	Pemco	7.5 up	1565	6.5	66.0
772602	0.65	1280	Pemco	7.5 up	1550	6.5	66.0
772611	1.10	1580	Stg	7.5 up	1550	6.5	66.0
772612	0.60	1580	Pemco	7.5 up	1540	6.5	66.0
772613	0.6	1580	Pemco	7.5 up	1535	6.5	66.0
816967	1.10	1580	Pemco	7.5 up	1555	6.5	66.0
816968	0.70	1580	Pemco	7.5 up	1560	6.5	66.0
816970	0.65	1530	Pemco	7.5 up	1558	6.5	66.0
816979	0.60	1580	Pemco	7.5 up	1550	6.5	66.0
816983	0.7. 0.8	1530	Pemco	7.5 up	1540	6.5	66.0
816984	0.70	1530	Pemco	7.5 up	1550	6.5	66.0
772629	0.75	1630	Pemco	7.5 up	1550	6.5	66.0
772636	0.60	1530	Stg	7.5 up	1535	6.5	66.0
816991	0.8, 1.0	1280	Stg	7.5 up	1520	6.5	66.0
816992	0.7, 0.8	1280	Stg	7.5 up	1530	6.5	66.0
816993	0.7	1280	Stg	7.5 up	1525	6.5	66.0
816994	0.7, 0.8	1230	Pemco	7.5 up	1545	6.5	66.0
816995	0.8, 1.0	1230	Pemco	7.5 up	1550	6.5	66.0
816996	1.0	1230	Pemco	7.5 up	1545	6.5	66.0
816997	0.8, 1.0	1230	Pemco	7.5 up	1545	6.5	66.0
816999	0.9	1230	Stg	7.5 up	1540	6.5	66.0
817007	0.65	1980	Pemco	15 down	1555	6.5	66.0
817008	0.60	1980	Pemco	15 down	1545	6.5	66.0
817009	0.50	1980	Pemco	15 down	1550	6.5	66.0
817014	0.50	1880	Pemco	15 down	1560	6.5	66.0
772758	0.9, 1.0	2030	Pemco	7.5 up	1550	6.5	66.0
772759	0.5, 0.7	2030	Pemco	7.5 up	1550	6.5	66.0
817187	0.6	2030	Pemco	7.5 up	1550	6.5	66.0
817190	0.75, 0.5	2030	Pemco	7.5 up	1535	6.5	66.0

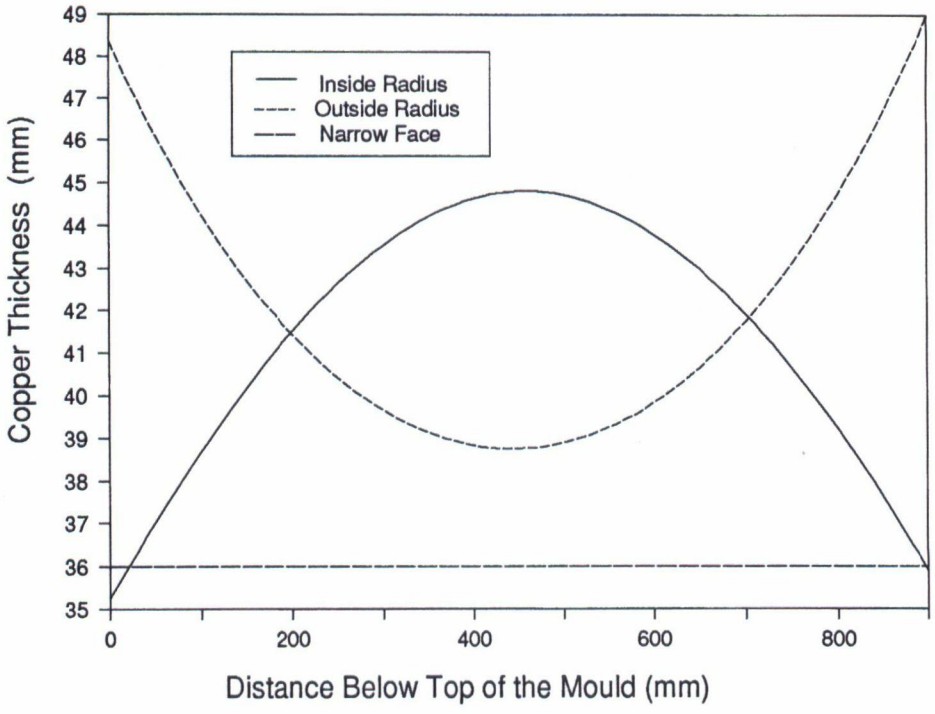

Figure 4.1. Thickness of the copper plates employed on the inside radius, outside radius and the narrow face.

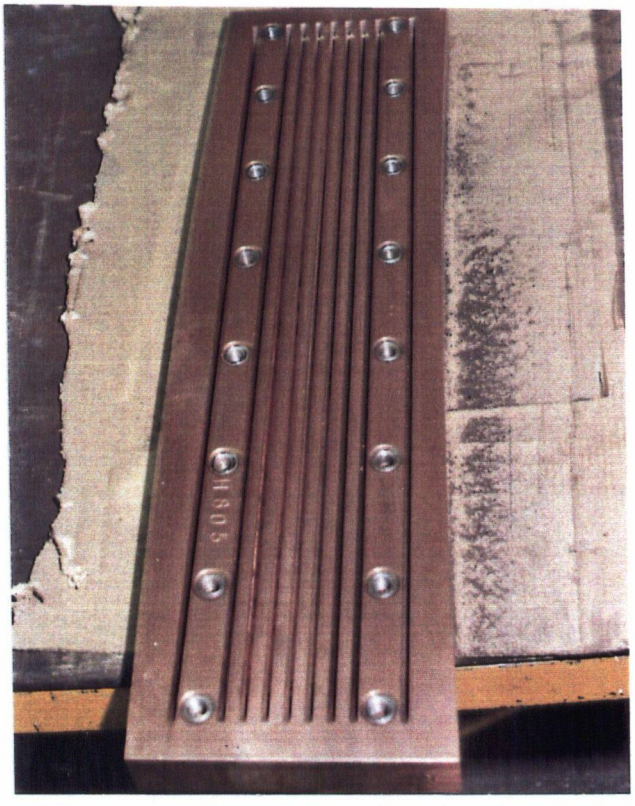

Figure 4.2. Photograph of the narrow face copper plate showing the location of cooling channels.

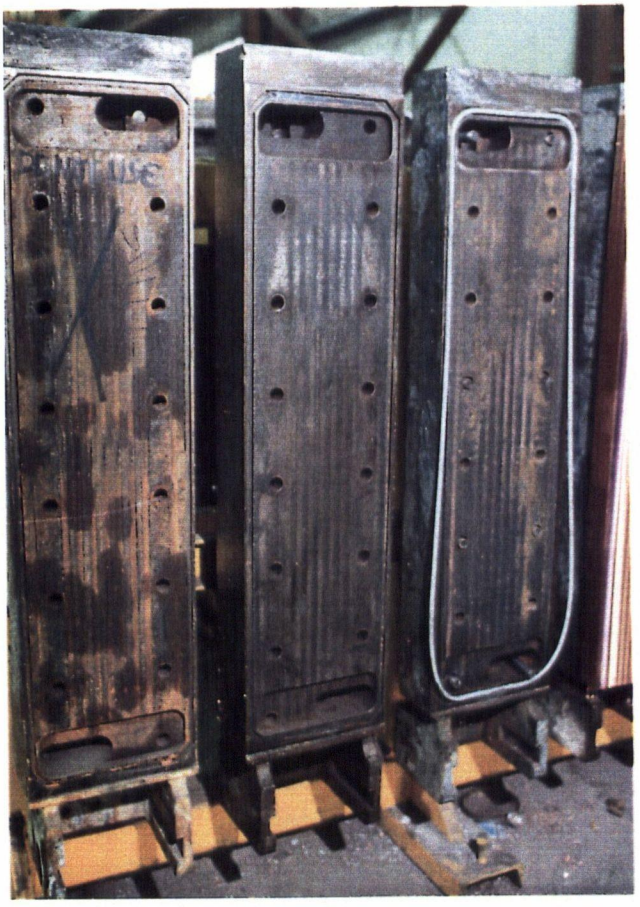

Figure 4.3. Photograph of a narrow face water jacket.

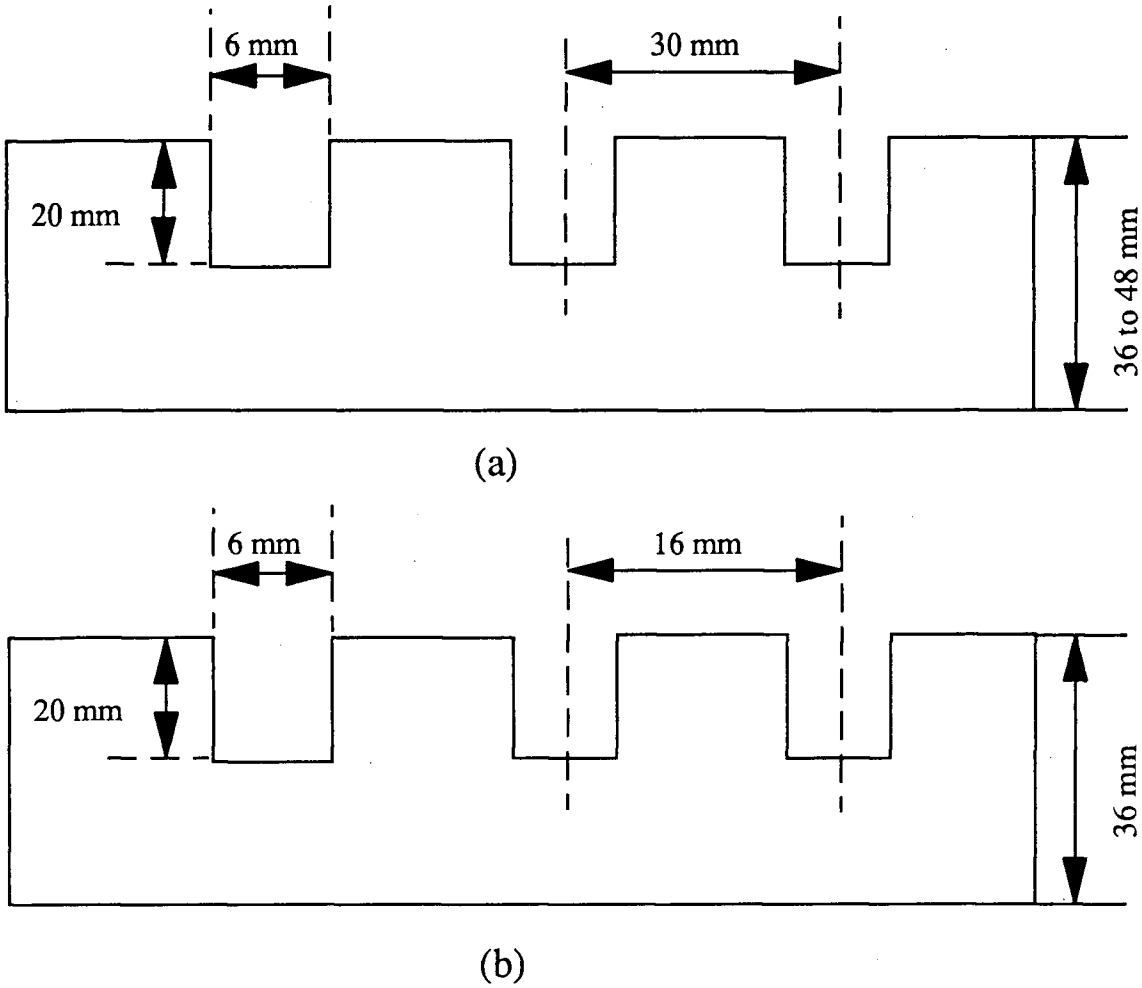

Figure 4.4. Transverse section across the copper plate showing the location of the cooling channels and their dimensions. (a) Broad face (b) Narrow face

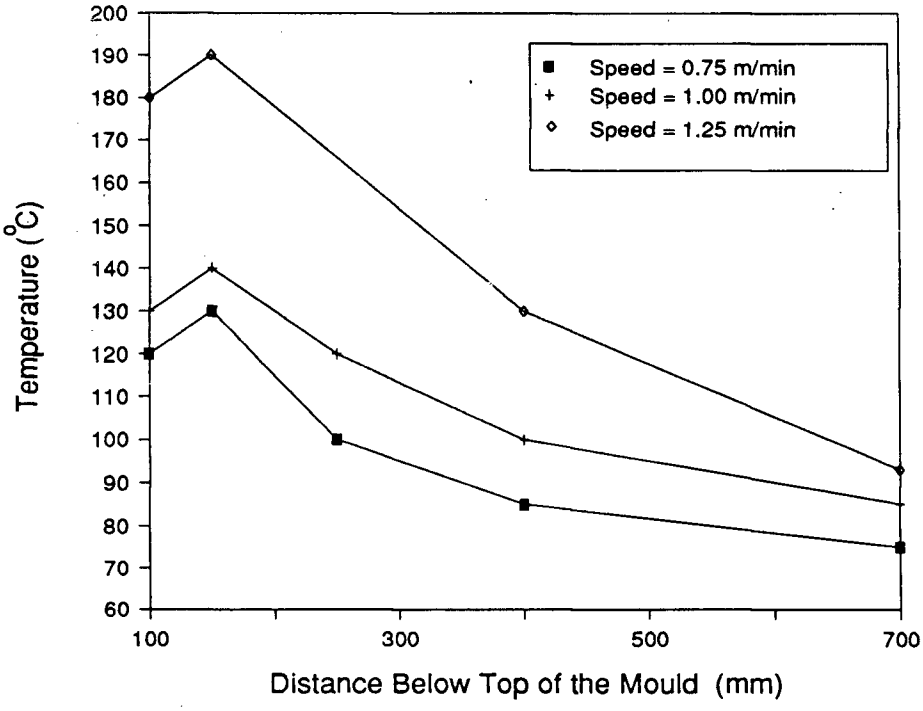

Figure 4.5. Axial mould temperature profiles obtained from the preliminary set of experiments conducted by Stelco personnel.

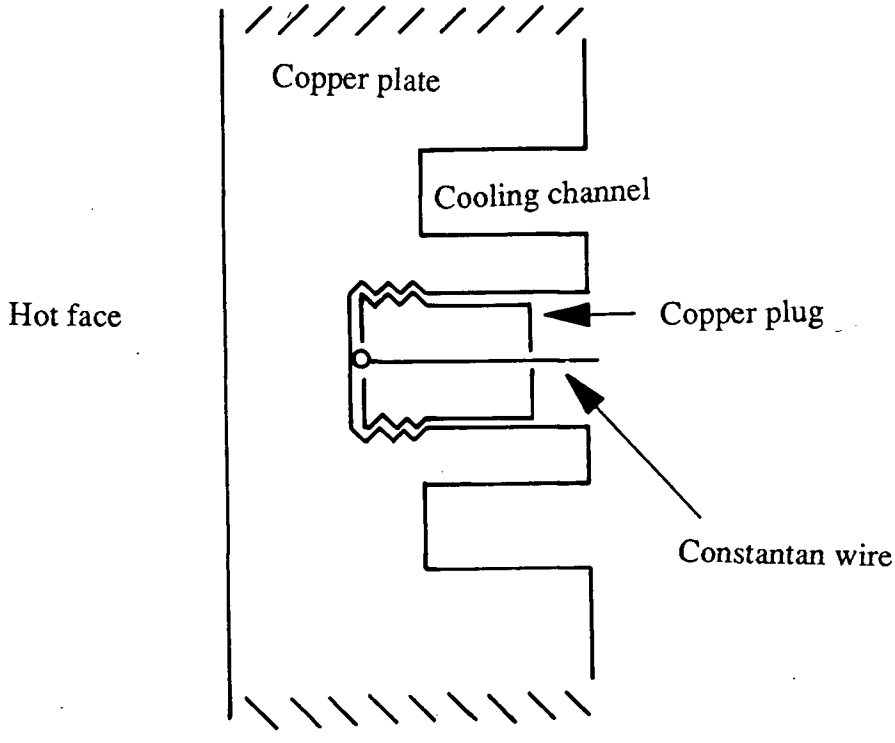

Figure 4.6. Schematic drawing showing the installation of a thermocouple on the mould wall.

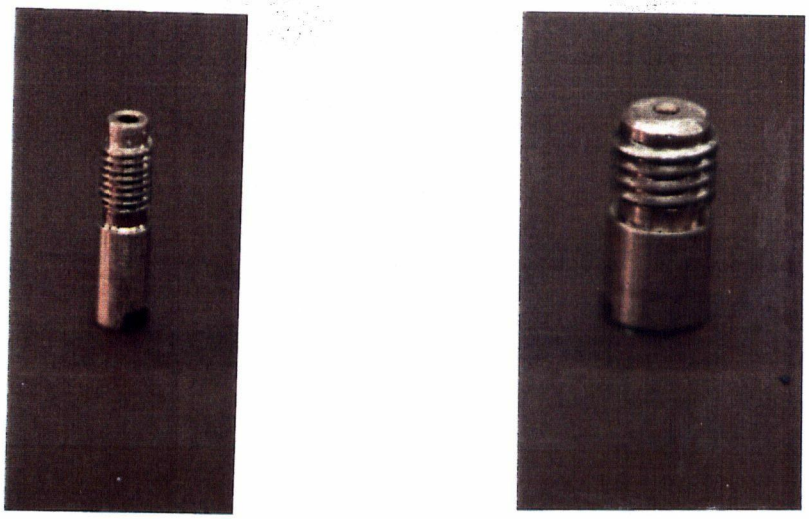

Figure 4.7. Photograph of the copper plugs employed on (a) Narrow face (b) Broad face.

Figure 4.8. Photograph of the screw driver used to screw the copper plugs into the mould wall.

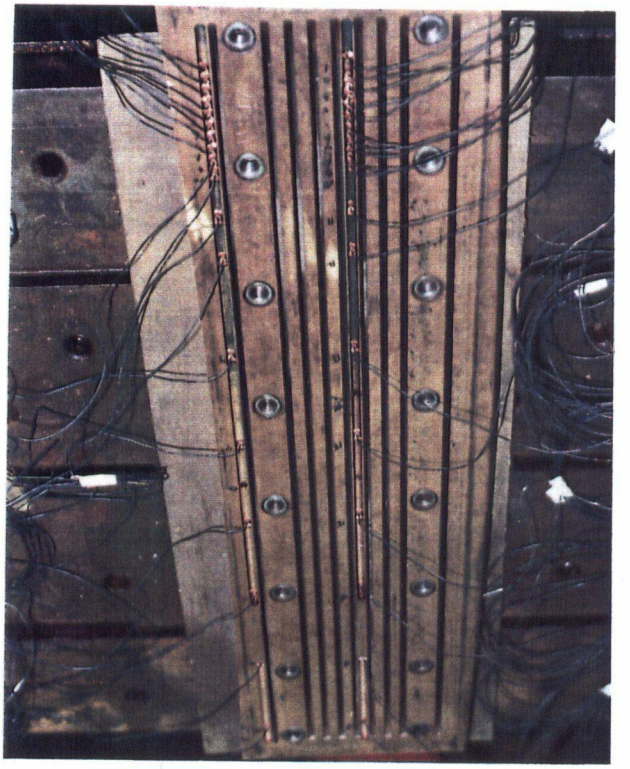

Figure 4.9. Photograph of an instrumented narrow face copper plate.

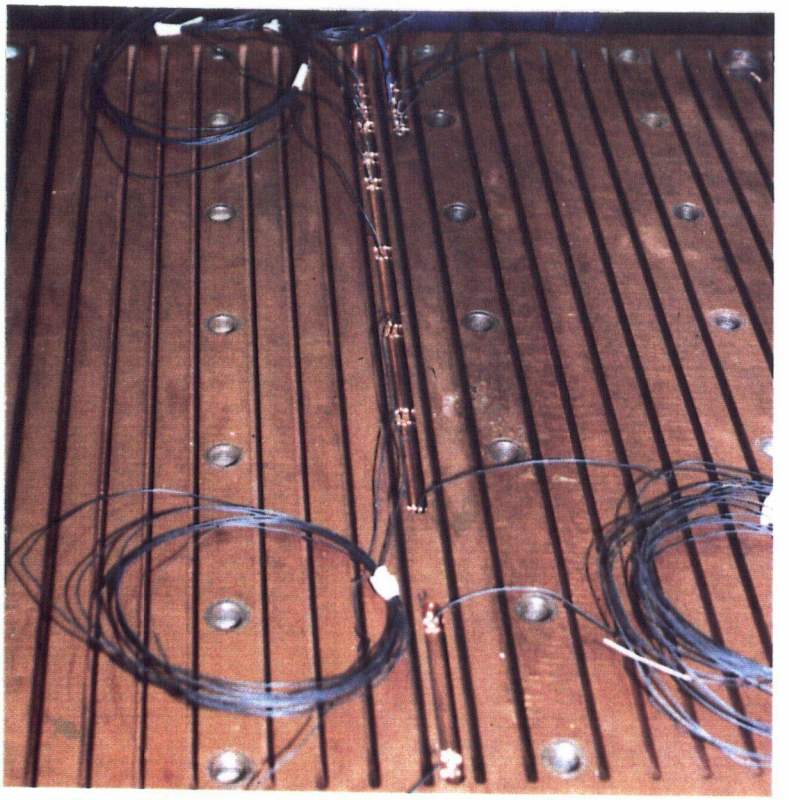

Figure 4.10. Photograph of an instrumented broad face copper plate.

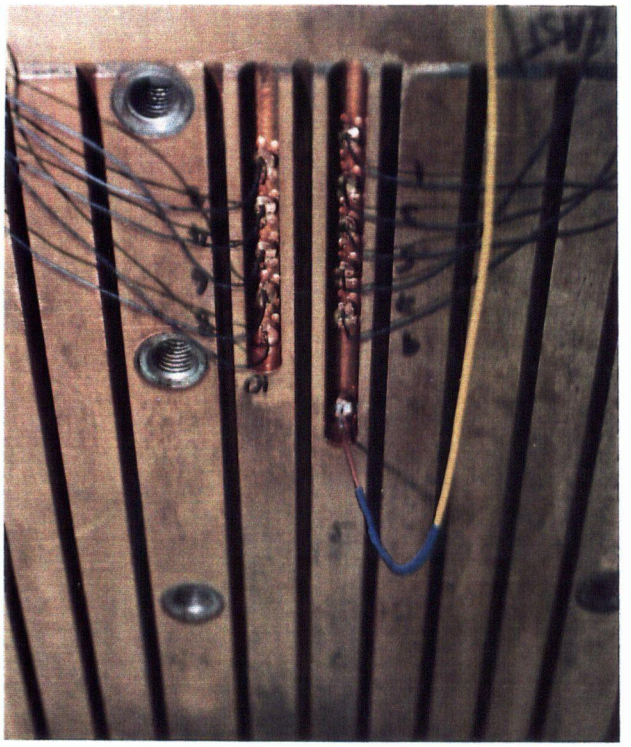

Figure 4.11. Photograph illustrating the peening of the copper plugs.

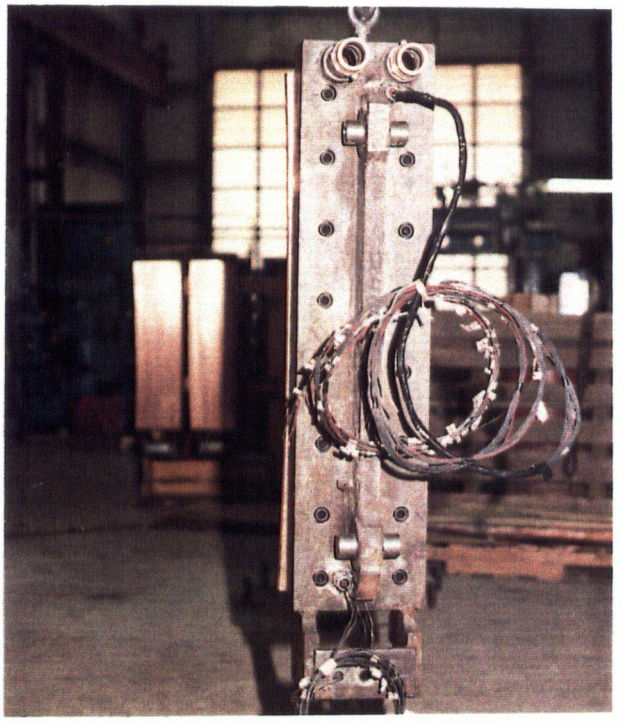

Figure 4.12. Photograph showing the exit of the thermocouples from the narrow face water jacket.

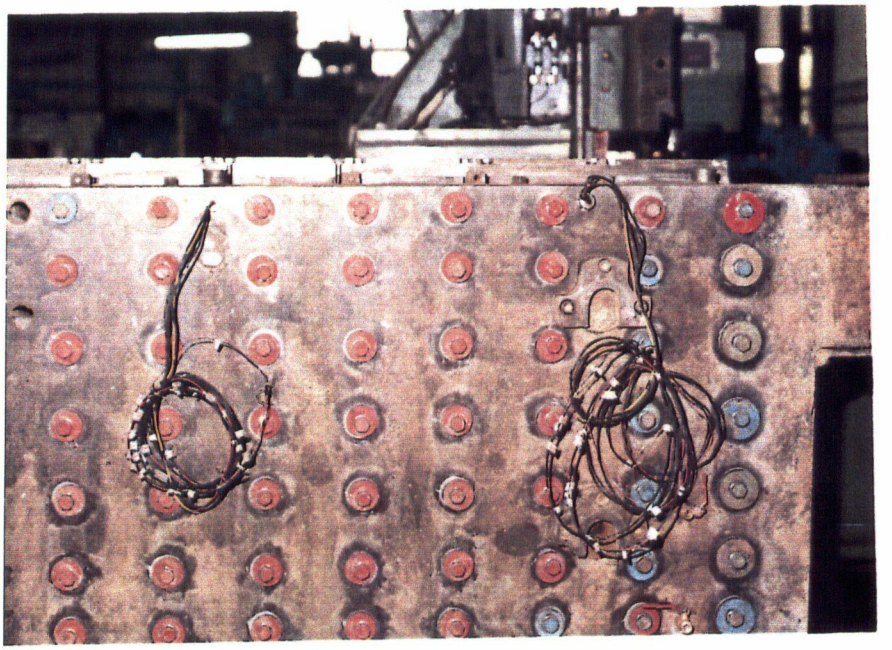

Figure 4.13. Photograph showing the exit of the thermocouples from the broad face water jacket.

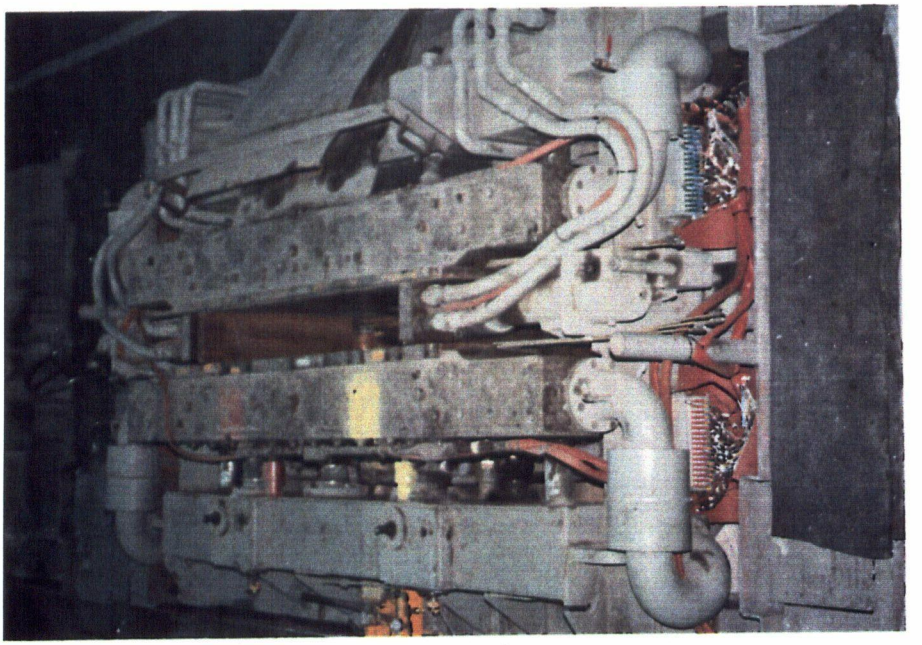

Figure 4.14. Photograph of the instrumented mould.

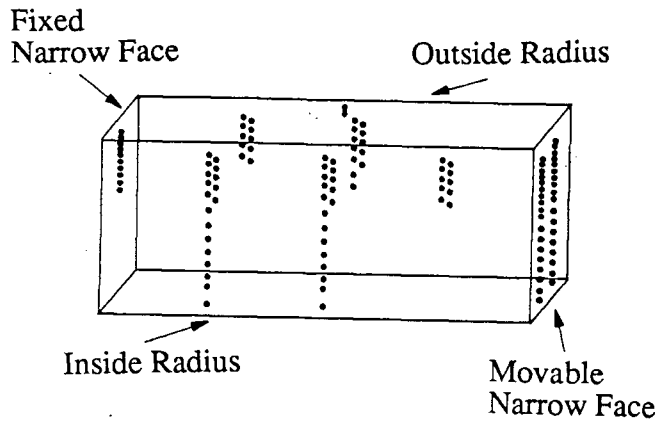

Figure 4.15. Schematic drawing of the mould showing the location of the thermocouples on the four faces.

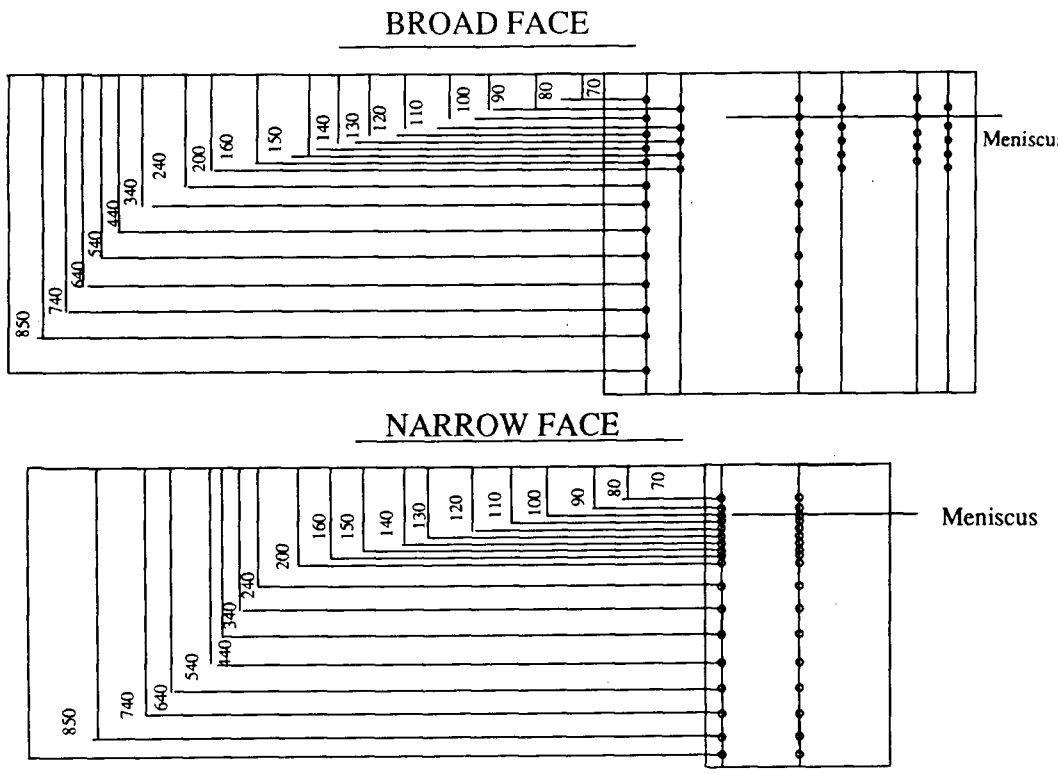

Figure 4.16. Schematic drawing showing the lay-out of the thermocouples on the broad and the narrow faces (all dimensions are in mm).

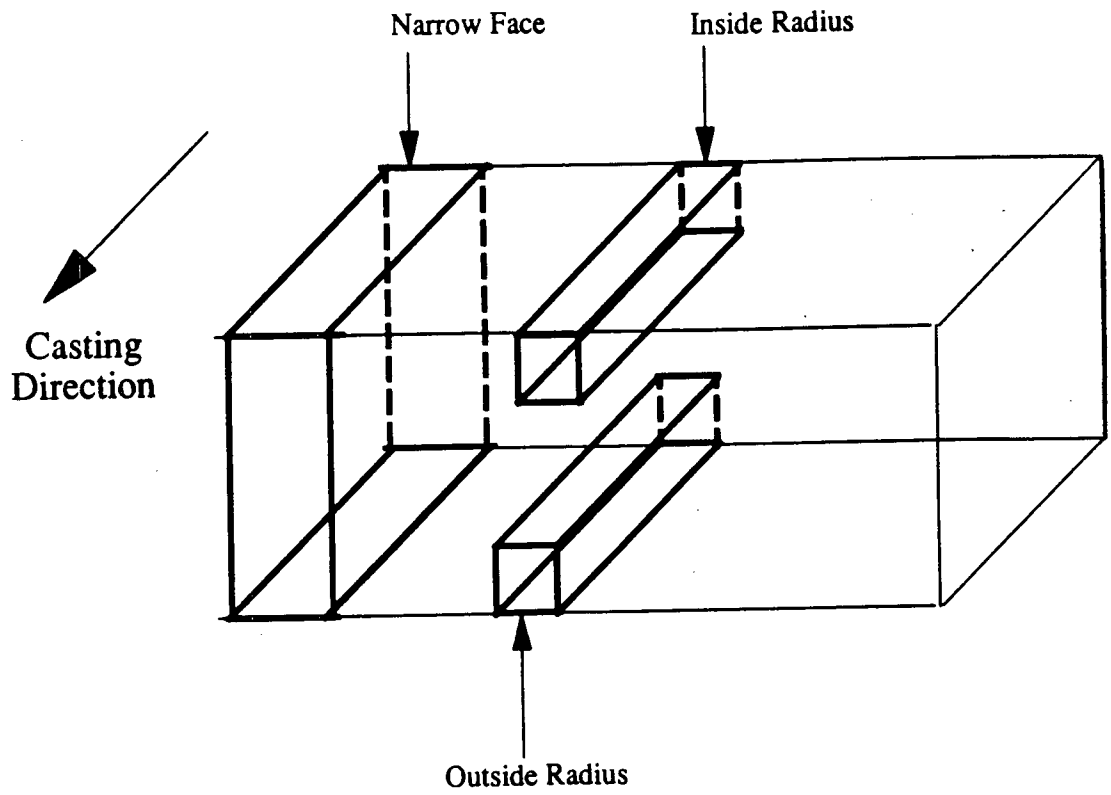

Figure 4.17. Cross-section of a slab showing the locations from where samples were cut.

Chapter 5 - MOULD TEMPERATURE MEASUREMENTS

The temperature of the copper plate is a good indication of the magnitude of heat transfer from the solidifying shell to the mould, although it is important to realize that the mould temperatures can only be utilized to estimate the heat extraction rates in the mould in a qualitative manner. In the following sections, the mould temperature measurements obtained from an operating slab mould will be presented and this information will be used to qualitatively assess the heat transfer rates along the length of the mould on both the broad and the narrow faces. In addition, it is also intended to examine the influence of process variables, mould flux and steel composition on heat transfer in the mould.

5.1 Mould Temperatures

As mentioned earlier, a total of 114 thermocouples were employed to measure the temperature of the mould at several locations on each of its four faces. It should be noted that there was a considerable fluctuation in the magnitude of the mould temperature with time and this particular aspect will be discussed in the subsequent sections. However, despite the mould temperature fluctuations, the shape of the axial mould-temperature profiles were nonetheless identical with respect to the location of the meniscus. The axial mould-temperature profiles have been examined to understand the nature of heat flow from the shell to the mould.

5.1.1 Typical Axial Mould-Temperature Profiles on the Narrow and the Broad Faces

Prior to presenting the axial temperature profiles, it is worthwhile to examine the arrangement of the thermocouples on the narrow and broad faces which has been schematically shown in Fig. 5.1. The thermocouples in the vicinity of the meniscus on the broad face (mid-face and near corner) are positioned along two vertical rows, unlike the

narrow face, on which the thermocouples are located only along one row. Therefore, on the broad face, the temperature read by thermocouples in both the rows are represented in a single axial temperature profile.

5.1.1.1 Narrow Face

The axial temperature profiles on the centreline and near the corner of the narrow face are shown in Figs. 5.2 and 5.3 respectively. It is evident that the location of the maximum temperature of the mould wall occurs below the meniscus which is located at a distance of 100 mm from the top of the mould. Below the maximum peak, there is a decrease in the mould temperature and finally towards the bottom of the mould there is an increase in the temperature. The higher temperature of the mould in the vicinity of the meniscus is an indication of enhanced heat extraction rates from the solidifying shell to the mould. The subsequent reduction in the mould temperature is a consequence of decrease in the heat transfer which is due to an increase in the dimensions of the gap between the steel shell and the mould wall. Needless to say, an increase in the dimension of the gap will increase the resistance of the gap which is known to control the heat-transfer in the mould. The rise in the mould temperature towards the bottom indicates a corresponding increase in heat transfer and this is probably as a result of either inadequate or excessive taper of the narrow face. Insufficient taper of the narrow face will reduce the heat extraction in the upper part of the mould resulting in a relatively thin shell and thus, towards the bottom of the mould the ferrostatic pressure is effective in pushing the solid shell towards the mould wall, thereby leading to a reduction in the gap dimensions. On the contrary, excessive taper of the narrow face will improve the contact between the shell and the mould and thus, increase the heat transfer. However, it will be shown later that the increase in the mould temperature towards the bottom is related to bulging of the narrow face and this topic will be addressed later.

A comparison of the axial temperature profiles along the centreline and off-corner region of the narrow face as shown in Fig. 5.2 and Fig. 5.3 reveals distinct differences.

The temperature profile near the corner is characterized by the presence of a spike near the meniscus; the thermocouple located at 120 mm from the top of the mould recorded a lower temperature than the thermocouples located at 90 mm and 100 mm and this observation was consistent from one heat to another. It may be interesting to note that despite large changes of the metal level in the mould, the spike was always seen at the same location. Sato et al. [52] have reported the occurrence of local reduction in the mould temperature below the meniscus which has been attributed to reduction in heat transfer due to the presence of local gaps generated by the break-down of the flux film. It is also apparent from the two mould-temperature profiles (Figs. 5.2 and 5.3) that the reduction in the mould temperature below the maximum peak is more rapid near the corner (Fig. 5.3) compared to the centre of the narrow face (Fig. 5.2); this is presumably a consequence of a larger gap near the corner of the narrow face relative to the centre. The large gap near the corner is an outcome of increased shrinkage of the shell as a result of enhanced solidification rates due to the two-dimensional nature of heat flow near the corner. Furthermore, it may be interesting to note that the curvature of the narrow face copper plate at the hot face as shown in Fig. 5.4 may further contribute towards enhancing the gap dimensions near the corner. These results indicate the necessity to modify the design (ie. curvature) of copper plate to minimize differences in heat transfer rates from the centre to the corner. It is also interesting to note that the magnitude of the mould temperature near the corner of the narrow face, particularly in the upper region was significantly higher than the corresponding temperature at the centreline. This may be a result of inadequate cooling of the copper plate (narrow face) near the corner as a result insufficient number of cooling channels in the vicinity of the corner. It is evident from Fig. 5.5 that the cooling channel nearest to the corner is located at a distance of 31.5 mm whereas the spacing between cooling channels in the other parts of the copper plate is 16 mm.

5.1.1.2 Broad Face

The axial temperature profile at the centreline of the broad face is shown in Fig. 5.6. Clearly, the mould temperature in the vicinity of the meniscus is higher than in the other regions of the mould and this is again similar to the measurements made on the narrow face. The temperature profile is an indication of higher heat extraction rates near the meniscus beyond which there is a reduction in heat transfer rates. However, a prominent feature of this profile is in the behaviour of the thermocouples located in the upper part of the mould (70 to 160 mm from the top of the mould). It is evident that the temperature of the mould near the bolts (indicated by the vertical row containing five thermocouples as shown in Fig. 4.10 and Fig. 5.1) was higher compared to the region of the mould away from the bolts suggesting a possibility of variation in the heat transfer rates along the width of the mould wall particularly in the proximity of the bolts.

5.1.1.3 Comparison of Axial Mould-Temperature Profiles Between the Narrow and the Broad Face

A comparison of the axial mould-temperature profiles measured on the narrow and the broad faces shows distinct differences in the mould temperatures particularly in the central region of the mould. On the narrow face, the reduction in the mould temperature below the maximum peak is relatively steep (Figs. 5.2 and 5.3) as compared to the broad face (Fig. 5.6) where the mould temperature is quite uniform. These findings imply that the rate of decrease in the heat transfer below the meniscus on the narrow face is more rapid in comparison to the broad face. This can be explained on the basis of the dimensions of the gap on the narrow face which is expected to be larger than that on the broad face due to the large aspect ratio of the slab. The gap dimension is largely determined by the magnitude of shrinkage during solidification; shrinkage of broad face will cause it to pull the narrow face from the mould wall which would obviously aid in the enhancement of the gap dimensions formed on the narrow face. This finding clearly

emphasizes the necessity to impart a proper taper to the narrow face in order to compensate for the increased gap dimensions due to the shrinkage of the broad face during solidification.

The axial temperature profiles have been immensely useful in assessing the heat extraction rates along the length of the mould and certainly, a qualitative understanding has been acquired. Clearly, in addition to the significant differences in the heat transfer between the broad and the narrow faces, considerable variation also prevails from centreline to the corner region of the same face.

5.1.2 Non-Uniformity of the Mould Temperatures in the Vicinity of the Bolts on the Broad Face

As mentioned earlier, a consistent feature of the axial temperature profile on the broad face was the non-uniformity of the mould temperature near the bolts. Evidently, the thermocouples adjacent to the vertical row of bolts measured a higher temperature and this effect is shown in Fig. 5.7. This may be an outcome of non-uniformity in the heat transfer near the bolts and obviously is not desirable from the standpoint of quality. It is probable that the thermal expansion of copper plate is restrained in the vicinity of bolts. This can assist in the outward bulging of the copper thereby resulting in differences in the gap dimensions; which can lead to a variation in the heat transfer. But, distortion of the copper plate is improbable due to its rigid attachment to the steel backup plate. The observation as shown in Fig. 5.7 can also be explained on the basis of differences in the resistance to heat flow along the width of the copper plate. It should be noted that the spacing between two consecutive cooling channels in the presence and absence of the bolts is 35 mm and 23 mm respectively. The increased spacing between the cooling channel near the bolts will presumably offer extra resistance to heat flow and consequently may result in the observed increase in the mould temperature near the bolts. Nevertheless, the above information available on the mould temperature is in itself

inadequate to determine any conclusive causes for the observed differences in the mould temperatures and therefore, a heat flow model of the mould wall will be utilized to provide further insight which will be discussed in the following chapter.

5.1.3 Mould-Temperature Profiles on the Inside and Outside Radius Copper Plates

Figure 5.8 is a plot of the axial temperature profiles along the centreline on the inside and the outside radius which clearly shows significant differences in the mould temperatures between the two broad faces. On the outside radius, thermocouples were located upto a distance of 240 mm from the top of the mould. It is evident from Fig. 5.8 that the temperature of the copper plate on the outside radius is higher compared to those at the same location on the inside radius. However, it is difficult to rationalize this observation strictly on the basis of differences in the heat transfer rates, because the heat fluxes on the inside and the outside radius are expected to be identical. It should also be noted that there are distinct differences in the design of the copper plate on the inside and the outside radius. It can be clearly seen from Fig. 4.1 that there is a considerable variation in copper thickness along the length of the mould on the inside and the outside radius copper plates. The depth of the cooling channels on the two copper plates are identical and the distance between the thermocouple bead and the hot face is similar on the two broad faces. In the upper region of the mould the copper is relatively thick on the outside radius (Fig. 4.1) and thus, the distance between the top of the cooling channel and the thermocouple tip is greater on the outside radius as compared with the inside radius copper plate. Therefore, thermocouples on the outside radius are likely to measure a higher temperature due to the increased distance between the thermocouple bead and the top of the cooling channel. However, it is difficult to ascertain the exact causes leading to the observed differences simply from a knowledge of the measured mould temperatures.

This topic will also be addressed in the next chapter by quantitatively characterizing the heat extraction rates on the two broad faces using a heat flow model of the mould wall in conjunction with the mould temperature data.

5.2 Mould Temperature Fluctuation

The influence of different process variables on heat transfer in the mould can be qualitatively assesed from a knowledge of the magnitude of the mould temperatures and therefore, the measured mould temperatures were time-averaged to generate axial mould-temperature profiles. In order to ensure that the time-averaging technique was appropriate, it was essential to examine the response of the thermocouples during casting. Figure 5.9 shows the temperature measured by two thermocouples located 90 mm and 850 mm from the top of the mould at different times from the start of casting. Evidently, the thermocouple located at 90 mm exhibited large fluctuation in temperature whereas the temperature of the mould at 850 mm is essentially uniform. It was important to characterize quantitatively the variation of the mould temperature at different locations and thus, the standard deviation of all the measurements as recorded by different thermocouples was determined. A distribution of this parameter along the length of the mould on the narrow face is shown in Fig. 5.10 and it can be seen that the thermocouples near the vicinity of the meniscus reveal higher values of standard deviation. These evidences indicate the presence of considerable variation in the mould temperatures particularly in the vicinity of the meniscus whereas the variations towards the bottom of the mould are quite nominal. Needless to say, it is inappropriate to simply utilize the time-averaged mould temperatures to estimate the heat transfer rates in the mould as this can lead to erroneous conclusions.

5.2.1 Analysis of the Mould Temperature Fluctuation

In an operating mould, the temperature of the copper plate at any desired location is not expected to remain constant during casting. The fluctuations in the temperature of the mould can occur due to numerous reasons. Factors like the shrinkage of the solidifying

shell, non-uniform flow of mould flux at the meniscus, mould distortion can change the dimension of the gap between the shell and the mould wall and thereby influence the heat transfer causing temperature variation of the mould wall. Besides, changes in the metal level in the mould, the oscillation of the mould can also lead to fluctuation of the mould wall temperature. Therefore, it was crucial to examine the pattern of fluctuations in the mould temperatures especially for thermocouples located in the vicinity of the meniscus to determine the underlying causes leading to the observed fluctuations.

It is expected that the oscillation of the mould will contribute towards the unsteadiness of the mould temperatures particularly near the meniscus since above the meniscus, the mould is at lower temperature and hence, it was intended to examine the effect of mould oscillation. It is important to note that the datalogger recorded the mould temperature at interval of 8 seconds and this is eqivalent to a scanning frequency of 8 cpm (cycles per minute). But, the frequency of the mould oscillation was 90 cpm. Due to the differences between the frequency of scanning and mould oscillation, the measurements obtained from the datalogger could not be utilized to determine the effect of the mould oscillation on the variation of mould temperature. This necessitated analysis of data recorded by a strip chart recorder which was employed during the trial to measure the temperature of the mould at few desired locations. The response of the two thermocouples located at 90 and 100 mm from the top of the mould obtained from the chart recorder is shown in Fig. 5.11 and a distinct periodic fluctuation of the voltage signal can be clearly seen. It is interesting to note that the frequency of these fluctuations (Fig. 5.11) is identical to the oscillation frequency of the mould. Therefore, the fluctuation of the voltage signals obtained from the thermocouples as shown in Fig. 5.11 can be attributed to the oscillation of the mould. But, it is important to realize that the magnitude of the temperature fluctuation due to mould oscillation is small and in the present example is in the range of $\pm 1.5^{0}$C and thus, the observed large fluctuations in the mould temperature can not be attributed to the oscillation of the mould.

Figure 5.12 shows the temperature recorded by thermocouples located on the narrow face at distances of 70, 80, 90 and 100 mm from the top of the mould. It should be noted that the temperature at 100 mm as shown in Fig. 5.12 is the absolute value measured by the thermocouple, but for thermocouples located at 70, 80, and 90 mm the respective temperatures have been magnified so as to avoid an overlap of the plots at the different locations and thus, it was possible to reveal the characteristics of the fluctuations more vividly. It is evident from Fig. 5.12 that the large components of the fluctuations in the temperature at each of the four locations occurred at the same instant of time. This is presumbaly an outcome of variation in the metal level in the mould. It should be noted that the location of the maximum temperature of the mould along its length is a good indication of the metal level. Therefore, to confirm the occurrence of metal level fluctuations, it was necessary to examine the axial temperature profiles particularly during the period over which the temperature fluctuation occurred. The axial temperature profiles obtained on the narrow face at three different times are shown in Fig. 5.13 and it is evident that there is a variation in the location of the maximum peak temperature with time which is a consequence of fluctuations in the metal level in the mould.

If the temperature fluctuation of the mould is a result of metal level changes, it is expected that this phenomenon be present on all the four faces of the mould at the same instant of time. This was verified by examining the response of the thermocouples on each of the four faces of the mould. Figure 5.14 shows the temperature recorded by thermocouples located at 100 mm from the top of the mould on the centreline of both the narrow faces and as well as broad faces. The temperatures as shown in Fig. 5.14 have essentially been magnified so as to avoid overlapping and show the fluctuations clearly. It is evident that the fluctuations in the temperatures on the four faces occur at the same instant of time and this is again an indication of metal level variation in the mould.

These aforementioned evidences clearly indicate that large variations in the mould temperatures are primarily a result of changes in the metal level. Thus, one of the findings of this work manifested in widely varying mould temperature is that the extent of metal level fluctuation in the mould is appreciable which in turn can lead to quality problems. The present practice of controlling the metal level manually is not adequate and therefore automatic metal level control system must be employed.

It is important to realize that metal level variation in the mould is not inherently related to the casting process and occurs mostly in the absence of relevant controlling devices as was the case on the present casting machine. Therefore, it is vital that the component of the fluctuation resulting from the metal level variation should be properly filtered out prior to further assessment of the heat transfer in the mould.

5.2.2 Data Filtration Technique

A filtration technique has been developed to eliminate the fluctuations in the mould temperature as a result of changes of the metal level in the mould and this technique is quite similar to the one employed by Samarasekera et al. [6] in the analysis of billet mould temperature data. It should be noted that the entire set of thermocouples are scanned every 8 seconds and the measurements obtained in each scan are referred to as a block of data. The filtration technique consisted of a sequence of steps as given below:

(i) Casting speed was not constant in a heat and measurements indicate a considerable variation in the speed and one example of this is shown in Fig. 5.15. Owing to the significant effect of the casting speed on the mould temperatures (to be discussed later), it was essential to select blocks of data pertaining to a constant speed and this was the first step of the filtration technique.

(ii) The location of the maximum temperature of the mould along its length is an indication of metal level in the mould which was generally found to be at 120 mm for a large number of heats. Subsequently, the next step of filtration comprised of selecting blocks from the previously chosen ones (step i) in which the maximum peak temperature of the mould was located at 120mm from the top.

(iii) It should be noted that the metal level is approximately located at 100 mm and thus, the fluctuation in the temperature of the mould at 70mm (Fig. 5.1) is predominantly due to variation in the metal level and therefore, a given temperature at 70 mm corresponds to a fixed position of the metal level. Based on this principle, a reference temperature range was designated for the top most thermocouple located at 70 mm. The final step of the filtration technique was essentially to select the blocks from the previous chosen ones (step ii), in which, temperature of the mould at 70 mm was within the above specified range.

Finally, the temperature recorded by all the thermocouples in each of the selected blocks were averaged and thus, time-averaged axial mould-temperature profiles were generated and utilized to elucidate the effect of a number of operating variables, mould flux and steel composition on the heat transfer in the mould.

5.3 Influence of Mould Flux, Steel Composition, Process Variables on the Mould Temperatures

In the following sections, the time-averaged axial temperature profiles in the mould will be presented. The magnitude of the mould temperatures can be utilized to qualitatively assess the heat extraction rates in the mould. However, it is important to note that the topic on the heat transfer in the mould will be dealt with in detail by quantitatively characterizing the heat fluxes in the mould for the temperature profiles presented in this section which will be discussed in the next chapter.

5.3.1 Mould Flux

Two types of mould fluxes are used in the plant on a regular basis, namely, Pemco 389 and Stg 179. Prior to examining the effect of the mould flux on heat transfer, it is important to establish the differences between the two types of mould flux and a comparison of the relevant properties are listed in Table 5.1. It is standard practice to use Pemco 389 mould flux during the casting of low (0.04-0.07 percent-carbon) and medium carbon (0.07-0.11 percent -carbon) grades and Stg 179 mould flux is usually employed for high carbon grades (0.18-0.21 percent-carbon). The effect of the two types of mould flux on the axial temperature profile during the casting of a 0.07 percent-carbon steel is shown in Fig. 5.16. It should be noted that the casting speed was constant in the two cases. Clearly, Pemco 389 results in higher mould temperatures compared to Stg 179 indicating that the heat transfer in the mould was enhanced with Pemco 389 and the effect is significant in the upper part of the mould.

5.3.2 Steel Composition

Usually, plain carbon steel grades are cast in the plant and therefore, the influence of carbon content only on the mould temperatures has been examined. As discussed in the preceding section, the nature of the mould flux employed during the casting can have a significant effect on the heat transfer. Therefore, it was imperative to study the influence of carbon content by considering steel grades which were cast using the same mould flux. Figure 5.17 is a plot of the axial mould-temperature profiles measured during casting of three steel grades containing 0.04, 0.09 and 0.29 percent-carbon cast with Pemco 389 mould flux. Evidently, the magnitude of the maximum temperature is the lowest for 0.09 percent-carbon and highest for 0.29 percent steel and also the diferences in mould temperature in the vicinity of the meniscus is significant for the three carbon content. These results indicate that carbon content of steel has a considerable influence on the heat transfer in the mould.

Figure 5.18 shows a comparison of the axial mould-temperature profiles for 0.18 and 0.36 percent-carbon steel cast with of Stg 179 mould flux. Clearly, the mould temperatures are higher for 0.18 percent as compared to the 0.36 percent-carbon, indicating an enhanced heat transfer in the mould. The lower mould temperature with 0.36 percent-carbon steel is unusual and will be shown to be related to the liquidus temperature of the steel and the melting characteristics of the flux.

5.3.3 Casting Speed

The influence of casting speed on the mould temperatures at the centreline of the narrow and the broad faces is shown in Fig. 5.19 and Fig. 5.20 respectively. It should be noted that the measurements are from the same heat which was cast at two different speeds. There is a significant rise in the mould temperature on both the broad and the narrow faces with an increase in casting speed indicating an enhancement in the heat extraction rates at higher casting speed.

5.3.4 Submergence Depth

The pouring of the molten steel from the tundish into the mould is accomplished by using a bi-furcated submerged nozzle shown schematically in Fig. 5.21 through which the molten steel is poured and the stream is directed towards the narrow faces. These nozzles are made from refractory materials like alumina graphite or fused silica. During the trial, ports having an angle of inclination of 7.5^0 upwards was frequently employed. These ports are usually oval shaped with the small and large diameters being 77 mm and 110 mm respectively. The effect of the submergence depth of the nozzle on the axial mould-temperature profile examined has been examined.

The distance between the meniscus and the top of the ports of the submerged entry nozzle is usually referred to as the depth of submergence (Fig. 5.21). To examine its effect on the heat transfer in the mould, the depth was altered from 175 to 300 mm in the same heat. The influence of the submergence depth on the axial temperature profile has been investigated on both the narrow faces. It may be interesting to note that mould width

is changed during casting by moving only one of the narrow faces and thus, the submerged entry nozzle is not always located at the centre of the mould. In the present experiment, the movable and the fixed narrow faces were located at a distance of 900 and 770 mm from the submerged entry nozzle respectively. On the fixed narrow face, thermocouples were present only upto a distance of 160 mm from the top of the mould. The effect of the submergence depth on the mould temperatures measured on the movable and the fixed narrow face is shown in Fig. 5.22 and Fig. 5.23 respectively. Evidently, the mould temperatures in the vicinity of the meniscus are higher at a submergence depth of 175 mm compared to 300 mm on both the narrow faces. But, the mould temperature towards the lower half of the mould (Fig. 5.22) were similar at the two depths of submergence. These measurements indicate that the heat transfer in the vicinity of the meniscus is enhanced with a reduction in the submergence depth and the depth of submergence (in the range examined) has no effect on the heat transfer towards the lower half of the mould. It should also be noted that the increase in the magnitude of the mould temperature with a reduction in the submergence depth is relatively more on the fixed narrow face (Fig. 5.23) compared to the movable narrow face (Fig. 5.22). Owing to the proximity of the fixed narrow face from the nozzle, the flow of the steel will be intense compared to that near the movable narrow face suggesting that the flow patterns in the liquid steel near the meniscus can influence the heat transfer.

Table 5.1 - Comparison of physical properties between Pemco 389 and Stg 179 mould fluxes

Properties	Pemco 389	Stg 179
Softening Temperature (^{0}C)	1050	1040
Melting Temperature (^{0}C)	1125	1165
Viscosity (poise)		
1400 ^{0}C	0.4	2.3
1300 ^{0}C	0.6	2.9
1200 ^{0}C	1.0	4.9

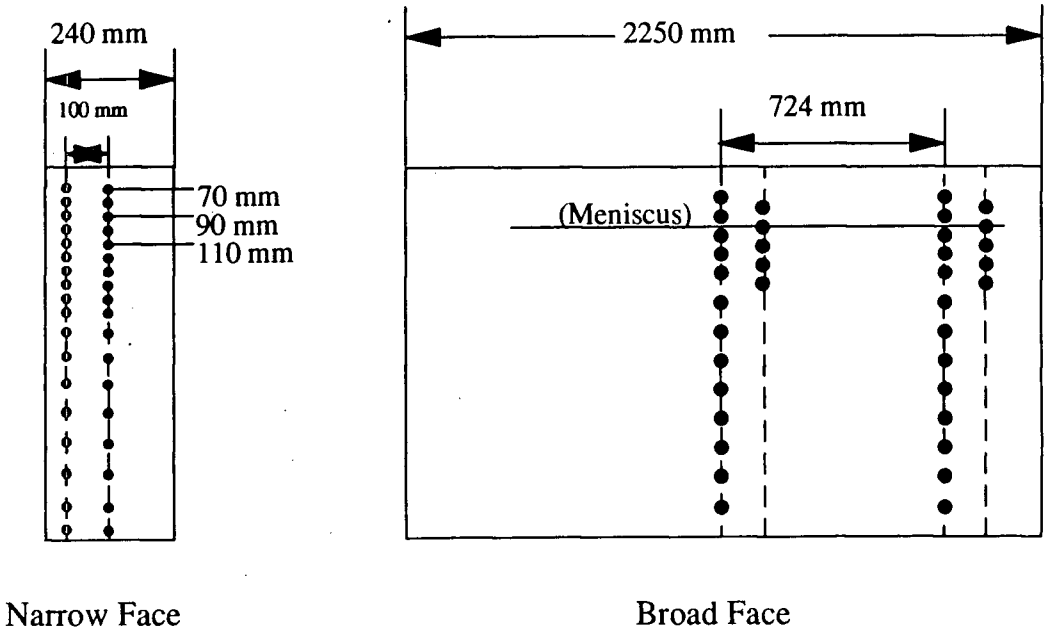

Figure 5.1. Schematic drawing showing the arrangement of the thermocouples on the broad and the narrow faces

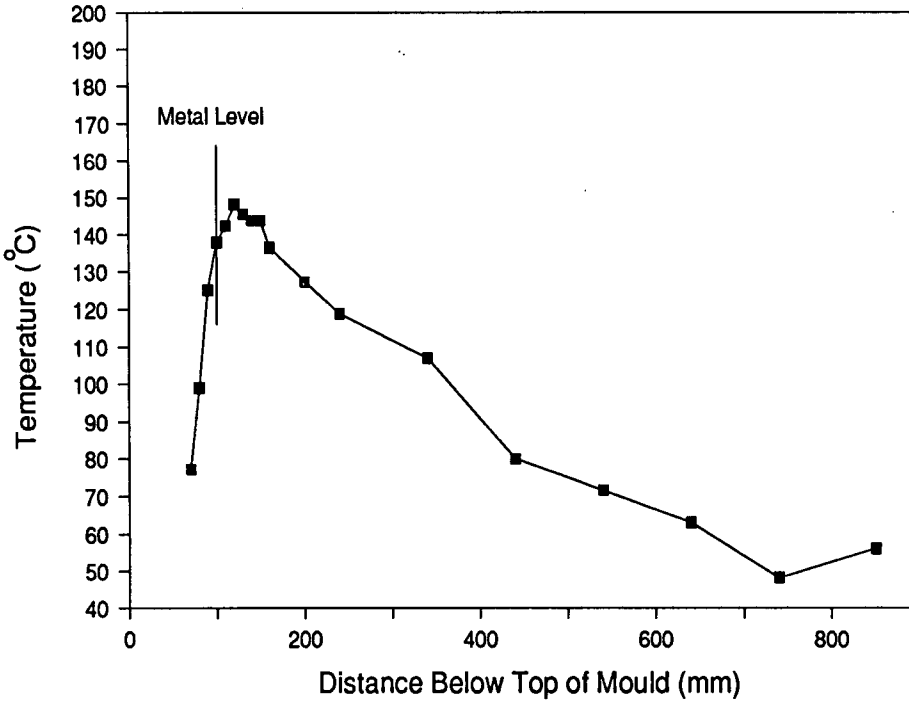

Figure 5.2. Axial temperature profile along the centreline of the narrow face.

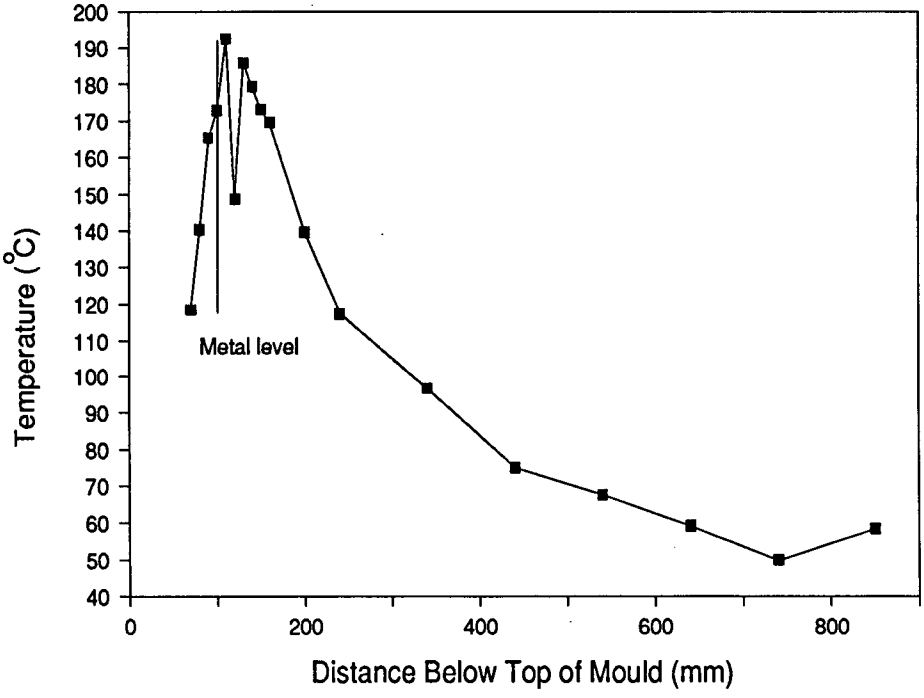

Figure 5.3. Axial temperature profile near the corner of the narrow face.

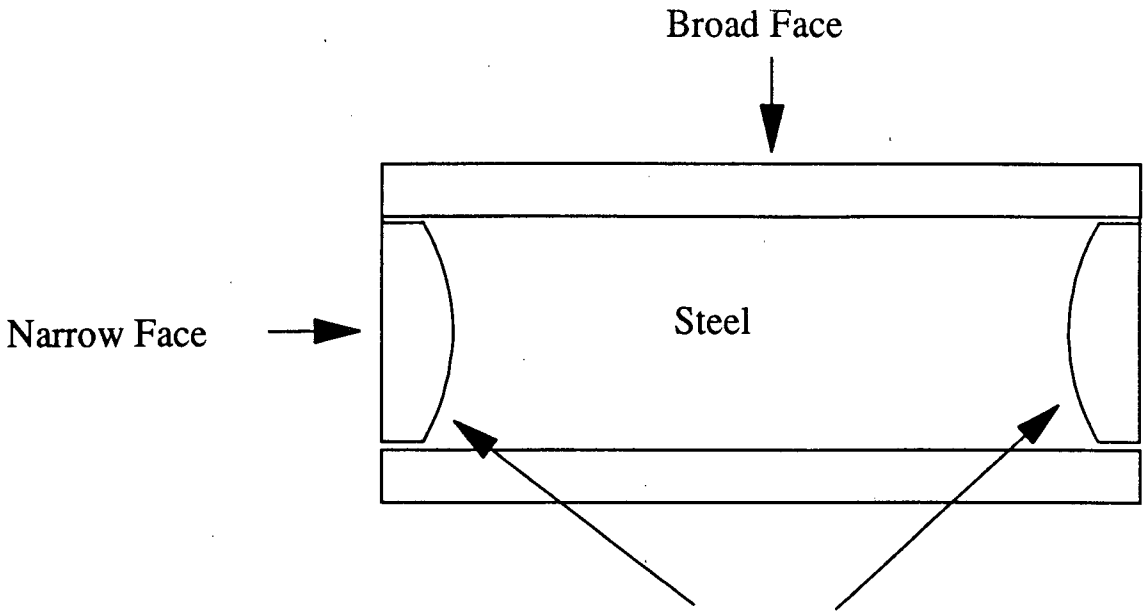

Figure 5.4. Schematic drawing depicting the curvature of the narrow face copper plate at the hot face.

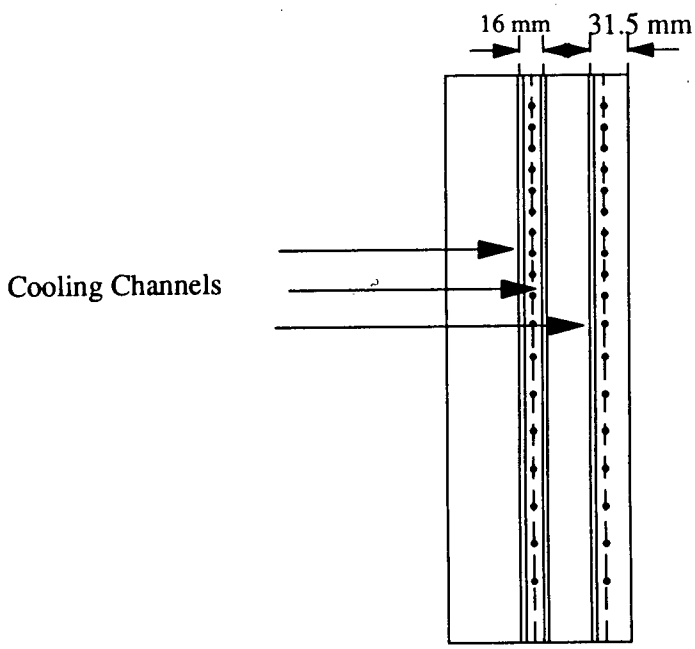

Figure 5.5. Schematic drawing comparing the location of the cooling channels near the corner and centre of the narrow face.

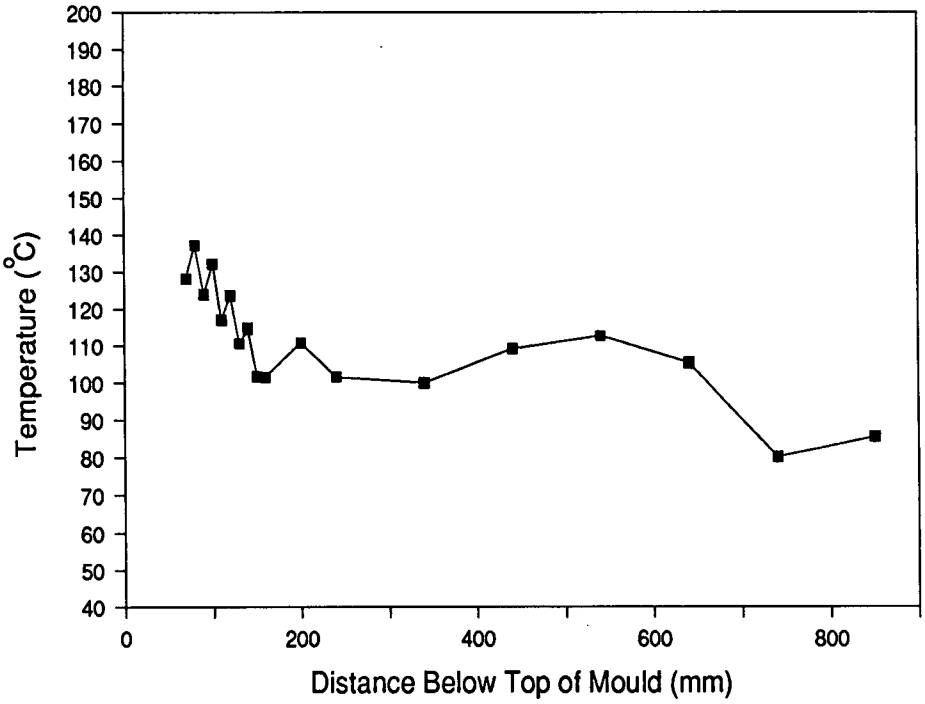

Figure 5.6. Axial temperature profile along the centreline of the road face.

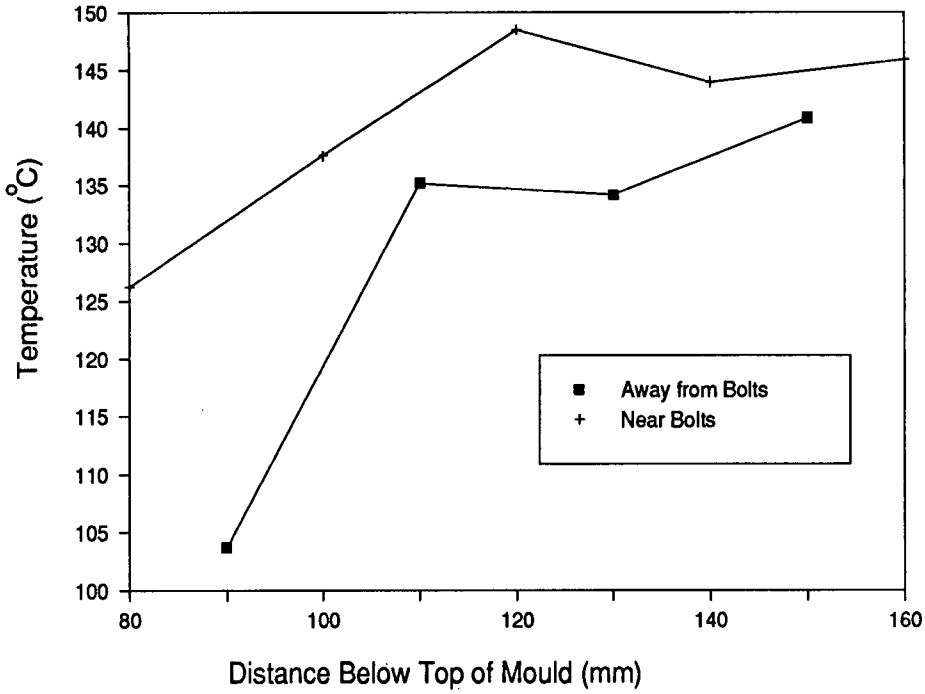

Figure 5.7. Comparison of the temperature of the mould wall in the vicinity of the bolts (inside radius centre)

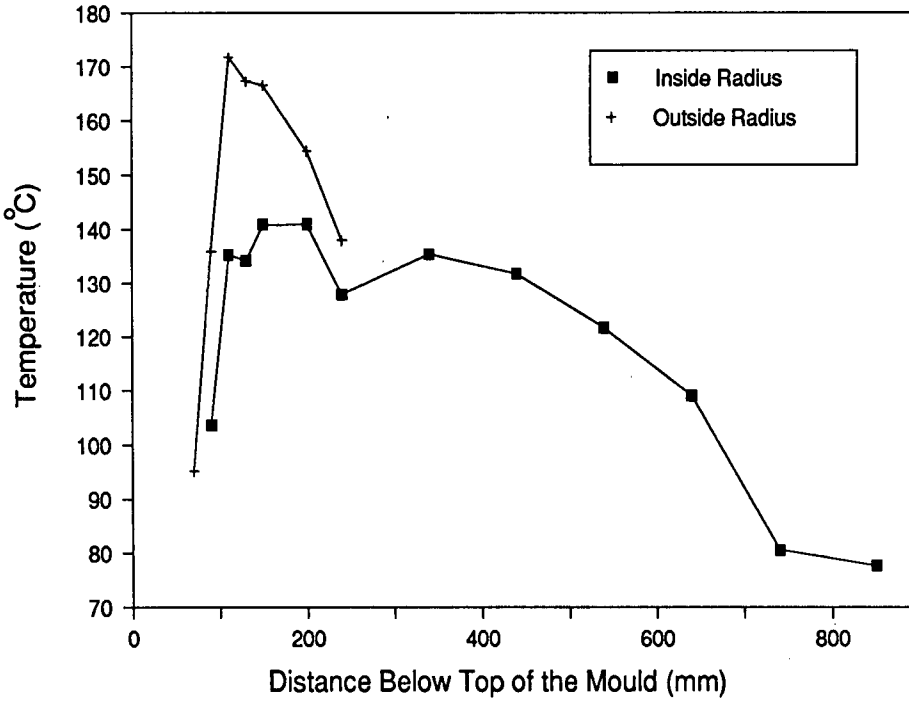

Figure 5.8. Comparison of the axial temperature profiles measured on the inside and outside radius copper plates (centreline).

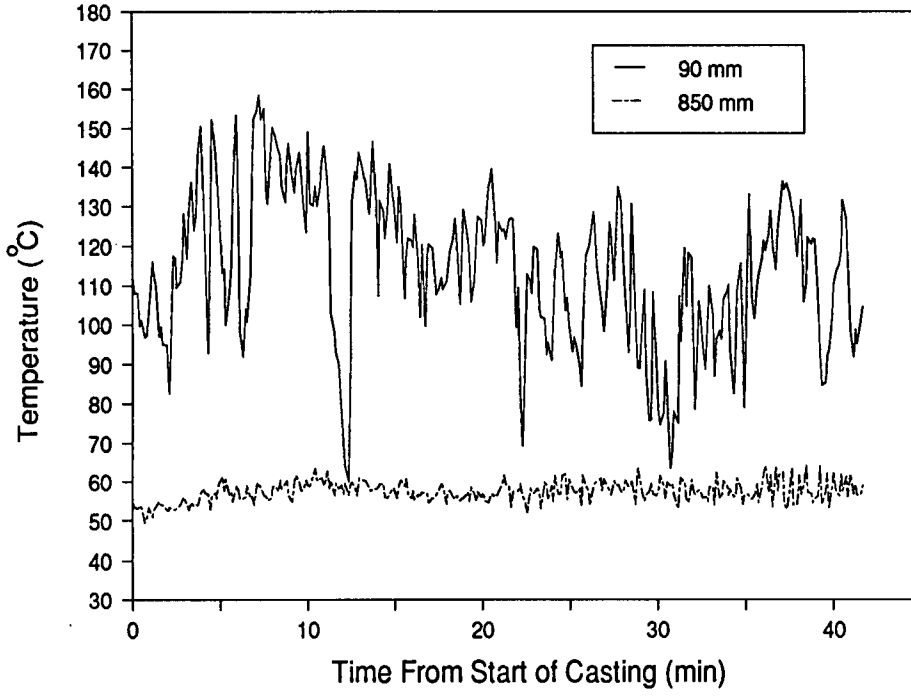

Figure 5.9. Measured temperature of the mould wall (narrow face) at 70 and 850 mm from the top during casting.

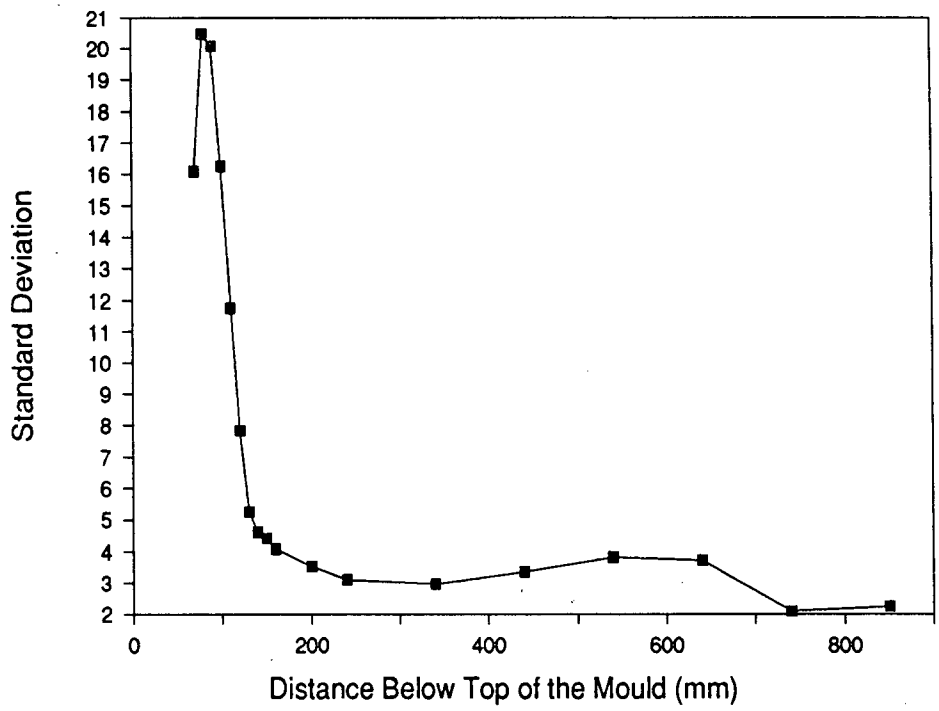

Figure 5.10. Standard deviation of the temperature measurements made at different locations on the narrow face.

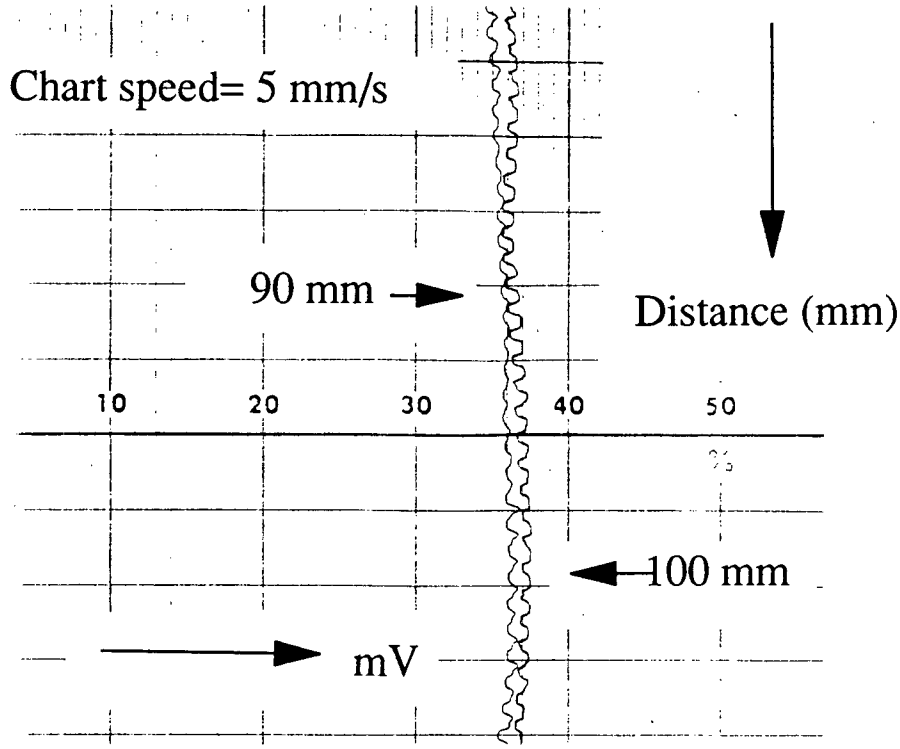

Figure 5.11. Variation of the mould temperature on the narrow face at 90 and 100 mm from the top of the mould obtained from the chart recorder measurements.

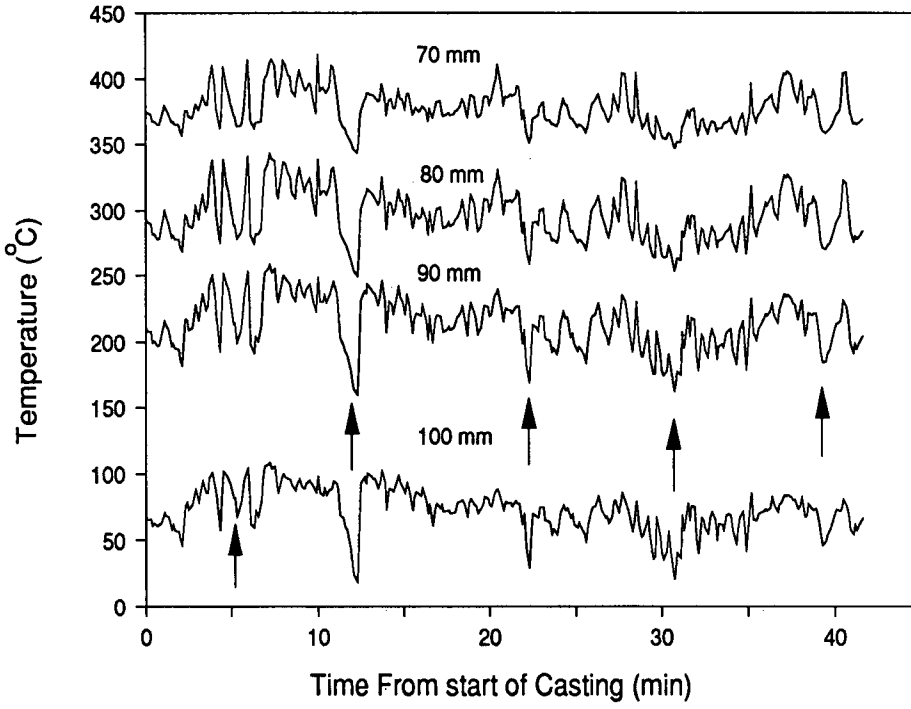

Figure 5.12. Variation of the temperature of the mould on the narrow face near the meniscus at 70, 80, 90, 100 mm from the top of the mould.

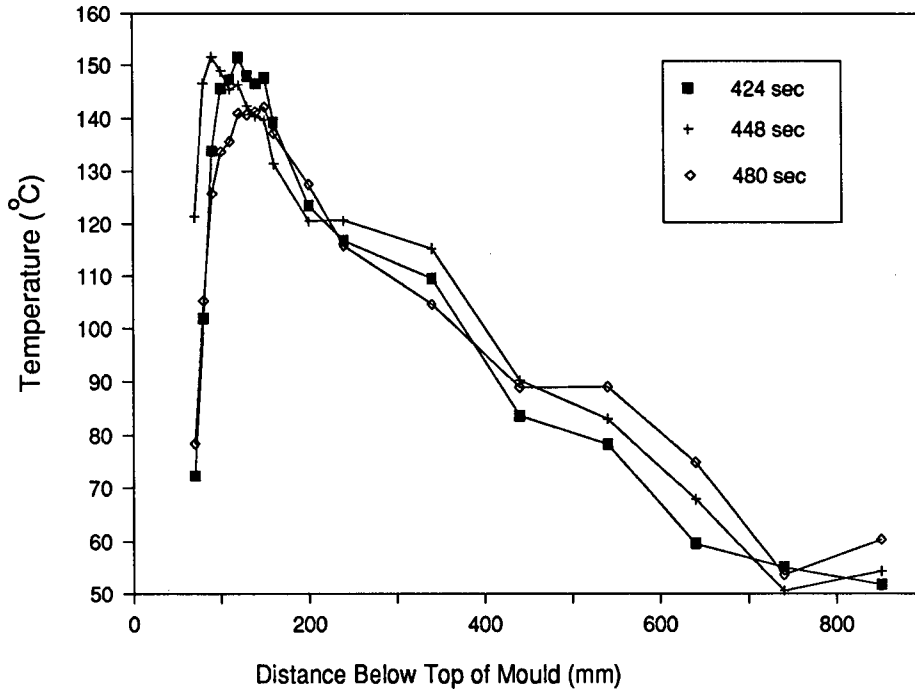

Figure 5.13. Axial mould-temperature profiles on the narrow face at three different times.

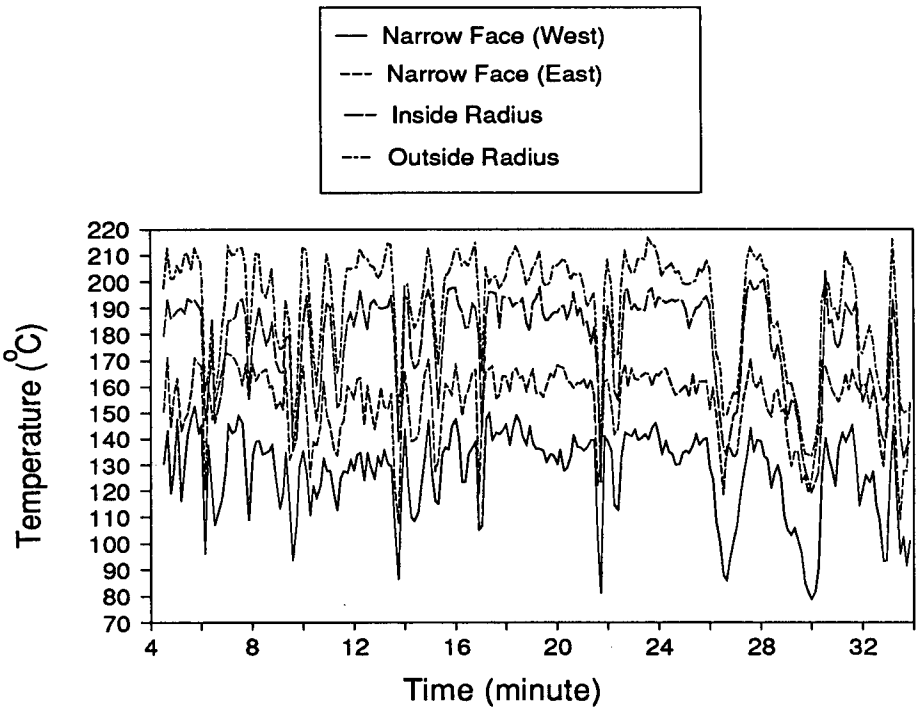

Figure 5.14. Temperature response of four thermocouples located at 100 mm from the top of the mould at the centreline of inside radius, outside radius and the two narrow faces.

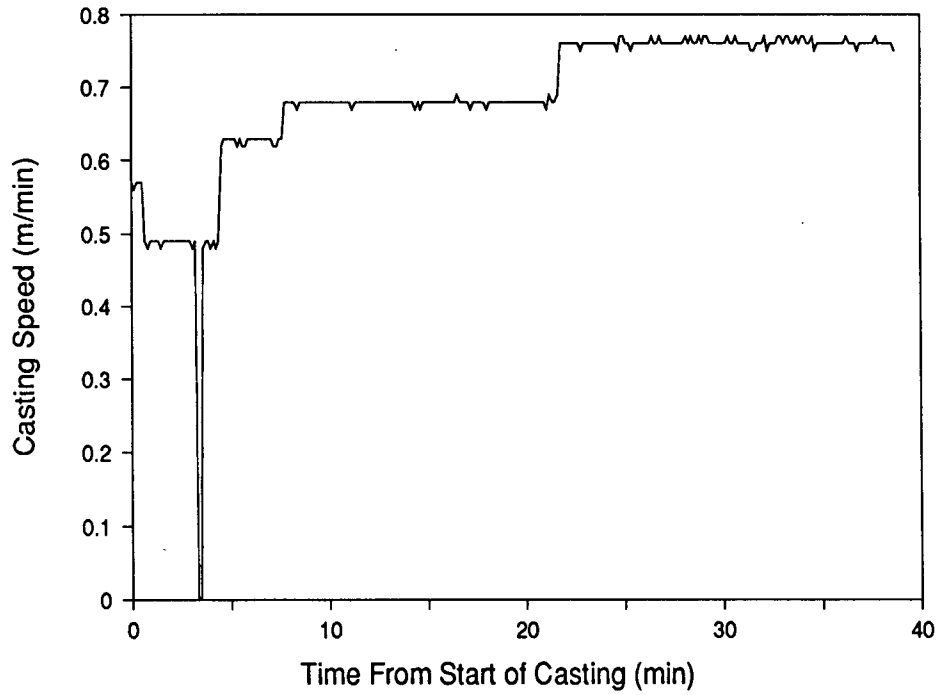

Figure 5.15. Typical example showing variation of casting speed with time in a heat.

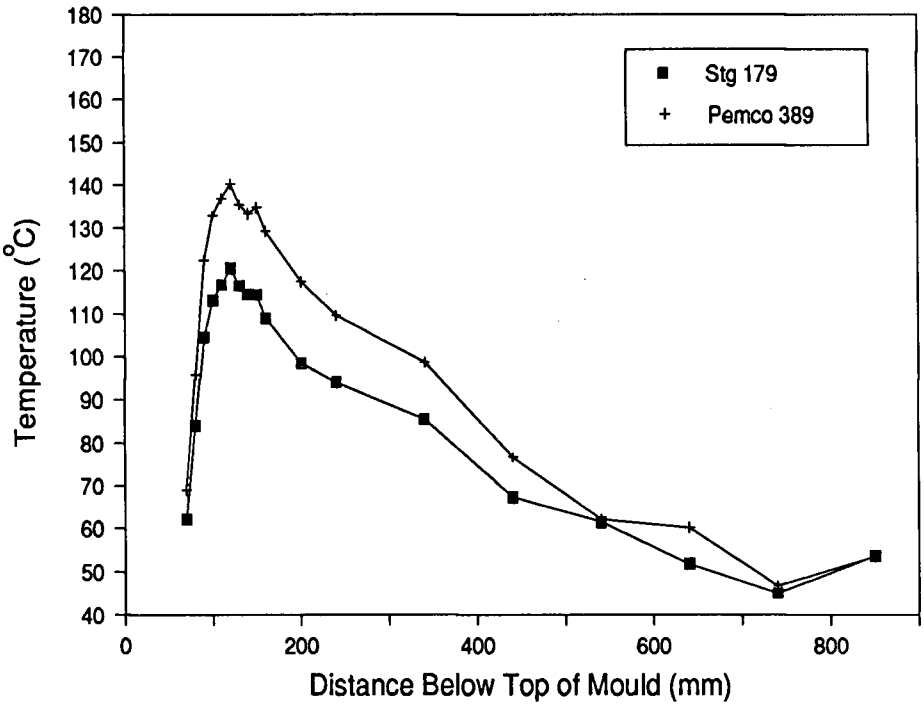

Figure 5.16. Influence of the type of mould flux on the axial mould-temperature profile.

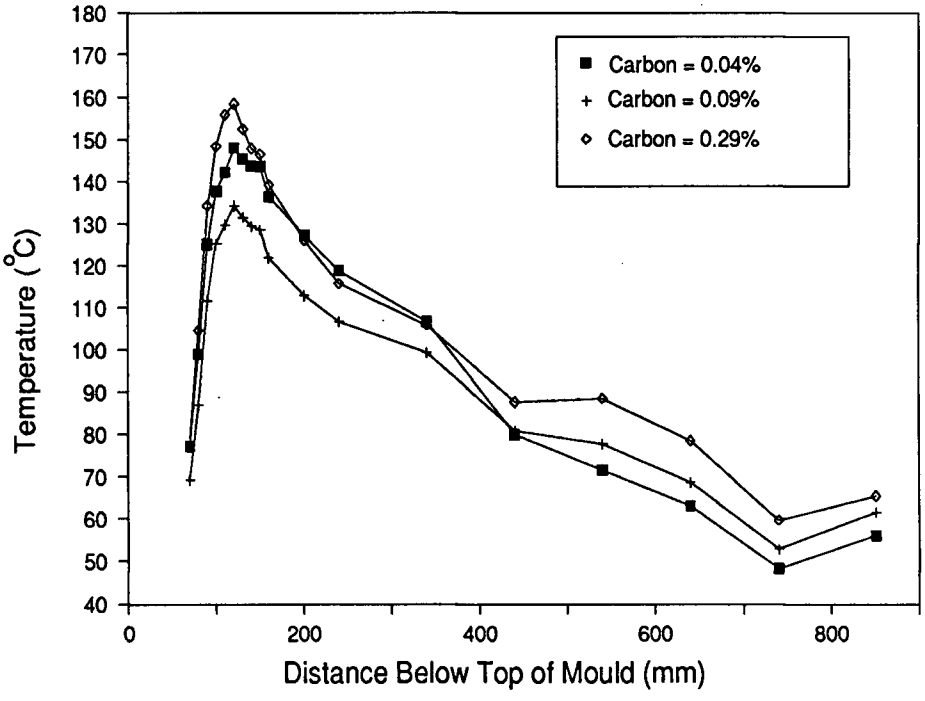

Figure 5.17. Influence of the steel carbon content on the axial mould-temperature profile with Pemco 389 mould flux.

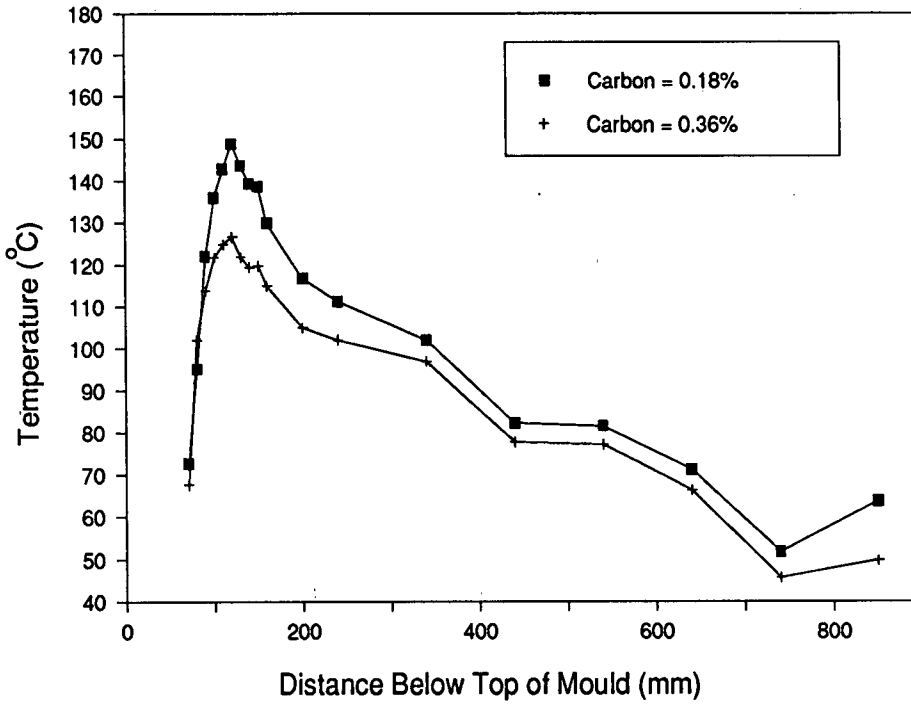

Figure 5.18. Influence of the steel carbon content on the axial mould-temperature profile with stg 179 mould flux.

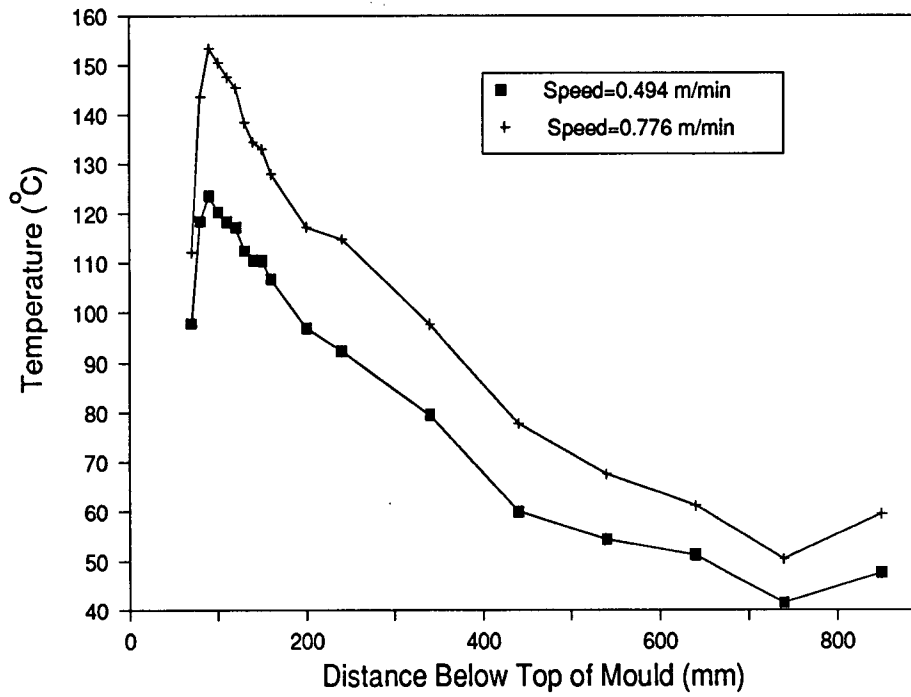

Figure 5.19. Influence of casting speed on the axial mould-temperature profile on the narrow face

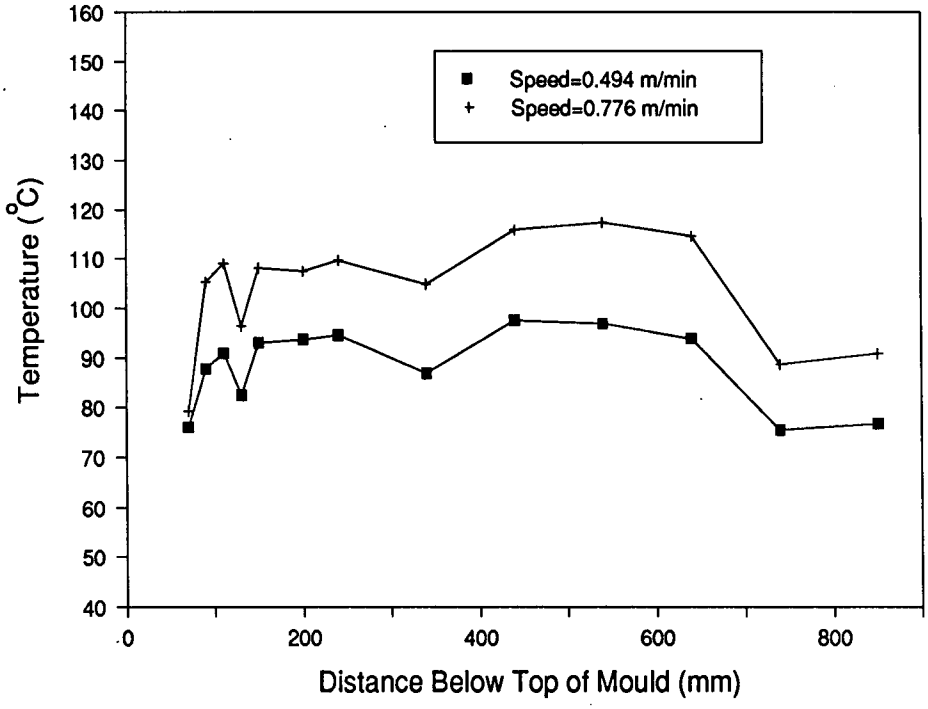

Figure 5.20. Influence of casting speed on the axial mould-temperature profile on the broad face.

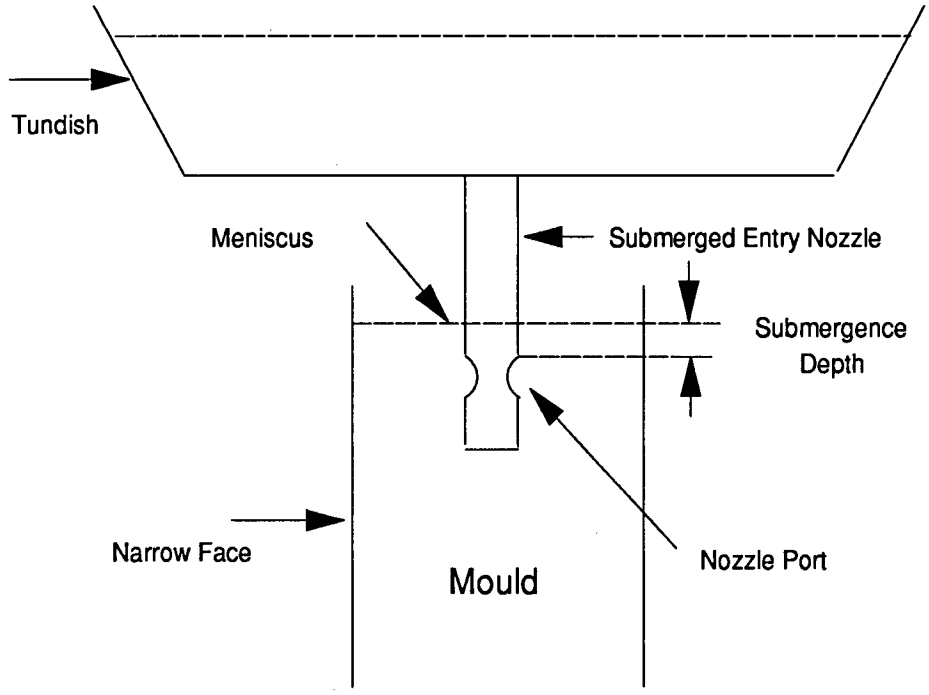

Figure 5.21. Schematic drawing showing the pouring of steel from the tundish into the mould through a submerged entry nozzle.

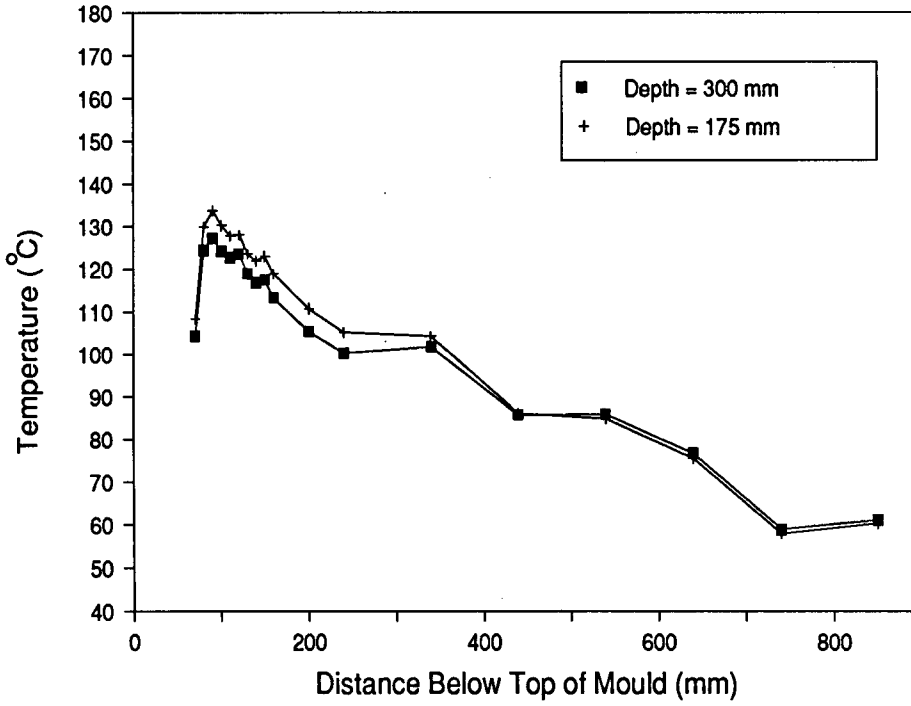

Figure 5.22. Influence of the submergence depth on the axial mould-temperature profile on the narrow face (movable) located at a distance of 900 mm from the submerged entry nozzle.

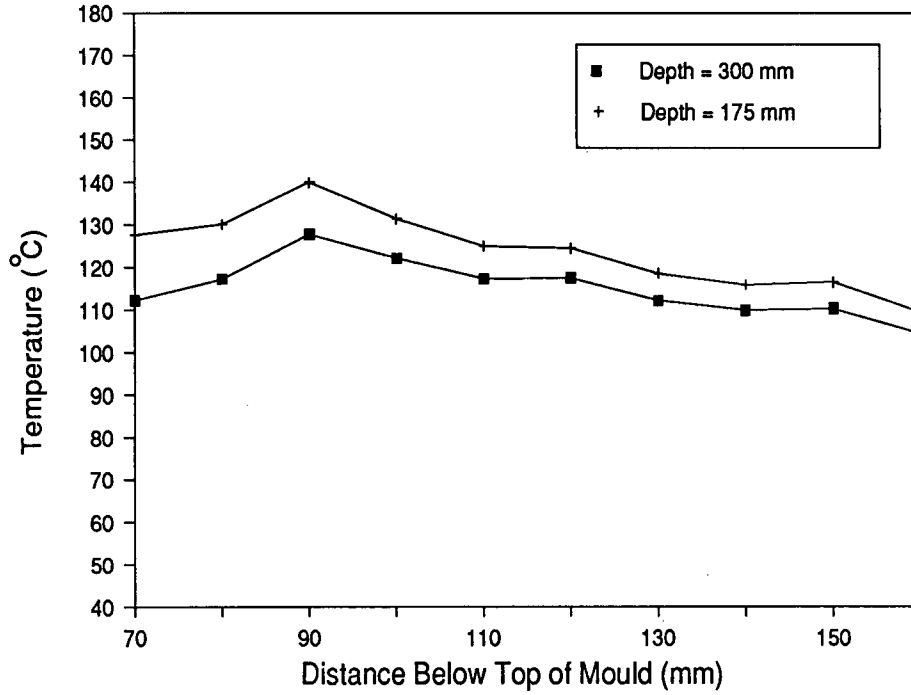

Figure 5.23. Influence of the submergence depth on the axial mould-temperature profile on the narrow face (fixed) located at a distance of 770 mm from the submerged entry nozzle.

Chapter 6 - MOULD HEAT TRANSFER

The mould temperature data reflecting the influence of a wide range of process variables on the heat transfer in the mould has been reported in the previous chapter. The insight gained on mould heat transfer from this data is qualitative at best and inadequate from the standpoint of making changes to mould design and operating practice that would yield consistent improvement in the final product quality. Furthermore some of the observations made in the measured mould temperatrure data such as the differences in the mould temperature between inside radius and outside radius (Fig. 5.8), non-uniformity in the mould temperatures near the bolts (Fig. 5.7) cannot be explained without a quantitative description of the mould heat transfer. Thus, a mathematical model of the mould wall has been developed to characterize the heat transfer rates in the mould quantitatively from the mould temperature data.

The thermal field in the copper plates particularly the temperature of the copper adjacent to the cooling channel governs the occurrence of nucleate boiling in the channel which is not desirable [139]. Moreover, a knowledge of the thermal field in the mould wall is essential to the characterization of its thermomechanical behaviour. It should be noted that a quantitative knowledge of the heat extraction rates in the mould will be useful in determining the thermal field throughout the copper plate. It is also important to characterize solidification of steel and the mould flux behaviour quantitatively because these phenomena strongly influence the quality of the slab; for this information the heat fluxes in the mould is required.

This chapter is devoted to the quantitative characterization of the heat extraction rates in the mould from the mould temperature data. As mentioned earlier, a

mathematical model of the mould wall has been developed and thus the details of the model will be presented. Furthermore, the influence of a number of process variables on the heat transfer in the mould also will be elucidated.

6.1 Development of the Mathematical Model of the Slab Mould

The principle mode of heat flow in the copper plate is conduction in the through thickness direction which has the smallest thermal resistance. Thus steeper temperature gradients are established through the thickness than in the other two directions. The exception is the region of the metal level which is usually located at a distance of 75 to 100 mm from the top of the mould. Above the meniscus the mould wall is relatively cold which leads to the establishment of steep axial temperature gradients. Therefore, at the meniscus there is also a significant axial component of heat flow as demonstrated by Samarasekera et al. [122]. It has been stated earlier that the mould wall is cooled by water flowing through a large number of cooling channels shown schematically in the transverse section of the copper plate as shown in Fig. 6.1. These cooling channels are located at fixed intervals and this arrangement can result in heat conduction along the width of the copper plate. Therefore, to accurately characterize heat flow in the mould wall, a three-dimensional model is required.

The temperature distribution in the mould wall is governed by the heat transfer from the shell to the mould, heat conduction in the mould wall and on the rate of heat extraction from the mould by the cooling water. The validity of the heat flow model is largely governed by the accuracy of the boundary conditions employed in the model to characterize the heat transfer rates at the cold face and hot face of the mould wall. In the present model, the relevant boundary condition to describe the convective heat transfer at the cold face of the mould wall was determined from available correlations in the literature. Needless to say, the heat transfer from the shell to the mould wall is complicated due to the presence of a gap and therefore has not been well quantified. Thus, quantification of the boundary conditions at the hot face, namely the heat transfer

from the solidifying shell to the mould wall was the main objective of the model. This was accomplished by a trial-and-error method in which the hot face heat-flux profile was adjusted in successive computer runs until the model-predicted temperatures agreed with the time-averaged measured temperatures.

It should be noted that the necessity of a trial-and-error procedure for the calculation of the heat fluxes at the hot face resulted in high computing costs particularly with the employment of the three-dimensional model of the mould wall. The initial assumed heat-flux profile was crucial because the number of iterations required to achieve the final solution was dependent on it. Hence a two-dimensional heat flow model of the mould wall was used to calculate the heat-flux profiles at the hot face which then was subsequently utilized as an initial guess for the three-dimensional model. Besides, the intention was also to examine the influence of different types of heat flow models of the mould wall on the computed heat-flux profiles. In the following sections, the salient features of the different models developed for the mould wall will be presented.

6.2 Two-Dimensional Model of the Mould Wall

6.2.1 Transverse Model

A two-dimensional model of the mould wall was developed to predict the thermal field in a transverse section of the copper plate as shown in Fig. 6.1. It should be noted that a similar model has been employed by Nakai et al. [29] to calculate the heat extraction rates in the mould. In this model, the direction of heat conduction was taken to be along the width and through the thickness of the copper plate; heat conduction down the length of the mould wall was neglected. Owing to the uniform spacing between the cooling channels, it was assumed that the heat flow is symmetrical across the centrelines AB and CD and therefore, calculations were performed only over the slice ABCD (Fig. 6.1). An explicit type finite-difference technique was employed to compute the temperature distribution; the details of input parameters utilized in the model are given in Table 6.1. A typical example of the predicted thermal field is shown in Fig. 6.2. Thus, it

is evident that the isotherms are parallel near the hot face so that the heat conduction in this region is locally uni-dimensional through the thickness of the copper plate. However, the curvature of the isotherms in the proximity of the cooling channel reveals the occurrence of two-dimensional heat flow. This model has been utilized at different locations along the length of the mould wall to back calculate the heat fluxes which will be presented in a later section.

6.2.2 Longitudinal Model

The mathematical model describing heat flow in a billet mould wall developed by Samarasekera and Brimacombe [122] has been utilized to estimate the axial heat-flux profiles. It should be noted, however, that the model is two dimensional and predicts the temperature distribution in the longitudinal plane of the mould wall as shown in Fig. 6.3 neglecting the transverse heat flow. Utilization of this model for calculating heat fluxes in the slab mould requires some degree of caution owing to the differences in design between the slab and billet mould. This can be better understood from Fig. 6.1 which is a schematic representation of a transverse section of a copper plate of the slab mould. It should be noted that the model of Samarasekera and Brimacombe [122] is only applicable to the plane through AB located at the centreline of the cooling channel since, by symmetry, there will be no heat flow perpendicular to this plane provided the hot-face heat flux is constant across the face. To back-calculate the heat fluxes utilizing this model, a knowledge of the temperature of the mould wall at several axial locations in the plane AB is required. In the present study, however, the mould temperature measurements were made at several locations on the longitudinal plane passing through CD (dark circle in Fig. 6.1). Consequently, it was necessary to examine the temperature predictions made by the transverse model to establish the applicability of the model of Samarasekera and Brimacombe [122] to the present study.

The temperature predictions for a transverse section are shown in Fig. 6.2 and clearly, the temperature of the mould wall near the hot face is the same in longitudinal

sections passing through AB and CD (Fig. 6.1). Therefore, it can be said that a thermocouple located on either longitudinal plane AB or CD would measure the same temperature provided it was located near the hot face. Since the temperature measurements of the mould were made 6 mm from the hot face; based on the above rationale it is appropriate to use the two-dimensional model of Samarasekera and Brimacombe [122] in the longitudinal plane AB in conjunction with the measured mould temperatures in the plane passing through CD (Fig. 6.1) to calculate the axial heat-flux profiles in the mould. The results obtained from this model will be presented later. It may be noted that Pozhivanov et al. [120] have used a two-dimensional longitudinal model to calculate the heat fluxes in a slab mould.

6.3 Three-Dimensional Model of the Mould Wall

A three-dimensional, heat-flow model of the slab mould wall which considers heat conduction through the thickness and over the width and the length of the copper plate was developed. It should be noted that a three-dimensional model has not been employed in the past to calculate the heat transfer rates in the mould. A photograph of one of the copper plates used in the trials is shown in Fig. 4.2 where it can be seen that the cooling channels are uniformly spaced except near the bolt holes. The depth and width of the cooling channels, the distance between two consecutive cooling channels on the narrow face and broad face copper plates were shown previously in Fig. 4.4. Longitudinal slots were machined into the copper plate between cooling channels to facilitate thermocouple placement; the slots can be seen in the photograph of an instrumented copper plate shown in Fig. 4.9. The dimensions of the slots are shown in the schematic drawing of the copper plate in Fig. 6.4. It may be noted that in addition to the differences in the length between the top and the bottom slots, the depth of the slots were different; namely the depth of the top slot was 12 mm compared to the bottom slot which was 4 mm. As mentioned earlier, the thermocouple wires were laid along the slot prior to their exit from the water jacket as shown in Fig. 6.5. It is important to note that the "medium" in the slot consisted of

thermocouple wires without a flow of cooling water.

It was important to examine the effect of the slot on the mould temperatures in order to establish whether or not the slots should be incorporated into the model. This was accomplished by utilizing the two-dimensional (transverse) model to calculate the mould temperature in a transverse section through the copper plate in the presence and absence of a slot as shown schematically Fig. 6.6. It should be noted that the slot boundary (Fig. 6.6a) was assumed to be adiabatic and the input data employed in the calculations are given in Table 6.2. Fig. 6.7 is a plot of the temperature of the copper plate at different distances from the hot face along the line AB (Figs. 6.6a and b) in the presence and absence of the slot. It is evident that the presence of a slot leads to a higher copper plate temperature and thus, it was necessary to include the slot in the model. It is worthwhile to point out that the presence of the slot on the copper plate furthermore justifies on the requirement of a three-dimensional model of the mould wall.

There was a significant difference in the thickness of the copper plates employed on the narrow face, inside radius and outside radius of the mould which is shown in Fig. 4.1. Furthermore, the broad face copper plates were curved at the hot face. Therefore, in order to incorporate the differences in the geometry of these copper plates, it was essential to develop three separate models. However, the underlying principles involved in the formulation of these models were same. It should be noted that the temperature measurements of the copper plate have been made exclusively at the mid-face and near the corner and, thus, owing to a lack of measurements along the width of the copper plate, the mathematical model has been formulated to calculate the heat fluxes only in the vicinity of the thermocouple measurements. The slots are located at equal distances from the two cooling channels (Fig. 6.4) and it is assumed that the heat flow is symmetrical across the longitudinal centreplanes in the slot and the cooling channel (planes perpendicular to the dashed lines in Fig. 6.4) and therefore, only half the width of the

cooling channel and the slot is considered in the model. The region of the narrow face, inside radius and outside radius copper plates over which calculations have been performed is shown schematically in Fig. 6.8.

In the subsequent sections, the assumptions made in the formulation of the model, the mathematical description of heat flow and finally the technique used to solve the governing differential equations will be discussed.

6.3.1 Assumptions

The following assumptions have been made in the heat flow model.

(i) The mould is at steady state and this assumption will be validated in a later section by examining the occurrence of the nucleate boiling in the cooling channel which is known to result in large variation of the mould wall temperature with time.

(ii) The mould is considered to be stationary. It has been shown in a previous chapter that the influence of the mould oscillation on the variation of the mould wall temperature near the meniscus is small and furthermore, the exact magnitude of the mould wall temperatures during each oscillation cycle is not known. Therefore, it was not worthwhile to consider the mould oscillation in the model.

(iii) The total length of the cooling channel is about 94 percent of the length of the copper plate and thus, it is assumed that the cooling channel extends from the top to the bottom of the copper plate. This assumption is expected to result in small errors owing to the fact that the regions of the mould wall not exposed to water cooling is small and moreover, the heat fluxes in these regions are quite low (only near the top and bottom of the copper plate).

(iv) The top and bottom surfaces of the copper plate, the surfaces of the slot and the surface at the back of the copper plate attached to backup plate are considered to be adiabatic.

(v) The water in the cooling channel is in plug flow and the heat transfer coefficient at the mould/water interface is constant throughout the length of the mould. The justification of the empirical correlation utilized to determine the heat transfer coefficient will be discussed later.

(vi) The heat transfer from the cooling water to the backing plate is negligible.

(vii) Thermal conductivity of copper is constant. This assumption will be validated later by comparing the thermal field in the mould wall computed both from a constant and a temperature dependent thermal conductivity.

6.3.2 Mathematical Description of Heat Flow in the Mould Wall and Cooling Water

The differential equation governing heat conduction in the mould wall in rectangular co-ordinates, under steady state conditions, is given by,

$$\frac{\partial^2 T_m}{\partial x^2} + \frac{\partial^2 T_m}{\partial y^2} + \frac{\partial^2 T_m}{\partial z^2} = 0 \qquad (6.1)$$

The cooling water is assumed to be in plug flow and therefore, the governing equation describing the heat transfer in the cooling channel is given by,

$$\rho_w c_{pw} u_w w_{ch} t_{ch} \frac{dT_w}{\partial z} - h_w[w_{ch}(T_m(x,y,z) - T_w(z)) + t_{ch}(T_m(x,y,z) - T_w(z))] = 0 \qquad (6.2)$$

6.3.3 Boundary Conditions

The appropriate boundary conditions for solving the differential equations (6.1) and (6.2) are given below (Fig. 6.9).

(i) hot face of the mould wall (ABCD)

$$-k_m \frac{\partial T_m}{\partial x} = q_m(y,z) \qquad (6.3)$$

It is assumed that the heat flux at the centre of the copper plate across its width is uniform. Therefore,

$$q_m(z) = q_m(y,z)$$

(ii) cold face of the mould wall (IJNM)

$$-k_m \frac{\partial T_m}{\partial x} = h_w[T_m(x,y,z) - T_w(z)] \quad (6.4)$$

region of the copper plate attached to the backup plate (KLPO) and the surface of the slot (EFHG),

$$-k_m \frac{\partial T_m}{\partial x} = 0 \quad (6.5)$$

(iii) Plane ABMI, due to symmetry,

$$-k_m \frac{\partial T_m}{\partial y} = 0 \quad (6.6)$$

cold face of the mould wall (JKON),

$$-k_m \frac{\partial T_m}{\partial y} = h_w[(T_m(x,y,z) - T_w(z))] \quad (6.7)$$

(iv) Plane CDGE, due to symmetry and at the surface of the slot (PFHL),

$$-k_m \frac{\partial T_m}{\partial y} = 0 \quad (6.8)$$

(v) bottom surface of the mould wall (ADLK),

$$-k_m \frac{\partial T_m}{\partial z} = 0 \quad (6.9)$$

(vi) top surface of the mould wall (BCPO),

$$-k_m \frac{\partial T_m}{\partial z} = 0 \quad (6.10)$$

(vii) inlet temperature of cooling water

$$z = 0, \quad T_w(z) = T_{iwat} \quad (6.11)$$

6.3.4 Solution of the Differential Equations

A complete mathematical description of heat flow in the mould wall and the cooling channel is expressed by Equations (6.1) and (6.2) which were solved numerically with the relevant boundary conditions (6.3) to (6.11) by employing a finite difference

technique. In the finite-difference scheme, the mould wall is divided into a large number of nodes and the present configuration of the mould wall resulted in 50 different types of nodes. The finite-difference equations were derived by performing heat balances on each of the control volumes. It should be noted that each node resulted in one equation and thus, the complete set of simultaneous equations are to be solved to compute the temperature in the mould wall. An over-relaxation method was selected to solve the equation governing the heat flow in the mould wall. In this technique, an initial approximate solution is assumed and then, an iterative scheme is utilized to determine the final solution.

The temperature distribution in the mould wall was computed by assuming that the temperature of the cooling water at different locations in the cooling channel intially varied linearly between the inlet and outlet temperatures of the water. Thereafter, heat balances were performed on the cooling water to recalculate its temperature which was subsequently utilized to calculate the mould wall temperature and this procedure was carried out until convergence was reached.

6.3.5 Input Data to the Model

6.3.5.1 Mould Wall Dimensions

The thickness of the copper plate was measured in the plant prior to its instrumentation with thermocouples. In addition to the copper thickness, the dimensions of the cooling channels and the slots were also measured. These measurements were carried out on each of the four plates. The relevant dimensions of the copper plates employed in the model are given in Tables 6.3a and 6.3b

6.3.5.2 Thermal Conductivity of Copper

The variation of the thermal conductivity of copper with temperature [140] is shown in Fig. 6.10. As mentioned earlier, a constant value of thermal conductivity has been assumed in the model and, thus, it will be necessary to examine the validity of the assumption which will be discussed later.

6.3.5.3 Heat-Transfer Coefficient at the Mould Wall/Cooling Water Interface

Heat transfer between the mould wall and the cooling water takes place by forced convection which has been characterized with the aid of a heat-transfer coefficient determined from the following dimensionless correlation [136],

$$\frac{h_w D_H}{k_w} = 0.023\left(\frac{\rho_w u_w D_H}{\mu_w}\right)^{0.8}\left(\frac{c_{pw}\mu_w}{k_w}\right)^{0.4} \qquad (6.12)$$

The above correlation is applicable only in the absence of nucleate boiling in the cooling channel. It should be noted that the occurrence of nucleate boiling is governed by the temperature of the copper adjacent to the water in addition to the saturation temperature of the cooling water. Therefore, in order to examine the possibility of presence of boiling, it is necessary to have a knowledge of the temperature of the copper at the cooling channel, which is currently not known. The temperature distribution in the mould can be assesed only after the heat fluxes are characterized and therefore, the aspect of nucleate boiling will be addressed later. The heat transfer coefficient is also strongly governed by velocity of water and in a later section the influence of variation of water velocity on the model predictions will be examined.

Furthermore, it may be noted that near the entrance region of the cooling channel the flow is not expected to be fully developed which can affect the heat transfer coefficient. It has been reported that in the case of flow through a pipe the length required to establish a fully developed flow is approximately equal to 20 times the hydraulic diameter of the pipe [137]. Based on this rationale, in the present case, the flow may not be fully established within a region which is approximately 25% of the length of the cooling channel. However, it was intimated earlier that the entrance is located at the bottom as the direction of the water flow is from bottom to the top of the mould and thus, only near the bottom of the mould the flow may not fully established. Therefore, the entrance effect will not affect the boundary conditions near the meniscus and

consequently the predictions of the heat fluxes in the upper region of the mould particularly near the meniscus which is of prime importance to this study will not influenced.

Besides, the employment of the correlation Eq. (6.12) depends on the following conditions.

(i) $0.7 < Pr < 120$

(ii) $10000 < Re < 120000$

(iii) $\frac{L}{D_H} > 60$

Calculations were performed to ensure that the above criteria were met and the results from the calculations are listed in Table 6.4. Thus, Equation (6.12) has been utilized to characterize the heat-transfer coefficient with the assumption that there is no boiling in the cooling channel.

6.3.6 Sensitivity Analysis

6.3.6.1 Node Size

The size of the nodes employed in the finite-difference mesh is very crucial from the standpoint of accuracy of the solution. In order to ascertain the appropriate node size, the temperature of the mould wall has been calculated for different mesh sizes; the effect of the total number of nodes on the axial temperature profile at the face is shown in Fig. 6.11. Thus, it is evident that beyond a total of 5733 nodes, the mould temperatures did not change with further refinement in the mesh size. The dimensions of the finite-difference nodes employed in the model were 4 mm along the x (thickness), 1 mm along the y (transverse) and 10 mm along the z (longitudinal) directions (Fig. 6.9).

6.3.6.2 Thermal Conductivity of Copper

As mentioned earlier, the thermal conductivity of copper has been assumed to be independent of temperature and its value at 127^0C has been employed in the calculations. However, owing to the dependence of thermal conductivity on temperature, calculations

were performed to determine the temperature of the copper plate utilizing a temperature dependent thermal conductivity as shown in Fig. 6.10. The calculated mould temperature for the two cases is given in Table 6.5. Clearly, the difference in the mould temperature is negligible and hence it was decided that a constant value of thermal conductivity of copper was adequate for the calculations.

6.3.7 Application of the Mathematical Model of the Mould Wall

6.3.7.1 Calculation of Heat-Flux Profiles in the Mould From the Measured Mould Temperature Data.

The major objective of the model was to calculate the heat-flux profiles in the mould from a knowledge of the measured values of the mould temperature. The back calculation of the heat fluxes in the mould will be illustrated with an example. A measured axial mould-temperature profile is given in Fig. 6.12. The heat-flux profile was calculated by assuming a heat-flux profile at the hot face and then computing the temperature distribution in the copper plate which was compared with the measured temperature. The procedure consisted of an iterative scheme in which the heat-flux profile was varied until there was a good agreement between the model predicted and the measured temperatures. It may be noted that in these calculations it was assumed that the meniscus level is at 100 mm from the top of the mould which was 20 mm above the location of the maximum mould temperature. For the axial mould-temperature profile shown in Fig. 6.12, the heat-flux profile calculated from the three-dimensional model is shown in Fig. 6.13 and a comparison of the model predicted and measured mould temperatures is shown in Fig. 6.14. Errors can be introduced in the estimate of the heat fluxes as a result of inaccurate measurements of mould temperature and therefore, it was essential to conduct an error analysis which is reported in Appendix I.

6.3.7.2 Comparison of Heat-Flux Profiles Calculated by Two and Three-Dimensional Models of the Mould Wall

The axial heat-flux profiles have been calculated for the mould temperature data as shown in Fig. 6.12 using the three different heat flow models of the mould wall (The two-dimensional model of the transverse plane, the two-dimensional model of the longitudinal plane and the three-dimensional model) and the results are shown in Fig. 6.15. Comparison of the heat fluxes calculated by the two-dimensional transverse and the three-dimensional model reveals that the differences in the magnitude of the heat fluxes for the two cases is largest near the meniscus relative to the other regions of the mould; also the location of the maximum heat flux is not same. The lower values of the heat fluxes calculated by the two-dimensional transverse model is a consequence of neglecting the axial heat flow in the model; neglect of the axial heat flow results in a maximum heat flux occurring at the location of the maximum mould temperature. It may be noted that the axial component of heat flow is of larger magnitude in the vicinity of the meniscus [122] and therefore, the differences in the heat fluxes predicted by the two models is largest near the meniscus.

Furthermore, it is also evident from Fig. 6.15 that the two-dimensional longitudinal model also predicts lower values of the heat fluxes when compared to the three-dimensional model, however, the magnitude of the difference in the heat fluxes is quite similar down the length of the mould. The main difference between the two models is in the incorporation of heat flow along the transverse direction in the three-dimensional model, the consequences of which on the mould wall temperature can be better understood by examining the results obtained with simple calculations performed on two copper plates the transverse sections of which are shown schematically in Fig. 6.16. In case I the heat flow is one-dimensional only (through the copper thickness) and in case II the heat flow is two-dimensional (thickness and width); the steady state temperature of the copper plate in case I was calculated using the Fourier's law and the same for the case

II was determined by a heat flow model. Figure 6.17 is a plot of the temperature of the copper plate at different distances from the hot face for identical boundary conditions at the hot and cold faces; it is evident that the temperature of the copper plate in case II is lower than case I. The lower temperature in case II can be explained on the basis that the depth of the cooling channel (20 mm) is large when compared to the spacing between the two consecutive channels (8 mm) (Fig. 6.16) leading to a greater surface area over which cooling occurs. Based on these calculations, it can be inferred that the lower values of the heat fluxes calculated by the two-dimensional longitudinal model is a consequence of neglecting the transverse heat flow resulting from the specific design of the cooling channels in the copper plate. Furthermore, owing to the constant dimensions of the cooling channel along the mould length, the magnitude of the transverse heat flow will be similar along the length of the mould wall and therefore, the differences in the heat fluxes down the length of the mould predicted by the two-dimensional longitudinal and the three-dimensional model is found to be the same.

Based on the above findings it may be concluded that the employment of two-dimensional model of the mould wall (transverse and longitudinal) will result in significant underestimation of the heat fluxes and thus, these models are not adequate for estimating the heat fluxes in the mould. It may be interesting to note that in the past, heat fluxes have been calculated using the Fourier's Law simply by utilizing the differences in the temperature recorded by two thermocouples located at different distances from the hot face and this technique will obviously result in inaccurate predictions. These findings have clearly demonstrated the importance of a three-dimensional model to calculate the heat fluxes in a slab mould from the measured mould temperatures.

6.3.7.3 Influence of the Heat Transfer Coefficient at the Water/Copper Interface on the Heat Fluxes Calculated by the Heat Flow Model

As mentioned earlier, the heat transfer coefficient between the cooling water and copper was characterized with the aid of a heat transfer coefficient determined from

Equation (6.12). It is evident that in addition to the influence of the thermo-physical properties of water, the heat transfer coefficient is also strongly dependent on the velocity of water. But the water velocity in the cooling channel could not be measured during the plant trial and thus was estimated from a knowledge of its flow rate and the dimensions of the cooling channel. It should be realized that theoretical estimation of water velocity by this method requires a knowledge of the cooling channel dimensions and thus, any local variation in the cross-sectional area of the cooling channel can result in an inaccurate estimation of water velocity; thus, the subsequent errors introduced in the estimation of the heat transfer coefficient can affect the model predictions of mould temperatures and consequenlty the heat fluxes predicted by the heat flow model will be influenced. Therefore, it was important to examine the effect of variation in the water velocity on the predicted heat fluxes. This was accomplished by calculating the axial heat-flux profiles for the same mould temperature data (Fig. 6.12); however the water velocity in the heat flow model was varied by 10 percent above and below the nominal value. The corresponding magnitude of the heat transfer coefficients were 20210 $W/m^2{}^0C$ and 17211 $W/m^2{}^0C$ respectively when compared to the nominal value of 18725 $W/m^2{}^0C$. The heat fluxes in the mould at three different locations for different values of the water velocity are shown in Fig. 6.18. The results clearly indicate that a 10 percent error in the theoretical estimate of the water velocity will have a small effect on the variation of the magnitude of the heat fluxes predicted by the model.

6.3.7.4 Occurrence of Nucleate Boiling in the Cooling Channel

The phenomenon of nucleate boiling in the cooling channel is dependent on the temperature of the copper adjacent to the cooling water and also on the saturation temperature of the water under the prevailing pressure. It has been reported that in a billet mould where the exit water pressure is about 240 KPa, boiling can be triggered, when the temperature of the cold face of the mould wall is in excess of 160 ^0C [122]. However, it may be noted that in a slab mould the water pressure is about 900 KPa which is relatively

higher than in a billet mould; the higher value of the water pressure will increase the saturation temperature of water which will further increase the lower limit of the temperature at which boiling initiates. The occurrence of boiling has been examined by calculating the temperature of the mould along the cooling channel from several different heat-flux profiles. As discussed earlier, an increase in the casting speed will result in a significant rise in the mould temperature particularly at the meniscus (Fig. 5.19). Therefore, it is logical to examine the mould temperature at the highest casting speed in order to investigate the occurrence of boiling in the cooling channel. The temperature of the copper adjacent to the cooling channel on the broad face was always lower than the corresponding temperature on the narrow face and this can be attributed to larger copper thickness and higher water velocity in the cooling channels on the broad face (Table 6.4). Thus, the mould temperatures only on the narrow face has been examined and Fig. 6.19 shows the axial mould-temperature profile near the cooling channel on the narrow face at a casting speed of 1.2 m/min. The maximum temperature of the copper plate near the meniscus is approximately 115^0C and is not sufficient to initiate boiling. Needless to say, boiling will lead to periodic fluctuation of the mould temperature and thus, the absence of boiling in the cooling channel of a slab mould justifies the assumption that the thermal fields in the copper plate are at quasi steady state with transients only being caused by metal level fluctuations and also the above finding justifies the use of the empirical correlation to determine the heat transfer coefficient (Eq. 6.12) which is applicable only in the absence of nucleate boiling.

6.3.7.5 Analysis of the Mould Temperatures Measured on the Inside and the Outside Radius Copper Plates

It has been mentioned earlier that the mould temperature on the outside radius was always higher than the same on the inside radius at the same distance from the hot face

(Fig. 5.8). This observation could be attributed to differences in the copper plate thickness between the two plates (Fig. 4.1) or may be a consequence of differences in heat-flux profiles.

The heat-flux profile on the inside radius copper plate was calculated utilizing the model (Fig. 6.8b) from the measured values of the mould temperature for low, medium and high-carbon steel grades and subsequently these heat-flux profiles were employed on the heat flow model of the outside radius copper plate (Fig. 6.8c) to compute the thermal fields to examine the influence of the copper thickness on the mould temperature. Figure 6.20 is a plot of the measured temperatures on the inside and outside radius copper plates, the calculated temperature on the outside radius using the inside radius heat-flux profile for three different grades of steel. It is evident that the thickness differences between the copper plates can not explain the observed differences in the measured temperature between the inside and the outside radius and therefore, the heat fluxes are expected to be different between the two broad faces.

A comparison of the magnitude of the heat fluxes at the meniscus on the inside and the outside radius for low, medium and high carbon grades of steel is shown in Fig. 6.21 and clearly, the heat flux at the meniscus on the outside radius is more than the same on the inside radius for the three different grades of steel. Furthermore, it may be noted that the heat fluxes on the outside radius was also higher than the same on the inside radius below the meniscus. Unfortunately, comparison of heat-flux profile along the entire length of the mould between the inside and the outside radius could not be made since thermocouples on the outside radius were only present near the meniscus. It may be interesting to note that temperature measurements made on a similar type of mould in Luken steel has also revealed the higher mould wall temperature of the outside radius compared to inside radius copper plate [141]. It will be shown later that the differences in heat flux on the two faces is due to the behaviour of the mould flux at the meniscus stemming from the differences in the wall thickness between the two faces and the associated temperature of the mould.

6.3.7.6 Analysis on the Observed Mould Temperatures Near the Bolts on the Broad Face

The plant measurements have shown that the temperature of the copper plate near the bolts was higher than the same away from it as shown in Fig. 5.7. It should be noted that spacing between two consecutive cooling channels in the presence of bolts was higher than the normal spacing. The mathematical model has been utilized to simulate the presence of a row of bolts simply by increasing the distance between the cooling channels. It was possible to calculate the temperature of the copper plate for two cases; one in which the spacing between the cooling channels was more than the other under similar heat flux conditions at the hot face. A comparison of the axial temperature profiles at the hot face for the two cases is shown in Fig. 6.22 and it is evident that with an increase in the spacing between the cooling channels (simulation of the copper plate near the bolts) the temperature of the copper plate is increased. These calculations indicate that the observed increase in mould temperature near the bolts is not due to an increase in heat flux but a consequence of larger spacing between the cooling channels near the bolts.

6.4 Mould Heat Transfer

The heat-flux profiles in the mould have been computed at the mid-face of the broad and narrow faces for different casting parameters, mould flux type and steel grades employing the time-averaged mould temperature data in conjunction with the three-dimensional heat flow model of the mould wall described in an earlier section. An example of a typical heat-flux profile at the centre of the narrow face is shown in Fig. 6.13. Evidently, the heat-flux profile is characterized by the presence of a maximum occurring at the metal level which was 100 mm below the top of the mould and with increasing distance from the metal level there is a decrease in the magnitude of the heat flux. The decrease in the heat transfer rates below the meniscus reflects the increase in the dimension of the gap between the shell and the mould which leads to an

corresponding increase in the resistance to heat flow. It should be noted that the thermal resistances to heat flow in the mould will be quantitatively characterized and its significance will be discussed in the next chapter. The shape of the heat-flux profile obtained in the present study is quite similar to the findings of earlier investigators [46,120,121,127]. However, direct comparison of magnitude of heat fluxes with the values reported in the literature will not be appropriate because the casting conditions for the different cases are not identical and also the technique used to convert the mould temperature into heat fluxes are not the same. Nonetheless, the magnitude of heat fluxes reported in the past [46,120,121,127] are similar to that obtained in the present study. It may be interesting to note that calculations have shown that heat flux at the meniscus in a slab mould varied between 2000 to 3000 kW/m^2 compared to a value of 3000 to 5000 kW/m^2 reported in the case of a billet mould in which oil is employed as a lubricant [6]. These results are in agreement with Riboud et al.[115] who have reported that when oil is used as a lubricant in the mould, the heat extraction in the mould is enhanced compared to the case in which mould flux is the lubricant. It is likely that the higher resistance to heat flow near the meniscus in a slab mould is probably a consequence of the insulating characteristics of the mould flux. Furthermore, the rate of reduction in the heat flux below the meniscus in a slab mould is lower when compared to the observations for a billet mould; in a high carbon steel grade (0.36 percent-carbon), the heat flux drops from 4700 kW/m^2 to 3000 kW/m^2 [6] within 50 mm from the meniscus compared to a corresponding drop 1900 kW/m^2 to 1450 kW/m^2 in a slab mould. The steep reduction in the heat flux in billet mould has been explained on the basis of distortion of the mould in the vicinity of the meniscus which affects the local gap width.

Figure 6.23 is a comparison of the heat-flux profiles at the centreline of the narrow face and the broad face (Inside radius). Evidently, the heat flux is maximum at the meniscus for the two cases. The magnitude of the meniscus heat flux on the narrow face was always higher than the same on the broad face and this observation is probably a consequence of the mould flux behaviour at the meniscus. The molten stream from the

submerged entry nozzle is directed towards the narrow face and consequently, the local temperature of the steel in the vicinity of the meniscus will be more near the narrow face relative to the broad face resulting in lower viscosity of the mould flux and the subsequent increase in the heat transfer. It will be shown later that a decrease in the viscosity of the mould flux will lead to an increase the heat flux. Another major difference between the two heat-flux profiles (Fig. 6.23) is in the reduction of the heat flux below the meniscus; on the narrow face, the drop in the heat flux is steeper compared to the broad face emphasizing on the importance of the taper of the narrow face. It was intimated earlier that a shrinkage of the broad face of the slab will generate gap near the corner by causing it to pull away from the mould wall; the rapid reduction in the heat flux on the narrow face is a consequence of large gap dimensions relative to the broad face. The heat fluxes in the central region of the broad face is fairly constant which is an indication of uniform gap dimensions.

6.4.1 Influence of the Process Variables, Mould Flux, Steel Composition on the Heat Extraction Rates in the Mould

6.4.1.1 Mould Flux

Two different types of mould flux namely, Pemco 389 and Stg 179 were employed in the plant trials and the differences in heat flux associated with the mould fluxes will be examined. The details of the two heats which were selected for this purpose are listed in Table 6.6 and clearly, the casting parameters and carbon content are quite similar. The heat-flux profiles at the centreline of the narrow face for the two types of the mould flux are shown in Fig. 6.24. It is clear the the heat transfer rates in the mould is increased with Pemco 389 when compared Stg 179 and the effect is more pronounced in the upper region of the mould. The physical properties of the two mould fluxes are listed in Table 5.1; Stg 179 mould flux is relatively more viscous when compared to Pemco 389. The softening temperature of the two mould fluxes are quite similar whereas the melting temperature of Stg 179 is higher than that of Pemco 389 (Table 5.1). The present findings

suggest that the viscosity and the melting temperatures of the mould flux are crucial from the standpoint of heat extraction in the mould. The dependence of the mould heat transfer on the viscosity of the mould flux has been reported in the literature [13,99,124] and the results of this study in which an increase in viscosity of the mould flux and the ensuing reduction in the mould heat transfer is in agreement with the findings reported in the literature [99,124]. Furthermore, the finding on the influence of the melting temperature of the mould flux, in which an increase in the melting temperature will lead to a reduction in the heat transfer in the mould agrees with the results reported in the literature [116].

The influence of the properties of the mould flux on the heat transfer in the mould has been explained simply from a knowledge of its viscosity as indicated by the suppliers of the mould flux. For instance, it is a standard practice to consider the viscosity of the mould flux at 1300^{0}C to assess its effect on the heat transfer. But, it is important to note that the viscosity of the mould flux at the meniscus is a critical factor in influencing the heat transfer and thus, its characterization is more meaningful. Furthermore, the design of the submerged entry nozzle is also important in determining the performance of the mould flux at the meniscus since it affects the fluid flow, the local temperature of the steel and hence viscosity of the mould flux. It will be shown later that differences in the submegence depth of the nozzle will influence the viscosity of the mould flux and the subsequent heat transfer in the mould.

6.4.1.2 Carbon Content of Steel

Figure 6.25 shows the axial heat-flux profiles at the centreline of the narrow face for three different steel grades containing 0.04, 0.09 and 0.29 percent-carbon and these heats were cast with Pemco 389 mould flux; the details of the three heats are given in Table 6.7. It can be seen from Table 6.7 that the casting speed is quite similar in the three cases, but there is a slight variation in the temperature of the steel in the tundish. It is evident from Fig. 6.25 that the heat transfer in the mould is influenced by the carbon content of steel. The peak heat fluxes at the meniscus for the three different grades of

steel are shown in Fig. 6.26 which shows that the heat flux is highest for 0.29 percent-carbon and lowest for 0.09 percent-carbon steel grade. These findings are in agreement with the results reported by Singh and Blazek [131] as shown in Fig. 2.33. It should be realized that the results obtained by Singh and Blazek [131] are based on measurements made on a non-reciprocating billet mould in which oil was employed as a mould lubricant. The observed reduction in the heat transfer for 0.09 percent-carbon steel is not a new finding and has been explained on the basis that, this paricular grade of steel undergoes larger shrinkage as a consequence of δ *to* γ transformation which occurs primarily in the solid state [132] and thus, the dimension of the gap between the shell and the mould wall is increased. It may be interesting to note that quality problems encountered with steel grades having a carbon content in the range 0.08 to 0.11 percent is more pronounced [28] and this may be an outcome of reduced heat transfer in the mould. Similarly, the observed heat transfer in the other two grades of steel can be rationalized on the basis of shrinkage during phase transformation. For the steel with 0.04 percent-carbon, it is evident from the Iron-Carbon phase diagram that the temperature at which the steel undergoes solid state δ *to* γ transformation is much lower and the transformation occurs below the meniscus unlike 0.09 percent-carbon steel and therefore, the heat fluxes at the meniscus are relatively higher for 0.04 percent-carbon steel than for 0.09 percent-carbon. The magnitude of shrinkage associated with δ *to* γ transformation is diminished for 0.29 percent-carbon steel due to the fact that the transformation occurs in the presence of liquid steel; thus the heat transfer rates are higher than for either 0.09 or the 0.04 percent-carbon grades.

Figure 6.27 shows the axial heat-flux profiles at the centreline of the narrow face for two steel grades containing 0.18 and 0.36 percent-carbon cast with Stg 179 mould flux and the details of the casting parameters, chemical composition of the two heats are given in Table 6.8. It is evident from Fig. 6.27 that the magnitude of the heat flux in the mould is reduced with increase in carbon content from 0.18 to 0.36 percent. In the literature, it has been reported that the heat extraction in a billet mould is a minimum at

0.1 percent-carbon steel and thereafter it increases with rise in carbon [131]. Samarasekera et al. [6] based on measurements made on an operating billet mould have reported that the heat flux in the mould is increased as the carbon content was increased in the range 0.14-0.36 percent. The present observations on the reduced heat transfer in a high carbon steel (0.36 percent, Fig. 6.27) is in apparent contradiction with the earlier findings. This anomaly can be explained by considering the liquidus temperature of the steel which is reduced with increase in carbon content; and therefore to maintain the same superheat, the 0.36 percent-carbon steel was cast at a lower temperature as compared with the pouring temperature for the 0.18 percent-carbon steel (Table 6.8). The observed differences in the heat transfer between the two grades can be rationalized on the basis that a lower temperature of the steel at the meniscus as is the case with 0.36 percent-carbon steel will reduce the melting rate of the mould flux and consequently, the viscosity of the mould flux is expected to be higher. It has been earlier shown that an increase in the viscosity of the mould flux will cause a reduction in the heat transfer in the mould (Fig. 6.24). Thus, from the above findings it is apparent that the mould flux behaviour at the meniscus can have a significant influence on heat transfer in the mould and can mask the effect of carbon content.

In the billet mould, the carbon content of steel has a pronounced effect on the mould heat transfer which has been mostly explained in terms of the shrinkage characterisitics of the different grades of steel during phase transformation. However, the findings of this study clearly indicate that in addition to the shrinkage during phase transformation, the effect of the steel grades on the heat transfer in the mould is also governed by behaviour of the mould flux at the meniscus. Also, the results imply that the choice of the mould flux should be governed by the carbon content and the pouring temperature of the steel from the standpoint of heat transfer in the mould.

6.4.1.3 Casting Speed

The influence of casting speed on the heat transfer has been examined in the same heat, details of the steel composition and casting condition are given in Table 6.9. This was possible because there were wide variations in the casting speed within the same heat (Fig. 5.15) and thus, the mould temperature data was time-averaged over periods of constant speed extracted for specific ranges of speed. Fig. 6.28 shows the axial heat-flux profiles at the centreline of the narrow face at two different casting speeds of 0.50 and 0.80 m/min. It is clear that an increase in the casting speeed results in an enhancement in the heat transfer in the mould and the influence is most significant in the vicinity of the meniscus. The magnitude of heat flux at the meniscus is increased from 1900 kW/m^2 to 2600 kW/m^2 with an increase in the speed from 0.5 m/mim to 0.8 m/min; at a distance of 440 mm from the meniscus the corresponding increase is from 575 kW/m^2 to 800 kW/m^2. In the literature there is large body of evidence reporting the enhancement of heat transfer in the mould with increase in the casting speed [115,120,123-128]. The findings of the present study are also in agreement with the results of Russian investigators [120] (Fig. 2.29) which corroborates with the findings of this study in that the heat fluxes near the meniscus increase more than the heat fluxes in the lower part of the mould with an increase in the casting speed. It is accepted that with an increase in the casting speed, the thickness of the solid shell in the mould is reduced and thus, the effect of casting speed on the mould heat transfer has been mostly explained in terms of the width of the gap which is reduced at higher casting speed because the ferrostatic pressure is more effective in pushing the thin shell towards the mould wall. Based on this rationale, the observed increase in the heat fluxes towards the bottom of the mould can be understood, but it is difficult to explain the profound influence of the casting speed in the vicinity of the meniscus where the ferrostatic pressure is low.

The influence of the casting speed particularly in the vicinity of the meniscus has not been explained in the past. In the next chapter, it will be shown that despite the use of

the same mould flux, variation in the casting speed will influence the behaviour of the mould flux at the meniscus which affects the depth of oscillation marks and consequently the heat transfer in the vicinity of the meniscus.

6.4.1.4 Submergence Depth

Figure 6.29 shows the axial heat-flux profile at the centreline of the narrow face at submergence depths of 175 and 300 mm; it should be noted that the submergence depth was varied in the same heat the details of which is given in Table 6.10. It can be seen from Fig. 6.29 that a reduction in the submergence depth leads to a small increase in the heat transfer in the upper region of the mould. The magnitude of the heat flux at the meniscus is increased from 2300 kw/m^2 to 2475 kw/m^2 with a reduction in the depth of submergence from 300 to 175 mm. There is no report on the effect of submergence depth on the mould heat transfer in the literature although it has been mentioned that the flow patterns in the molten steel is dependent on submergence depth [16]. It has been shown that the temperature of the molten steel at the meniscus is increased and also, the thickness of the molten flux layer above the meniscus is enhanced with an increase in the angle of the ports (upward) owing to an enhancement in the turbulence near the meniscus [138]. Similarly it can be argued that with the nozzle in which the ports are angled 7.5^0 upwards, a reduction in the submergence depth enhances the intensity of turbulence of the steel at the meniscus. The mould flux comes in contact with steel at a higher temperature which results in a reduction in its viscosity and consequently the heat transfer is increased. This finding again shows the relevance of the mould flux behaviour at the meniscus in influencing the heat transfer in the mould.

Table 6.1 - Input parameters employed in the two-dimensional transverse model of the mould wall.

Copper thickness	50 mm
Depth of cooling channel	20 mm
Width of the cooling channel	6 mm
Heat flux	2000 kW/m^2
Thermal conductivity of copper	392 W/m .K
Heat Transfer coefficient	27977.79 W/m^2 ^{0}C
Water temperature	25.0 ^{0}C
Node size (thickness)	1.0 mm
Node size (transverse)	1.0 mm

Table 6.2 - Input parameters to calculate the tempertaure of the copper plate in the presence and absence of the slot using the two-dimensional model (transverse).

Copper thickness	36 mm
Depth of cooling channel	20 mm
Width of the cooling channel	6 mm
Depth of slot	12 mm
Width of slot	8 mm
Heat flux	2000 kW/m^2
Heat transfer coefficient	27977.79 W/m^2 ^{0}C
Thermal conductivity of copper	392 W/m .K
Water temperature	25.0 ^{0}C
Node size (thickness)	1.0 mm
Node size (transverse)	1.0 mm

Table 6.3a - Thickness of the copper plates employed in the three-dimensional mathematical model of the mould wall.

Distance below mould top (mm)	Copper plate thickness (mm)		
	Narrow face	Inside radius	Outside radius
0	36	36	48
100	36	39	44
200	36	42	41
300	36	44	40
400	36	45	39
500	36	45	39
600	36	44	40
700	36	42	42
800	36	39	45
900	36	36	48

Table 6.3b - Dimensions of the cooling channel employed in the three-dimensional model of the mould wall.

Dimensions (mm)	Narrow face	Inside radius	Outside radius
Length of cooling channel	900	900	900
Depth of cooling channel	20	20	20
Width of cooling channel	6	6	6

Table 6.4 - Testing of conditions to establish the applicability of the correlation (Eq. 6.12) for obtaining the heat transfer coefficient

Hydraulic diameter of the cooling channel	9.23 mm
Velocity of water (Broad face)	8.08 m/s
Velocity of water (Narrow face)	5.56 m/s
Specific heat of water	4182 J / kg. K
Density of water	998.2 kg / m^3
Thermal conductivity of water	0.597 W / m . K
Viscosity of water	993×10^{-6} N. s / m^2
Prandtl number	7.0
Reynolds number (broad face)	74969
Reynolds number (narrow face)	51585
Ratio of length and hydraulic diameter of cooling channel	97.5

Table 6.5 - Effect of thermal conductivity of copper on the mould temperature at the hot face.

Distance below top of the mould (mm)	Mould temperature at the hot face. (^{0}C) obtained with constant and variable conductivity	
	Constant thermal conductivity (127^{0}C)	Temperature dependent thermal conductivity
0	30.79	30.81
100	172.41	172.30
200	148.58	148.41
300	132.14	131.91
400	111.07	110.79
500	101.72	101.42
600	91.95	91.64
700	78.13	77.82
800	79.69	79.37
900	96.07	95.73

Table 6.6 - Steel composition and casting conditions of the heats investigated to examine the influence of the mould flux on heat transfer in the mould.

C (%)	Mn (%)	Si (%)	P (%)	S (%)	Casting speed (m/min)	Tundish temp (^{0}C)	Mould flux
0.07	1.34	0.30	0.008	0.005	0.63	1550	Stg 179
0.07	0.40	0.008	0.007	0.011	0.68	1558	Pemco 389

Table 6.7 - Steel composition and casting conditions of the heats investigated to examine the influence of steel carbon content on heat transfer in the mould.

C (%)	Mn (%)	Si (%)	P (%)	S (%)	Casting speed (m/min)	Tundish temp (^{0}C)	Mould flux
0.04	0.26	0.008	0.004	0.013	0.77	1550	Pemco 389
0.09	0.30	0.017	0.007	0.021	0.76	1540	Pemco 389
0.29	1.25	0.19	0.016	0.005	0.82	1550	Pemco 389

Table 6.8 - Steel composition and casting conditions of the heats investigated to examine the influence of steel carbon content on heat transfer in the mould.

C (%)	Mn (%)	Si (%)	P (%)	S (%)	Casting speed (m/min)	Tundish temp (^{0}C)	Mould flux
0.18	0.78	0.13	0.011	0.014	0.78	1535	Stg 179
0.36	0.80	0.013	0.013	0.006	0.68	1520	Stg 179

Table 6.9 - Steel composition and casting conditions of the heat investigated to examine the influence of casting speed on heat transfer in the mould.

C (%)	Mn (%)	Si (%)	P (%)	S (%)	Casting speed (m/min)	Tundish temp (^{0}C)	Mould flux
0.21	1.40	0.14	0.013	0.005	0.50 and 0.80	1545	Stg 179

Table 6.10 - Steel composition and casting conditions of the heat investigated to examine the influence of submergence depth on heat transfer in the mould.

C (%)	Mn (%)	Si (%)	P (%)	S (%)	Casting speed (m/min)	Tundish temp (^{0}C)	Mould flux
0.05	0.28	0.16	0.004	0.009	0.68	1550	Pemco 389

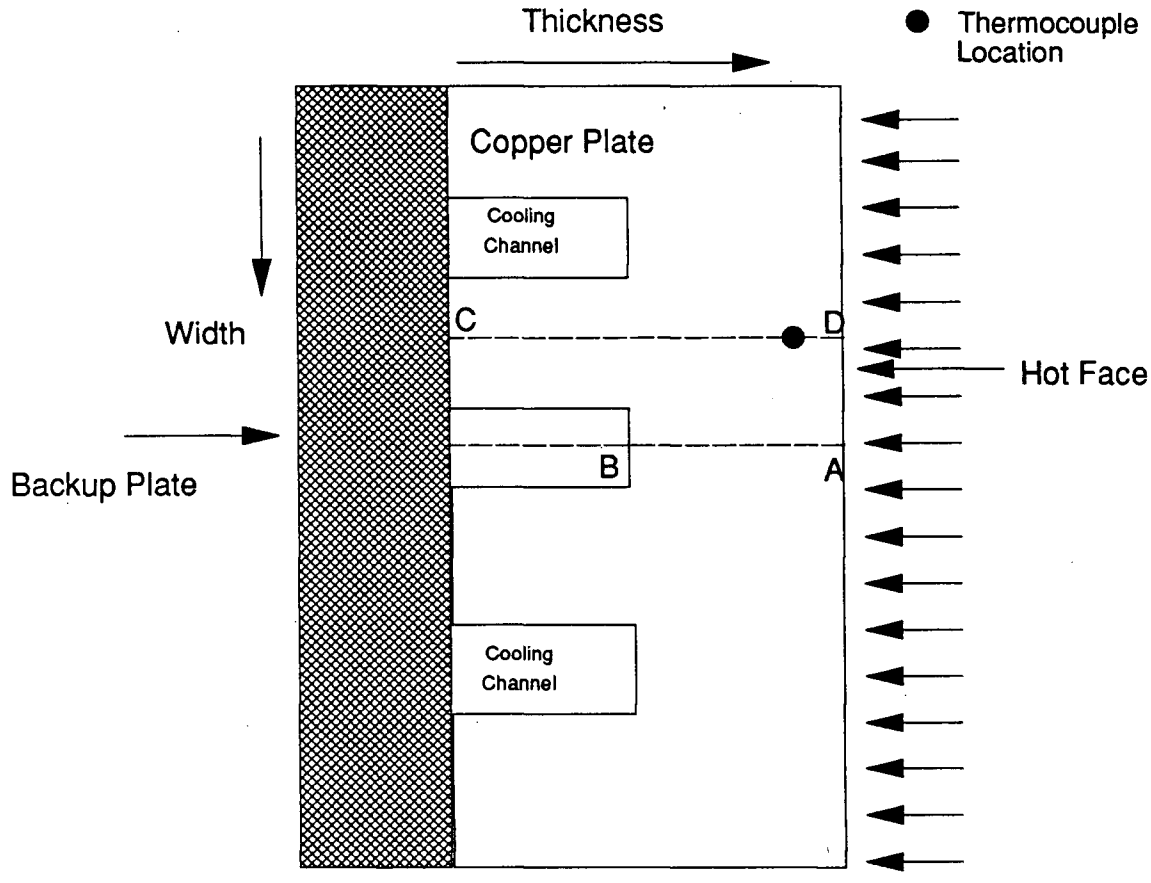

Figure 6.1. Schematic diagram of transverse section of a copper plate employed in the two-dimensional model of the mould wall.

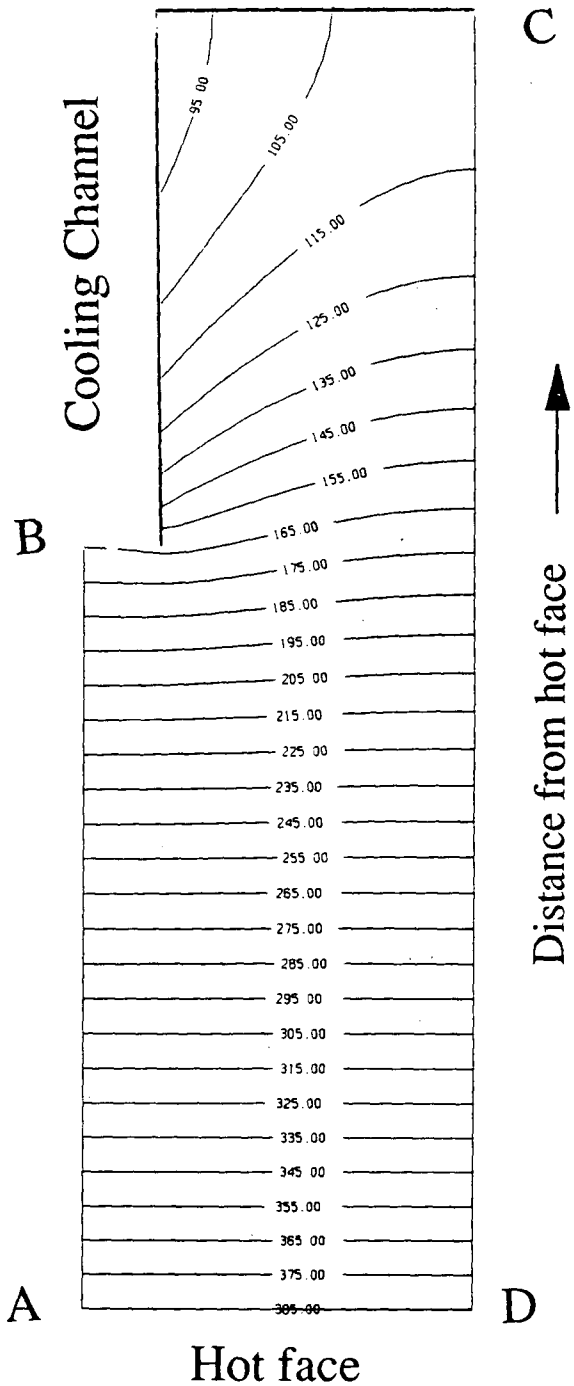

Figure 6.2. Model predicted isotherms on the transverse section of the copper plate.

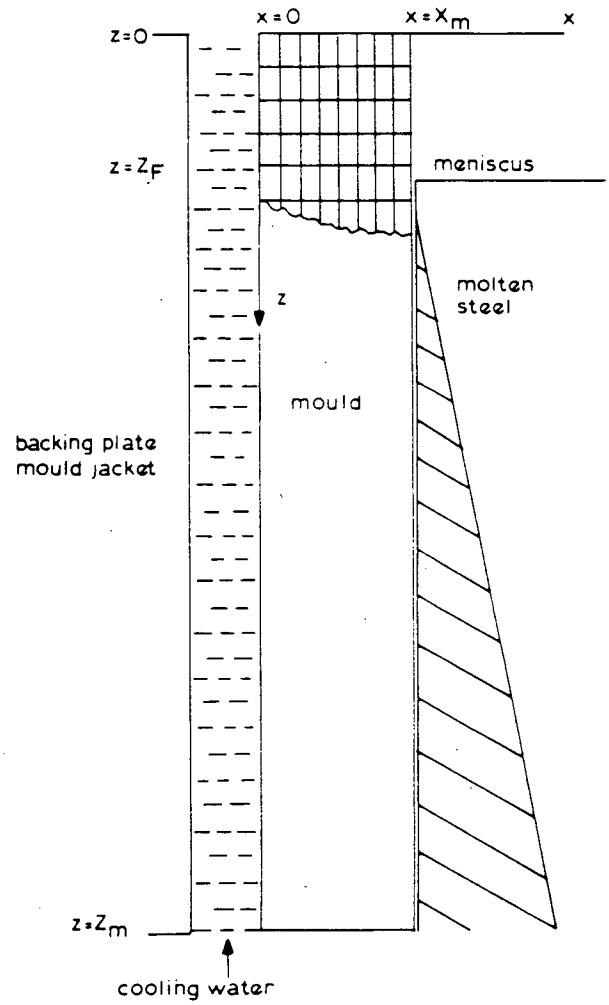

Figure 6.3. Schematic diagram of a longitudinal mid-plane through the mould wall employed in the two-dimensional longitudinal model [122].

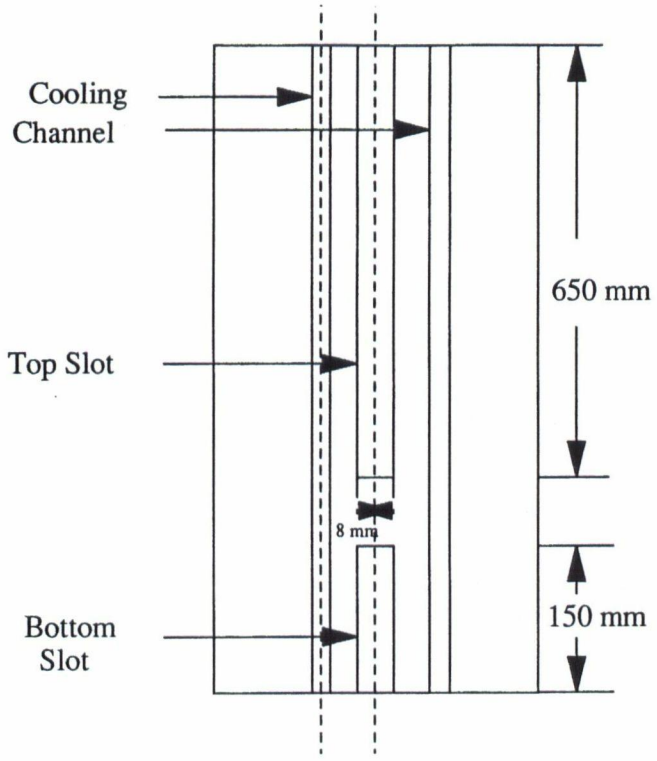

Figure 6.4. Schematic diagram of a copper plate showing the location of the slots and their dimensions.

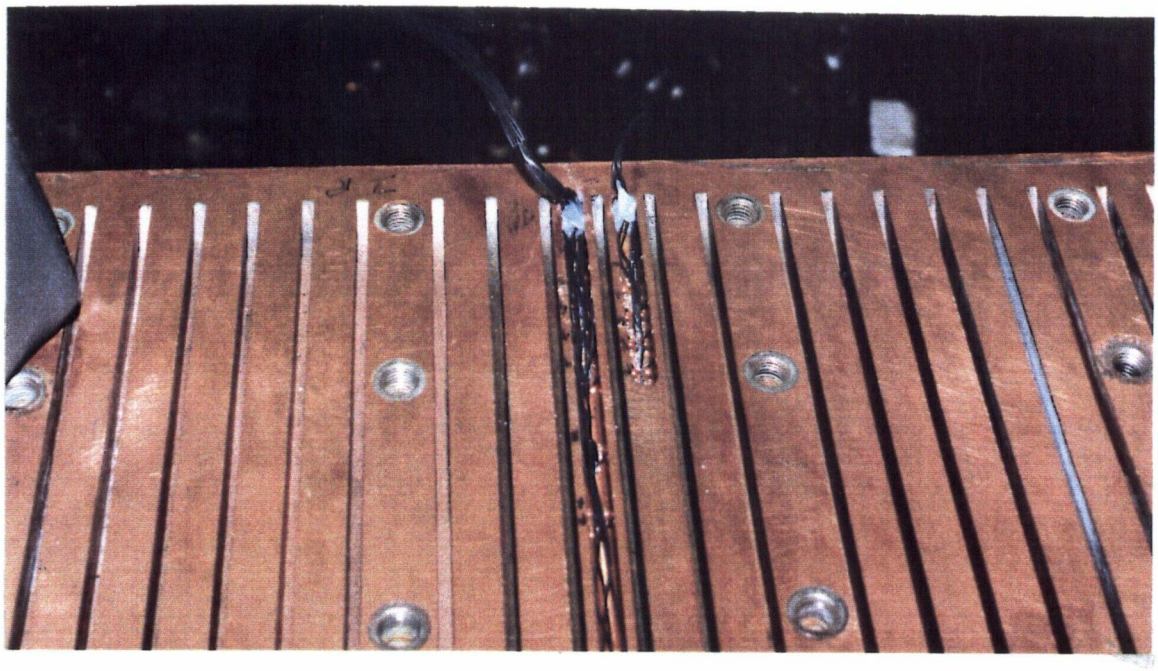

Figure 6.5. Photograph of a copper plate showing the thermocouple wires in the slot.

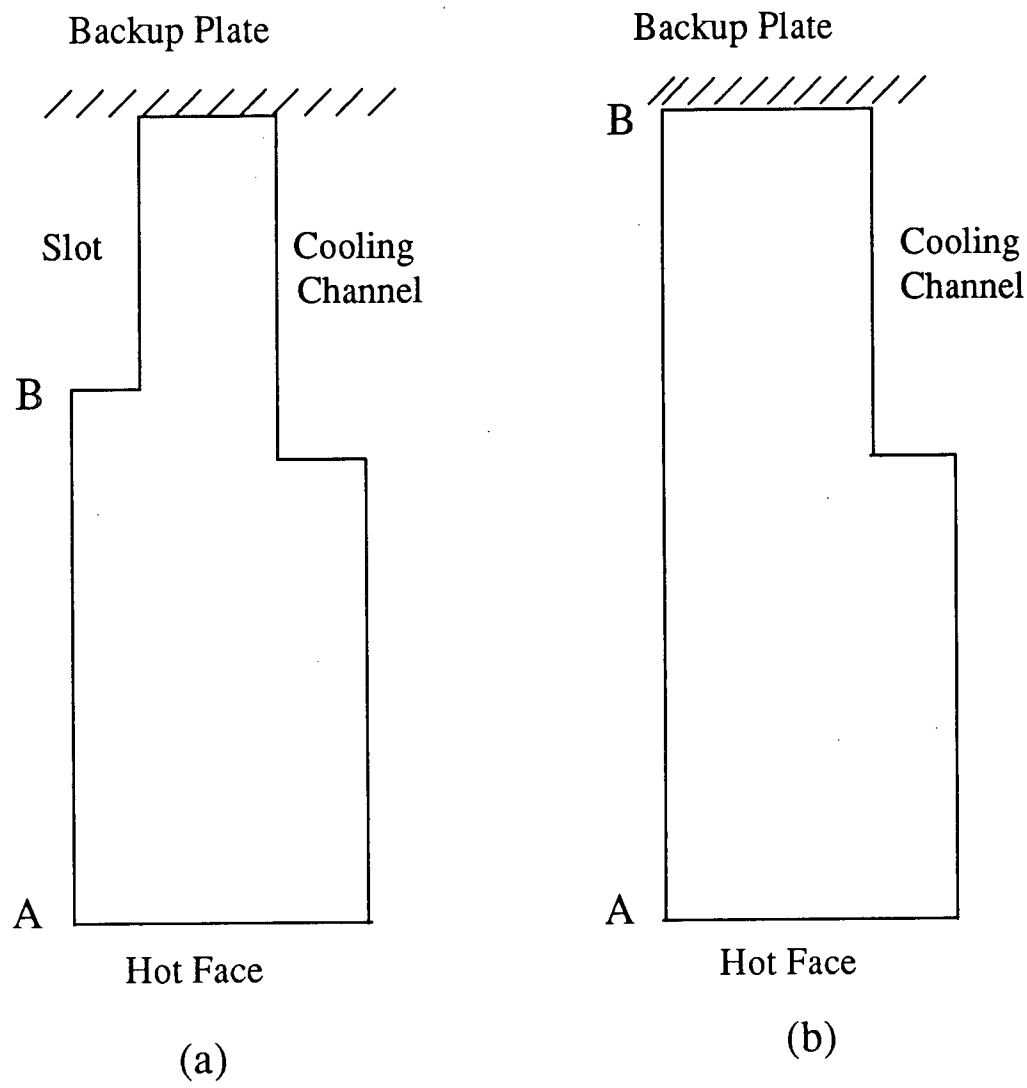

Figure 6.6. Transverse section of the copper plate showing the (a) presence and (b)absence of the slot (only half the width of the cooling channel and the slot has been shown).

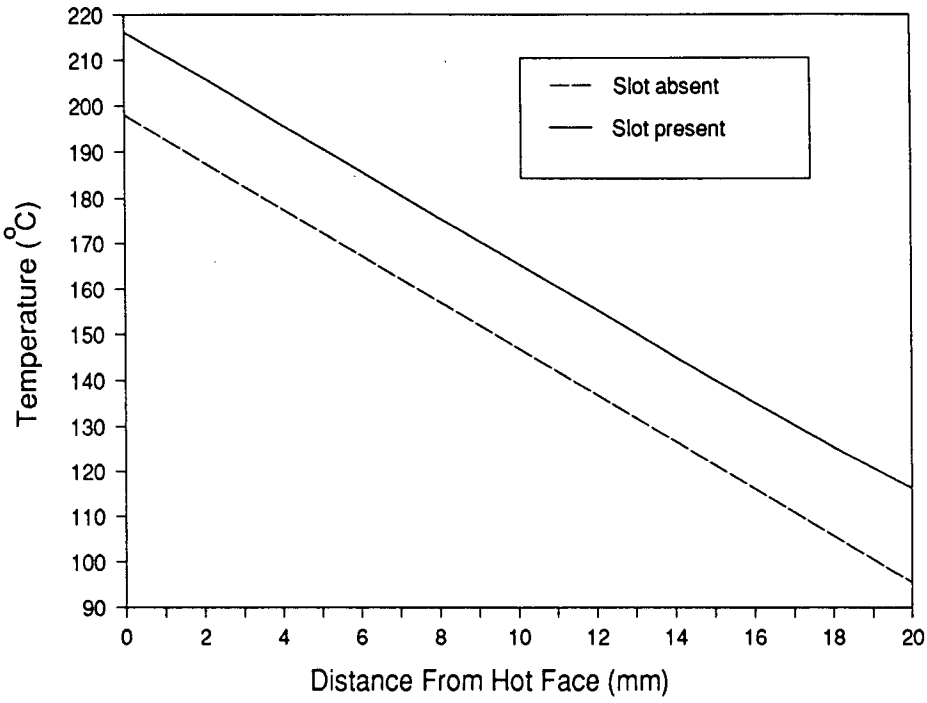

Figure 6.7. Model predicted temperature of the copper plate at different distances from the hot face in the presence and absence of the slot as shown in Fig. 6.6 a-b.

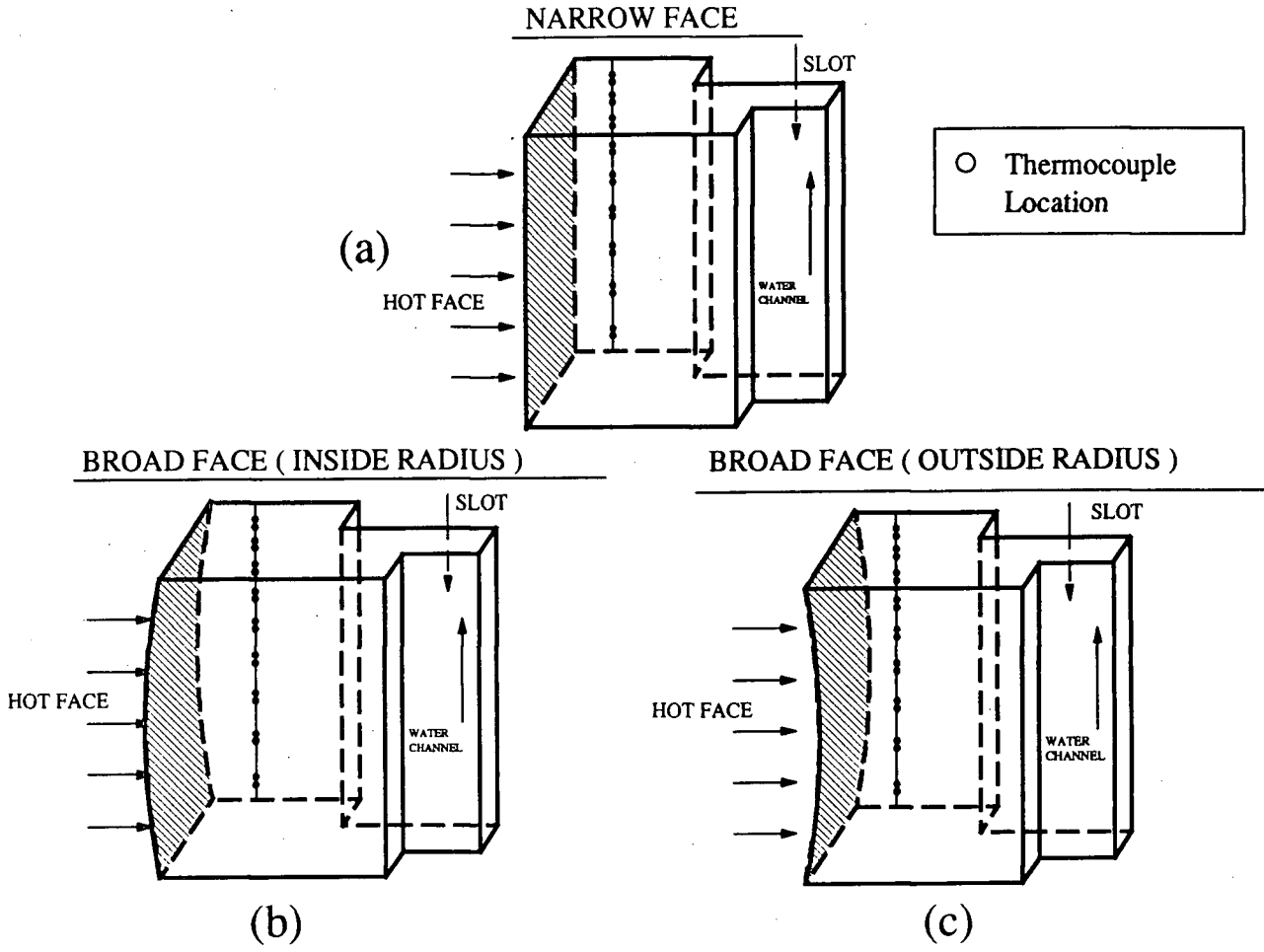

Figure 6.8. Schematic diagram of the copper plates over which calculation have been performed with the three-dimensional model (a) Narrow face (b) Inside radius (c) Outside radius

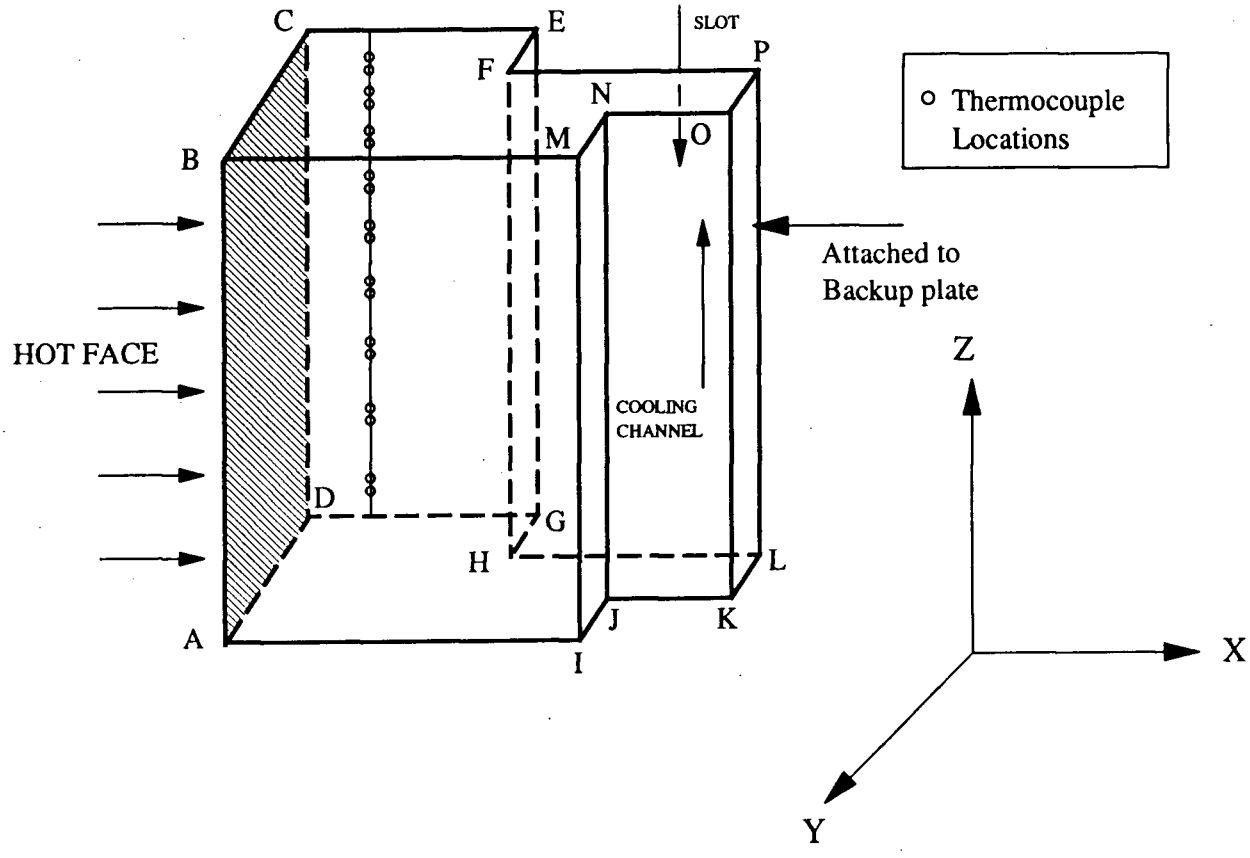

Figure 6.9. Schematic drawing of a copper plate used to describe the boundary conditions at different faces.

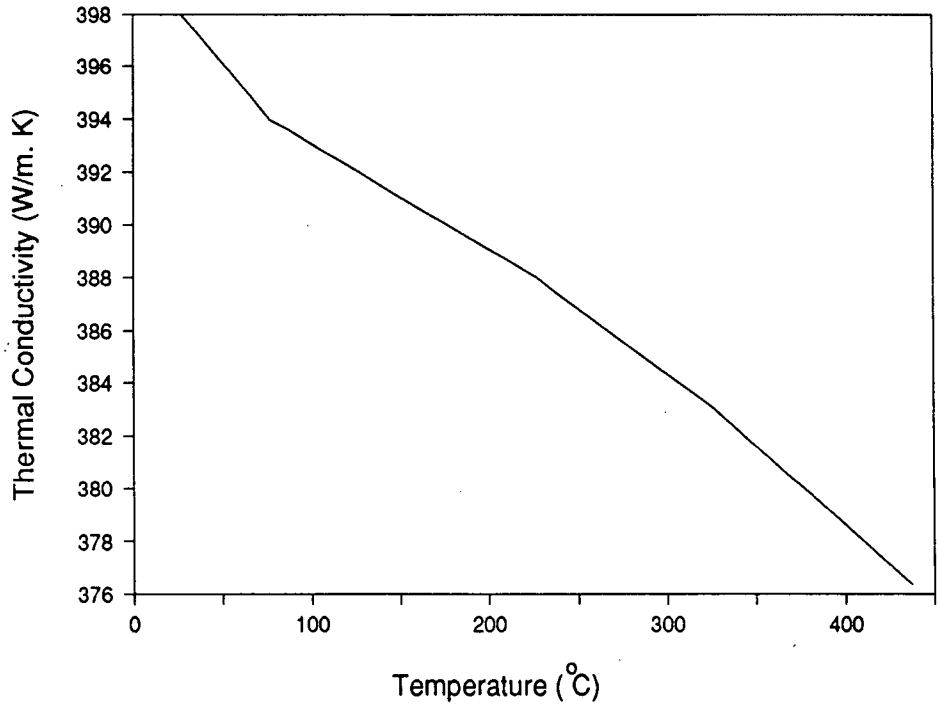

Figure 6.10. Variation of thermal conductivity of copper with temperature [140].

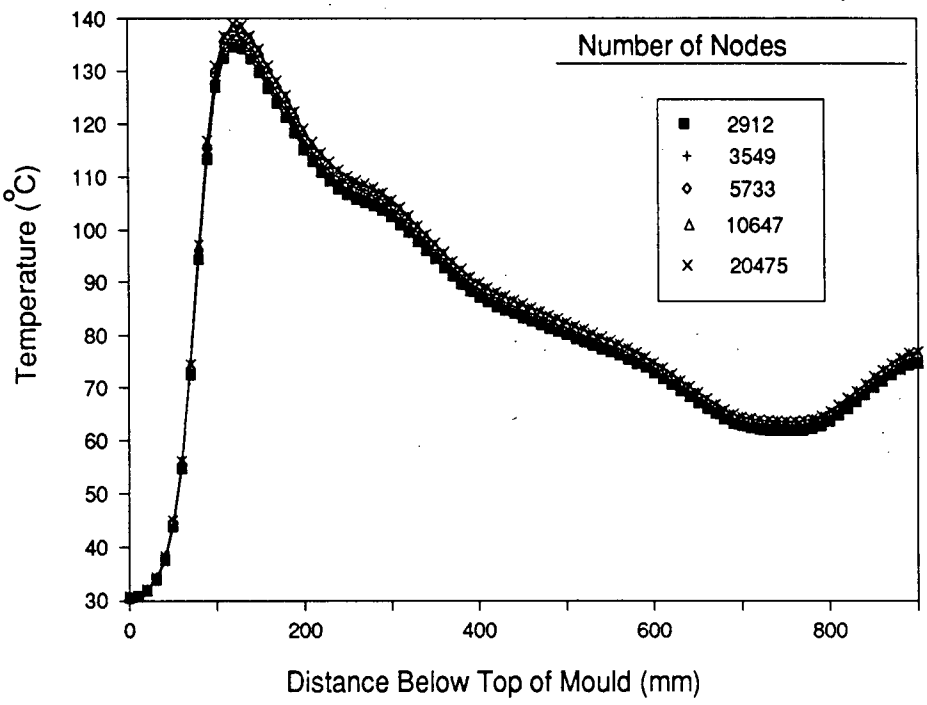

Figure 6.11. Effect of the total number of nodes (generated due to different mesh size) on the axial hot-face temperature profile.

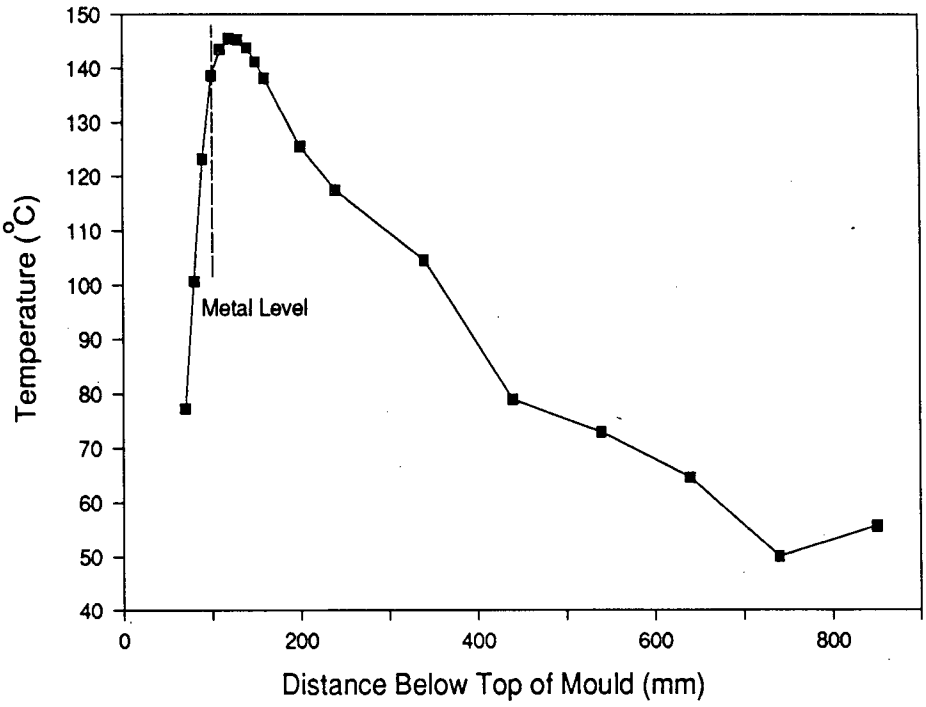

Figure 6.12. A typical example of measured axial mould-temperature profile.

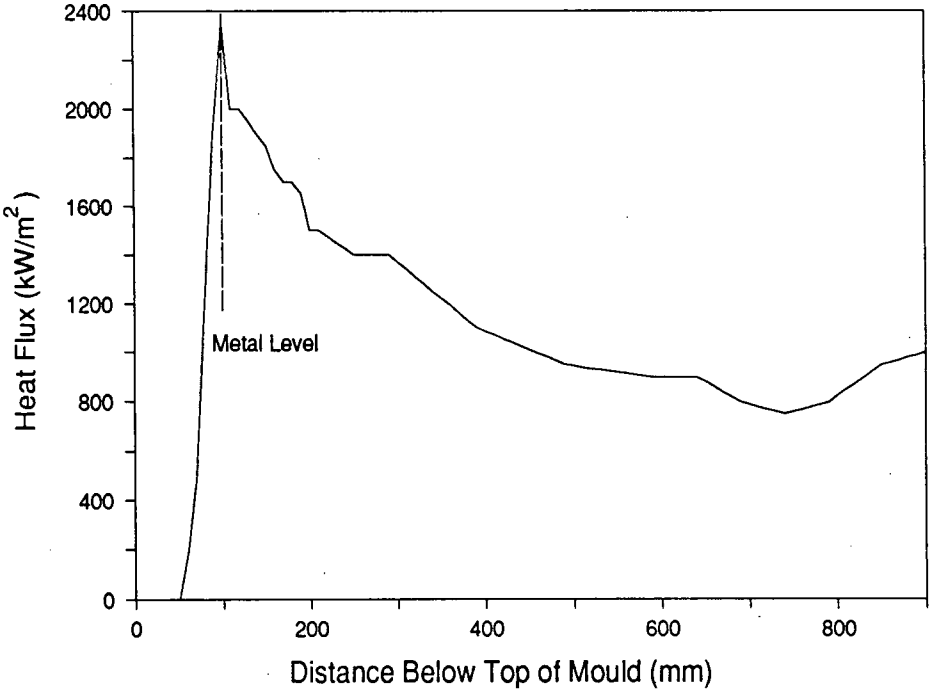

Figure 6.13. Model predicted axial heat-flux profile obtained with the measured mould-temperature profile shown in Fig. 6.12.

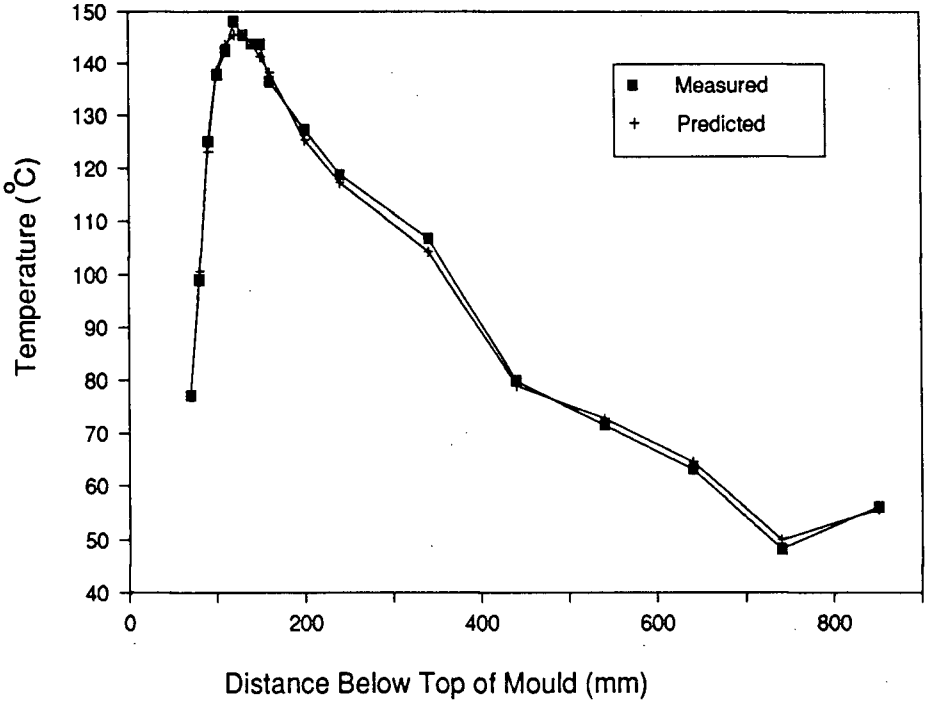

Figure 6.14. Comparison of the measured and calculated mould-temperature profiles for the heat-flux profile shown in Fig. 6.12.

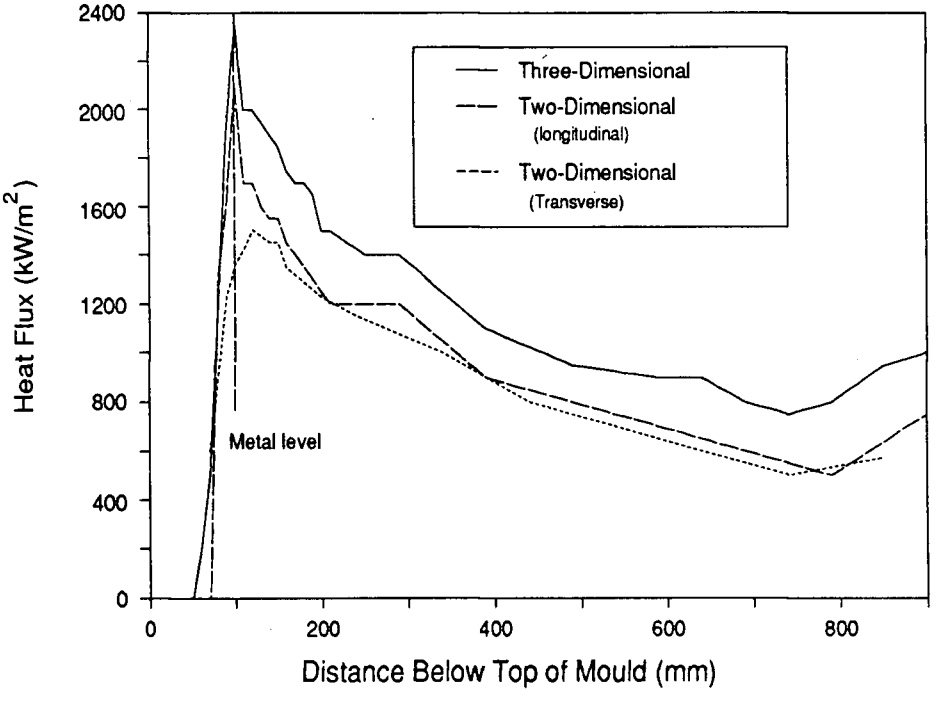

Figure 6.15. Comparison of heat-flux profiles predicted by two-dimensional (transverse and longitudinal) and three-dimensional model of the mould wall for the same mould temperature data (Fig. 6.12).

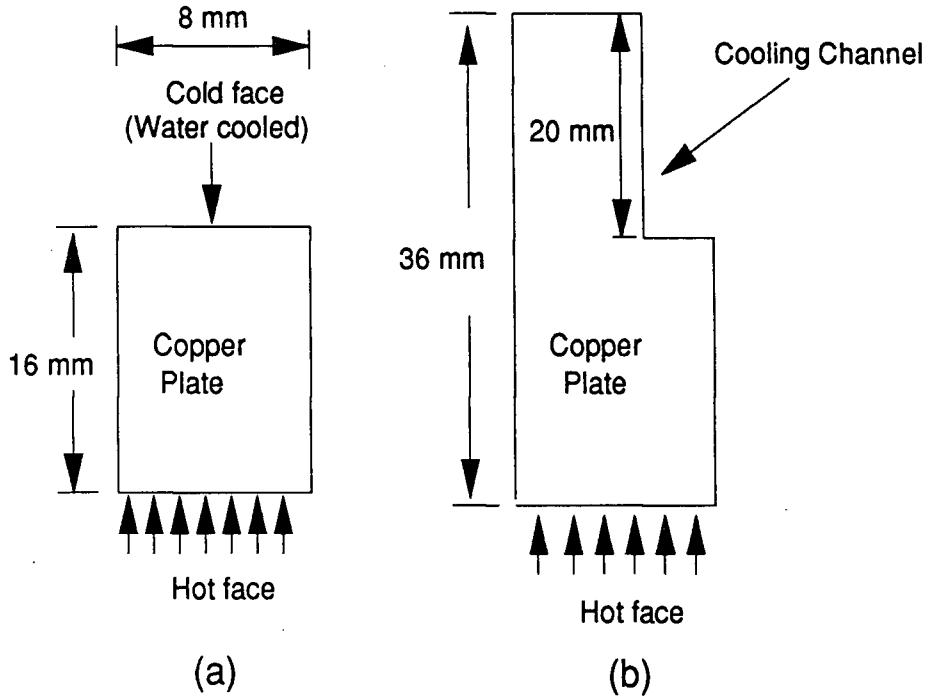

Figure 6.16. Schematic drawing of the transverse sections of the copper plates considered to examine the influence of the transverse heat flow on mould wall temperatures (a) Case I, one-dimensional heat flow, no transverse heat flow (b) Case II, two-dimensional heat flow.

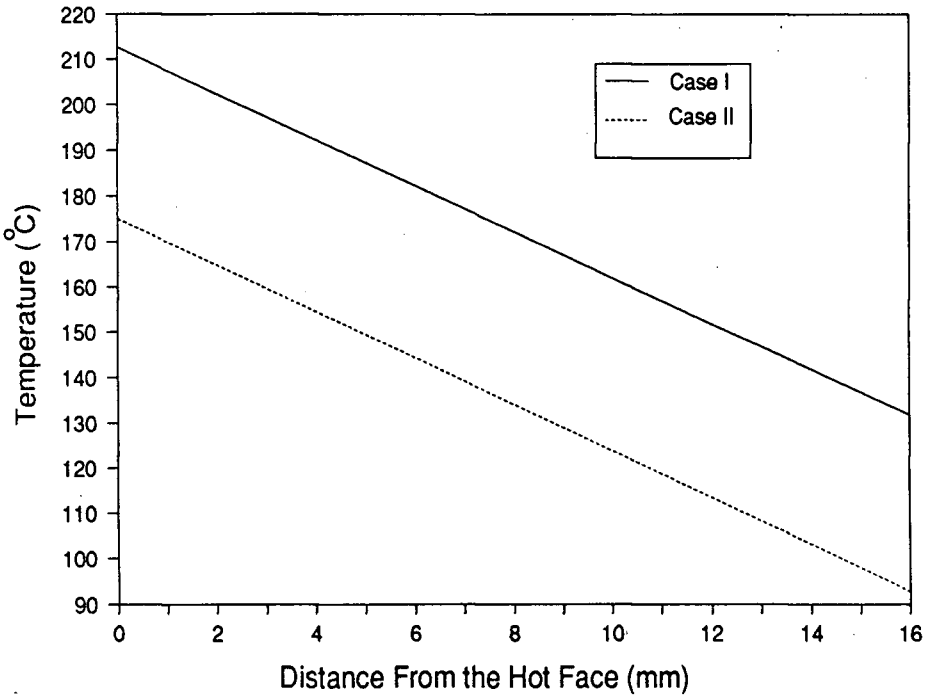

Figure 6.17. Model predicted temperature of the mould wall as a function of distance from the hot face for case I and Case II shown in Figs. 6.16 a-b.

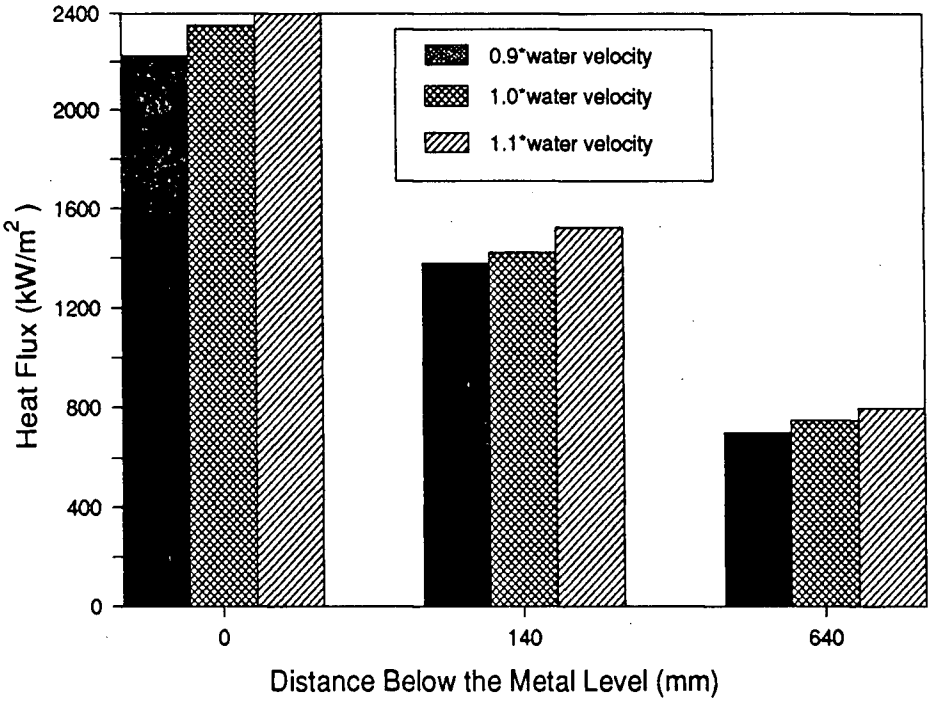

Figure 6.18. Influence of water velocity in the cooling channel on the model predictions of heat fluxes in the mould.

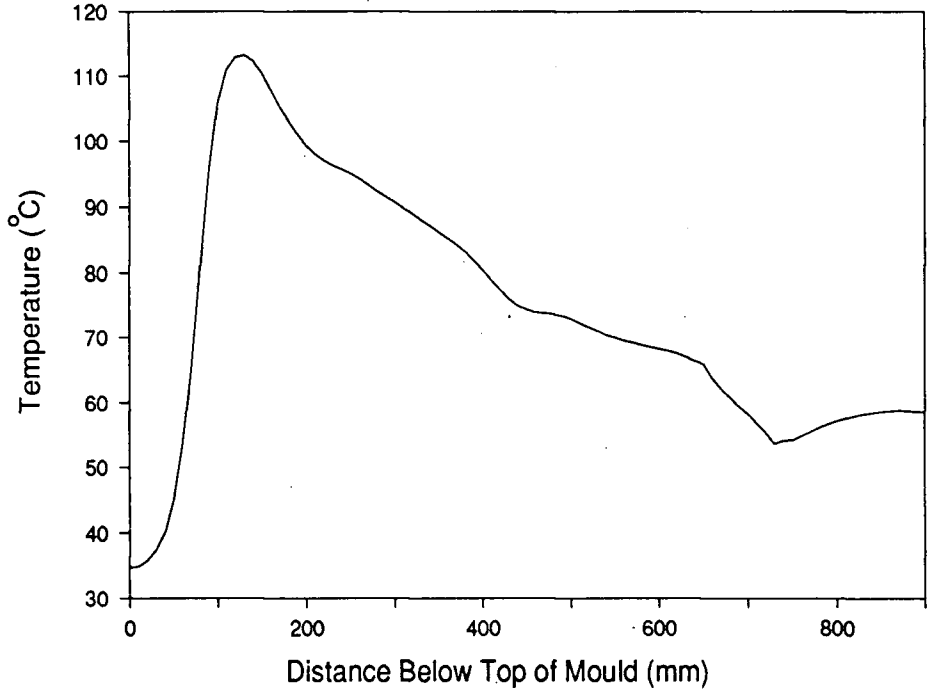

Figure 6.19. Model predicted axial temperature profile in the cooling channel (Narrow face, casting speed= 1.2 m/min).

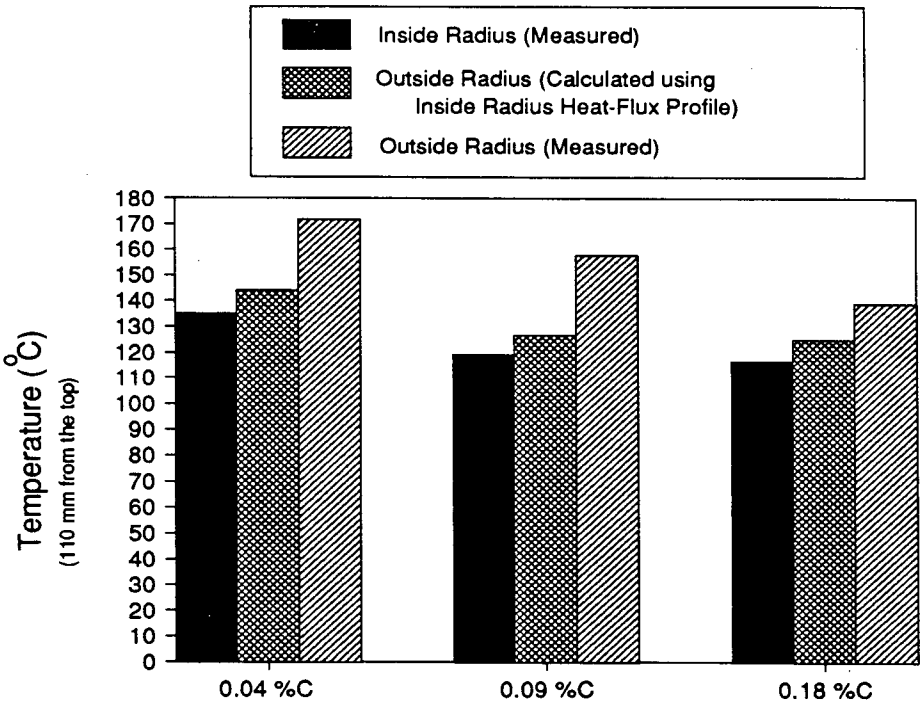

Figure 6.20. Comparison of the mould wall temperature at a fixed location obtained from measurements on the inside and outside radius copper plates and also model predicted temperature at the outside radius using the inside radius heat-flux profile.

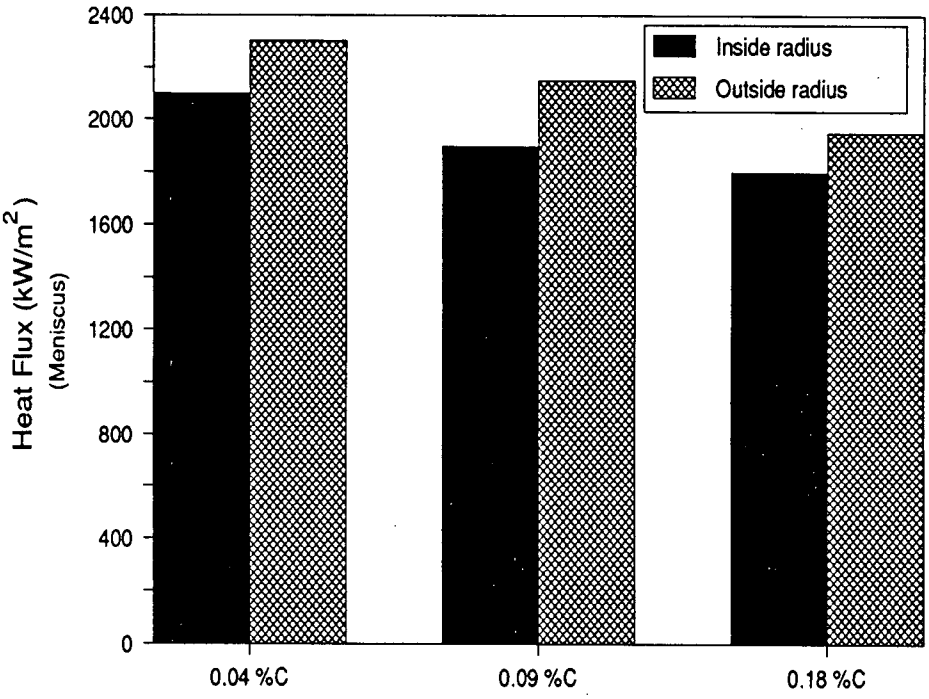

Figure 6.21. Comparison of model predicted heat flux at the meniscus at the inside and the outside radius for different grades of steel (casting speed=0.75 m/min).

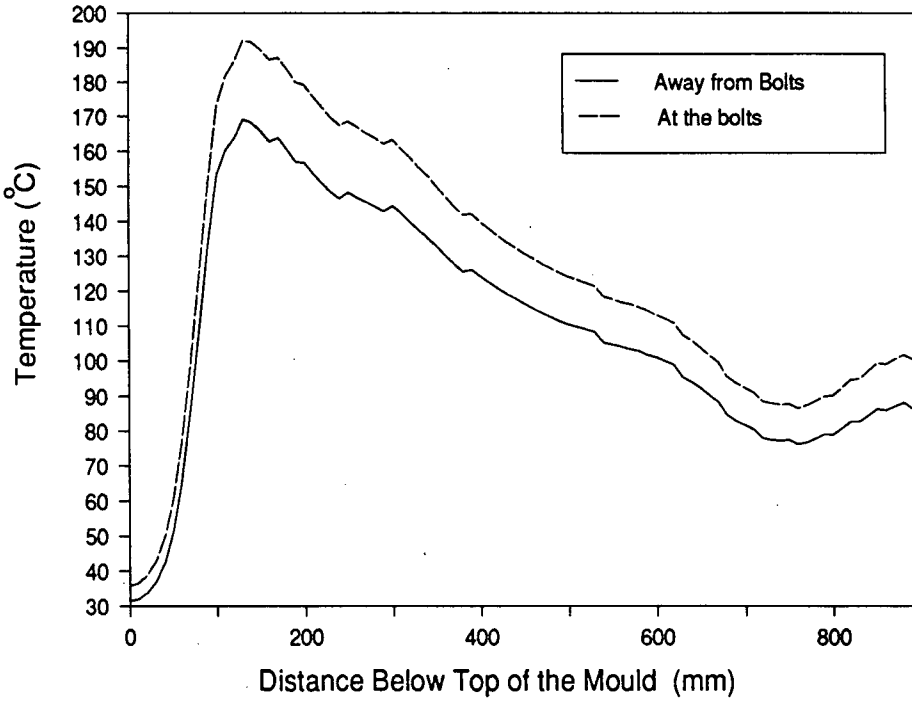

Figure 6.22. Comparison of the model predicted axial mould-temperature profiles near and away from the bolts.

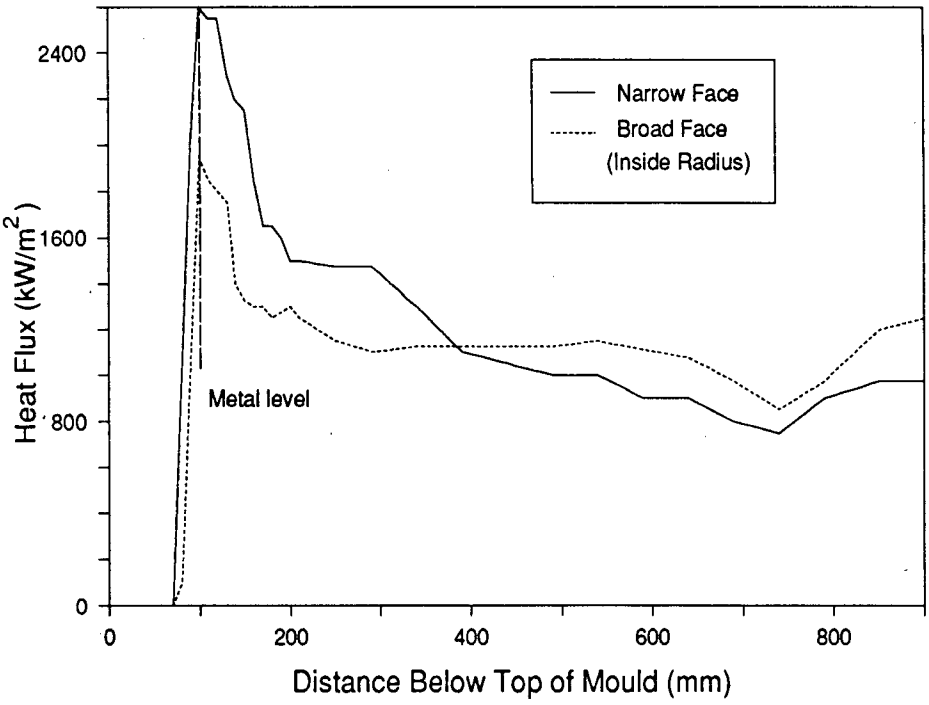

Figure 6.23. Comparison of the heat-flux profiles between the narrow face and the broad face (inside radius) (C=0.17%, casting speed=0.996 m/min).

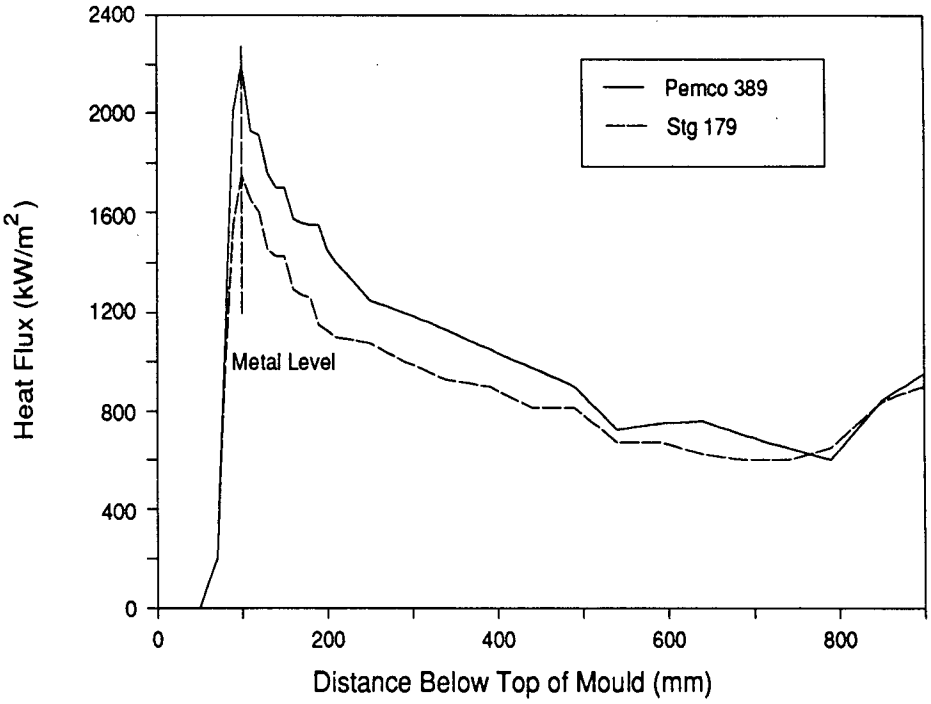

Figure 6.24. Influence of the type of the mould flux on the axial heat-flux profiles (narrow face).

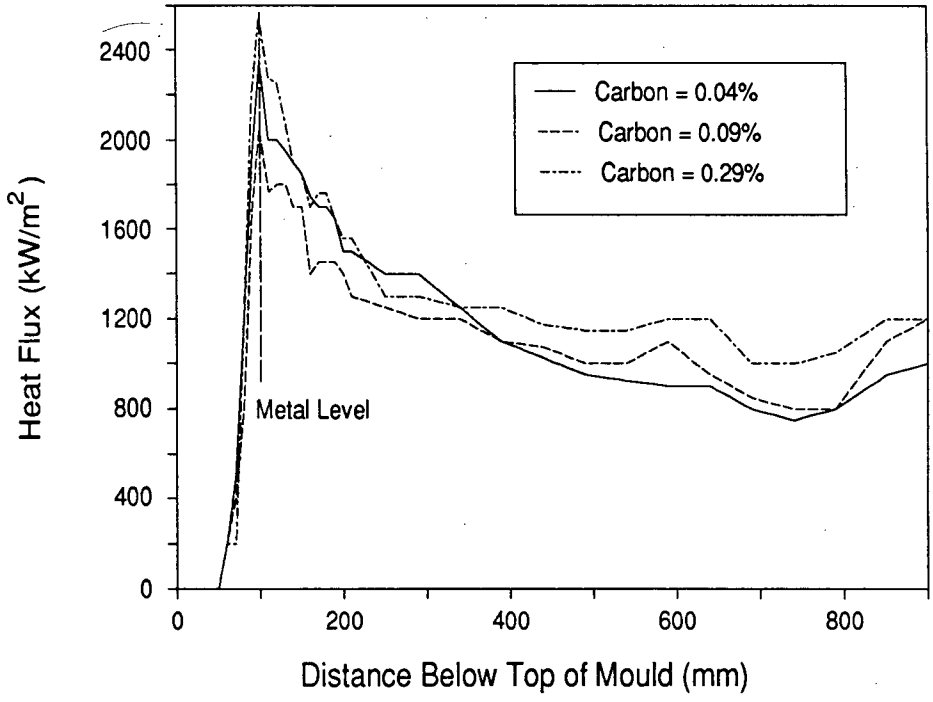

Figure 6.25. Influence of steel carbon content on the axial heat-flux profiles (Pemco 389 mould flux, narrow face).

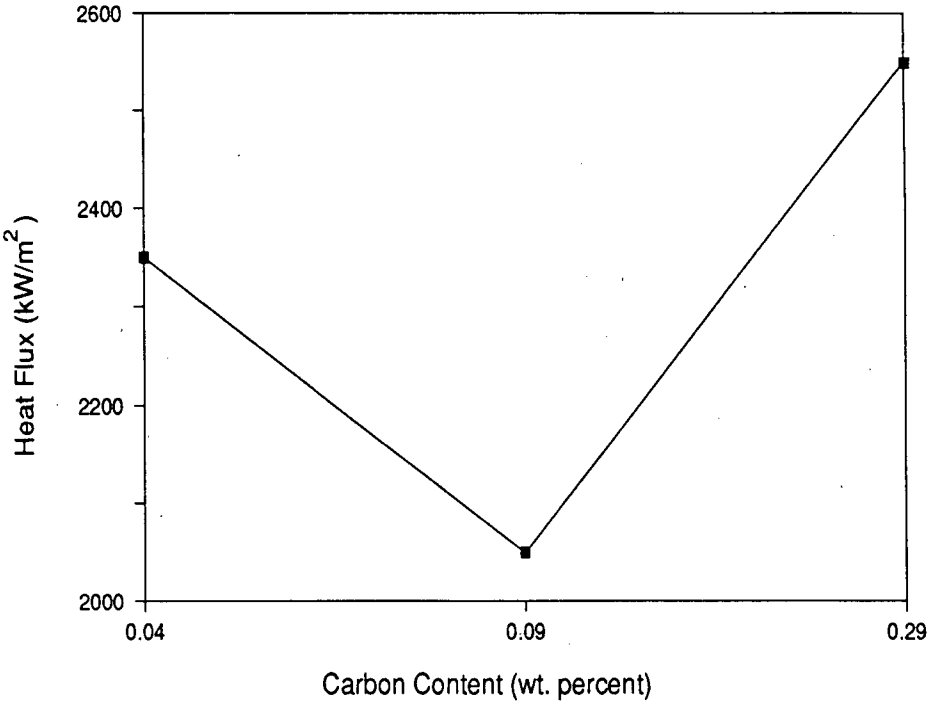

Figure 6.26. Meniscus Heat Flux for three steel grades containing 0.04, 0.09 and 0.29 percent-carbon.

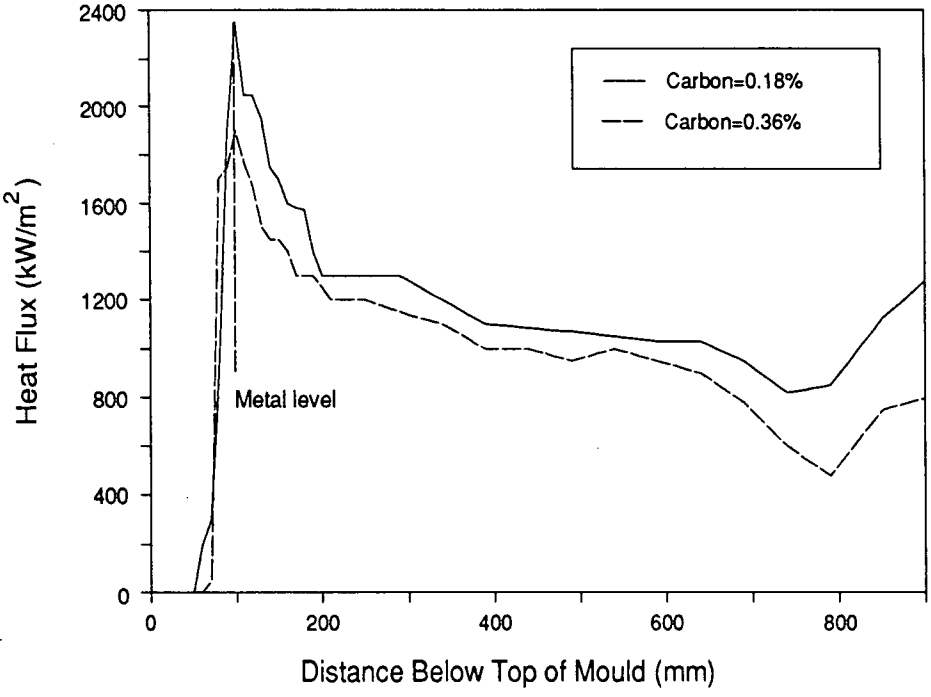

Figure 6.27. Influence of steel carbon content on the axial heat-flux profiles on the narrow face (Stg 179 mould flux).

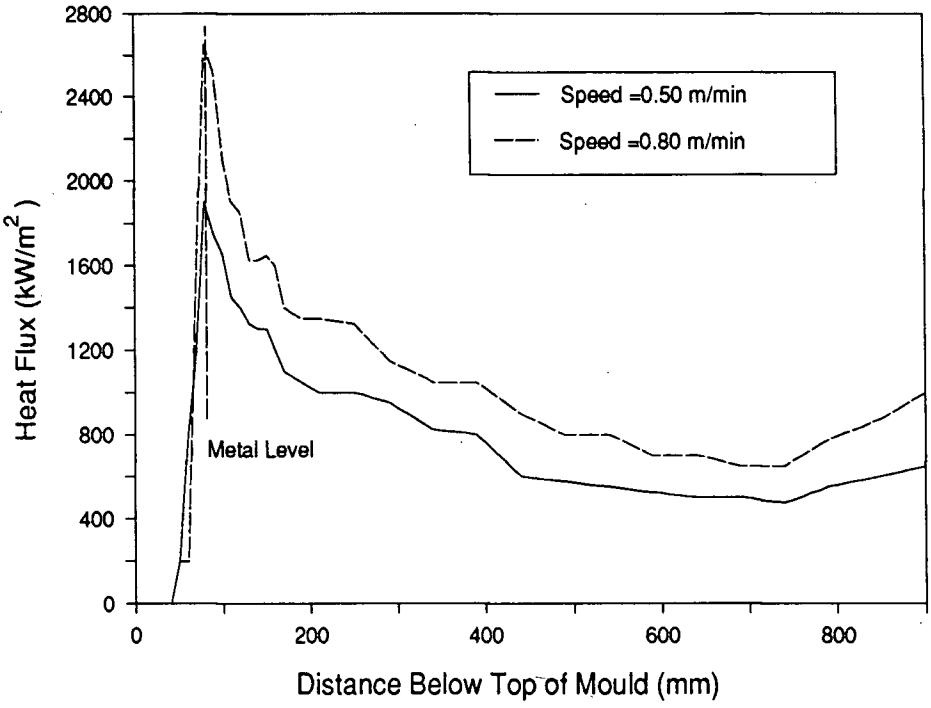

Figure 6.28. Effect of casting speed on the axial heat-flux profiles at the narrow face.

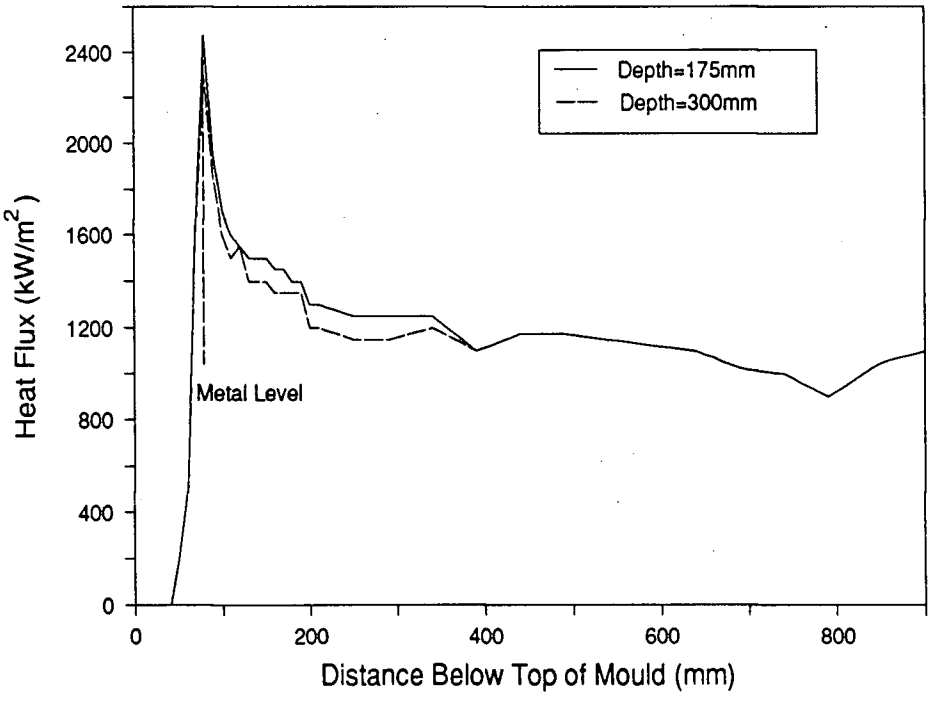

Figure 6.29. Influence of the depth of submergence on the axial heat-flux profiles on the narrow face.

Chapter 7 - SOLIDIFICATION PHENOMENON AND QUALITY ASPECT OF SLABS

Understanding the solidification phenomenon of steel in the mould is crucial because of the strong influence it has on the surface/sub-surface quality of the cast slab and also on operating problems encountered during casting, such as break-outs. A quantitative characterization of the temperature distribution in the steel during solidification is necessary to estimate the shell profile in the mould, a knowledge of which is essential in optimizing the casting speed. Furthermore, a knowledge on the shrinkage characteristics of the steel shell during solidification can be utilized to provide insight on mould design, particularly the taper of the mould wall. Needless to say, the rate of solidification is largely governed by the heat extraction rates in the mould which has been well established in the present study. This chapter will be devoted to the solidification phenomenon in the mould which has been examined by combining mathematical modelling with metallographic analyses. Furthermore, the characterization of oscillation marks and longitudinal off-corner cracks have also been examined and will be discussed in this chapter.

7.1 Solidification Model

Mathematical models have been frequently utilized in the past to quantitatively characterize the thermal field in the steel during casting primarily to determine the pool depth and shell growth in the different zones of the casting machine. It should be noted that the models employed in the past have usually assumed values of heat fluxes to characterize the boundary conditions at the surface of the slab. This approach can lead to inaccurate predictions particularly in the mould, owing to the complex nature of heat transfer. This difficulty has been overcome in the present study by employing the heat

extraction rates calculated from the time-averaged mould temperatures as boundary condition in the solidification model. The salient features of the solidification model will be presented in the following section.

7.1.1 Assumptions

The following assumptions have been made in the model.

(i) The temperature distribution in the strand is at steady state with respect to a fixed reference frame

(ii) Heat conduction along the casting direction is small compared to the heat flow by bulk motion of the strand and therefore has been neglected.

(iii) Heat flow in the molten steel occurs by conduction; the convection in the molten pool is taken into account by increasing the thermal conductivity of the molten steel.

(iv) Thermal conductivity and specific heat of steel is considered to be a linear function of temperature and the density of the steel is assumed to be constant.

7.1.2 Mathematical Formulation of Heat Flow in the Strand

An infinitesimal control volume is located in the solid shell as shown in Fig. 7.1 and the strand passes through it at a constant speed. If the control volume is fixed in space, heat balance on the control volume resulting from heat conduction and bulk motion of the strand will yield the following differential equation.

$$\frac{\partial}{\partial x}\left(k_s\frac{\partial T_s}{\partial x}\right)+\frac{\partial}{\partial y}\left(k_s\frac{\partial T_s}{\partial y}\right)+\frac{\partial}{\partial z}\left(k_s\frac{\partial T_s}{\partial z}\right)-u_s\rho_s c_{ps}\frac{\partial T_s}{\partial z} = \rho_s c_{ps}\frac{\partial T_s}{\partial t} \qquad (7.1)$$

It is important to note that the above differential equation has been derived on a control volume located in the solid shell (Fig. 7.1), but the same equation will also be valid in the liquid steel because it is assumed that the heat flow in the liquid steel takes place by conduction. The next step is to examine the possibility of simplification of Eq. (7.1). The casting process is assumed to be at steady state with respect to a fixed reference frame and thus,

$$\frac{\partial T_s}{\partial t} = 0$$

Furthermore, Peclet number was calculated to be greater than 100 (Appendix II) and thereby indicating that heat conduction along the casting direction is small compared to the heat flow by bulk motion.

$$k_s \frac{\partial T_s}{\partial z} = 0$$

Substituting $k_s \frac{\partial T_s}{\partial z} = 0$ and $\frac{\partial T_s}{\partial t} = 0$

in Equation (7.1) will result in the following.

$$\frac{\partial}{\partial x}\left(k_s \frac{\partial T_s}{\partial x}\right) + \frac{\partial}{\partial y}\left(k_s \frac{\partial T_s}{\partial y}\right) = u_s \rho_s c_{ps} \frac{\partial T_s}{\partial z} \tag{7.2}$$

From the standpoint of computation, it is convenient to consider a slice of steel which moves at the casting speed from an intial position at the meniscus (z=0, or time, t=0). Axial position from the meniscus can then be related by casting speed, $z = u_s t$ and thus, Equation 7.2 can be rewritten as,

$$\frac{\partial}{\partial x}\left(k_s \frac{\partial T_s}{\partial x}\right) + \frac{\partial}{\partial y}\left(k_s \frac{\partial T_s}{\partial y}\right) = \rho_s c_{ps} \frac{\partial T_s}{\partial t} \tag{7.3}$$

A schematic drawing of the transverse section of the slab is shown in Fig. 7.2 and it should be noted that the heat extraction rates from the slab surface is known at the centre of the broad and the narrow faces. Thus, due to a lack of appropriate boundary conditions (between the centre and corner of the face), the two-dimensional heat flow equation (Eq. 7.3) cannot be solved to determine the temperature distribution in the whole section of the slab (Fig. 7.2). Owing to these difficulties, calculations have been performed over a slice of steel located in the central region of the slab as shown in Fig. 7.2 and thus, the heat conduction in the transverse direction has been ignored which further reduces the heat flow problem into a one-dimensional one. The governing equation is given below,

$$\frac{\partial}{\partial x}\left(k_s \frac{\partial T_s}{\partial x}\right) = \rho_s c_{ps} \frac{\partial T_s}{\partial t} \tag{7.4}$$

Equation (7.4) represents an one-dimensional unsteady state heat flow model of the solidifying steel applicable to a slice of the strand of unit thickness moving at the casting speed and it should be noted that identical equation has been employed in the past to simulate solidification during continuous casting of slabs [145]. One initial condition and two boundary conditions are required to solve the differential Eq. (7.4).

Initial Condition is dependent on the temperature of steel at the meniscus. In the present model it has been assumed that the temperature of the steel at the meniscus is equivalent to the steel temperature in the tundish which was regularly monitored during casting.

$$t = 0, \quad 0 \le x \le x_m, \quad T_s(x) = T_p \tag{7.5}$$

Boundary Condition at the surface of the slab is governed by the heat extraction rates which have been well established in the present study. However, it is important to note that the surface boundary condition varies considerably along the casting direction.

$$t \ge 0 \quad x = 0, \quad -k_s \frac{\partial T_s}{\partial x} = q_m \tag{7.6}$$

At the centreline of the slab it is assumed that there is no net flow of heat due to symmetry and thus the appropriate boundary condition is given below (Fig. 7.2)

$$t \ge 0 \quad x = x_m, \quad -k_s \frac{\partial T_s}{\partial x} = 0 \tag{7.7}$$

7.1.3 Solution

Equation (7.4) along with the initial and boundary conditions Eqs. (7.5 to 7.7) are a complete mathematical description of heat flow in the solidifying slab. The differential equation (7.4) cannot be solved by analytical means owing to the temperature dependence of the thermo-physical properties of steel and the varying nature of the

boundary conditions at the surface of the slab and it was thus essential to utilize a numerical technique. The explicit finite difference technique was chosen to solve the Equation (7.4) with the appropriate initial and boundary conditions. The slice as shown in Fig. 7.2 was divided into nodes and finite-difference equations were derived by performing heat balances on each of the nodes.

7.1.4 Input Parameters Employed in the Model

The values of thermo-physical properties of steel such as latent heat, specific heat, density, thermal conductivity employed in the model were obtained from the literature [142,143] and are listed in Table 7.1. Furthermore, the liquidus and solidus temperatures of the steel for different compositions were also obtained from the literature [144] and are given in Table 7.1.

7.1.5 Sensitivity Analysis

It was essential to examine the effect of the node size and the time step on the accuracy and stability of the computed solution. Therefore, calculations were performed using various node sizes and time steps to determine the optimum magnitude of these independent variables which are listed in Table 7.1.

The precise manner in which the latent heat of fusion is released within the solidus and the liquidus temperature range is unknown due to the complex nature of solidification in the mushy region. Owing to the fact that the latent heat of fusion is of considerable magnitude when compared to the sensible heat and superheat of steel, the mathematical treatment of the removal of latent heat from the melt during solidification is crucial and could have a significant influence on the model predictions. This has been investigated by examining the influence of various assumed modes of solidification in the mushy region as shown in Fig. 7.3 on the temperature predictions by the model. The latent heat of fusion is incorporated in the model by artificially increasing the value of the specific heat as shown in Fig. 7.4 corresponding to the different solidification modes illustrated in Fig. 7.3.

Figure 7.5 shows the surface temperature of the slab at different locations in the mould computed with the different solidification modes (Fig. 7.3) and evidently, the variation in the temperature is small and furthermore, it should be noted that the shell thickness was essentially the same for the three cases. These findings have clearly demonstrated the nominal influence of the solidification mode on the temperature predictions made by the model and thus, the latent heat is assumed to be released in a linear fashion within the solidus and liquidus temperature range. The value of the specific heat in the mushy region employed in the model is given below,

$$c_{pm} = c_{p_s} + \frac{L_s}{T_{liq} - T_{sol}} \tag{7.8}$$

This technique of latent heat release must be applied with caution because it can lead to erroneous results as illustrated below with examples. In the event of high heat extraction rates or when large time steps are employed in the model, it is likely that the temperature of any particular node after one time step can drop from above the liquidus temperature to below the solidus temperature and consequently, the latent heat is not taken into account in the model (Fig. 7.6). Similarly, a drop in the temperature of a node from within the mushy region to below the solidus temperature does not consider the appropriate amount of latent heat. Therefore, it is crucial to ensure that exact amount of latent heat is removed from the different nodes during solidification. This was accomplished by employing a correction procedure in which at the end of each time step, heat balances were performed on nodes which have undergone solidification to correct their temperature. The details of the correction procedure is given in Appendix III.

7.1.6 Application of the Solidification Model

7.1.6.1 Shell Thickness

During casting, it is essential that the shell thickness of the strand is sufficient to withstand the ferrostatic pressure of the steel melt or else a break-out would occur below the mould. Furthermore, it will be shown later that a knowledge of the shell profile can be

utilized in the analysis of crack formation. Thus, the solidification model has been employed to compute the temperature distribution in the strand and the shell profile is generated from a knowledge of the solidus isotherm. The influence of casting speed on the shell profile is shown in Fig. 7.7 and not surprisingly, the rate of the shell growth is higher in the upper region of the mould than in the lower which is a reflection on the higher rates of heat extraction in the vicinity of the meniscus (Fig. 6.13). The significant influence of the casting speed on the shell thickness in the mould is also evident from Fig. 7.7 in which it is seen that an increase in speed results in a decrease in shell thickness at a given location in the mould due to the decrease in the residence time of a slice of steel. From these results it is easy to understand that a higher casting speed will enhance the possibility of a break-out. It is also interesting to note that the increase in the heat fluxes corresponding to an increase in casting speed (Fig. 6.28) is insufficient to offset the effect of a decrease in the residence time of steel in the mould. Needless to say, the heat extraction capability of the mould must be enhanced to be able to safely operate at higher casting speed and in the next chapter it will be shown that this can be accomplished by changing the mould design.

The influence of the mould flux on the shell thickness at the bottom of the mould is shown in Fig. 7.8. Evidently Pemco 389 mould flux results in a higher thickness than Stg 179 mould flux and this can be explained on the basis of higher rates of heat extraction in the mould with Pemco 389 compared to Stg 179 (Fig. 6.24). A plot of the shell thickness at the bottom of the mould as a function of the carbon content is shown in Fig. 7.9. It may be noted that the three steel grades were cast with the same mould flux and the casting speed was similar. It is interesting to note that despite the higher rates of heat extraction observed with carbon content of 0.29 percent compared to 0.04 and 0.09 percent-carbon grades (Fig. 6.25), the shell thickness is the lowest for 0.29 percent-carbon steel. The reduction in the shell thickness with increase in the carbon content is because of the lower solidus temperature of 0.29 percent-carbon steel grade compared to 0.04 and 0.09 percent-carbon grades.

7.1.6.2 Slab Surface Temperature

Figure 7.10 is a plot of the surface temperature of a low carbon steel slab as a function of casting speed. As expected, it can be seen that an increase in the casting speed results in higher temperature of the slab surface. A knowledge of the slab surface temperature profile in the mould can be utilized to elucidate the mould flux behaviour in the gap and also to examine the mould wall taper design and each of these aspects will be discussed in the subsequent sections.

7.1.6.3 Behaviour of the Mould Flux in the Gap.

The infiltration of the liquid flux into the gap between the strand surface and the mould wall results in the formation of a flux film which plays an important role during casting because of its ability to control heat transfer and lubrication in the mould. Behaviour of the mould flux film in the gap has been examined in the past in a qualitative manner [95,96] and a quantitative analysis requires a knowledge of the thermal field in the flux film which is bounded by the mould wall (hot face) and the strand surface. Therefore, the temperature distribution in the flux film is strongly governed by the temperatures of the mould wall and the slab surface both of which have been quantitatively characterized in the present study. The temperatures of the strand surface of a low-carbon steel grade (0.04 percent-carbon) cast with Pemco 389 mould flux and the mould wall at two different casting speeds are shown in Figs. 7.11 and 7.12 and it should be noted that the vertical line denotes the melting temperature of the mould flux which is of significance owing to the fact that flux film is presumably in solid state and thus, highly viscous below this temperature. It has been reported that the thermal resistance at the strand surface/flux film interface is small as the flux readily wets steel surface [115]. Therefore, it is reasonable to assume that the temperature of the flux film adjacent to the strand surface will be same as the slab surface temperature. It is evident from Figs. 7.11 and 7.12 that a large temperature gradient exists across the flux film; the mould flux adjacent to the mould wall in both the cases will exist in the solid state

because temperature of the mould wall is much lower than the melting temperature of the mould flux. However, it may be interesting to note that when casting with higher speed (Fig. 7.11), the surface temperature of the strand is always higher than the melting temperature of the mould flux which will lead to the presence of liquid flux adjacent to the strand surface. On the contrary at a lower casting speed (Fig. 7.12), towards the bottom of the mould the slab surface temperature is lower than the mould flux melting temperature and thus, the flux adjacent to the strand surface will be in solid state and will increase the friction between the strand and the mould wall. Needless to say, a liquid flux film is desirable as it would be beneficial from the standpoint of lubrication in the mould.

The above findings have demonstrated that the same mould flux can behave quite differently under different conditions and it is important to realize that the mould fluxes with appropriate melting temperatures must be utilized at different casting speeds; mould flux with a lower melting temperature should be employed at lower casting speed.

7.1.6.4 Taper of the Narrow Face Copper Plate

In the earlier chapter on mould temperature measurements, it was shown that the reduction in the mould temperature beyond the maximum peak on the narrow face (Fig. 5.2) is relatively steep when compared to the broad face (Fig. 5.6) and thus emphasizing the importance of tapering the narrow face copper plate. In addition to the significant influence of the taper of the mould wall on the heat extraction rates in the mould [123], the taper of the narrow face copper plate is strongly related to the occurrence of longitudinal corner cracks and this topic will be addressed in a later section. An examination of the slab surface temperature profile (Fig. 7.10) reveals that the reduction in the surface temperature is more rapid in the vicinity of the meniscus when compared with the lower part of the mould. This is more evident from Fig. 7.13 which is a comparison of reduction in slab surface temperature over two different regions in the mould and clearly, the drop in temperature is considerable near the meniscus which will lead to larger shrinkage of the shell. The non-uniformity in shrinkage of the shell will be

reflected in the thermal resistance of the gap and the shell which has been quantitatively characterized and will be addressed in the next section. It is important to note that owing to the enhanced shrinkage of the steel shell near the meniscus, the taper of the copper plate in the vicinity of the meniscus must be increased when compared to the lower region of the mould in order to accommodate the shrinkage. On the contrary, a linear taper of the narrow face is frequently employed in slab moulds, whereas the present finding indicates that the non-uniformity in shrinkage of the shell will consequently require a non-linear taper of the narrow face copper plate.

7.1.6.5 Thermal Resistances to Heat Flow in the Mould

From a knowledge of the heat fluxes and shell profile in the mould it was possible to estimate the major thermal resistances to heat flow in the mould. Figure 7.14 is a typical comparison between the resistance of the gap and the steel shell at different locations in the mould (narrow face). Evidently, the resistance of the gap is always larger than the shell resistance, but it may be interesting to note that in the vicinity of the meniscus, the resistance of the gap is much larger than the corresponding resistance of the shell. On the contrary, towards the lower region of the mould, the magnitude of the shell resistance approaches the gap resistance. It may be noted that Samarasekera et al. [146] have also reported that the magnitude of shell resistance is significant towards the bottom of a billet mould. From these findings it is concluded that the gap resistance dominates in the upper region of the mould and thus, controls the heat extraction whereas the heat flow towards the bottom of the mould is governed by the gap as well as the shell resistance. Therefore, the heat extraction rates near the vicinity of the meniscus can be further enhanced by increasing the taper of the narrow face since this will lead to a reduction in the gap resistance. The higher gap resistance in the upper part of the mould is because the surface temperature of the slab decreases rapidly which causes the shell to shrink more as discussed in the earlier section. On the otherhand, in the lower part because the shell resistance is significant, the surface temperature does not change very

much (Fig. 7.10) resulting in very little shrinkage. Thus if the same taper is used from the top to the bottom of the mould, binding between the shell and the mould wall will occur in the lower region of the mould which is undesirable. The above findings have also provided an insight on the mould wall taper and it clearly stems that a double taper of the narrow face will be more effective when compared to a linear taper from the standpoint of heat removal and slab quality.

7.2 Solidification Bands

Metallographic examination was conducted on samples cut from different locations as shown on the schematic drawing of the transverse section of the slab (Fig. 7.15). The photograph of a macroetched sample near the narrow face is shown in Fig. 7.16 and the presence of a number of distinct white continuous lines is evident. These white lines are commonly referred to as the white solidification bands. However, it may be interesting to note that the macroetched samples near the centre of both the broad faces (Fig. 7.15) did not reveal similar white solidification bands as observed on the sample near the narrow face. The presence of white bands on the macrostructure of billet sections has also been reported [5]. Electromagnetically stirred sections are frequently characterized by the presence of white bands [147] and it should be noted that the width of these bands is much larger when compared to the same observed on the slab sections in the present study (Fig. 7.16). Bridge et al. [147] have carried out chemical analysis in the region within the white band and have reported that the white band is a zone of negative segregation and usually depleted of elements like sulphur, phosphorus, manganese and carbon which tend to segregate positively. The formation of white bands in the billet section has been linked to the bulging of the shell in the mould or upper sprays which induces fluid flow at the solidification front removing the positively segregated elements [5]. It is generally believed that in a slab mould the molten stream from the immersion nozzle can penetrate the dendritic array resulting in the washing of the solute enriched interdendritic liquid and thus, leading to the formation of a white band. Furthermore, it

may be interesting to note that in a slab mould, molten stream from the immersion nozzle is directed towards the narrow faces, and owing to the relative stagnant flow conditions prevailing in the molten steel near the centre of the broad faces, white bands cannot be formed which is in agreement with the present findings. But based on this mechanism, it is difficult to explain the presence of a large number of discretely spaced white bands on the narrow side (Fig. 7.16). It can also be seen from the macrograph in Fig. 7.16 that cracks have originated from the innermost white band. It will be shown in the next section that these cracks are a consequence of bulging of the narrow face in the lower region of the mould and thus, the white bands as seen in the macrograph may be linked to bulging phenomenon as suggested by Bommaraju et al. [5]

It is well understood that the white bands delineate the location of the solid/liquid interface during solidification at the time fluid flow occurred and therefore, the shell profile in the mould can be used to establish the location on the casting machine at which these bands form. Heat extraction rates at the centre of the narrow face obtained from the mould temperature measurements were employed as a boundary condition in the solidification model described in the earlier section and the location of the solidification front at the narrow face at different locations in the mould is shown in Fig. 7.17. It should be noted that the innermost white band is located at a distance of 24 to 25 mm from the surface on the narrow face (Fig. 7.16) and an examination of the shell profile (Fig. 7.17) clearly indicates that the white band is formed in the lower region of the mould, approximately 700 mm below the top of the mould.

The most prominent feature of the macrograph shown in Fig. 7.16 is in the location of the white bands on the two opposite broad faces. On the inside radius, the distance between the innermost white band and the slab surface is 26 mm when compared to a distance of 28.5 mm on the outside radius which is an indication of difference in the shell thickness between the two broad faces. Wolf [50] based on measurements made on a break-out shell has also reported that the shell was thicker on the outside radius when compared to the inside radius, although no valid explanation was given to substantiate the

observation. The heat extraction rates obtained on the broad faces from the time-averaged mould temperatures have been employed in the solidification model and Fig. 7.18 shows a comparison of the shell thickness on the two opposite broad faces at a distance of 200 mm from the meniscus. Clearly, the shell thickness on the outside radius is always found to be more than the same on the inside radius for the three different grades of steel examined which is also apparent from the location of the solidification bands. It should be noted that comparison of shell thickness between the two broad faces along the entire length of the mould could not be made owing to the fact that the mould temperature measurements on the outside radius copper plate was made over a distance of 240 mm from the top of the mould. It is evident that the non-uniformity in the location of the white band on the two opposite broad faces is a consequence of differences in the heat extraction rates between the two broad faces which further confirms the measurements made in the present study, namely, the heat transfer rates on the outside radius face is greater than that on the inside radius (Fig. 6.21).

The macrostructure (Fig. 7.16) also shows the entrapment of mould flux beneath the surface on the narrow face which obviously is detrimental to the quality of the slab. It is likely that mould flux entrapment is a consequence of metal level fluctuation in the mould, the occurrence of which has been established in the present study from the mould temperature measurements made in the plant.

7.3 Slab Quality

7.3.1 Longitudinal Off-Corner Cracks

Longitudinal cracks were observed near the corner region of the broad face and details of the samples in which these cracks were found are given in Table 7.2. It may be noted that the cracks were found in low-carbon as well as high-carbon steel grades. A typical example of these type of cracks in a low-carbon steel grade is shown in the macrograph of the transverse section of the slab at the narrow face (Fig. 7.19). Macrographs of the transverse sections of the slab at the narrow face and in the off-corner

region of the broad face for a high carbon steel grade are shown in Fig. 7.20. Longitudinal corner cracks can be seen at the broad face near the corner (Fig. 7.20a) which is again similar to the cracks shown in Fig. 7.19. Furthermore, it may be noted that a depression can be seen in a small region of the surface of the broad face sample (Fig. 7.20b) and very fine cracks of the same orientation as the cracks shown in Fig. 7.19 and Fig. 7.20a are also present beneath the depression. It has been reported that longitudinal depressions are frequently seen on the surface of the broad faces in the off-corner region [34,148]. Brimacombe et al. [8] have examined the surfaces of the longitudinal mid-face cracks and have reported the smooth appearance of the crack surface which is an indication that the cracks are interdendritic in nature and formed by hot tearing close to the solidification front. The location of these cracks with respect to the surface varied in different samples (Table 7.2), but the orientation of the cracks was always the same indicating that transverse tensile strains initiated the cracks.

7.3.1.1 Mechanism of Formation of Longitudinal Off-Corner Cracks and the Depression

It can be seen in Fig. 7.19 that the innermost tip of the cracks are located at a distance of about 15 to 16 mm from the surface and since these cracks are known to be formed by hot tearing close to the solidification front, the solidification model can thus be utilized to determine the position of solidification front at different times and thereby, ascertain the location in the machine where these cracks form. From mould temperature measurements near the corner of the broad face (approximately 100 mm from the location of the cracks), heat fluxes were calculated using the mathematical model of the mould wall and employed in the solidification model to compute the shell thickness. From the shell profile near the corner of the broad face as shown in Fig. 7.21, it is evident that the cracks were initiated towards the bottom of the mould. As mentioned earlier, temperature measurements on the narrow face copper plate always indicated an increase in the mould temperature towards the bottom and this behaviour was very consistent (Fig.

5.2) from one heat to the next. The heat-flux profile along the centreline of the narrow face is also shown in Fig 7.21 and clearly, below 750 mm from the top of the mould there is an increase in the magnitude of the heat flux which may be a consequence of bulging of the shell due to the ferrostatic pressure of the liquid core which leads to a reduction in the gap dimensions and an increase in the heat flux. From Fig. 7.21 it appears that the phenomenon of bulging of the narrow face and initiation of the cracks occur approximately at the same location in the mould. The links between bulging of the narrow face shell and the concomitant cracks on the broad face is not difficult to explain. The bulging of the narrow face will impose transverse tensile strains on the broad face which will concentrate at the hot spots present in the vicinity of the corner. It should be noted that at the solidification front the steel can not withstand tensile strains owing to its poor ductility [4] and thus the tensile strains will lead to the formation of cracks. Needless to say, the bulging of the narrow face occurs due to insufficient taper of the narrow face copper plate. There is evidence in the literature suggesting that the occurrence of longitudinal corner cracks can be reduced by increasing the taper of the narrow face [17] which is in accordance with the present mechanism formulated for the formation of longitudinal cracks. It may be noted that the longitudinal cracks in different samples were not located at the same distance from the surface; for instance for the same grade of steel, cracks were found at 26 mm (Fig. 7.16) and also at 16 mm from the surface in Fig. 7.19. The differences in the location of the cracks in the two samples is a consequence of the difference in casting speed; the sample which showed cracks at a distance of 26 mm was cast at a low speed (0.5 m/min) than the sample in which cracks were formed at 16 mm from the surface (1.1 m/min).

The occurrence of longitudinal depression on the surface of the broad face may also be related to the bulging of the narrow face. It should be noted that towards the bottom of the mould, the temperature of the slab surface as calculated from the solidification model is found to be approximately 1150^{0}C to 1175^{0}C and thus, the surface has good ductility when compared to the solidification front. Owing to the bulging of the narrow face, the

shell near the broad face is subjected to transverse tensile strains which results in plastic flow of the surface much like in a tension test and consequently, the depression is formed at the surface. The formation of the longitudinal depression is schematically illustrated in Fig. 7.22. The results clearly indicate that the longitudinal depressions are formed in the mould which agrees with the findings of Yamamoto et al. [33]. Thomas et al. [34] based on their investigation conducted on stainless steel slabs have also reported that the bulging of the narrow face will lead to the formation of longitudinal depression on the broad face. However, they have suggested that the bulging of the narrow face will lead to the rotation of the shell near the corner of the broad face resulting in the formation of the depression.

It may be possible that the increase in the heat flux at the narrow face towards the bottom of the mould (Fig. 7.21) can also be a consequence of excessive taper of the narrow face which will enhance the contact between the shell and the mould wall. Simple calculations were performed to determine the thermal shrinkage of the broad face based on the temperature at the meniscus and at the mould bottom. The results indicate that thermal shrinkage will result in a reduction of the slab width from 1880 mm to 1862.7 mm at the bottom of the mould. From a knowledge of the taper of the narrow face (1 %/m), the width at the bottom of the mould was calculated to be 1863 mm. These results indicate that the taper at the bottom of the mould may be excessive which can lead to an enhancement in the heat flux. However, the above calculations are very simple in nature and thus it is necessary to do a complete calculation to establish the thermal shrinkage of the broad face. It may also be noted that the magnitude of increase in the mould temperature towards the mould bottom was more near the corner of the narrow face relative to the centre; this observation indicates that taper of the narrow face at the bottom may be too high. It may be interesting to note that excessive taper of the narrow face will result in compression of the broad face and result in the buckling of the shell thereby leading to the formation of the depression. The ensuing tensile strains generated at the

solidification front will lead to the formation of cracks. Thomas et al. [34] also have suggested that the depression at the broad face can be formed due to compression of the broad face resulting from excessive taper of narrow face.

7.3.2 Oscillation Marks

The slab samples from the narrow face and the broad face were shotblasted and the typical appearance of the surface of the sample on the narrow face is shown in Fig. 7.23. The surface of the narrow face sample is characterized by the presence of distinct oscillation marks. However, the oscillation marks on the broad face samples were not clearly seen owing to the fact that these marks are rolled out by the containment rolls in the sub-mould region.

The distance between consecutive oscillation marks was not always identical over the whole length of the sample which is probably a consequence of the metal level fluctuation in the mould. Nonetheless, it is quite evident from the photograph shown in Fig. 7.23 that these marks are frequently uniformly spaced and the distance between two consecutive oscillation marks is approximately equal to the pitch calculated from the ratio of casting speed and the mould oscillation frequency. This finding is in agreement with previous measurements and confirms that one oscillation mark is formed in each oscillation cycle of the mould [13]. Owing to the significant influence of the oscillation mark depth on the product quality and the casting operation, it was important to quantitatively characterize the depth of oscillation marks and thereby relate it to the process variables. The depth of oscillations marks were measured on the samples of the narrow face using a profilometer. A typical trace of surface of the sample generated by the profilometer is shown in Fig. 7.24 and the depth of oscillation marks were determined from the trace. It should be noted that there was a variation in the depth of the oscillation marks and the average depth of oscillation marks and the corresponding standard deviation is given in Table 7.3.

The variation of the oscillation mark depth with carbon content of the steel at different casting speeds is shown in Fig. 7.25. It can be seen that the depth of the oscillation mark is reduced with increase in carbon content of steel. However, it is also seen that the oscillation marks are deeper when the carbon content is near 0.08 to 0.10 percent range. The above findings on the influence of carbon content is in agreement with the measurements reported in the literature [40,41]. The increase in the depth of oscillation marks near 0.10 percent-carbon grades can be attributed to larger shrinkage of the steel because of the solid state $\delta to \gamma$ transformation. The lower depth of oscillation marks at higher carbon content of steel has been explained on the basis of the lower strength of the partially solidified meniscus which is drawn back toward the mould wall during the positive strip of the mould oscillation [41].

It should be noted that the stroke length and the frequency of oscillation of the mould in the present study was fixed and thus, casting speed is the only variable which can influence the negative strip time. The casting speed was approximately known for the duration in which the sample was cast in the mould and this value was utilized in conjunction with the stroke length and oscillation frequency to determine the negative strip time. Fig. 7.26 is a plot of the oscillation mark depth at different negative strip times and clearly, an increase in the negative strip time resulted in an increase in the depth of oscillation marks for the different grades of steel examined. These findings are in agreement with the earlier studies in the literature [20,28,40]. It has been suggested in the literature that an increase in the negative strip time will enhance the positive pressure developed in the mould flux channel and consequently increase the depth of oscillation marks [41]. However, it appears from Fig. 7.26 that a small increase in the negative strip time resulted in a considerable increase in the depth of oscillation marks which is difficult to explain on the basis of the mechanism proposed in the literature [41].

The influence of the casting speed on the depth of oscillation marks is shown in Fig. 7.27. It is evident that an increase in the casting speed will lead to a reduction in the oscillation mark depth. This observation was consistent in all the steel grades examined.

The finding on the influence of the casting speed agrees well with the results reported by Cramb et al. [40]. It appears that despite a fairly constant negative strip time, changes in the casting speed can have a significant effect on the depth of oscillation marks. In the next chapter which will be devoted to the mould flux behaviour at the meniscus, it will be shown that casting speed has a considerable effect on the behaviour of the mould flux at the meniscus which can strongly influence the oscillation mark depth.

Table 7.1 - Input parameters employed in the solidification model

Thermal Conductivity (W/m^0C) [142]	17.0 + 0.012 x Temperature
Specific Heat (J/kg^0C) [142]	540 + 0.094 x Temperature
Density (kg/m^3) [143]	7400
Latent Heat (kJ/kg) [143]	272.0
Solidus Temperature (^0C) [144]	1536- (415.5 x %C + 12.3 x %Si + 6.8 x %Mn + 124.5 x %P + 183.9 x %S + 4.3 x% Ni + 1.4 x% Cr + 4.1 x %Al)
Liquidus Temperature (^0C) [144]	1536 - (78 x %C + 7.6 x %Si + 4.9 x %Mn + 34.4 x %P +38.0 x %S + 4.7 x %Cu + 3.1 x %Ni + 1.3 x %Cr + 3.6 x %Al)
Time step Node Size	0.01 sec 0.001 m

Table 7.2 - Details of the samples showing longitudinal corner cracks.

Carbon content (wt. %)	Casting cpeed (m/min)	Location of the cracks from the surface (mm)
0.05	1.10	16.0
0.05	0.52	26.0
0.29	0.75	22.0

Table 7.3 - Summary of the oscillation mark depth measurements from the profilometer.

Carbon content (wt. %)	Casting speed (m/min)	Negative strip time (sec)	Average depth of oscillation mark (mm)	Standard deviation
0.04	0.52	0.2987	1.2537	0.0813
0.05	0.52	0.2987	1.0493	0.1813
0.06	0.87	0.2732	0.6865	0.1766
0.05	1.1	0.2567	0.5357	0.1092
0.05	1.12	0.2552	0.4172	0.1093
0.05	1.12	0.2552	0.4816	0.1573
0.09	0.49	0.2998	1.1267	0.2333
0.08	0.56	0.295	0.9799	0.3293
0.08	0.56	0.295	0.8296	0.2013
0.09	0.62	0.2908	1.0753	0.2247
0.09	0.75	0.2817	0.9308	0.1842
0.09	1.07	0.2588	0.7717	0.1016
0.09	1.07	0.2588	0.8345	0.1352
0.09	1.1	0.2567	0.9321	0.3051
0.09	1.1	0.2567	0.8361	0.2988
0.18	0.8	0.2782	0.5660	0.1448
0.18	0.8	0.2782	0.6633	0.1234
0.17	0.98	0.2657	0.5364	0.1594
0.19	1.11	0.2559	0.4168	0.0690
0.28	0.53	0.2971	0.5029	0.0524
0.28	0.53	0.2971	0.5073	0.0615
0.29	0.82	0.2768	0.3531	0.0487
0.29	0.82	0.2768	0.3305	0.0709
0.36	0.78	0.2796	0.7980	0.1315
0.36	0.78	0.2796	0.7771	0.0563

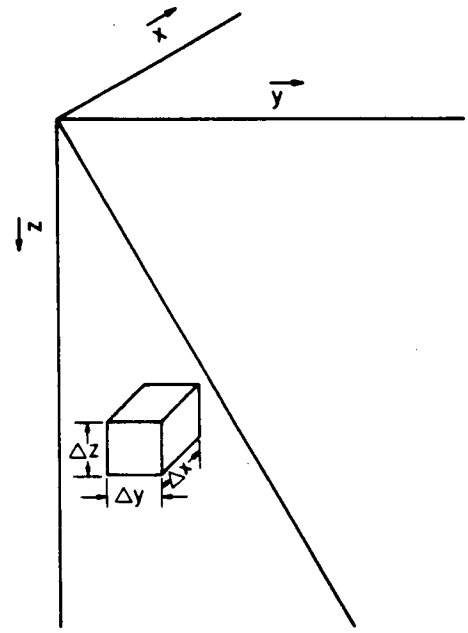

Figure 7.1. Schematic drawing showing the location of the control volume in the solid shell.

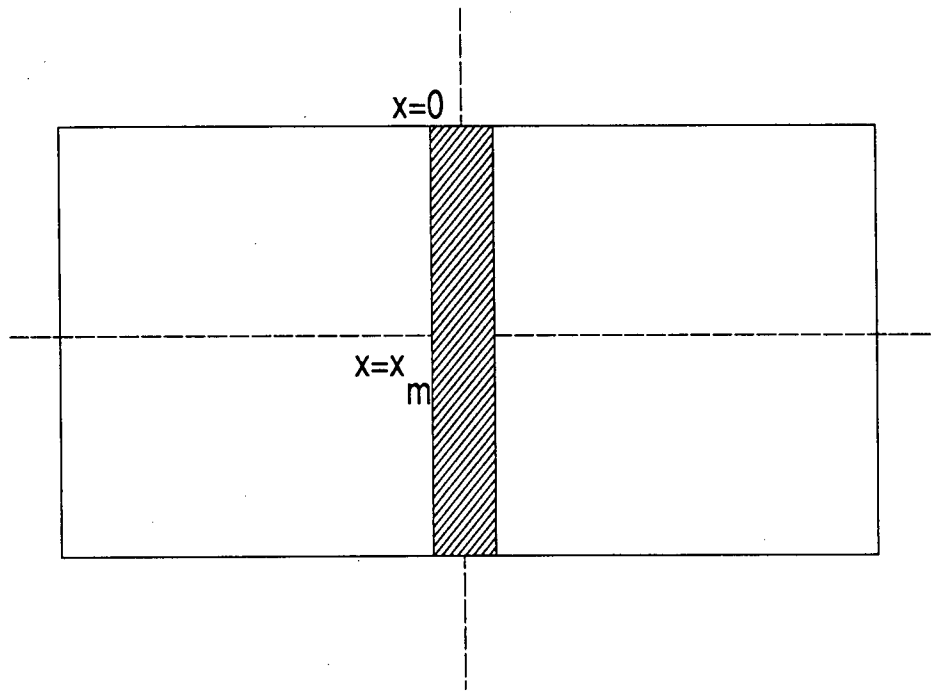

Figure 7.2. Schematic drawing of the transverse section of the slab.

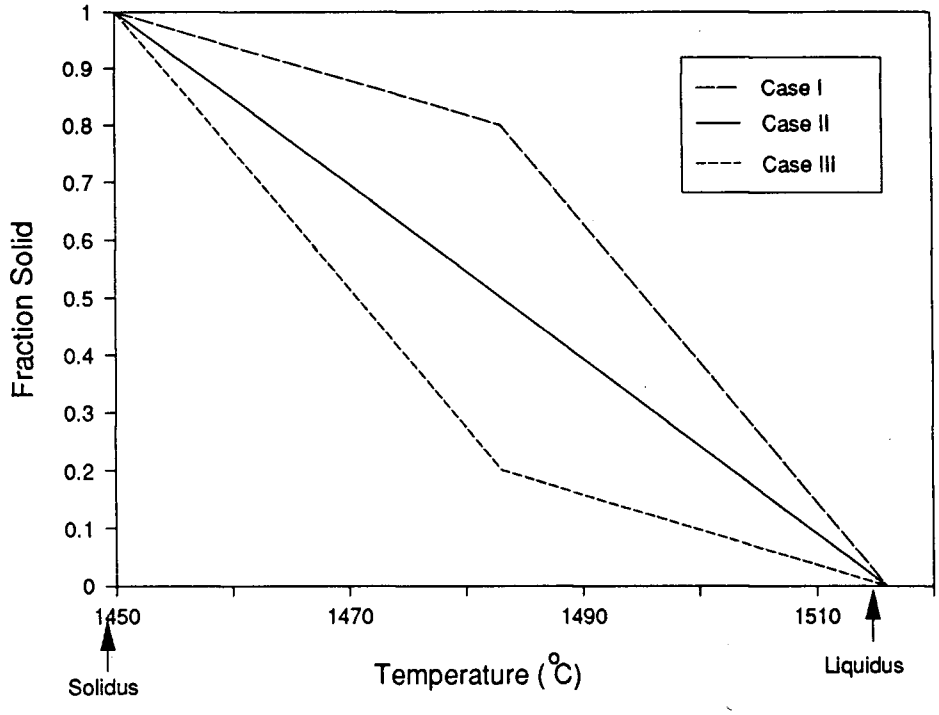

Figure 7.3. Variation of solid fraction in the mushy region for three different assumed solidification modes.

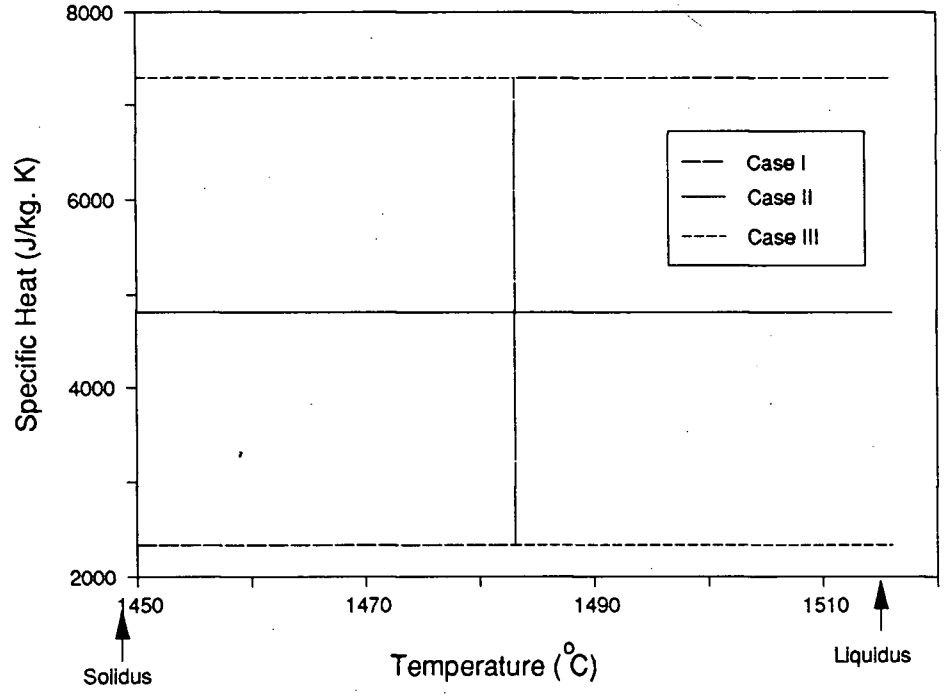

Figure 7.4. The magnitude of the specific heat in the mushy region for the three solidification modes shown in Fig. 7.3.

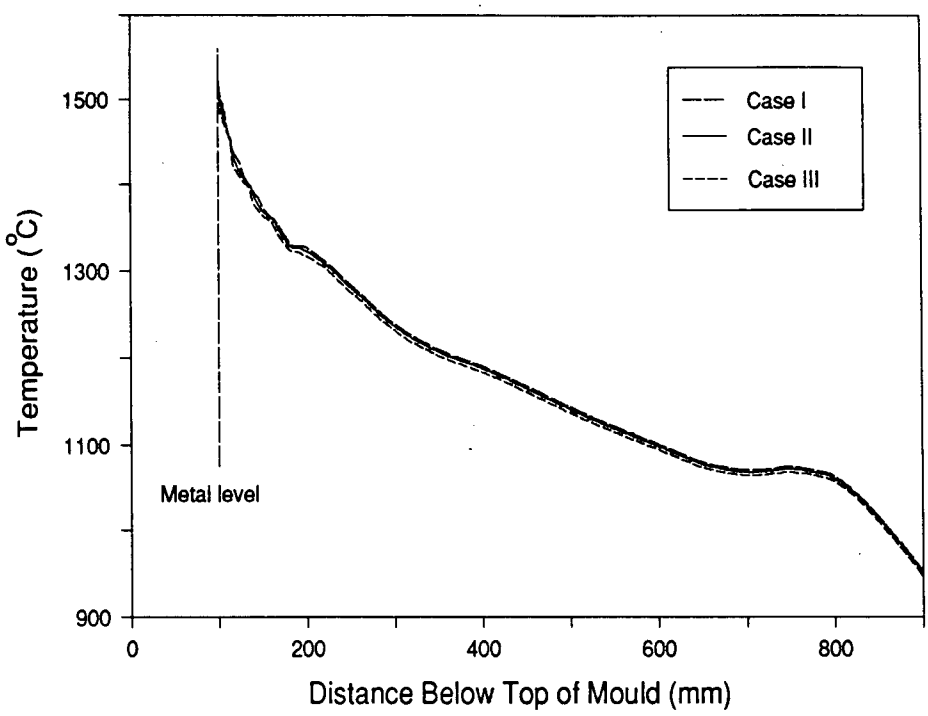

Figure 7.5. Model predicted surface temperature of the slab for different modes of latent heat release shown in Fig. 7.4.

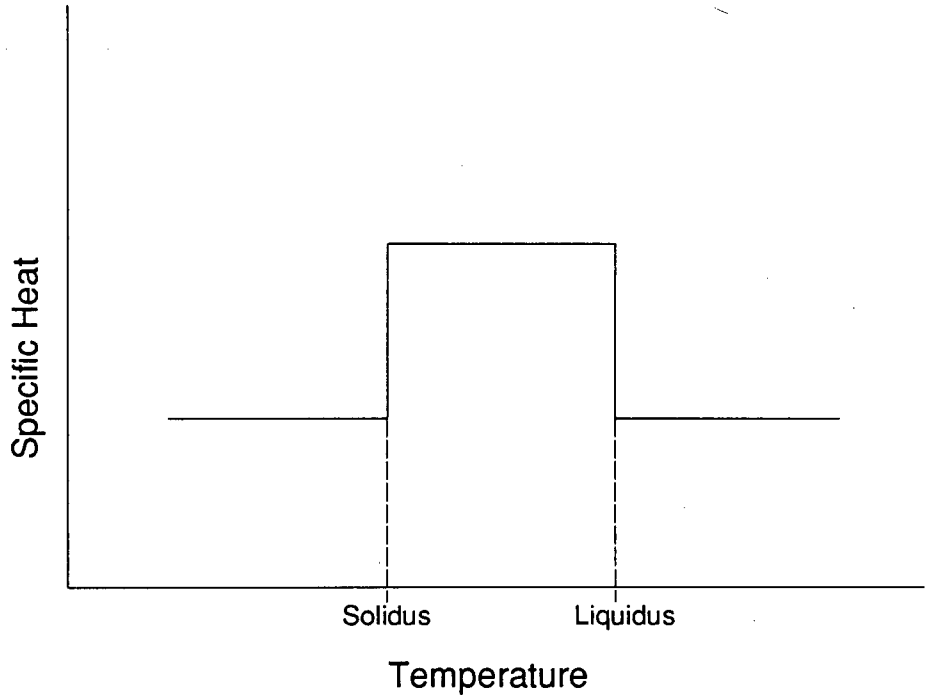

Figure 7.6. Schematic drawing to illustrate the incorporation of latent heat by increasing the specific heat in the mushy region.

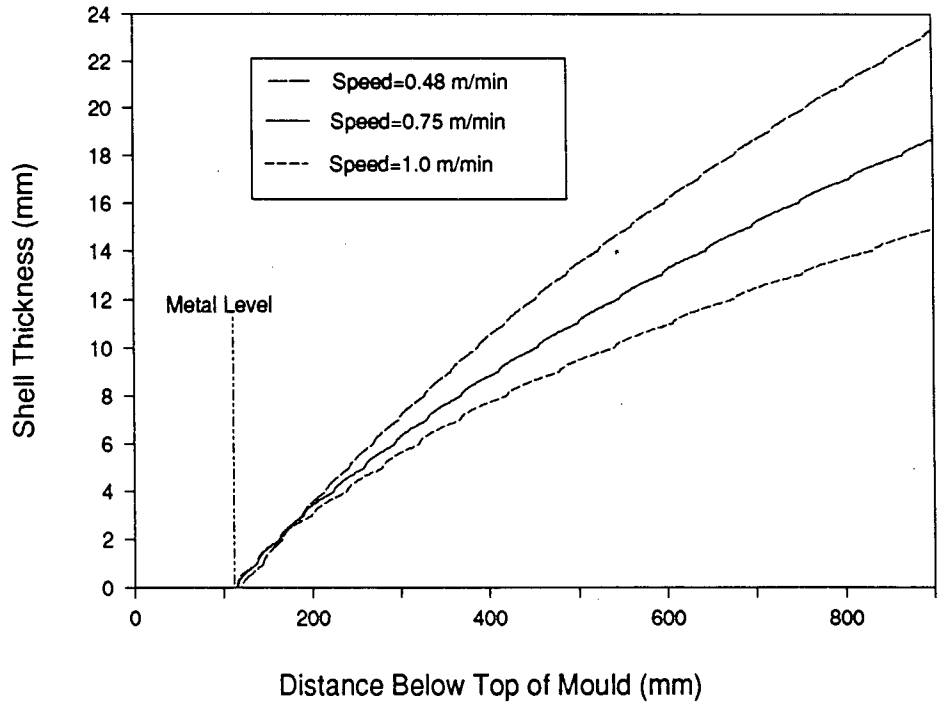

Figure 7.7. The influence of casting speed on the shell profile in the mould for a high carbon steel (C=0.18-0.21 %).

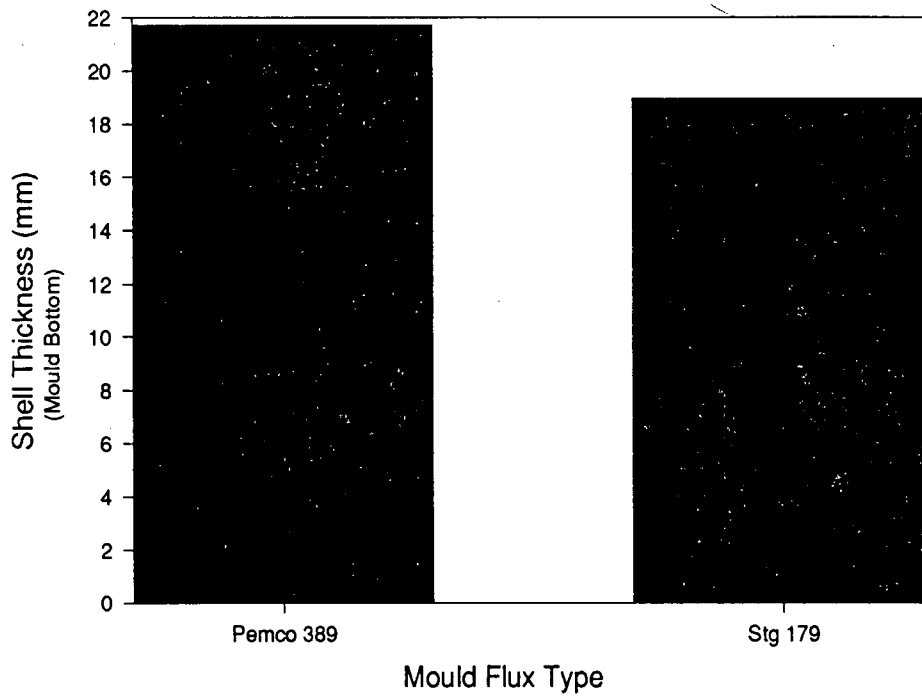

Figure 7.8. The influence of mould flux type on the shell thickness at the bottom of the mould.

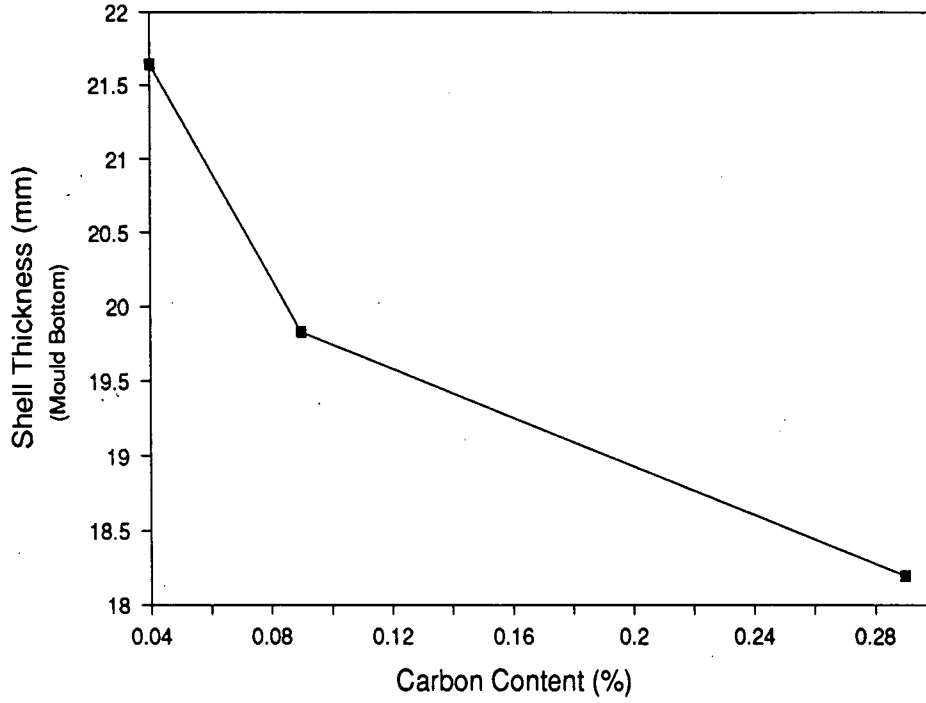

Figure 7.9. The influence of steel carbon content on the shell thickness at the bottom of the mould. (casting speed=0.75 m/min)

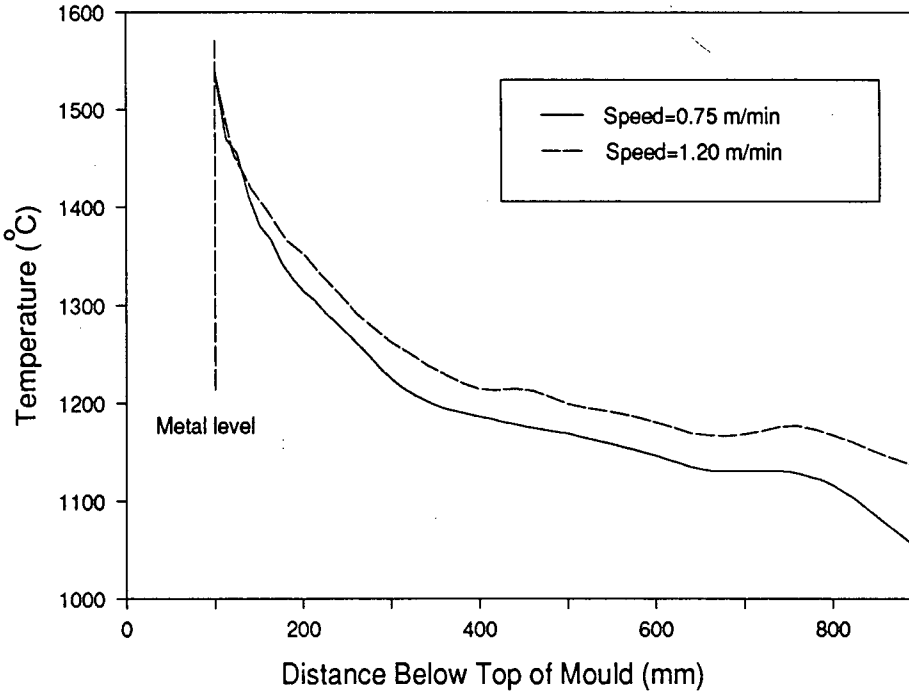

Figure 7.10. The influence of the casting speed on the surface temperature of the slab (%C=0.04).

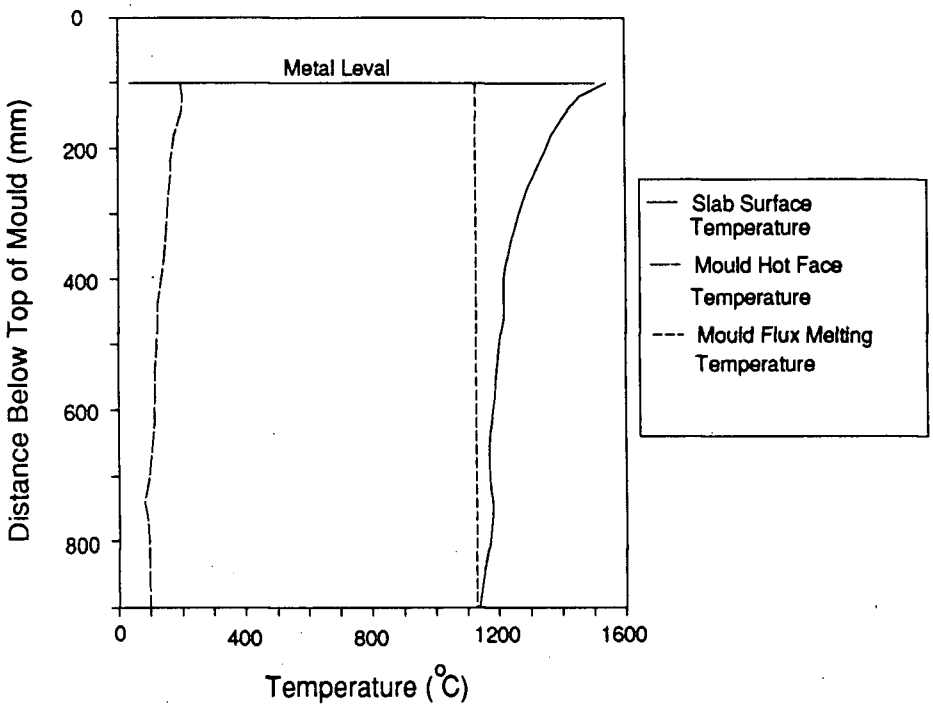

Figure 7.11. Illustration of the behaviour of the mould flux in the gap between the shell and the mould wall (Pemco 389 mould flux, C=0.05%, casting speed=1.2 m/min)

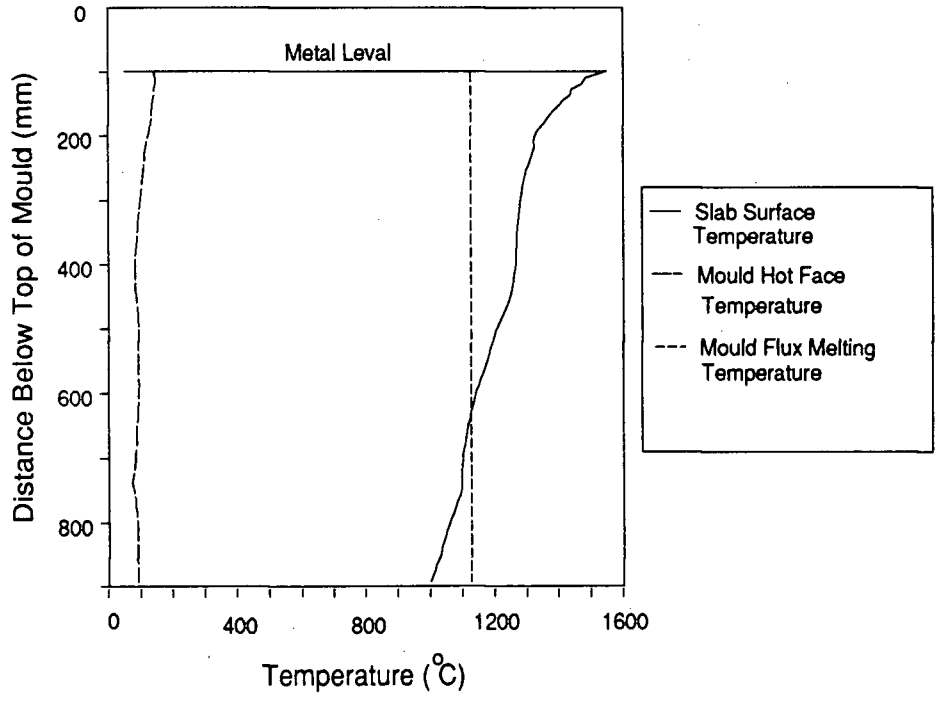

Figure 7.12. Illustration of the behaviour of the mould flux in the gap between the shell and the mould wall (Pemco 389 mould flux, C=0.05%, casting speed=0.54 m/min)

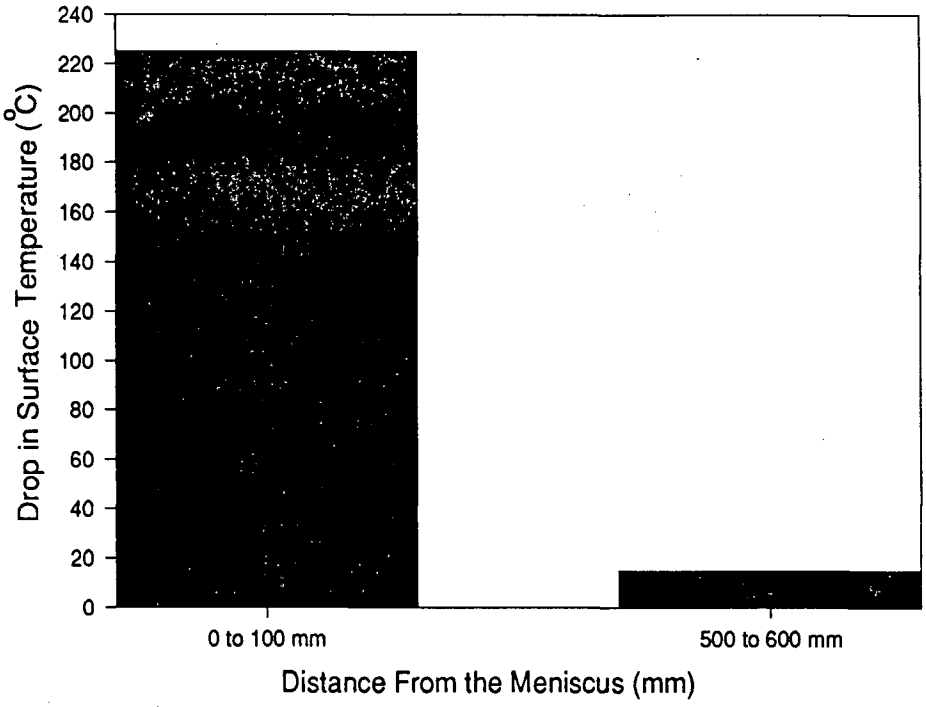

Figure 7.13. Reduction in the slab surface temperature over two different zones in the mould obtained from the model (C=0.04%, casting speed=0.75 m/min, Pemco 389 mould flux)

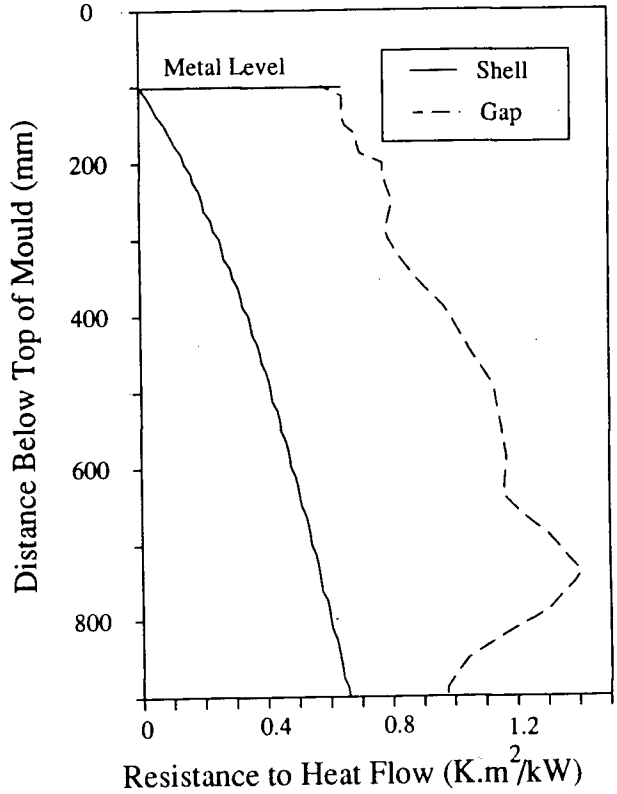

Figure 7.14. Comparison between the gap and the shell resistance at different locations in the mould (C=0.04%, casting speed=0.75 m/min, Pemco 389 mould flux).

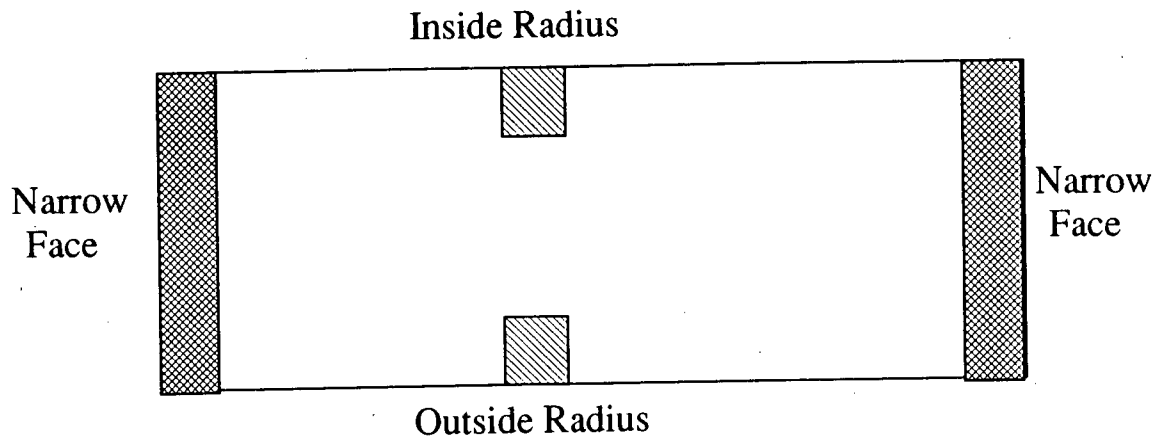

Figure 7.15. Schematic drawing of the transverse section of the slab illustrating the location of samples metallographically examined.

Figure 7.16. Macrostructure showing the presence of white solidification bands, Mag X0.8 (C=0.05%, casting speed=0.52 m/min, Pemco 389 mould flux).

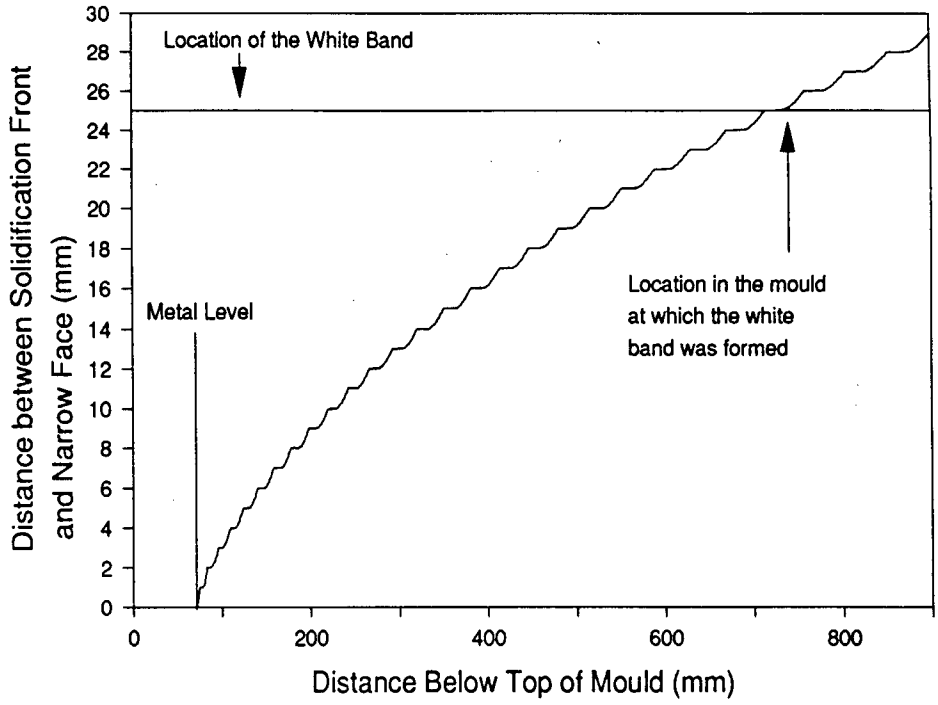

Figure 7.17. Location of the solidification front near the narrow face at different times in the mould showing that the white band is formed in the mould.

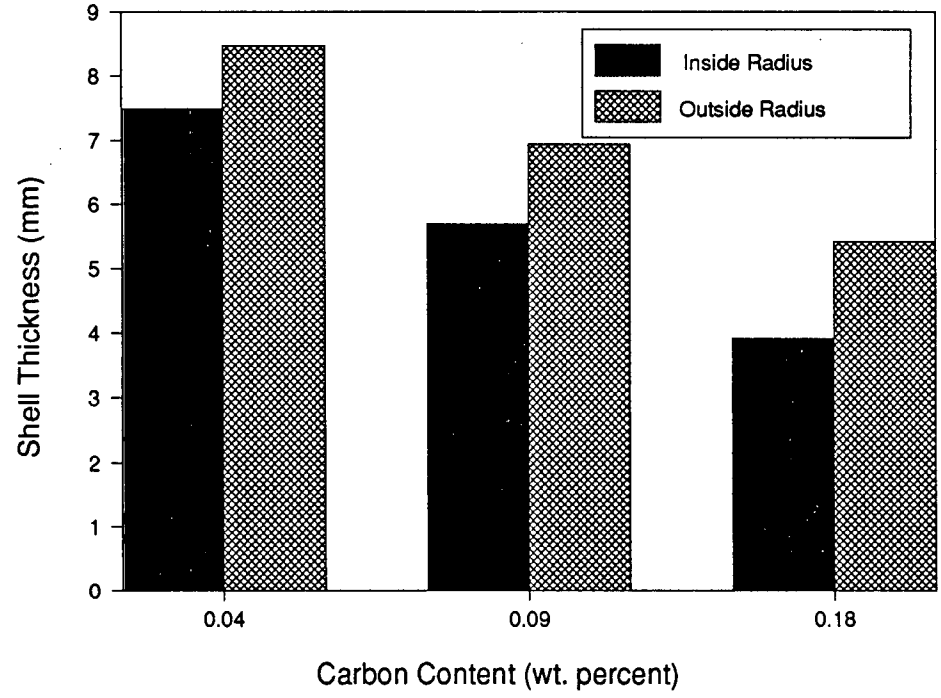

Figure 7.18. Comparison of the model predicted shell thickness at the two broad faces at 200 mm from the meniscus for three different grades of steel at a casting speed of 0.75 m/min.

Figure 7.19. Macrograph of a transverse section of sample cut at the narrow face showing longitudinal corner cracks on the broad face near the corner, Mag. X1.4 (C=0.05%, casting speed=1.10 m/min).

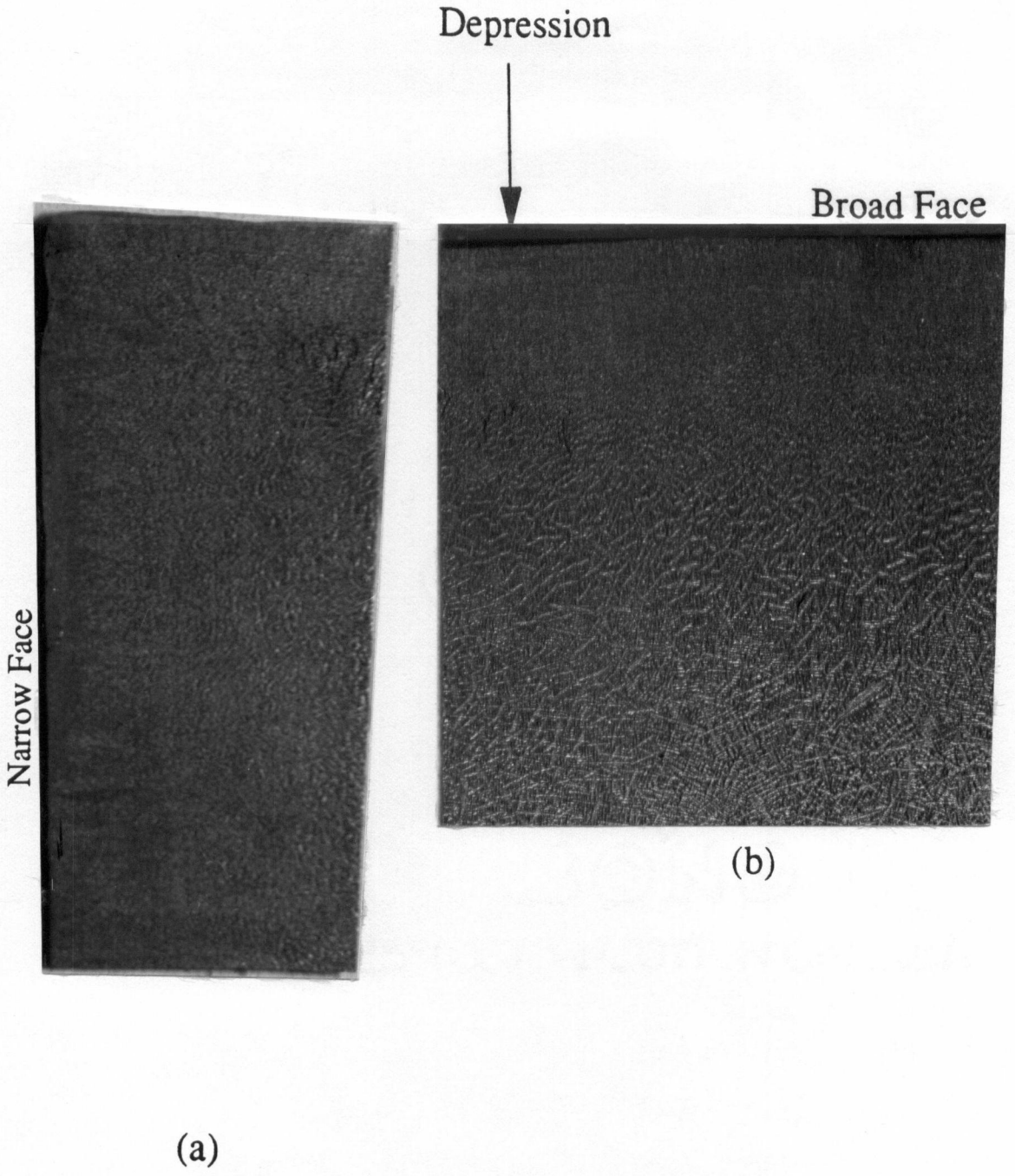

Figure 7.20. Macrographs of transverse sections of (a) sample cut near the narrow face showing longitudinal corner cracks, Mag. 0.8X (b) sample from the off-corner region of the broad face showing a depression on the surface, Mag. 1.1X (C=0.29%, casting speed=0.75 m/min).

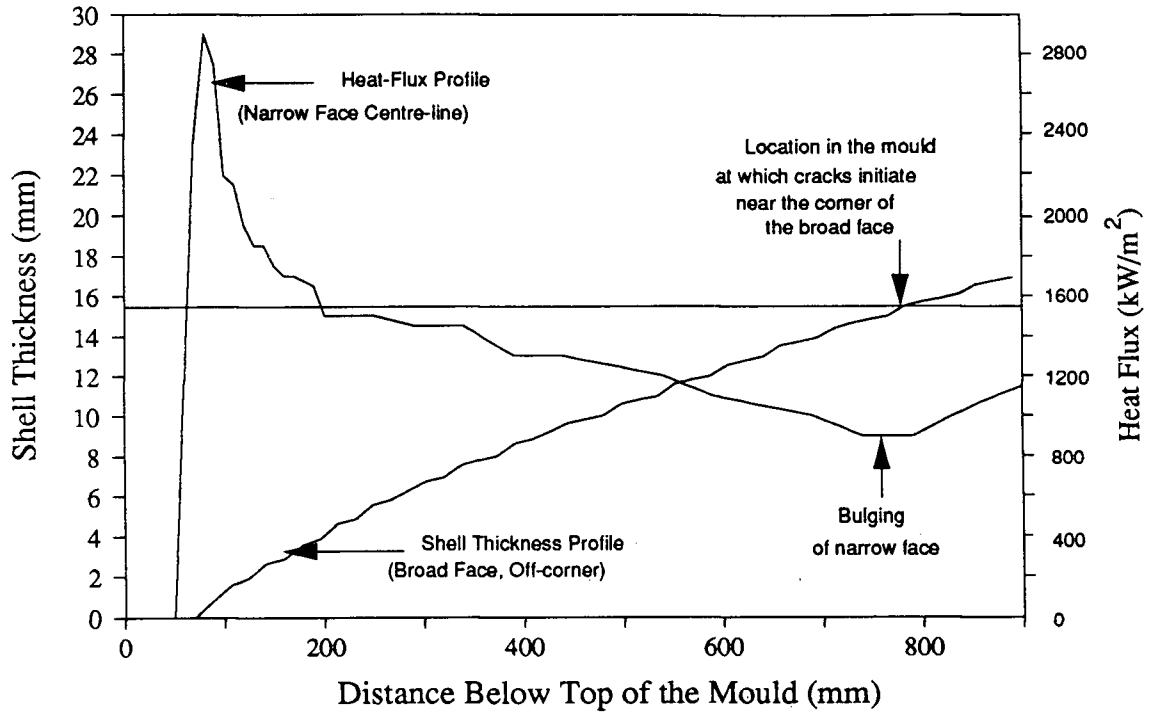

Figure 7.21. Heat-flux profile indicating the bulging of narrow face towards the bottom of the mould and the concomitant occurrence of longitudinal cracks on the broad face (C=0.05%, casting speed=1.1 m/min).

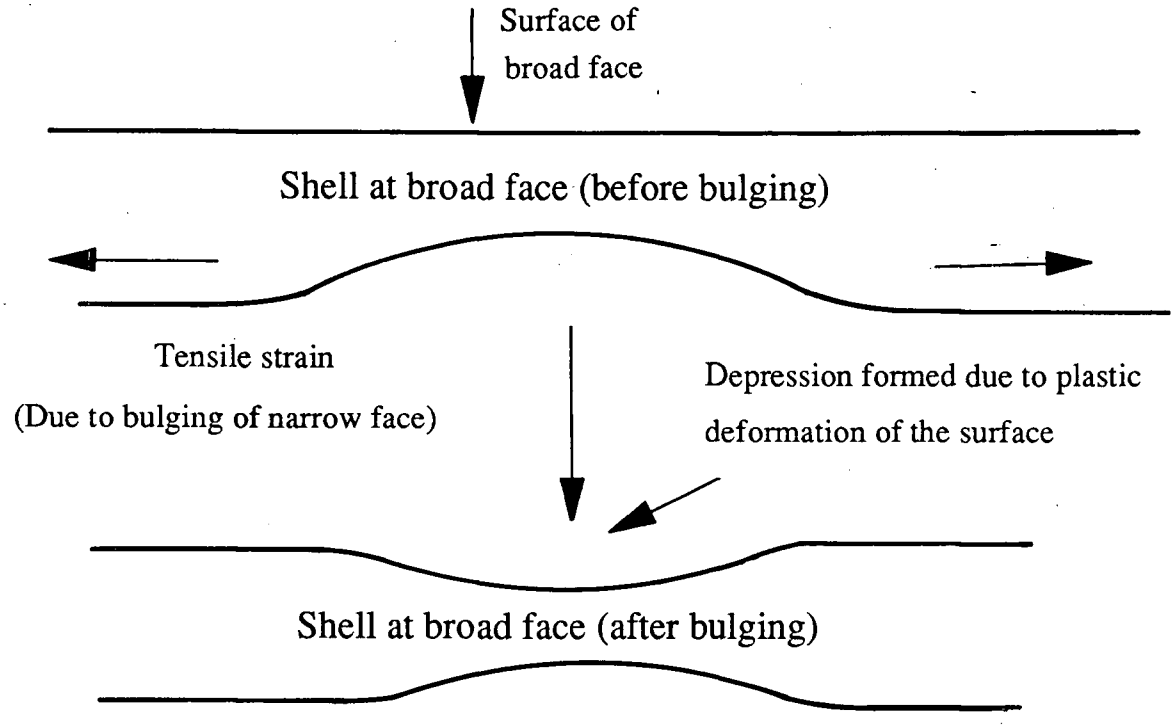

Figure 7.22. Schematic drawing to illustrate the formation of a depression on the slab surface due to bulging of the narrow face.

Figure 7.23. Typical surface appearance of the slab on the narrow face showing the presence of oscillation marks, Mag. 1.1X.

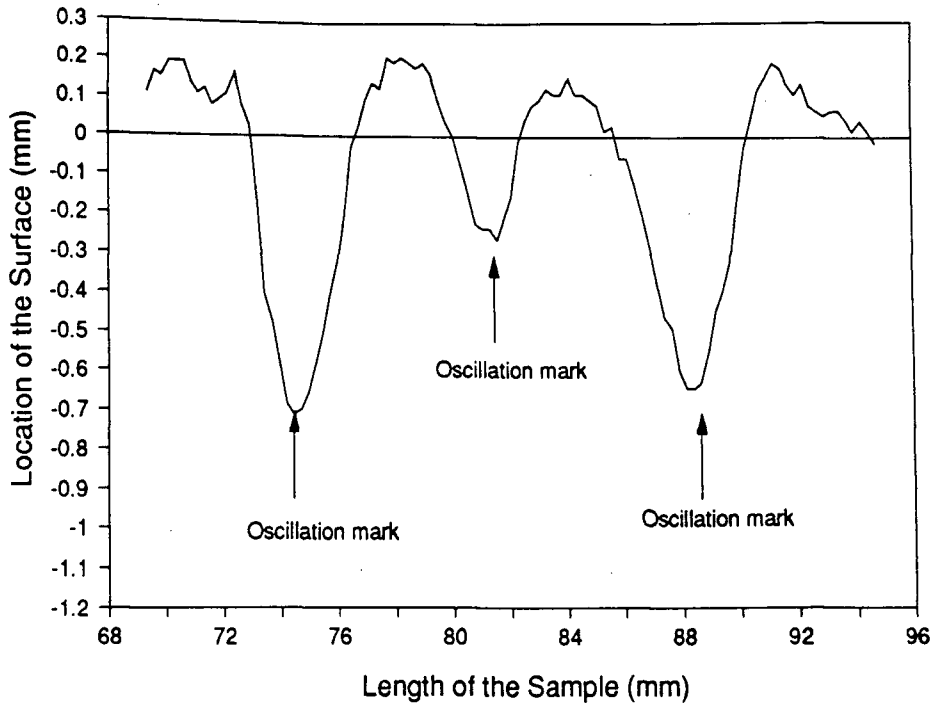

Figure 7.24. Typical trace of the slab surface generated by the profilometer.

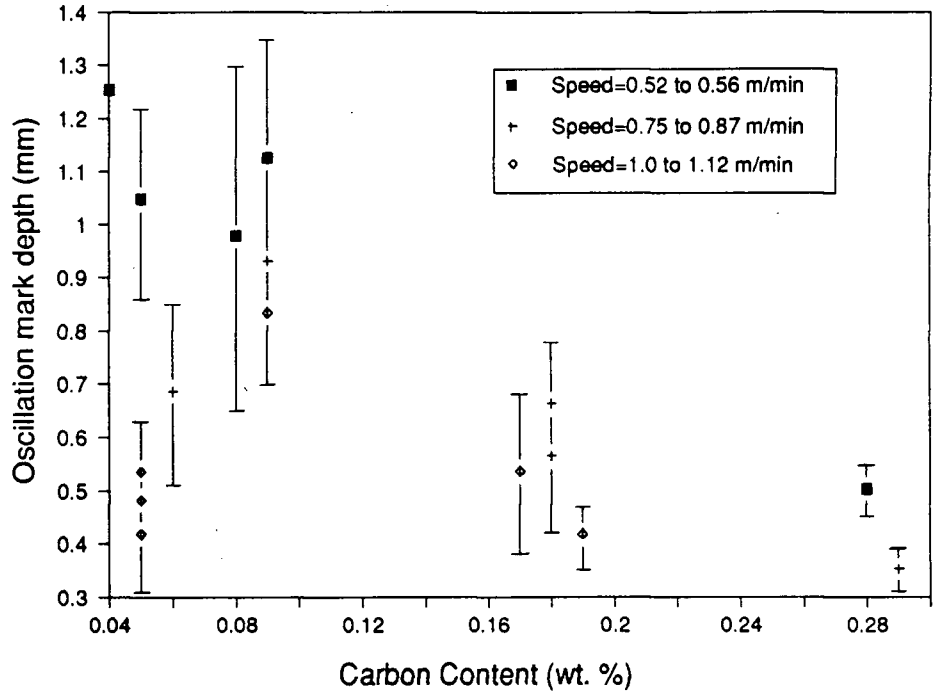

Figure 7.25. Influence of steel carbon content on the oscillation mark depth.

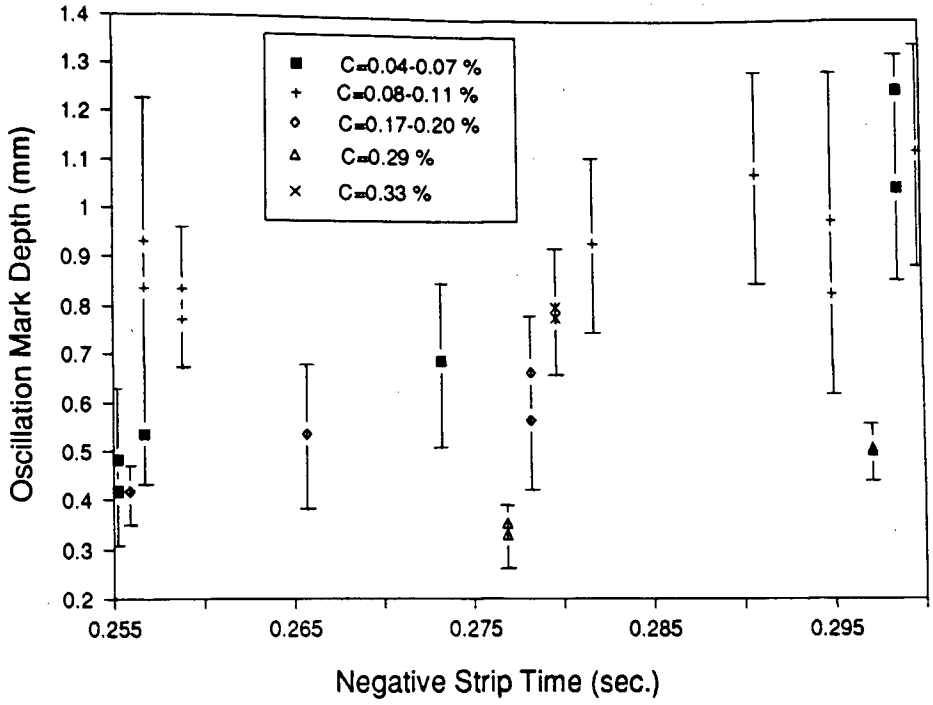

Figure 7.26. Influence of negative strip time on the depth of oscillation marks.

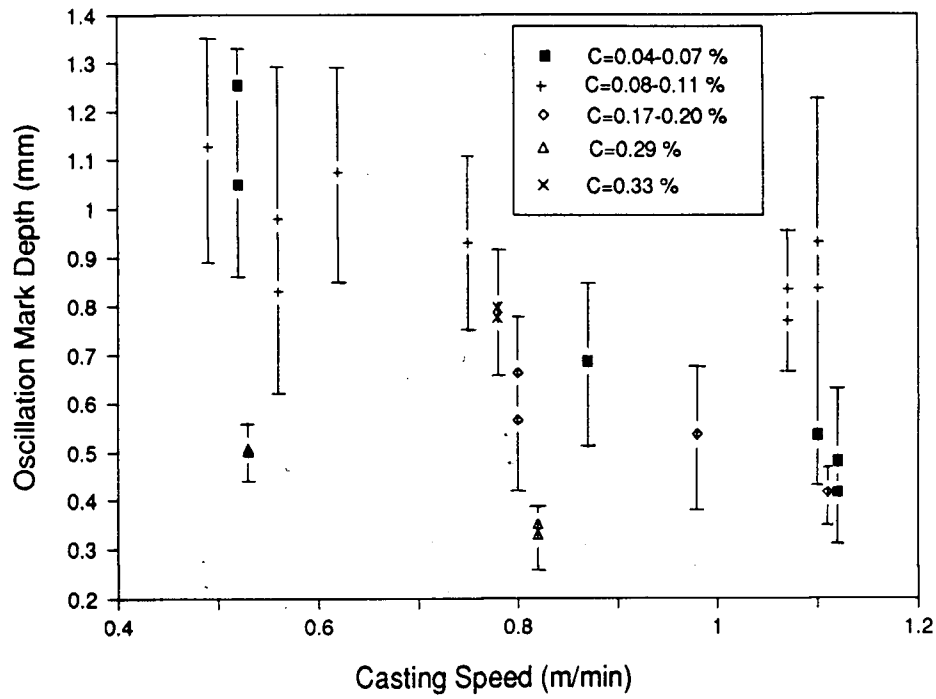

Figure 7.27. Influence of casting speed on the depth of oscillation marks.

Chapter 8 - MOULD FLUX BEHAVIOUR AT THE MENISCUS

In the present study the influence of two different types of mould flux on heat transfer has been examined and the results as presented in Chapter 6 have clearly demonstrated the importance of the mould flux from the standpoint of heat transfer in the mould. Furthermore, it has been intimated that the influence of process variables like casting speed, submergence depth and in some instances even carbon content is related to the mould flux behaviour at the meniscus. One of the important findings of the present study, the differences in the heat extraction rates on the two opposite broad faces, could also be a consequence of differences in the mould flux behaviour owing to its strong influence on the heat transfer in the mould as established in Chapter 6. Needless to say, an assessment of the mould flux behaviour at the meniscus requires a quantitative characterization of the thermal field in the mould flux which was accomplished by developing an one-dimensional heat flow model of the mould flux, the salient features of which will be presented in this chapter. The model predictions have been utilized to rationalize the differences in the heat transfer characteristics on the two broad faces and has also aided in the formulation of a mechanism to explain the differences in the observed depth of oscillation marks under different casting conditions.

8.1 Mathematical Model of the Mould Flux

The mould flux surrounding the meniscus exists in different physical states, namely, liquid, sinter and powder as shown schematically in Fig. 8.1. During casting the liquid flux flows down between the shell and the mould wall and thus, lubrication and heat transfer in the mould are influenced by the infiltration rate of the liquid flux at the meniscus. Therefore, in the model only the liquid layer of the mould flux has been taken into consideration which further simplified the modelling exercise.

8.1.1 Assumptions

The assumptions made in the heat flow model of the mould flux are given below,

(i) The temperature distribution in the mould flux is at steady state.

(ii) The thermal resistance at the mould flux-mould wall interface is assumed to be constant. The implications of this assumption will be discussed later.

(iii) Heat flow in the liquid flux occurs by conduction only. It may be noted that molten steel from the submerged entry nozzle is directed toward the narrow faces and thus, convection in the mould flux particularly adjacent to the broad faces is expected to be small and hence ignored in the calculations.

(iv) Heat conduction along the height of the liquid flux layer has been neglected. Simple calculations indicate that the heat flux in this direction is approximately 40 kW/m^2 which is smaller compared to the heat flux from the surface of the flux to the mould wall.

(v) The thermophysical properties of the mould flux are assumed to be constant.

8.1.2 Formulation

The steady state temperature distribution in the mould flux cannot be directly determined from Fourier's Law owing to phase changes occurring in the mould flux during its solidification which results in the release of latent heat of fusion. This was overcome by developing an unsteady state heat flow model which was utilized to compute the steady state thermal fields in the mould flux. A heat balance on an infinitesimal volume located in the mould flux as shown in Fig. 8.2 will result in the following differential equation.

$$\frac{\partial}{\partial x}\left(k_{flux}\frac{\partial T_{flux}}{\partial x}\right)+\frac{\partial}{\partial y}\left(k_{flux}\frac{\partial T_{flux}}{\partial y}\right)=\rho_{flux}c_{pflux}\frac{\partial T_{flux}}{\partial t} \qquad (8.1)$$

Heat conduction along the height of the liquid flux layer has been neglected, and thus, Equation (8.1) can be simplified to the following.

$$\frac{\partial}{\partial x}\left(k_{flux}\frac{\partial T_{flux}}{\partial x}\right) = \rho_{flux}c_{pflux}\frac{\partial T_{flux}}{\partial t} \qquad (8.2)$$

Equation (8.2) represents a one-dimensional unsteady-state heat flow model of the mould flux. The solution to the above equation requires one initial condition and two boundary conditions.

The **initial condition** is necessary to specify the initial temperature of the mould flux. It may be noted that the one-dimensional model has been utilized at different locations in the mould flux ($0 \le y \le y_m$, Fig. 8.2) to determine the two-dimensional temperature distribution in the mould flux. The temperature of the mould flux is expected to vary along its height; the temperature will be maximum near the meniscus and will then be expected to decrease with increasing height (Fig. 8.2). Thus, the initial temperature of the mould flux at the meniscus (y=0 in Fig. 8.2) is taken to be 1400^0C, however, the initial temperature of the mould flux at $y = y_m$ is expected to be slightly more than its melting temperature and hence is taken to be 1200^0C in all the calculations.

$$t = 0, \quad 0 \le x \le x/2, \quad T_{flux}(x) = T_{iflux} \qquad (8.3)$$

Boundary Conditions: A constant temperature boundary condition was specified at the surface of the mould flux adjacent to the mould wall, which was determined from the magnitude of the heat flux, the thermal resistance at the flux/mould wall interface and the temperature of the mould wall. In the present study, extra precaution was taken to install thermocouples above the metal level, and from these measurements heat fluxes from the mould flux to the mould wall were established. Figure 8.3 is a plot of the variation of the heat fluxes with distance above the meniscus at different casting speeds as determined from the time-averaged mould temperatures. It is important to note that the depth of the liquid flux layer is approximately 10 mm [148] and thus, the magnitude of the heat fluxes adjacent to the liquid flux is known (Fig. 8.3). The temperature of the

mould wall adjacent to the mould flux was determined from the mathematical model of the mould discussed in Chapter 6. The surface temperature of the mould flux needed as a boundary condition was calculated from the following equation.

$$T_{sur} = q_{flux} R_{flux} + T_m \tag{8.4}$$

The boundary condition at the surface is given by, (Fig. 8.2)

$$t \geq 0 \quad x = 0, \quad T_{flux} = T_{sur} \tag{8.5}$$

There is no heat flow across the centreline (x=x/2, Fig. 8.2) and thus, the boundary condition is given by,

$$t \geq 0 \quad x = x/2, \quad -k_{flux} \frac{\partial T_{flux}}{\partial x} = 0 \tag{8.6}$$

8.1.3 Solution

The explicit finite difference technique was employed to solve Equation (8.2) with the appropriate initial and boundary conditions Eqs. (8.4 to 8.6) to compute the temperature distribution in the mould flux. It may be noted that the method utilized to incorporate the latent heat of fusion during mould flux solidification was identical to that used in the model of the solidifying strand discussed in the previous chapter. From a knowledge of the heat flux, surface temperature, solidus temperature and thermal conductivity of the mould flux, the dimension of the steady state slag rim was determined. Comparisons were made at the end of each time step between the computed thickness of the solidified mould flux adjacent to the mould wall and the steady state slag rim thickness until an agreement was reached between the two thicknesses and thus the steady state temperature distribution in the mould flux was determined. The two-dimensional temperature distribution in the liquid flux layer was established by employing the one-dimensional model at different heights in the liquid flux layer (Fig. 8.2) but, utilizing the appropriate heat fluxes and the mould temperature values at the corresponding locations to determine the relevant boundary conditions.

8.1.4 Characterization of the Input Parameters Employed in the Model

As mentioned earlier, a constant value for the thermal resistance at the mould wall/flux interface determined from the literature has been utilized to calculate the surface temperature of the mould flux required as a boundary condition in the model. Riboud et al. [115] have reported that the value of the contact resistance between the solid mould flux and the copper plate is within the range $1x10^{-3}$ to $5x10^{-4}$ W^{-1} m^2 K based on results obtained with different types of mould fluxes. Ohmiya et al. [117] also have made measurements in the laboratory to estimate the heat fluxes with different mould fluxes and have reported that the mean contact resistance (average of the mould flux/mould wall and mould flux/shell resistance) varied between 0 to $3x10^{-4}$ W^{-1} m^2 K. It may be noted that in the model, calculations have been performed with different assumed values of the contact resistance which will be discussed later.

The thermophysical properties of the mould flux such as density, thermal conductivity, specific heat and heat of fusion are important input parameters into the model. Unfortunately, the relevant information on these properties were not provided by the mould flux manufacturers. However, a few investigators have reported values of physical properties of the mould fluxes obtained from laboratory measurements [113,150]. The composition of the mould fluxes in the present investigation was different from those on which measurements have been conducted and thus, the available information on the values of the properties could not be utilized in the present study. However, it should be noted that the thermophysical properties of components like CaO, SiO_2, Al_2O_3 which constitute a major fraction of the mould flux are available in the literature [149]. From a knowledge of the weight fractions of the different components constituting the mould flux, the thermophysical properties of the mould fluxes have been estimated, the values of which are quite similar to the measurements reported in the literature for a variety of mould fluxes.

The softening and the melting temperatures of the mould fluxes were provided by the mould flux manufacturers and this information was utilized to represent the solidification temperatures of the mould flux. The details of the various input parameters employed in the model are listed in Table 8.1.

8.2 Model Predictions of Temperature Distribution in the Mould Flux

A typical example of a temperature distribution in the mould flux with distance from the mould wall, at two different levels from the meniscus, as predicted by the model is shown in Fig. 8.4 and it is evident that the temperature of the mould flux adjacent to the copper plate is lower than its melting temperature which will consequently lead to the formation of a solid layer of mould flux, which is usually referred to as the slag rim. The presence of a slag rim is considered to be detrimental as it can physically obstruct the inflow of the mould flux at the meniscus and thereby affect heat transfer and lubrication. The steady state temperature distribution was utilized to determine the slag rim thickness from a knowledge of the melting (Liquidus) isotherm. The temperature predictions in Fig. 8.4 are based on an interface resistance of zero between the flux and the copper plate. Model predictions also were made for interface resistances of $1x10^{-4}$ W^{-1} m^2 K and $2x10^{-4}$ W^{-1} m^2 K. Fig. 8.5 is a profile of the slag rim above the meniscus for three interface resistance values and clearly, the model predicts a finite thickness of the slag rim in each of the cases, but the absolute magnitude of the slag rim thickness is influenced by the value of the interface resistance chosen. It is important to note that the magnitude of the interface resistance will vary with the nature of the mould flux, but its value will be expected to stay constant for the same mould flux. Therefore, based on this rationale, relative comparison of the slag rim dimensions formed under different operating conditions with the same mould flux can be made by employing a constant value of the interface resistance in the model; a value of zero interface resistance has been incorporated in the model because the exact value is not known. The model predictions

have been utilized in conjunction with the findings of the present study to ascertain the significance of the mould flux behaviour from the standpoint of heat transfer and product quality (oscillation marks) which will be discussed in the subsequent sections.

8.3 Discussion on the Heat Transfer in the Mould

It was shown earlier that the heat extraction rates were different on the two broad faces; the higher heat fluxes on the outside radius as determined from the time-averaged mould temperatures (Fig. 6.21) were supported by the shell thickness measurements on the two faces indicated by the location of the white band seen on the macrostructure (Fig. 7.16). A typical example of the heat-flux profiles above the metal level on the two broad faces are shown in Fig. 8.6 and this information has been utilized to determine the relevant boundary conditions for the heat flow model of the mould flux. A comparison of the slag rim thickness profile above the metal level adjacent to the two broad face copper plates is shown in Fig. 8.7 and clearly, the slag rim is thicker on the inside radius as compared to the outside radius. The influence of the slag rim on heat transfer can be better understood from the schematic drawing in Fig. 8.8 which shows the presence of a slag rim adjacent to the mould wall above the meniscus. It is easy to imagine that the slag rim will act as a physical barrier and thus, impede the infiltration of the mould flux into the gap between the strand surface and the mould wall which will subsequently affect the the heat transfer. Nakano et al. [25] have reported that the heat transfer in the mould is reduced when the height of the liquid flux is small; it is easy to understand that the slag rim will be more effective in inhibiting the inflow of mould flux particularly when the depth of the liquid flux layer is small compared to the mould oscillation stroke length. Based on this logic, it can be said that the lower values of heat flux on the inside radius is a consequence of a thicker slag rim which will enhance the restriction of the mould flux infiltration at the meniscus as compared with the outside radius. Furthermore, the model has been utilized to perform similar calculations on a number of different heats and the results consistently show that the slag rim is thicker on the inside radius compared to the

outside radius as shown in Fig. 8.9. The reason for the differences in heat transfer and consequently the differences in the slag rim thickness at the two broad faces need to be clarified. Although the flow patterns and the temperature of the steel in the vicinity of the meniscus will influence the temperature distribution in the mould flux and consequently, the dimensions of the slag rim; it is difficult to explain the differences in the slag rim thicknesses by this rationale because the submerged entry nozzle is symmetrically located between the two broad faces and will presumably result in identical flow patterns and local temperature of the molten steel near the meniscus. Therefore, another reason must exist for the differences in the slag rim dimensions at the two broad faces.

Further insight on the different characteristics on the mould flux behaviour near the broad faces can be gained by examining the design of the two copper plates and its influence on the mould wall temperature. Comparison of the copper thickness of the two plates employed on the broad face is shown in Fig. 4.1 and it was intimated earlier that the differences in the copper thickness is a consequence of the curvature of the mould wall only at the hot face. It is important to note that in the vicinity of the meniscus the copper thickness on the outside radius is of greater magnitude than at a corresponding location on the inside radius copper plate (Fig. 4.1). An increase in the copper thickness will result in an increase in the resistance to heat flow through the thickness which further leads to higher temperatures at the hot face on the outside radius. Furthermore, it should be noted that the depth of the cooling channels on the two copper plates is identical and thus, the increased distance between the hot face and the top of the cooling channel on the outside radius (Fig. 4.4a) will lead to higher temperature of the hot face. The axial hot face temperature profiles above the metal level on both the broad faces are shown in Fig. 8.10 and clearly, the temperature of the outside radius is higher than the inside radius copper plate. It follows from the above discussion that the liquid mould flux comes in contact with two copper plates which are at different temperaturess. Thus, the lower slag rim thickness associated with the outside radius can be attributed to the higher temperature of the copper plate in the region adjacent to the mould flux which in turn

enhances the the heat extraction rates at the meniscus. From the above findings, it can be inferred that the heat extraction capability of the mould can be enhanced by minimizing the slag rim dimensions which can be accomplished by increasing the hot face temperature of the copper plate in the vicinity of the meniscus; this aspect will be discussed later. Wolf [123] has implied that an increase in the water velocity in the mould resulted in a reduction in heat transfer. Fogleman et al. [151] of Luken Steel have reported that a reduction in the water flow rate in the mould from 110 l/s to 98 l/s resulted in an increase in the heat transfer from 62.8 kJ/kg to 81.4 kJ/kg. These results are in apparent agreement with the present findings because a reduction in the water velocity will lead to higher temperature at the hot face which will consequently result in thinner slag rim and thus, a subsequent increase in the heat transfer.

It is necessary at this point to provide a rationale for the strong dependence of the slag rim thickness on the magnitude of the mould wall temperatures. It is important to note that the thermal conductivity of the mould flux is quite low and therefore, a small change in the slag rim thickness can result in large change in its thermal resistance which is crucial because the slag rim offers the largest resistance to heat flow. A small decrease in the mould wall temperature at the hot face will increase the slag rim dimensions which will further increase the resistance to heat flow thereby resulting in a reduction in the heat flux which consequently will lead to a further drop in the mould wall temperature. There is a synergism between heat transfer, mould wall temperature and slag rim thickness since they are interrelated.

8.4 Discussion on Oscillation Marks

The oscillation marks present on the broad faces of the slab are rolled by the containment rolls located in the sub-mould region of the casting machine as shown in Fig. 8.11. Thus, it was not possible to quantitatively characterize the depth of oscillation marks present on these samples. However, careful visual examination of the surfaces of these samples (Fig. 8.11) consistently revealed that the oscillation marks present on the

inside radius sample are relatively more distinct when compared to same on the outside radius sample. This observation suggests that the oscillation marks on the inside radius sample were originally deeper than those on the outside radius sample. The mechanism responsible for the differences in oscillation mark depth between the two broad faces can be elucidated by examining the interaction between the solid slag rim and solidified shell at the meniscus. It has been proposed by Kawakami et al. [12] that the slag rim which is attached to the mould wall moves with the mould during its oscillation and thus, during negative strip when the downward velocity of the mould is greater than that of the strand, the solid slag rim adjacent to the mould wall will compress the shell at the meniscus resulting in its deformation and forming an oscillation mark. Furthermore, it may be noted that Tada et al. [64] have attempted to examine the influence of the size of the slag rim on the positive pressure developed in the flux channel and their results indicate that an increase in the size of the slag rim will increase the pressure and thereby enhance the deformation of the meniscus. The chain of events occurring in each oscillation cycle of the mould leading to the formation of an oscillation mark as proposed by Kawakami et al. [12] are schematically illustrated in Fig. 8.12. It emerges from the above mechanism that the depth of an oscillation mark will be largely governed by the magnitude of the deformation of the shell at the meniscus which in turn will be influenced by the dimension of the slag rim, the mechanical properties of the steel and the downward displacement of the slag rim during the negative strip period. Needless to say, the stroke length of the mould oscillation is fixed and the high temperature mechanical properties of steel will remain the same. Therefore, the presence of deeper oscillation marks on the inside radius when compared to the outside radius can only be rationalized on the basis of the slag rim dimension; a thicker slag rim adjacent to the inside radius (Fig. 8.9) results in an increase in the depth of oscillation marks compared to the outside radius face.

A key finding which was apparent from the oscillation mark depth measurements conducted on the narrow face samples was the influence of the casting speed on the oscillation mark depth; an increase in the casting speed resulted in a decrease in the

oscillation mark depth (Fig. 7.27). Cramb et al. [40] have also reported the strong dependence of oscillation mark depth on casting speed. The influence of casting speed on the depth of oscillation marks has been explained in the past by linking an increase in casting speed to a decrease in the negative strip time which will subsequently reduce the depth of oscillation marks. However, it may be noted that within the range of casting speeds examined (0.5 to 1.1 m/min) and with an oscillation frequency of 90 cycles per minute and a stroke length of 11 mm, the resultant negative strip time is between 0.26 to 0.29 seconds and thus the variation in the negative strip time is small rendering it difficult to explain the observed influence of the casting speed on the depth of oscillation marks. The latter effect can be rationalized in light of the mechanism proposed by Kawakami et al. [12] for the formation of oscillation marks. In other words, casting speed must have a strong influence on the slag rim thickness which in turn affect the oscillation mark depth; this is to be expected since casting speed has a strong influence on the heat transfer. The heat flow model of the mould flux has been utilized to assess the influence of casting speed on the slag rim thickness at the narrow face and the results as shown in Fig. 8.13 depict a trend; an increase in the casting speed resulted in a reduction in the slag rim thickness. Therefore, the observed reduction in depth of oscillation marks at higher casting speeds (Fig. 7.27) is an outcome of thinner slag rim. The significant increase in the heat transfer in the vicinity of the meniscus at higher casting speed (Fig. 6.28) is a consequence of increase in the rate of heat input to the mould flux which increases its melting rate, temperature and reduces the slag rim dimensions.

It is possible to draw parallels from the observations made in the present study to studies conducted earlier on oscillation marks. It has been reported in the literature that oscillation mark depth can be reduced by inserting insulating sleeves on the mould wall in the vicinity of the meniscus [59]. It is likely that the presence of insulating sleeves will increase the temperature of the mould wall which will minimize the slag rim thickness and consequently, the depth of oscillation marks will be reduced. Takeuchi and Brimacombe [41] have reported the presence of sub-surface hooks beneath the oscillation

marks which formed a larger angle with the surface on high carbon steel grades when compared to low carbon grades. This observation is probably a consequence of thicker slag rim adjacent to the mould wall, the interaction of which can physically bend the partially solidified meniscus and result in the large angle between the hook and the slab surface.

8.5 Recommendations for Improvements in Mould Design

The influence of the thickness of the copper plate in the vicinity of the meniscus on the heat transfer in the mould has been well established in the present study and for the first time demonstrates quantitatively the link between mould design and mould heat-transfer. It also provides an effective method for increasing production rates and reducing the depth of oscillation marks. In the past attainment of higher production rates has been generally accomplished at high speeds with the attendant risk of break-outs. It is possible however as a result of this study to increase the heat extraction capability of the mould particularly at high casting speeds simply by increasing the mould wall thickness thereby increasing the productivity without enhancing the possibility of a break-out. The influence of the mould wall thickness on the heat transfer and the concomitant influence on the production rates will be illustrated with an example. The heat-flux profiles at the two broad faces were calculated at two casting speeds from the mould temperature data and utilized in the solidification model to compute the shell profiles. Figure 8.14 is a plot of the computed shell thickness at the mould exit on the two opposite broad faces for the same heat cast at two different speeds. Not surprisingly, an increase in the casting speed leads to a reduction in the shell thickness on the two broad faces and moreover, the influence of the copper thickness on the magnitude of the shell thickess is clearly seen. It can be shown with simple calculations that the shell thickness at the mould exit (16.58 mm), corresponding to a speed of 0.985 m/min can be attained at a higher speed (1.155 m/min) simply by increasing the copper thickness at the meniscus from 38 to 44 mm.

This increase in the casting speed is equivalent to an increase of 17 percent in the production rate demonstrating the significance of the benefits that could be achieved through an increase in the mould wall thickess.

The influence of the copper thickness on the heat transfer in the mould has been explained on the basis of the relative dimensions of the slag rim at the meniscus. This rationale has been employed to predict the heat fluxes as a function of copper thickness at the meniscus. The mathematical model of the mould wall was utilized to compute the temperature of the copper near the meniscus and based on this information the slag rim dimensions were obtained as a function of the copper thickness. From a knowledge of the slag rim thickness, heat fluxes were estimated and a plot of the meniscus heat flux values at different copper thickness values are shown in Fig. 8.15. The details of these calculations are presented in Appendix IV. From the above results it can be inferred that the heat extraction capability of the mould can be enhanced by increasing the magnitude of the copper thickness at the meniscus. It is a standard practice to remachine and reuse the copper plates until the thickness reaches a specified minimum value. This procedure warrants re-examination in light of the findings of this study, since this practice will lead to a reduction in heat transfer over the life of the mould plates which can have an adverse effect on the slab quality.

In addition to the copper thickness, the temperature of the mould wall is also governed by the water velocity in the cooling channel, inlet temperature of cooling water. Based on the findings of this study, it can be said that a reduction in the water velocity and an increase in the water inlet temperature will result in higher heat extraction rates in the mould by increasing the temperature of the mould wall which will reduce the slag rim thickness. The enhancement of the heat transfer rates in a slab mould due to a reduction in the water velocity has been reported in the literature [151]. However, it may be noted that a decrease in the water velocity and an increase in the water temperature may result in the occurrence of nucleate boiling in the cooling channel which is not desirable and thus can offset the advantages interms of the heat transfer. Unlike the effect of mould

wall thickness, it was not possible to quantitatively establish the influence of water velocity and temperature on heat transfer primarily due to a lack of data because these variables were constant during plant trials.

Table 8.1 - Input parameters employed in the heat flow model of the mould flux

Specific Heat (J/kg^0C)	1025.7
Density (kg/m^3)	3040.0
Latent Heat (J/kg)	615296.0
Thermal Conductivity (W/m^0C)	2.0
Softening Temperature (^0C)	1050
Melting Temperature (^0C)	1125
Node Size (mm)	0.1 and 1.0
Time Step (sec)	0.01

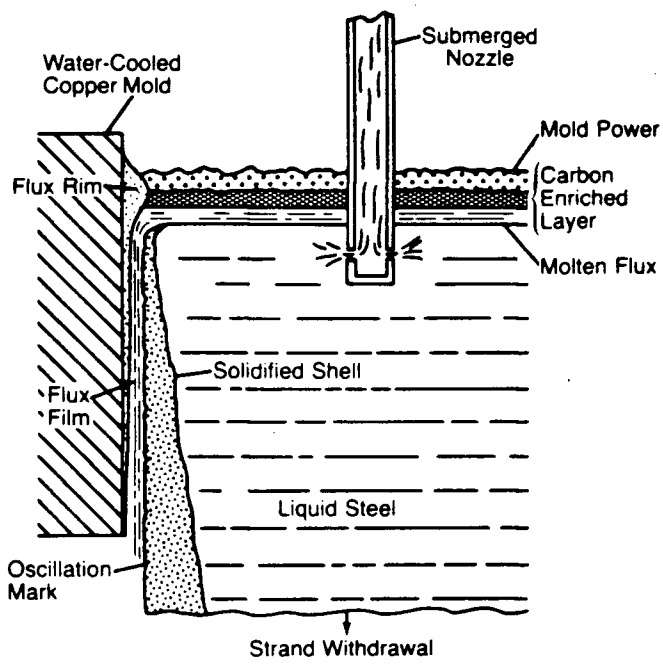

Figure 8.1. Schematic drawing showing the presence of mould flux above the molten steel meniscus.

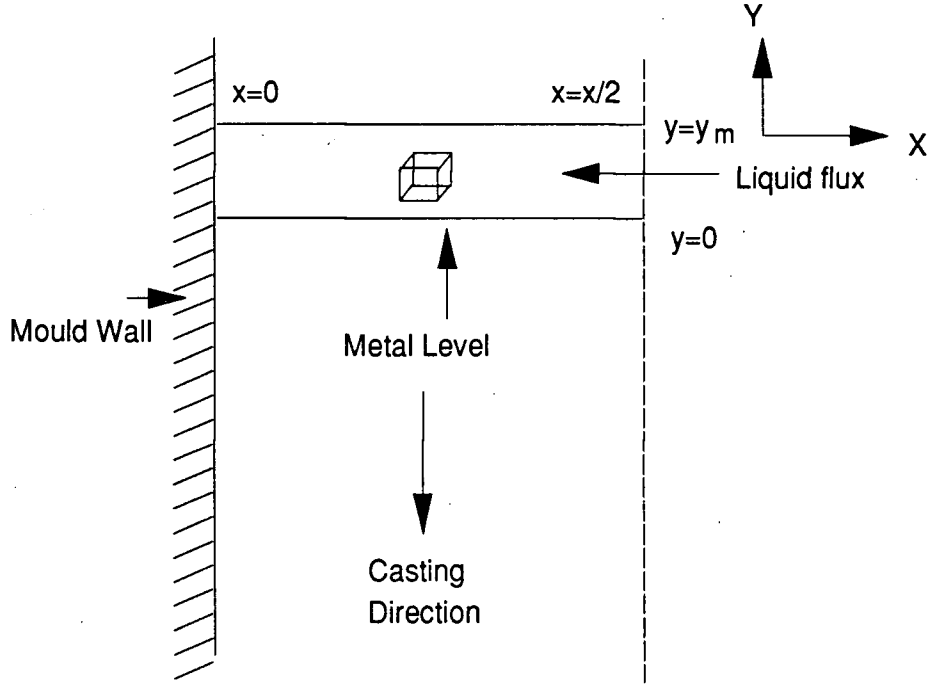

Figure 8.2. Location of the control volume in the mould flux.

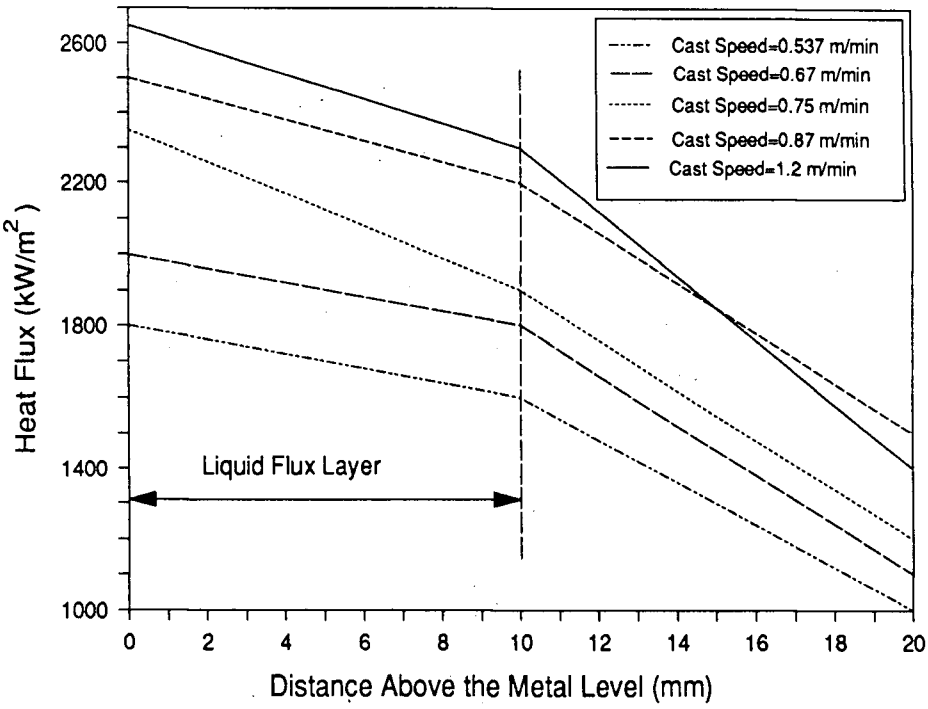

Figure 8.3. Heat-flux profile above the meniscus at the narrow face (centreline) at different casting speeds (%C=0.04 to 0.06%).

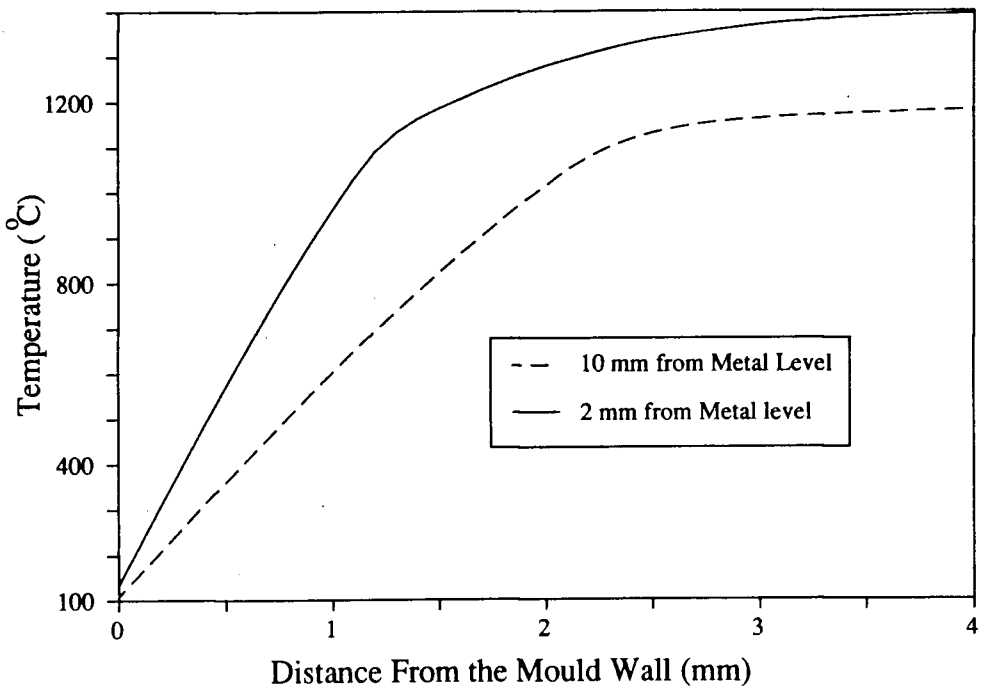

Figure 8.4. An example of the model predicted temperature distribution in the liquid mould flux (Pemco 389 mould flux).

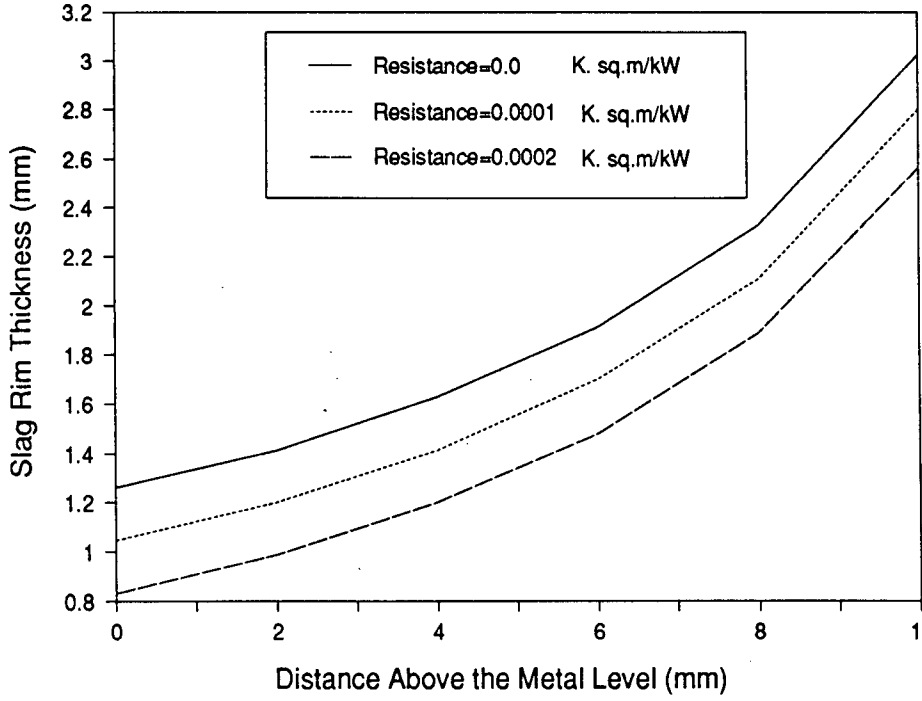

Figure 8.5. Computed profiles of the slag rim thickness at different assumed values of the interface resistance.

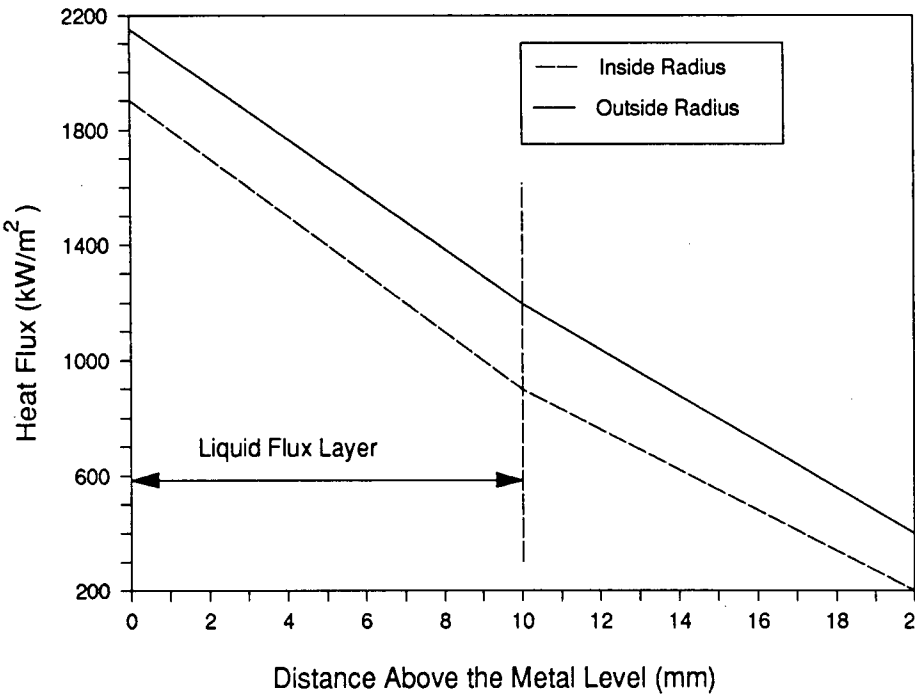

Figure 8.6. Heat-flux profiles at the two broad faces above the metal level.

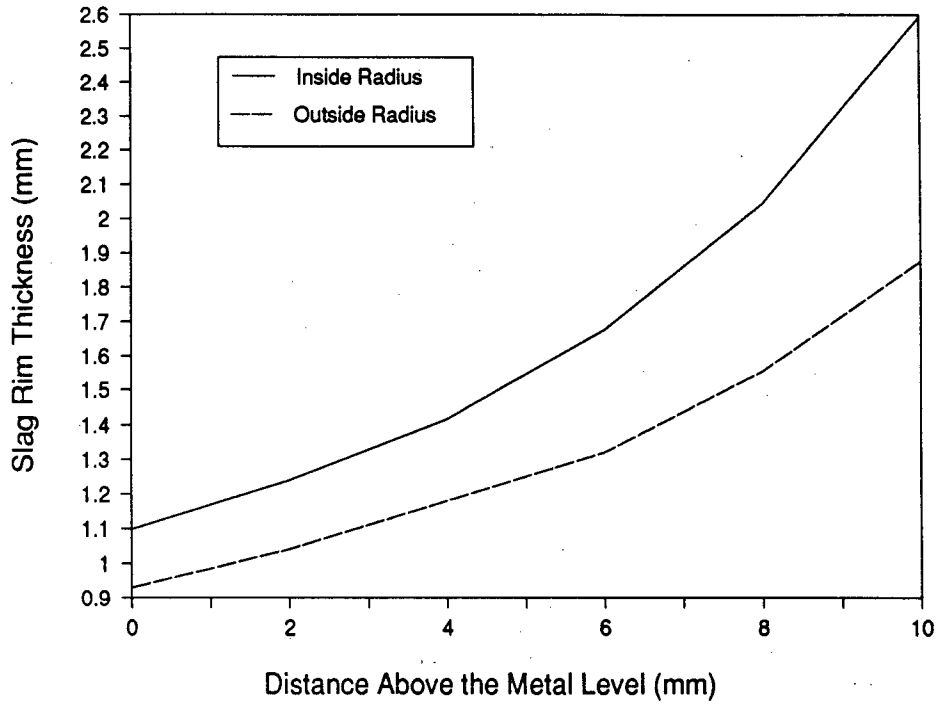

Figure 8.7. A comparison of the model predicted slag rim thickness profiles adjacent to the inside and the outside radius faces. (Pemco 389 mould flux, C=0.09%)

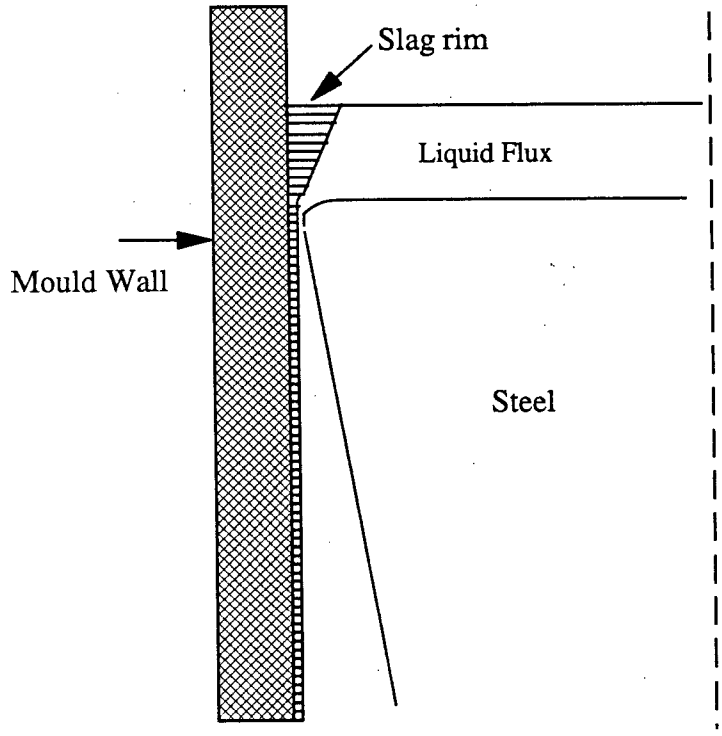

Figure 8.8. A schematic drawing showing the presence of the slag rim adjacent to the mould wall to illustrate its influence on the inflow of the mould flux at the meniscus.

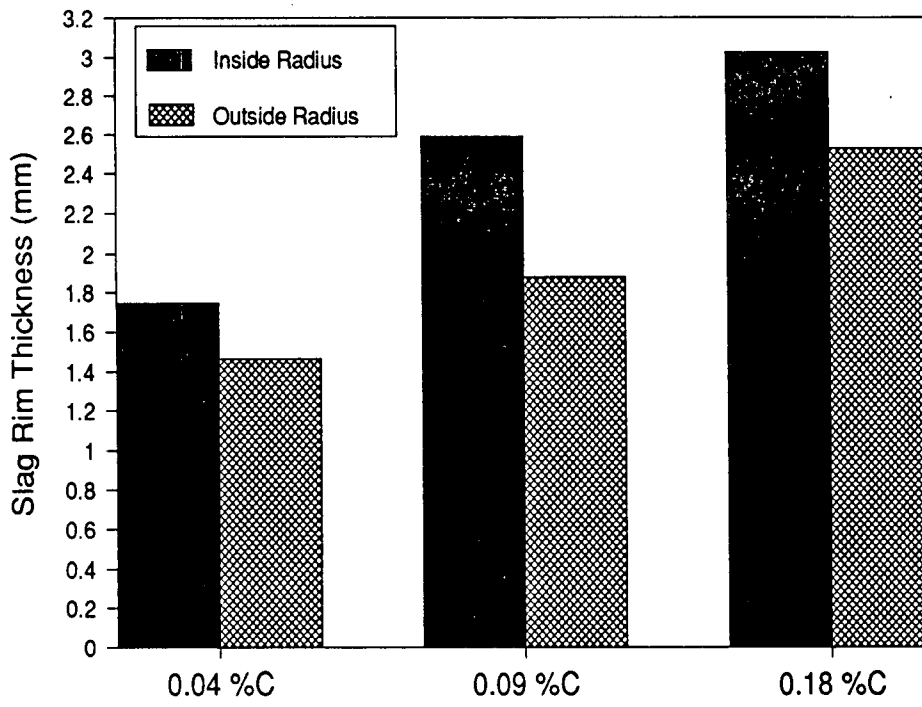

Figure 8.9. Comparison of the maximum slag rim thickness on the two broad faces for three different steel grades (Pemco 389 mould flux).

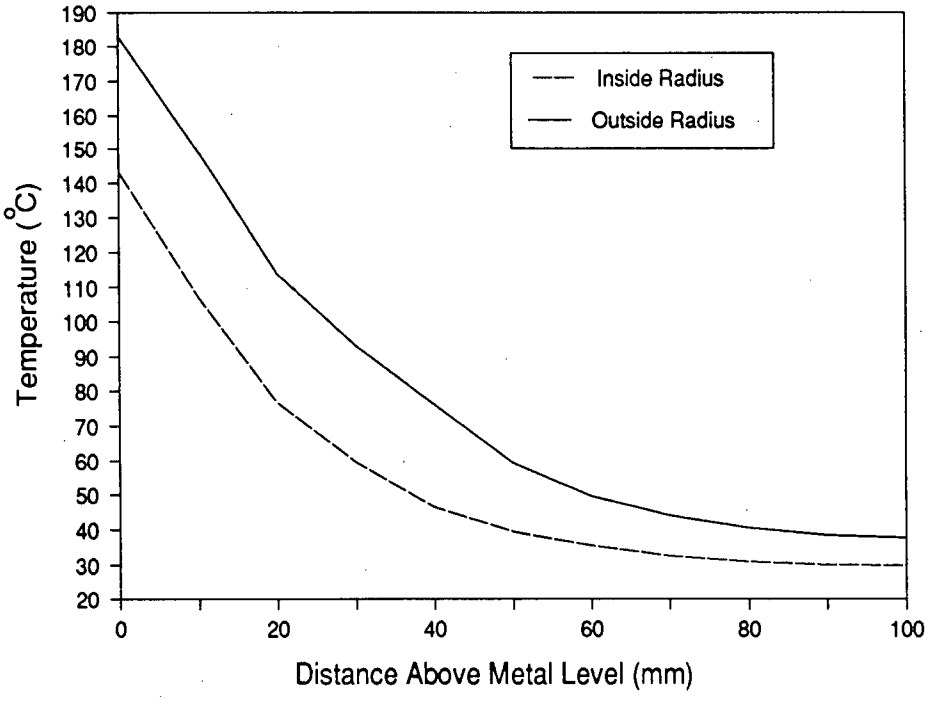

Figure 8.10. Comparison of the model predicted hot-face temperature profile above the meniscus on the inside and the outside radius copper plates.

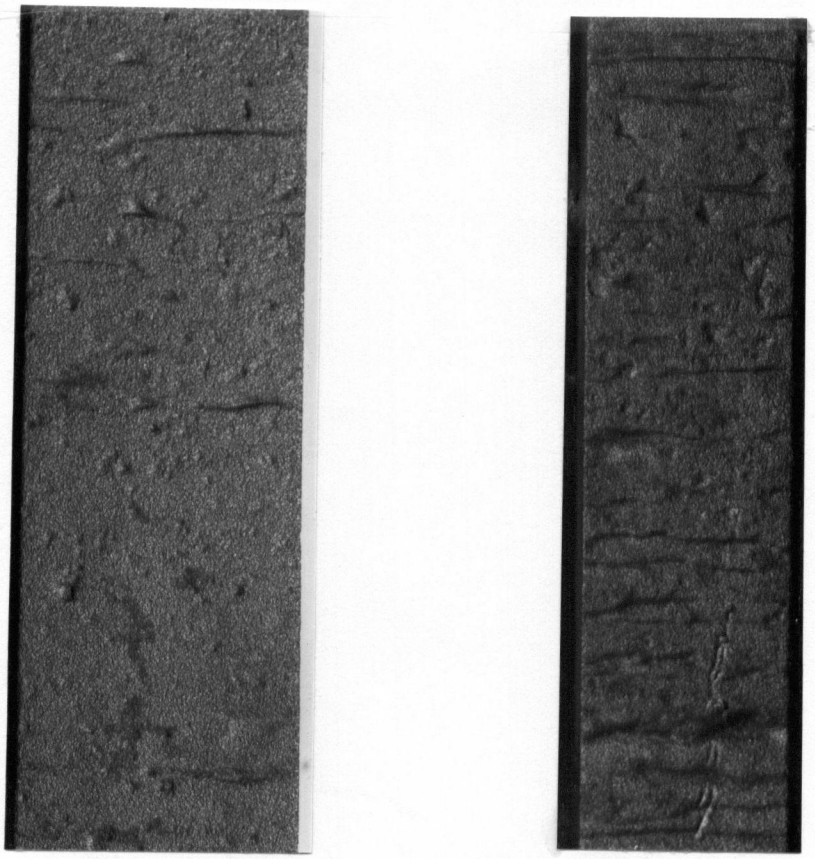

Figure 8.11. Surface appearance of the samples on the inside and the outside radius showing the rolled-out oscillation marks.

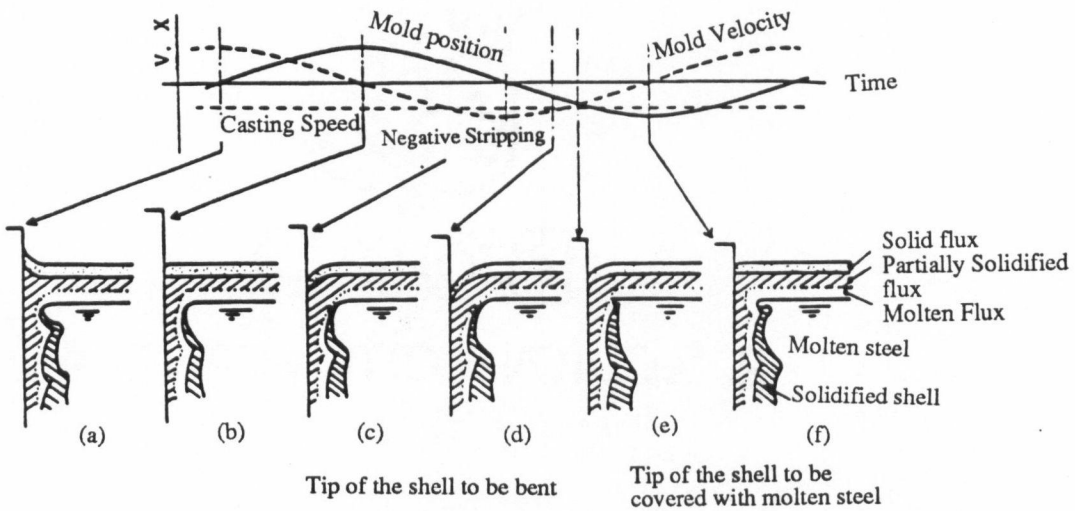

Figure 8.12. Schematic drawing showing the interaction between the slag rim and the meniscus leading to the formation of an oscillation mark [12]

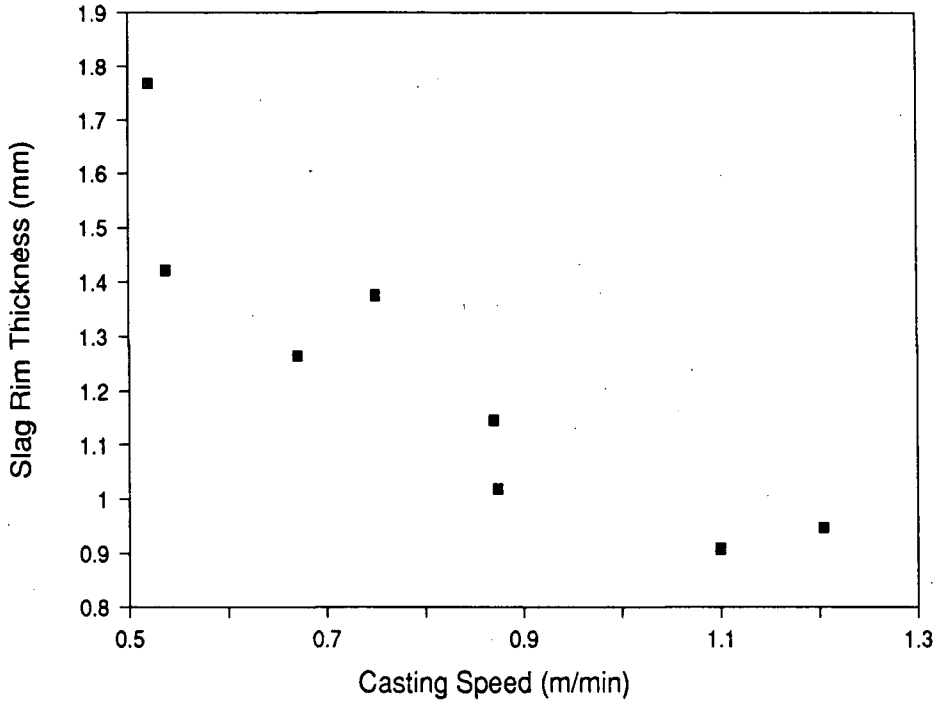

Figure 8.13. Influence of the casting speed on the thickness of the slag rim at the narrow face (C=0.04 to 0.06%).

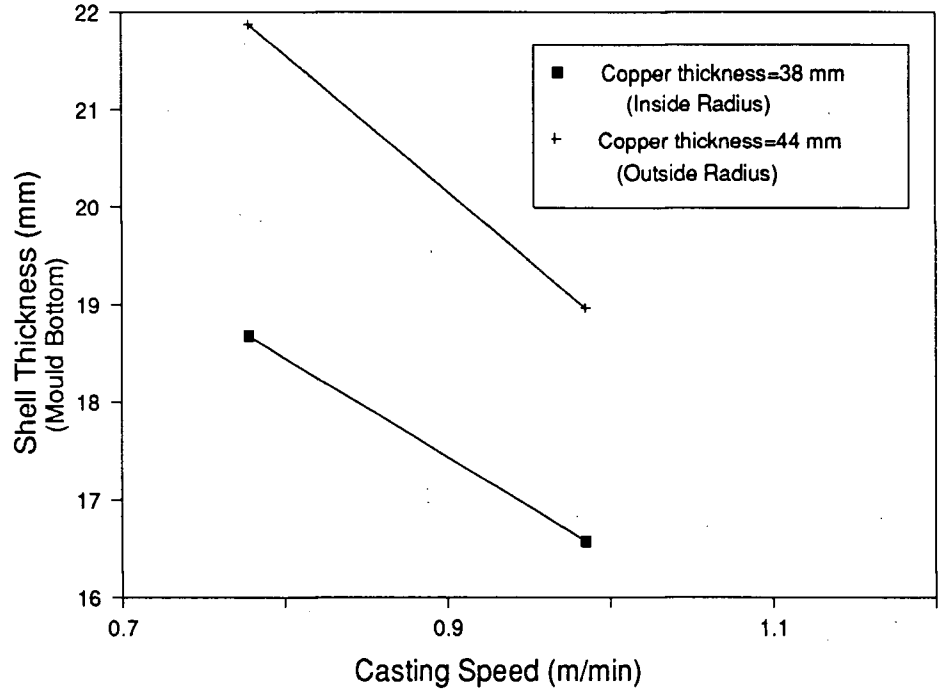

Figure 8.14. Shell thickness at the bottom of the mould on the inside and the outside radius faces at two casting speeds (C=0.20%).

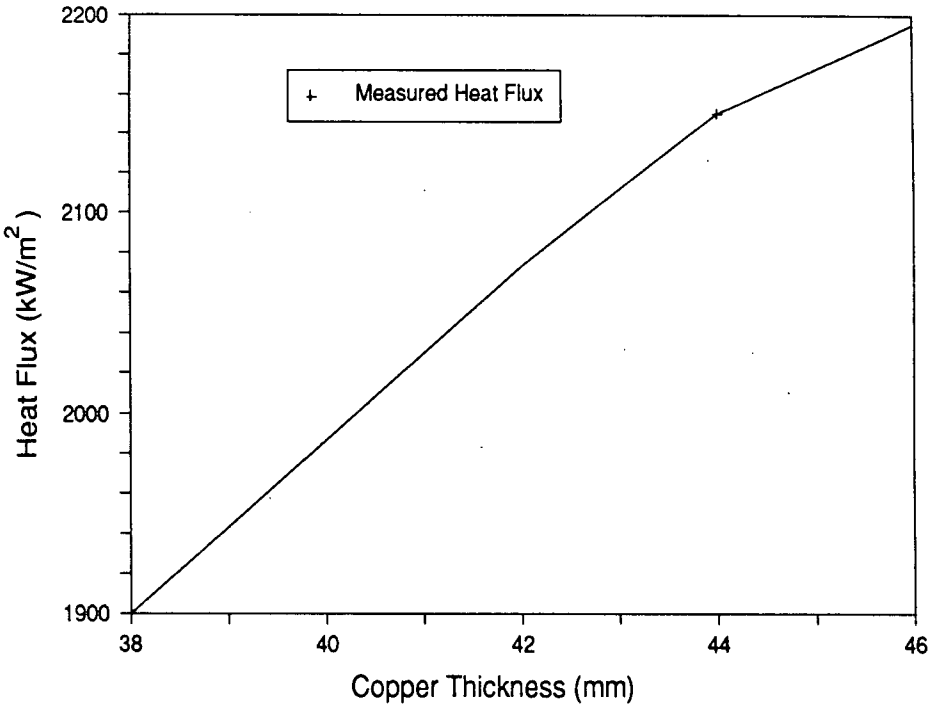

Figure 8.15. Anticipated values of the meniscus heat flux at different thickness of the copper plates (C=0.09%).

Chapter 9 - SUMMARY AND CONCLUSIONS

A comprehensive study comprising of industrial measurements, mathematical models, metallographic analysis has been conducted to elucidate the mould behaviour during casting and its influence on the slab quality. An operating slab mould was instrumented with a large number of thermocouples and the temperature of the mould wall was measured for a wide range of casting conditions. A three-dimensional heat flow model of the mould wall was developed and utilized to calculate the heat flux profiles on the broad and narrow faces of the mould from the thermocouple measurements. Furthermore, mathematical models also were developed to simulate solidification of the steel in the mould and to ascertain the behaviour of the mould flux at the meniscus; the heat fluxes obtained from the time-averaged mould temperature data were employed as boundary conditions in these models. The samples collected during the trials were metallographically examined to determine the presence of cracks, solidification bands. The pitch and depth of oscillation marks present on the narrow face samples were measured with a profilometer.

The mould temperature measurements particularly at the meniscus revealed significant variation due to metal level fluctuations. Thus a filtering technique was implemented to obtain time slices of temperature corresponding to a fixed metal level and casting speed. Implementation of a metal level control system is strongly recommended. It has been shown that a three-dimensional model of the mould wall is absolutely essential for accurate computation of the mould heat fluxes from the mould temperature data. This is because heat flow is fully three-dimensional in the mould wall and thus, two-dimensional models either in the transverse or in the longitudinal plane neglect the third component of heat flow which leads to an underestimation of the heat flux. With the aid of a three-dimensional heat transfer model of the mould wall, a heat transfer model to predict solidification in the steel and a third model to quantify heat-transfer in the mould

flux, it has been unambiguously established that the behaviour of the mould flux determined by the thickness of the slag rim has a strong influence on mould-heat transfer. With this concept, which is central to this study the influence of variables on the mould heat-transfer have been analysed. The following conclusions may be drawn from the mould heat-transfer analysis.

(i) The axial heat-flux profile is characterized by the presence of a maximum at the metal level and thereafter with increasing distance below the meniscus there is a reduction in the heat extraction rate. The decrease in the heat flux below the meniscus is more rapid on the narrow face than the broad face and this finding emphasizes the importance of the narrow face taper.

(ii) The heat flux at the meniscus in a slab mould varies between 2000 to 3000 kW/m^2 as compared to values of 3000 to 5000 kW/m^2 for a billet mould.

(iii) Heat extraction rates on the outside radius face were greater than that on the inside radius. The differences in the heat fluxes are a consequence of differences in the mould wall thickness near the meniscus and the concomitant influence on the dimensions of the slag rim at the meniscus. Higher temperature of the outside radius copper plate led to a reduction in the slag rim thickness relative to inside radius face which resulted in an increase in the heat fluxes.

(iv) Heat transfer in the mould is strongly governed by the type of the mould flux; viscosity and melting temperature of the mould flux are important parameters from the standpoint of heat transfer.

(v) Steel carbon content has a measurable influence on the heat transfer in the mould; however the influence of carbon is also governed by the type of mould flux employed. In general it was found that for a 0.09 percent carbon steel grade the heat transfer rates were lower than either 0.04 percent or 0.29 percent carbon steels. On the otherhand, heat extraction rates in the mould

for a 0.36 percent-carbon steel was lower than for 0.18 percent-carbon steel owing to the lower temperature of the steel at the meniscus which increased the viscosity of the mould flux.

(vi) Casting speed has a strong influence on the heat extraction rates in the mould. An increase in the casting speed resulted in an enhancement in the heat fluxes down the length of the mould; however, the effect was most prominent near the meniscus. With an increase in the casting speed the rate of heat input to the mould flux is enhanced which increases its melting rate and subsequently lowers the viscosity.

(vii) The submergence depth of the submerged entry nozzle has an effect on the heat transfer particularly in the upper region of the mould. The flow patterns and the temperature of the steel is affected by the submergence depth; the enhanced turbulence and higher temperature of steel at the meniscus with shallower submergence depth will increase the heat input to the mould flux and consequently decrease its viscosity and thereby increasing the heat transfer.

The heat-transfer solidification model for the steel has shown that the surface temperature of the steel decreases very rapidly in the upper part of the mould, whilst in the lower part of the mould the surface temperature remains virtually constant or decreases slightly. This is because the principal thermal resistance to heat flow in the upper part is the gap whilst with increasing distance below the meniscus the shell offers larger resistance to heat flow. The following is a summary of the major findings.

(i) The shell thickness in the mould is strongly governed by the casting speed. With an increase in casting speed the residence time of a slice of steel in the mould is reduced which leads to a decrease in the shell thickness and thus enhance the propensity for break-outs.

(ii) The type of mould flux also has an influence on the shell thickness; it was shown that Pemco 389 mould flux led to an increase in the shell thickness relative to Stg 179 as a result of higher heat fluxes in the mould.

(iii) The computed shell thickness on the outside radius was found to be more than that on the inside radius face corroborating the evidences obtained from the white bands seen in the macroetched sample. Increase in the shell thickness on the outside radius face is a consequence of higher heat fluxes relative to inside radius face.

(iv) The reduction in the slab surface temperature is more rapid near the meniscus compared to the lower half of the mould. Consequently, the steel shrinks more in the upper region of the mould relative to the lower part. Therefore, it is important to impart a double taper to the narrow face copper plate; the taper should be increased near the meniscus to accomodate the large shrinkage relative to the lower region of the mould.

(v) Longitudinal cracks were observed near the corner region of the broad face and the location of these cracks from the surface varied with casting speed. A depression was present on the surface beneath which cracks were located. It was shown that these cracks are formed in the mould. The bulging of the narrow face in the lower region of the mould (approximately 750 mm from the mould top) generated transverse tensile strains near the corner region of the broad face which led to the formation of cracks initiating at the solidification front. Owing to the good ductility of steel at the surface, the transverse strains resulted in the plastic deformation of the surface much like tensile testing which resulted in the depression.

Based on the importance of the slag rim it is proposed that oscillation marks form during the negative strip time due to the mechanical interaction between the slag rim and the newly solidifying shell, which is in accordance with the mechanism proposed by Kawakami et al. [12]. The following observations and conclusions are of importance.

(i) The oscillation marks on the inside radius face were deeper than those on the outside radius. The increased depth of oscillation marks on the inside radius is a consequence of thick slag rim at the meniscus. Increase in the slag rim thickness will lead to more deformation of the shell at the meniscus and therefore, the depth of oscillation mark is increased.

(ii) The oscillation mark depth is strongly governed by the casting speed; an increase in the casting speed resulted in a decrease in the slag rim thickness which decreased the mark depth. Despite a constant negative strip time, changes in casting speed can have a strong influence on the oscillation mark depth.

As a result of this study, for the first time links have been established between mould design and mould heat-transfer.

(i) The mould wall thickness has a strong influence on the heat transfer in the mould, an increase in the mould wall thickness will result in an increase in the heat fluxes in the mould. With an increase in the mould wall thickness, the temperature of the mould wall will be increased which will reduce the slag rim thickness and subsequently increase the heat transfer. It was shown that the production rate can be increased by increasing the mould wall thickness which will enhance the heat extraction capability of the mould.

9.1 Suggestions for Future Work

The findings of the present study have clearly demonstrated the significance of the mould flux behaviour near the meniscus from the standpoint of heat extraction and product quality and thus, it is essential to examine this phenomenon for a wide range of mould fluxes to evaluate their performance. This can be accomplished by conducting experiments in the laboratory by simulating the conditions prevailing at the meniscus in an operating slab mould. These experiments should mainly be aimed at establishing the slag rim dimensions and characterizing the infiltration rate of the mould flux at the

meniscus. A major variable which need to be considered is the copper plate temperature and experiments should be conducted over a wide range of copper temperature to examine its influence on the slag rim thickness. Besides, the other variables which need to be considered are the steel temperature at the meniscus, depth of the liquid flux layer, melting characteristics of the mould flux. The results of these experiments can be utilized to provide a greater insight into the behaviour of the mould flux and also in the assessment of its applicability in a real casting operation.

The industrial trials of the same nature as conducted in the present study will also be essential primarily to characterize the heat fluxes to elucidate the mould flux behaviour. However, in addition to the variables considered in the present study, it will be important to examine the influence of variables like copper plate thickness, water velocity, inlet water temperature, molten flux pool depth on the heat transfer and the slab quality.

REFERENCES

1. N.A. McPherson and S. Henderson: Ironmaking and Steelmaking, 1983, Vol. 10, No. 6, pp. 259-268.

2. Y. Takamura, S. Mizoguchi, O. Tsubakihara, T. Kuwabra and M. Saito: Nippon Steel Technical Report, 1983, No. 21, pp. 198-201.

3. F. Weinberg: Metall. Trans. B, 1979, Vol. 10B, pp. 219-227.

4. B.G. Thomas, J.K. Brimacombe and I. V.Samarasekera: ISS Trans., 1986, Vol. 7, pp. 7-29.

5. R. Bommaraju, J.K. Brimacombe and I.V. Samarasekera: ISS Trans., 1984, Vol. 5, pp. 95-105.

6. I.V. Samarasekera, J.K. Brimacombe and R. Bommaraju: ISS Trans., 1984, Vol. 5, pp. 79-94.

7. Charles R. Taylor: Metall. Trans. B, 1975, Vol. 6B, pp. 359-375.

8. J.K. Brimacombe, F. Weinberg and E.B. Hawbolt: Metall. Trans. B, 1979, Vol. 10b, pp. 279-292.

9. T. Nakano, M. Fuji, K. Nagano, S. Mizoguchi, T. Yamamoto and K. Asano: Transactions ISIJ, 1981, Vol. 21, pp. B-306.

10. A. Byrne, J. Powell, A. Perkins, and N. Hunter: Proceedings of the 4th International Conference on Continuous Casting, Brussels, 1988, pp. 177-188.

11. K. Chihara, T. Komai, Y. Sawada, K. Iga, M. Matsumoto and J. Osida: Transactions ISIJ, Vol 22, 1982, pp. B-267.

12. K. Kawakami, T. Kitagawa, M. Komatsu, H. Mizukami, A. Mausi and T. Ishida: Nippon Kokan Tech. Report, Overseas, No. 36, pp. 1-9.

13. T. Emi, H. Nakato, Y. Iida, K. Emota, R. Tachibana, T. Imai and H. Bada: Steelmaking Conference Proceedings, 1978, Vol. 61, pp. 350-361.

14. S. Farkas, J. W. Shaw and J. D. Gricol: Open Hearth Conference Proceedings, 1971, Vol. 54, pp. 68-80.

15. H. Nakato, S. Omiya, Y. Habu, T.Emi, K. Hamagami, and T. Kushikawa: Journal of Metals, 1984, No. 3, pp. 44-49.

16. A. Delahalle, J. F. Moriotton, J. P. Birat J. Foussal, M. Larrecq and G. Tourscheo: Steelmaking Conference Proceedings, 1984, Vol. 67, pp. 21-35.

17. H. Funanokawa, T. Wada, A. Siroyami, T. Mori and K. Okomoto: Tetsu-To-Hagane, 1987, Vol. 73, pp. 187.

18. M. Hashio, T. Watanabe, T. Echigo, H. Kato, Y. Nakatsuka and K. Mafus: Presented at the 100th ISIJ Meeting, October 1980, Lecture No. S857.

19. K. Sorimachi, M. Kuga, K. Marumoto, T. Koshikawa, K. Hamagami and H. Kitaoka: Transactions ISIJ, 1982, Vol. 22, No. 2, pp. B-17.

20. A. Fujiwara, T. Isoda, H. Nishikawa and K. Emoto: Proceedings of the McMaster Symposium, 1985, No. 13, pp. 287-301.

21. T. Wada, M. Suzuki and T. Mori: Steelmaking Proceedings, 1987, Vol. 70, pp. 197-204.

22. M. Vereecke, W. Vermeirsch and U. Meers: Proceedings of the 4th International Conference on Continuous Casting, Brussels, 1988, pp.128-141.

23. B. Mairy, D. Ramelot, M. Dutrieux, L. Deliege, N. Nourricier, and J. Dellieu: Process Technology Conference Proceedings, 1985, Vol. 5, pp. 101-117.

24. S. Ogibayashi, K. Yamaguchi, T. Mukai, T. Takahashi, Y. Mimura, K. Koyama, Y. Nagano and T. Nakano: Nippon Steel Technical Report, July 1987, No. 34, pp. 1-10.

25. T. Nakano, M. Fuji, K. Nagano, S. Mizoguchi, T. Yamamoto and K. Asano: Transactions ISIJ, 1981, Vol. 21, No. 7, pp. B-307.

26. M. Yanagida, M. Fujine, Y. Kawakami and T. Ohtsuka: Transactions ISIJ, 1981, Vol. 21, No. 9, pp. B-395.

27. R. Gray and H. Marston: Steelmaking Conference Proceedings, 1979, Vol. 62, pp. 93-102.

28. W. R. Irving, A. Perkins and R. Gray: Ironmaking and Steelmaking, 1984, Vol. 11, No. 3, pp. 146-151.

29. K. Nakai, M. Kowasaki, K. Nakajima, T. Sakashita and Y. Sugitani: Continuous Casting '85, Proceedings of the Conference by the Institute of Metals, London, 1985, pp. 71.1-71.8.

30. H. Nakata, M. Ozawa, K. Kinoshita, Y. Habu and T. Emi: Transactions, ISIJ, 1984, Vol. 24, pp. 957-965.

31. T. Fujiyama, S. Miyagawa, S. Deshimaru and H. Mizota: Steelmaking Conference Proceedings, 1985, Vol. 68, pp. 215-221.

32. P. H. Dauby, W. H. Emling and R. Sobolewski: Iron & Steelmaker, Feb. 1986, pp. 28-36.

33. H. Yamamoto, Y. Nuri and T. Ohashi: Transactions ISIJ, 1982, Vol. 22, 1982, pp. B-336.

34. W.R. Storkman and B.G. Thomas: "Modeling of Casting and Welding Processes", Engineering Foundation Conference, Palm Coast, FL, April 17-22, 1988.

35. N.T. Mills and R.W. Joseph: Ironmaking and Steelmaking, 1977, No. 3, pp. 181-189.

36. E. Takeuchi and J.K. Brimacombe: Metall. Trans. B, 1985, Vol. 16B, No. 3, pp. 605-625.

37. H. Takeuchi, S. Matsumura, Y. Ikehara, T. Kosuge and R. Hidaka: Transactions ISIJ, 1982, Vol. 22, No. 7, pp. B-205.

38. S. Tanaka, H. Misumi, H. Kibe, T. Ota, S. Mizoguchi and H. Horiguchi: Presented at 102nd ISIJ Meeting, November 1981, Lecture No. S852.

39. S. Watanabe, K. Harada, N. Fujita, Y. Tamura and K. Noro: Tetsu-to-Hagane, 1972, Vol. 58, No. 11, pp. 393-394

40. A.W. Cramb and F.J. Mannion: Steelmaking Conference Proceedings, 1985, Vol. 68, pp. 349-359.

41. E. Takeuchi and J. K. Brimacombe: Metall. Trans. B, 1984, Vol. 15B, No. 3, pp. 493-509.

42. M. Wolf: Transactions ISIJ, 1982, Vol. 22, No. 4, pp. B-91

43. H. Takeuchi, S. Matsumura, R. Hidaka, Y. Nagano and Y. Suzuki: Presented at 102nd ISIJ Meeting, Nov. 1981, Lecture No. S906.

44. M. Hashio, T. Watanabe, T. Yamamoto, K. Marukawa and M. Kawasaki: Transactions ISIJ, 1983, Vol. 23, 1983, pp. B-88.

45. M. Wolf: Electric Furnace Proceedings, 1982, Vol. 40, pp. 335-346.

46. M. Suzuki, Y. Kitagawa, S. Uchida, T. Masaoka, K. Ozawa and T. Mori: Tetsu-to-Hagane, 1985, Vol. 71, pp. 246.

47. Y. Kobayashi, Y. Hasegawa and S. Maruhashi: Tetsu-to-Hagane, 1984, Vol. 70, pp. 274.

48. E. Takeuchi: Ph. D Thesis, 1984, Univ. of British Columbia.

49. S. Ando, J. Ikeda, K. Yamaguchi, N. Hagibayashi and T. Mukai: Tetsu-to-Hagane, 1985, Vol. 71, pp. 251.

50. M. Wolf: Ironmaking and Steelmaking, 1986, Vol. 13, pp. 248-257.

51. J. Savage and W.H. Pritchard: JISI, November 1954, pp. 269-277.

52. R. Sato: Steelmaking Conference Proceedings, 1979, Vol. 62, pp. 48-67.

53. E. I. Akimova, A.V Leites, N.V. Dolgunov and V.M. Kukartsev: Steel in the USSR, 1983, No. 10, pp. 440-443.

54. H. Nakato, T. Nozaki, Y. Habu, H. Oka, T. Ueda, Y. Kitano and T. Koshikawa: Steelmaking Conference Proceedings, 1985, Vol. 68, pp. 361-365.

55. I.G. Saucedo: Steelmaking Conference Proceedings, 1987, Vol. 70, pp. 449.

56. A. Howe and I. Stewart: Steelmaking Conference Proceedings, 1987, Vol. 70, pp. 417-425.

57. M. Wolf: Transactions ISIJ, 1980, Vol. 20, pp. 710-717.

58. H. Yasunaka, T. Mori, H. Nakata, F. Kamei and S. Harada: Transactions ISIJ, 1985, Vol. 25, pp. B-90.

59. A. Delhalle, M. Larrecq, J. Petegnief and J.P. Radot: Proceedigs of the 4th International Conference on Continuous casting, Brussels, 1988, pp.38-48.

60. H. Tomono, P. Ackermann, W. Kurz and W. Heinemann: "Solidification Technology in the Foundry and Cast house", Proceedings of the Conference Organised by The Metals Society, Coventry, September 1980, pp. 524-531.

61. I. G. Saucedo, J. Beech and G. J. Davies: "Solidification Technology in the Foundry and Cast house", Proceeding of the Conference Organised by the Metals Society, Coventry, September 1980, pp. 461-468

62. I. Saucedo, J. Beech and G. J. Davies: Metals Technology, 1982, Vol. 9, pp. 282-291.

63. R. S. Laki, J. Beech and J. Davies: Ironmaking and Steelmaking, 1984, Vol. 11, No. 5, pp. 283-291.

64. K. Tada, J.P. Birat, P. Riboud, M. Larrecq and H. Hackl: Tetsu-to-Hagane, 1984, Vol. 70, pp. 155.

65. T. Takawa, T. Takamoto, H. Tomono and K. Tada: Tetsu-to-Hagane, 1988, Vol. 74, No. 11, 1988, pp. 70-76.

66. H. Nakato and I. Muchi: Tetsu-to-Hagane, 1980, Vol. 66, pp. 33-42.

67. Y. Iida, K. Moriwaki, N. Ueda and Y. Habu: Tetsu-to-Hagane, 1973, Vol. 59, pp. S89.

68. T. Soejima, N. Kobayashi, S. Kita, M.Kimura Y. Matsushita and H. Yasunaka: Tetsu-to-Hagane, 1988, Vol. 1, pp. 308

69. S. Tanaka, H. Misumi, S. Mizoguchi and S. Horiguchi: Presented at 101st ISIJ Meeting, April 1981, Lecture No. S172.

70. A. Tsuneoka, W. Ohashi, S. Ishitobi, T. Kataoka and M. Tenma: Steelmaking Conference Proceedings, 1985, Vol. 68, pp. 3-10.

71. H.T. Tsai and J.C. Mastervich: Steelmaking Conference Proceedings, 1988, Vol. 71, pp. 167-173.

72. S. Itoyama, H. Yamanaka, S. Tanaka, T. Yunde and T. Kuroki: Steelmaking Conference Proceedings, 1988, Vol. 71, pp. 97-102.

73. K. Blazek and I. Saucedo: Proceedings of the 4th International Conference on Continuous Casting, Brussels, 1988.

74. M. Washio, K. Hamagami, S. Kokura, M. Onishi, T. Koshikama: Tetsu-to-Hagane, 1988, Vol. 1, pp. 150-152.

75. K. Sorimachi, M. Kuga, H. Nishikawa, K. Marumoto and H. Nakati: Transactions ISIJ, 1981, Vol. 21, No. 9, pp. B-435.

76. T. Imai, Y. Kurose, S. Omiya, K. Sorimachi and K. Suzuki: Transactions ISIJ, 1986, Vol. 26, pp. B-95.

77. T. Koyano, O. Terada, S. Uchida and M. Ishikawa: Steelmaking Conference Proceedings, 1986, Vol. 69, pp. 449-456.

78. M .Maeda, H. Nakamura, M. Tawala and T. Yamagami: Tetsu-to-Hagane, 1988, Vol. 1, pp. 143-144.

79. K. Yui, Y. Katoh, M. Yamada, M. Uehera, T. Nakamura and M. Tezuka: Transactions ISIJ, 1988, Vol. 28, No. 2, pp. B-55

80. M. Yamada, Y. Katoh, K. Yamaguchi, S. Ogibayashi, M. Tezuka and K. Shio: Transactions ISIJ, 1988, Vol. 28, No. 2, pp. B-56

81. T. Nakato, T. Nozaki, Y. Kakeu, H. Oka, N. Ueda and H. Baba: Tetsu-to-Hagane, pp. 149.

82. H. Mizukami, K. Kawakami, S. Miyahara, M. Suzuki, T. Kitagawa and O. Terada: Transactions ISIJ, 1985, Vol. 25, pp. B-300.

83. H. Mizukami, A. Ozeki, A. Kuribayashi, N. Hasabe, S. Uchida and T. Kitagawa: Transactions ISIJ, 1985, Vol. 25, pp. B-301.

84. H. Mizukami, K. Kawakami, T. Kitagawa, M. Suzuki, S. Uchida and Y. Komatsu: Tetsu-to-Hagane, 1986, Vol. 72, pp. 50-57.

85. T. Yamashita, J. P. Radot, I. McNeil and M. Wolf: Proceedings of the 4th International Conference on Continuous Casting, Brussels, 1988, pp. 329-340.

86. T. Mukai, K. Yamaguchi and S. Ogibayashi: Transactions ISIJ, 1986, Vol. 26, pp. B-163.

87. H. Takeuchi, H. Mori, T. Nishida, T. Yanai and K. Mukunashi: Transactions ISIJ, 1979, Vol. 19, pp. 274-282.

88. W.L. McCauely and M.K. Koul: Steelmaking Conference Proceedings, 1986, Vol. 69, pp. 87-93.

89. L.J. Heaslip, A. Mclean and I.D. Somerville: Continuous Casting, Vol. 1, A Publication of the Iron and Steel Society of AIME.

90. W. L. McCauely and D. Apelian: Iron and Steelmaker, 1983, Vol. 10, No. 8, pp. 45.

91. W. L. McCauely and D. Apelian: Iron and Steelmaker, 1983, Vol. 10, No. 9, pp. 50.

92. W. L. McCauely and D. Apelian: Iron and Steelmaker, 1983, Vol. 10, No. 10, pp. 39-41.

93. W. L. McCauely and D. Apelian: Iron and Steelmaker, 1983, Vol. 10, No. 11, pp. 56-58.

94. W. L. McCauely and D. Apelian: Iron and Steelmaker, 1983, Vol. 10, No. 12, pp. 42-43.

95. R. V. Branion: Iron and Steel Maker, 1986, No. 9, pp. 41-50.

96. M.D. Layni and C.J. Rosa: Ironmaking and Steelmaking, 1982, No. 1, pp. 25-31.

97. P.V. Riboud and M. Olette: Steelmaking Conference Proceedings, 1978, Vol 61, pp. 411-417.

98. B.N. Bhat and N.T. Mills: Continuous Casting, 1983, Vol. 1 pp. 147-154.

99. R. Scheel, H. Stahl, A. G. Dortmund and W. Korte: Stahl Eisen, 1988, Vol. 107, No. 17, pp. 781-787.

100. M. K. Koul: Natco Inc., Private Communication.

101. P. Grievson, S. Bagha, N. Machingawuta, K. Liddel and K. C. Mills: Ironmaking and Steelmaking, 1988, Vol. 15, No. 4, pp. 181-186.

102. I.V. Samarasekera and J.K. Brimacombe: International Metals Reviews, 1978, No. 6, pp. 286-300.

103. I.M.D. Halliday: Continuous Casting Steel Publication, Nov 1964, The Iron and Steel Institute, Special Report No. 89.

104. H. Nemoto: Tetsu-to-Hagane, 1974, Vol. 60, pp. 755.

105. H. Marti and J. Barbe: Iron and Steel International, June 1978, pp. 167-177.

106. B. A. Otterman and J. D. Young: Steelmaking Conference Proceedings, 1988, Vol. 71, pp. 227-232.

107. M. Kitamura, T. Soejima, S. Kawasaki J. Abu and S. Ishiguro: Transactions ISIJ, Vol. 23, pp. B-370

108. J.K. Brimacombe, I.V. Samarasekera: Steelmaking Conference Proceedings, 1986, Vol. 69, pp. 409-423.

109. W.R. Irving: JISI, 1967, Vol. 205, pp. 271-277.

110. A. Mitchell: Canadian Metallurgical Quarterly, 1981, Vol. 20, No. 1, pp. 101-112.

111. E. Turkdogan: Physico-Chemical Properties of Molten Slag and Glasses, 1983.

112. K.C. Mills, P. Grieveson, A. Olusanya and S. Bagha: :"Continuous Casing " 85', Proceedings of the International Conference, Organised by Institute of Metals, London,1985, pp. 57.1-57.6.

113. R. Taylor and K.C. Mills: Ironmaking and Steelmaking, 1988, Vol. 15, No. 4, pp. 187-194.

114. T. Fukushima, N. Kobayashi, K. Matsuo, H. Yokoyama, H. Yasuna and H. Matsuda: Tetsu-to-Hagane, 1988, Vol. 1, pp. 161-164.

115. P.V. Riboud and M. Larrecq: Steelmaking Conference Proceedings, 1979, Vol. 62, pp. 78-92.

116. H. Kyoden, T. Doihara and O. Nomura: Steelmaking Conference Proceedings, 1986, Vol. 69, pp. 153-159.

117. S. Ohmiya, K. H. Tacke and K. Schwerdtfeger: Ironmaking and Steelmaking, 1983, Vol. 10, No. 1, pp. 24-30.

118. S.N. Singh and K.E. Blazek: Open Hearth Proceedings, 1974, Vol. 57, pp. 16-38.

119. D.P. Evteev: Stal in English, August, 1969, pp. 708-711.

120. A.M. Pozhivanov, V.I. Dozhdikov, V.M. Kukartsev, V.P. Farafonov, I.I. Sheinfel'd and V.E. Berezhanskii: Steel in the USSR, 1986, Vol. 16, pp.324-325.

121. S. Deshimaru, S. Omiya, H. Mizota, M. Yao, M. Maeda and T. Imai: Transactions ISIJ, 1984, Vol. 24, pp. B-339.

122. I.V. Samarasekera and J.K. Brimacombe: Can. Met. Quart, 1979, Vol. 18, pp. 251-266

123. M. Wolf: Transactions ISIJ, 1980, Vol. 20, pp. 718-724.

124. M. Ozawa, K. Suzuki, E. Hina, Y. Wada, H. Take and M. Shibata: Presented at 98th ISIJ Meeting, Oct 1979, Lecture No. S748.

125. K. Nakai, T. Kimura, T. Watanabe and T. Nakayama: Tetsu-to-Hagane, 1988, Vol. 1, pp. 145.

126. M. Sugitani, M. Nakamura, M. Okuda, M. Kawasaki and K. Nakajima: Transactions ISIJ, 1985, Vol. 25, pp. B-91.

127. M. Suzuki, S. Miyahara, T. Wada and Y. Shiratani: Trans. Presented at 100th meeting, 1980, Lecture No. S853.

128. H. Nagano and E. Takeuchi: Tetsu-to-Hagane, 1988, Vol. 1, pp. 146-149.

129. H. Yasunaka, T. Mori, H. Nakata, F. Kamei ans S. Harada: Steelmaking Conference Proceedigs, 1986, Vol. 69, pp. 497-502.

130. N.I. Revtov, E.A. Kazachkov, J.M. Young, G.H. J. Bennet and L.I. Kuzhelnay: Metals Technology, 1983, Vol. 10, No. 10, pp. 401-405.

131. S.N. Singh and K.E. Blazek: Open Hearth Proceedings, 1976, Vol. 59, pp. 264-283.

132. A. Grill and J.K. Brimacombe: Ironmaking and Steelmaking, 1976, No. 2, pp. 76-79.

133. J. K. Brimacombe, I. V. Samarasekera, N. Walker, I. Bakshi, R. Bommaraju, F. Weinberg and E. B. Hawbolt: Trans. ISS, 1984, Vol. 5, pp. 71-77.

134. Omega Temperature Handbook, Vol. 26, 1988.

135. I.A. Bakshi, E. Osinski, I.V. Samarasekera and J.K. Brimacombe: Presented at the CIM Conference, August 1988, Montreal, Canada.

136. J. Szekely and N.J. Themelis: Rate Phenomena in Process Metallurgy, Wiely-Interscience, New York, 1971.

137. J.K. Vennard: Elementary Fluid Mechanics, Wiley, New York, 4th ed., 1961.

138. H. Nakato, K. Saito, Y. Oguchi, N. Namura and K. Sorimachi: Steelmaking Conference Proceedings, 1987, Vol. 70, pp. 427-431.

139. I.V. Samarasekera and J.K. Brimacombe: Ironmaking and Steelmaking, 1982, Vol. 9, pp. 1-15.

140. Y.S. Touloukian and E.H. Buyko: Thermophysical Properties of Matter, IFI/Plenum, New York, 1970.

141. M. Nicholos: Luken Steel, Personal Communication.

142. R.V.S.S. Bommaraju: Master's Thesis, Univ. of British Columbia, 1984.

143. B.G. Thomas, I.V. Samarasekera and J.K. Brimacombe: Metall. Trans. B, 1987, Vol. 18B, pp. 119-129.

144. Iron and Steel Hand Book, 3rd ed., Published by ISIJ, 1982, Vol. 1, pp. 205.

145. E. A. Mizikar: Trans TMS-AIME, 1967, Vol. 239, pp. 1747-1753.

146. I.V. Samarasekera and J.K. Brimacombe: Presented at the "Philbrook Memorial Symposium", Organised by Iron and Steel Society, 1988, Toronto, Canada.

147. M.R. Bridge and G.D. Rogers: Metall. Trans., 1984, Vol. 15B, pp. 581-588.

148. E. Patterson: Stelco Inc, Private Communication.

149. A. Goldsmith, T.E. Waterman and H.J. Hirschhorn: Hand Book of Thermophysical Properties of Solid Materials, Vol III, Ceramics, The Macmillan Co., New York, 1961.

150. K.C. Mills, A. Olusanya, R. Brooks, R. Morrell and S. Bagha: Ironmaking and Steelmaking, 1988, Vol. 15, No. 5, pp. 257-264.

151. E. L. Fogleman and R. T. Orie: Journal of Metals, 1974, Vol. 26, No. 10, pp. 37-42

152. E. G. Hauptmann: University of British Columbia, Private Communications.

Appendix I - Errors in the Estimation of Heat Fluxes

Heat fluxes in the mould have been determined from the measured mould temperature data and thus, any error in the measured mould temperature value will subsequently lead to errors in the estimation of heat fluxes. Errors in the estimation of the heat fluxes can be attributed to the following.

(i) Calibration error of the thermocouple, which is in the range of $\pm 2.8^{0}C$ [134]. Heat flux calculations indicate that the subsequent error in the estimate of the heat fluxes due to this parameter will be within ±2.85%

(ii) Inaccurate measurements on the distance of the thermocouple bead from the hot face will also introduce error in the heat flux estimation, however the error was found to be quite small. For example, if the thermocouple bead was actually located at 6.2 mm from the hot face, but a distance of 6 mm was considered in the model, the corresponding error on the heat fluxes was calculated to be within ±0.70%

From the above calculations, it can be said that the total error in the estimate of the heat fluxes will be in the range of ±3.55%

Appendix II - Calculation of the Peclet Number

Peclet number can be utilized as a criteria to make comparisons on the relative magnitudes of heat flow due to axial conduction in the strand to the heat flow as a result of bulk motion of the strand. The heat flow due to bulk motion is considered to be dominant if the Peclet number is greater than 100 [152].

Peclet number = Reynolds number * Prandtl number

$$\text{Peclet number} = \frac{\rho_s D_H C_{ps} u_s}{k_s}$$

ρ_s = 7400 kg/m^3

D_H = 0.416 m

C_{ps} = 671.6 J/kg.K

u_s = 0.017 m/s

k_s = 33.7 W/m.K

Substituting the above values, the Peclet number is found to be 1043 and therefore, the assumption on the neglect of axial heat conduction relative to the bulk motion of the strand is justified in the heat flow model of the strand.

Appendix III - Correction Procedure Employed to Incorporate the Exact Amount of Latent Heat of Fusion in the Model

(i) If the temperature of the node before and after the time step was above the liquidus temperature and also if the temperature of the node before the time step was below the solidus temperature, then the correction procedure is not employed.

(ii) If the temperature of a node before a time step was above the liquidus temperature and after the time step was below the liquidus temperature, then the following condition is checked.

If $(T_{liq} - T_{new}) \times c_{pliq} > (T_{liq} - T_{sol}) \times c_{pm}$, then the corrected temperature of the node is

$$T_{cor} = T_{sol} - ((T_{liq} - T_{new}) \times c_{pliq} - (T_{liq} - T_{sol}) \times c_{pm})) / c_{psol}$$

However, if $(T_{liq} - T_{new}) \times c_{pliq} < (T_{liq} - T_{sol}) \times c_{pm}$, then the corrected temperature is

$$T_{cor} = T_{liq} - (c_{pliq}/c_{pm}) \times (T_{liq} - T_{new})$$

(iii) If the temperature of a node before a time step was between the liquidus temperature and solidus temperature then the following condition is checked.

If $(T_{old} - T_{new}) \times c_{ps} > (T_{old} - T_{sol}) \times c_{pm}$, then the corrected temperture of the node is,

$$T_{cor} = T_{sol} - c_{ps}/c_{psol} \times (T_{old} - T_{new}) - c_{pm}/c_{psol} \times (T_{old} - T_{sol})$$

However, if $(T_{old} - T_{new}) \times c_{ps} < (T_{old} - T_{sol}) \times c_{pm}$, then the corrected temperture of the node is,

$$T_{cor} = T_{old} - (T_{old} - T_{new}) \times c_{ps}/c_{pm}$$

Appendix IV - Calculation of Heat Fluxes at the Meniscus for Different Copper Thickness Values

The calculations are performed on 0.09 percent-carbon steel. Based on the measurements the following information was obtained.

Copper thickness (mm)	Slag rim thickness (mm)	Heat flux at the mould flux (kW/m^2)	Meniscus heat flux (kW/m^2)
38	2.595	900	1900
44	1.878	1200	2150

The relationship between the slag rim thickness and meniscus heat flux is as given below,

$$q_{me} = 2804.8 - 348.68 \times t_{rim} \qquad (A1.1)$$

where q_{me} is the meniscus heat flux in kW/m^2 and t_{rim} is the slag rim thickness in mm.

The relationship between the copper thickness and heat flux at the mould flux is as given below,

$$q_{fl} = 50 \times t_{Cu} - 1000 \qquad (A1.2)$$

where q_{fl} is the the heat flux at the mould flux in kW/m^2 and t_{Cu} is the copper thickness in mm.

The mathematical model of the mould wall was run for copper thickness of 42 and 46 mm. Then, from a knowledge of the mould wall temperature at the meniscus and heat flux at the mould flux (Eq. A1.2) corresponding to the copper thickness, the heat flow model of the mould flux was utilized to compute the slag rim thickness for copper

thickness of 42 and 46 mm. Subsequently, the heat flux at the meniscus was obtained from known values of slag rim thickness by using Eq. (A1.2). The results are given below.

Copper thickness (mm)	Slag rim thickness (mm)	Heat flux at the mould flux (kW/m^2)	Meniscus heat flux (kW/m^2)
42	2.1	1100	2072.58
46	1.748	1300	2195.316